



University
of Glasgow

Ali, Abdalla Elsadig (1982) *Investigation of Seasat: a synthetic aperture radar (SAR) for topographic mapping applications.*

PhD thesis

<http://theses.gla.ac.uk/4060/>

Copyright and moral rights for this thesis are retained by the author

A copy can be downloaded for personal non-commercial research or study, without prior permission or charge

This thesis cannot be reproduced or quoted extensively from without first obtaining permission in writing from the Author

The content must not be changed in any way or sold commercially in any format or medium without the formal permission of the Author

When referring to this work, full bibliographic details including the author, title, awarding institution and date of the thesis must be given

INVESTIGATION OF SEASAT-A SYNTHETIC APERTURE RADAR (SAR)
FOR TOPOGRAPHIC MAPPING APPLICATIONS

By

ABDALLA ELSADIG ALI

B.Sc.(Hons.) (Civil Eng. (University of Khartoum))

A Thesis Submitted for the Degree of
Doctor of Philosophy (Ph.D.) in
Remote Sensing

to the
University of Glasgow

May, 1982

Volume 2

CHAPTER VIII

DESIGN AND PROCEDURES OF ACCURACY TESTS

8.1 Introduction

The purpose of this series of tests is to establish the inherent metric accuracy of the Seasat SAR imagery in the three main forms which are available to users, i.e. survey optically processed, precision optically processed and digitally processed images. The tests have been made by first establishing a test field of well defined control points whose terrain coordinates have been derived from medium-scale topographic maps. The image coordinates of the same points have then been measured on the SAR images and transformed into the corresponding terrain values using various alternative coordinate transformation procedures. Certain of these points have been used as the control points on which the computation of the transformation parameters has been based, while others have been used as check points to enable an assessment of the overall accuracy of the imagery and the efficiency of the different transformations to be made. Comparisons of the known terrain coordinates and the transformed image coordinates will give residual values in position over the whole terrain field. These allow various statistical tests to be carried out, resulting in the derivation of various indicators of the geometrical accuracy of the imagery and of the efficiency of the algorithm used for processing. A number of different control point patterns were tested with varying numbers and distribution of control points with a view to establishing the most suitable density and arrangement to achieve a given accuracy in the final results.

Due to the sheer volume of computational work involved in the transformations of large numbers of measured test points, the statistical

analyses of the residual errors and the plotting of these errors with a view to establishing their distribution and character, a suite of computer programs has been written by the author. These have taken a long time to develop and check but, without them, the programme of tests of metric accuracy could not have been carried out. Once developed, they will be available for the testing of other remote sensing imagery and not only SAR data.

8.2 Test Areas and Materials

Three areas were selected for the purpose of testing the Seasat SAR imagery. These were located as follows:-

- (i) along the banks of the River Tay in Scotland, including the cities of Dundee and Perth and the area of South Angus and North Fife;
- (ii) in East Anglia; and
- (iii) in South-western Wales around the port of Milford Haven.

Each of the selected areas is of a different topographic character to the others so that a wide variety of conditions would be encountered. Not only would this be useful from the metric point of view, but it would also allow interpretative tests to be devised to establish the degree to which the Seasat SAR imagery can supply information for the compilation and revision of topographic maps.

8.2.1 River Tay Test Area

The image covers an area approximately 48 x 36 km in extent, from $02^{\circ}43.0'$ to $03^{\circ}38.4'W$ in longitude and from $56^{\circ}0.2'$ to $56^{\circ}33.1' N$ in latitude (Fig 8.1). The terrain in this area is very varied with some large urban areas (Dundee, Perth and several smaller towns), a considerable area of flat and undulating ground, and some quite hilly

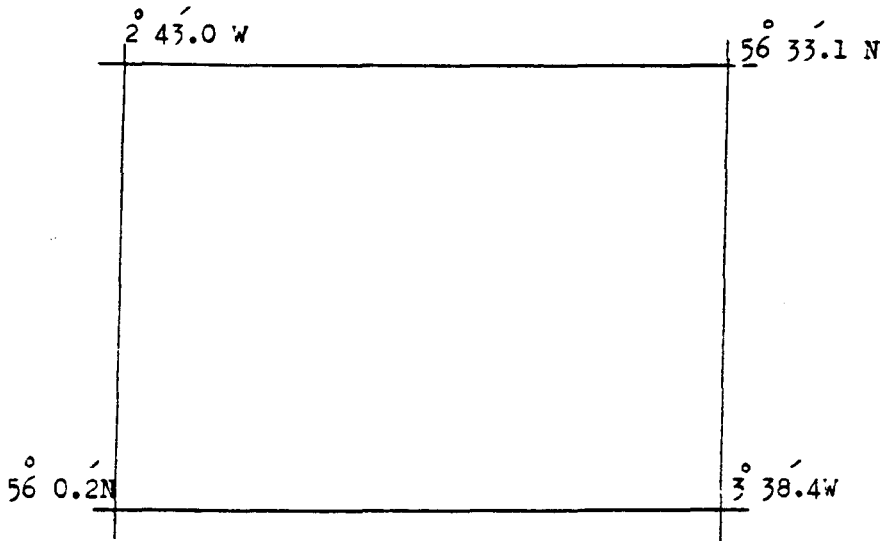


Fig 8.1 Geographic boundary of the River Tay test area

areas. The topographic relief ranges from sea level to around 350 metres. There is a considerable area of agricultural land, a number of large forests and smaller woods and certain expanses of moorland. Also the estuary of the River Tay produced islands, sand and mud banks, bridges, etc, all of which added to the variety of objects available in this test area.

The SAR imagery was acquired on 19th August 1978 at 06.40.44 from orbit 762 of Seasat. The imagery from this orbit was supplied in the form of a negative transparency 120 cm long by 24 cm wide. It contains two sub-swaths, each of 70 mm width and at a scale of 1:685,000 in ground range. The test area lies in the first sub-swath of this imagery. Positive film transparencies of this area were produced on stable polyester material at 1:250,000 scale (i.e. at approximately 2.75 times enlargement) using a Philips PCS130 70 mm enlarger installed in the Department of Geography. This was done for both the survey processed (Fig 8.2) and precision processed (Fig 8.3) images of the area originally produced on the ERIM tilted-plane optical correlator.

8.2.2 East Anglia Test Area

The East Anglia test area is covered by a three-look image also obtained from Seasat orbit 762. The image covers an area of 15 x 30 km from $00^{\circ}59.6'W$ to $00^{\circ}30.1'E$ in longitude and from $52^{\circ}41.0'$ to $52^{\circ}55.8'N$ in latitude (Fig 8.4). The area is rather flat, with topographic relief ranging from sea level to around 90 metres. Basically, it is a very highly developed agricultural area with few towns of any size, the most striking man-made objects being two large military airfields. The digital processing gave a pixel spacing of 12 m and a nominal resolution of 20 metres.

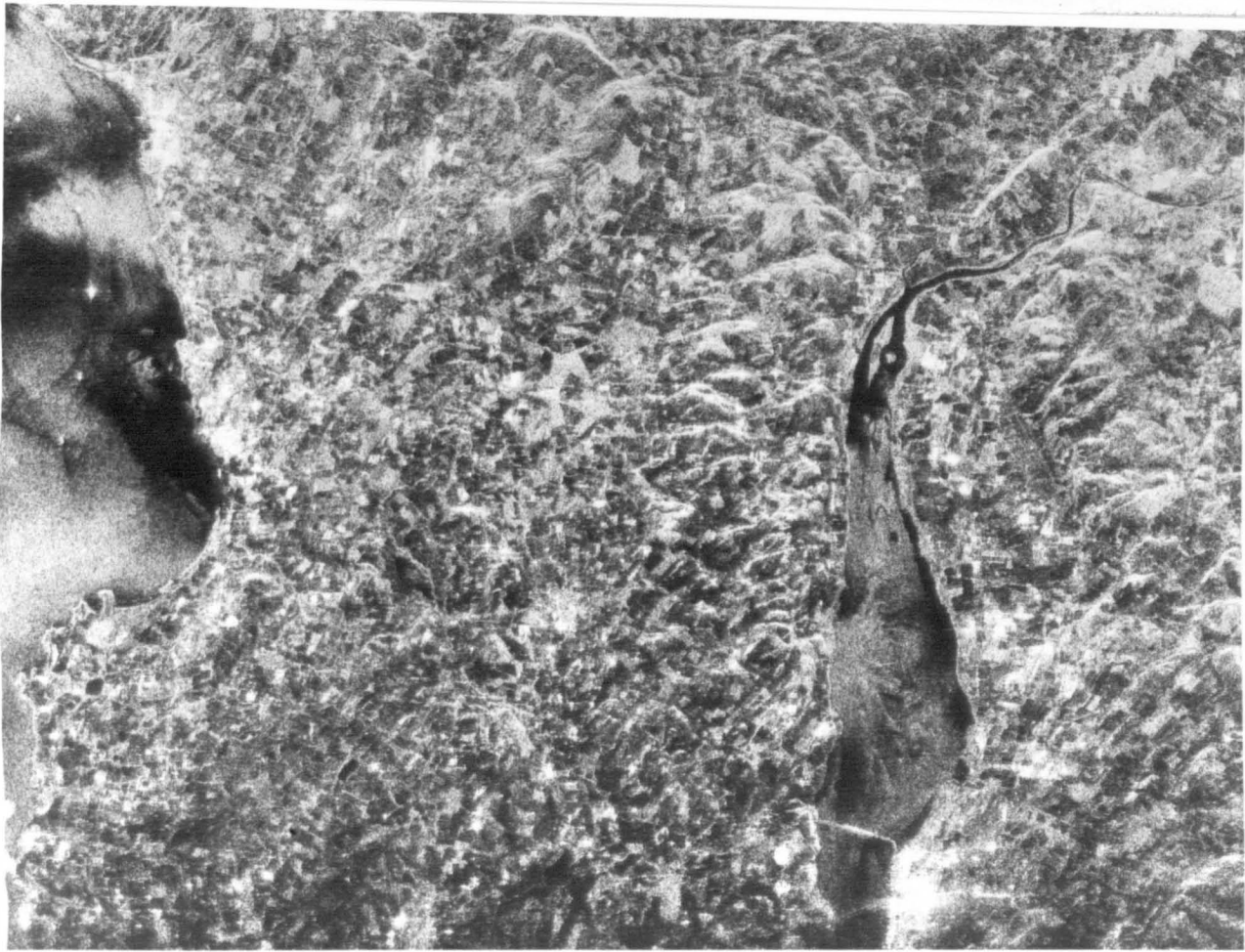


Fig 8.2 Survey optically processed image of River Tay Test Area

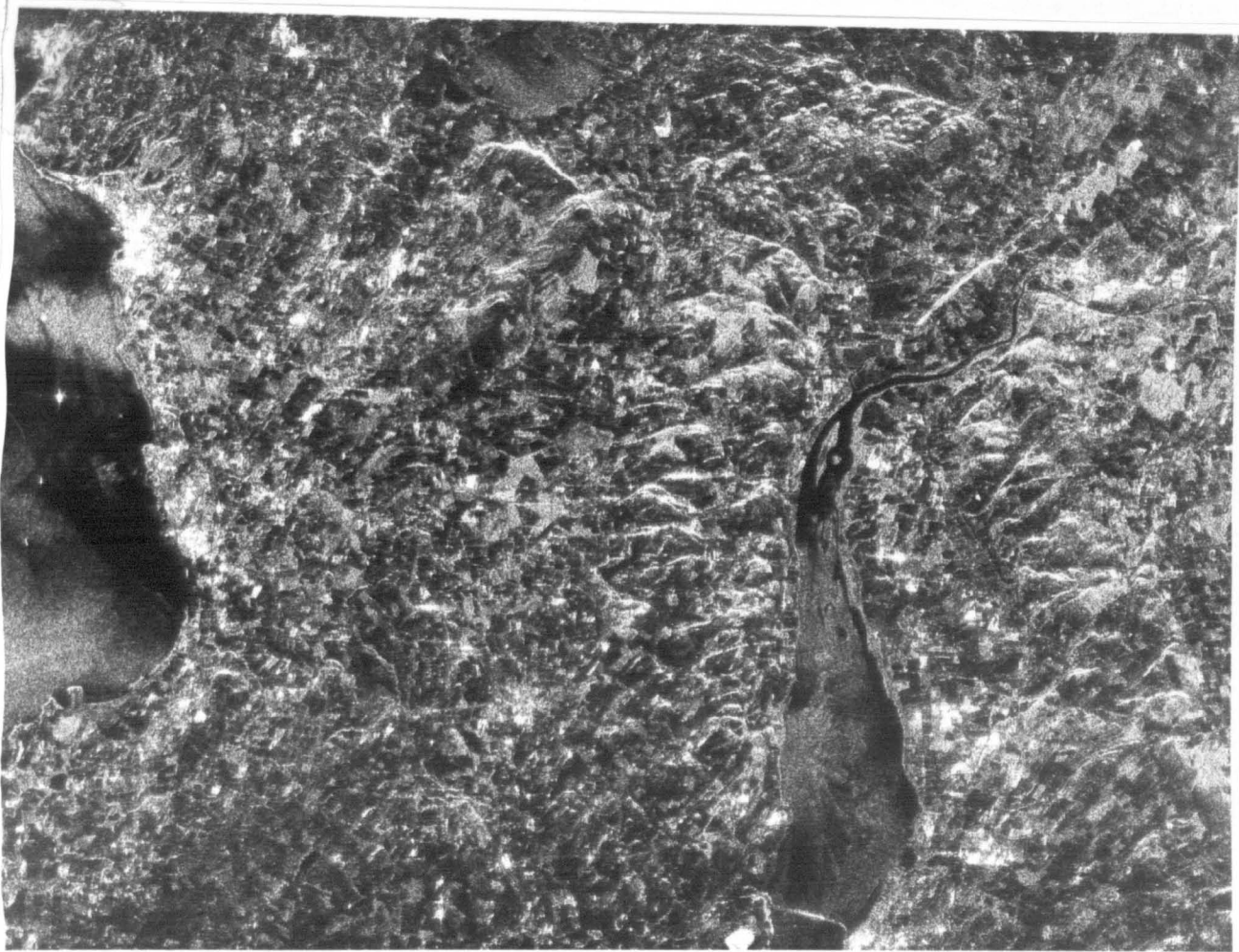


Fig 8.3 Precision optically processed image of River Tay test area

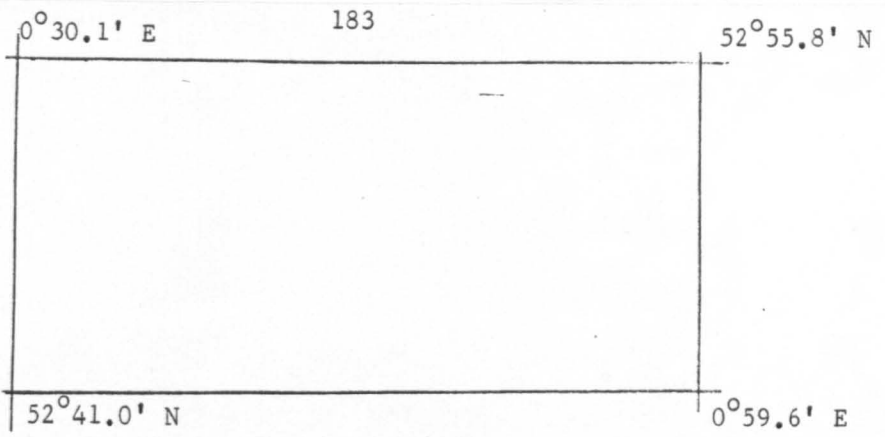
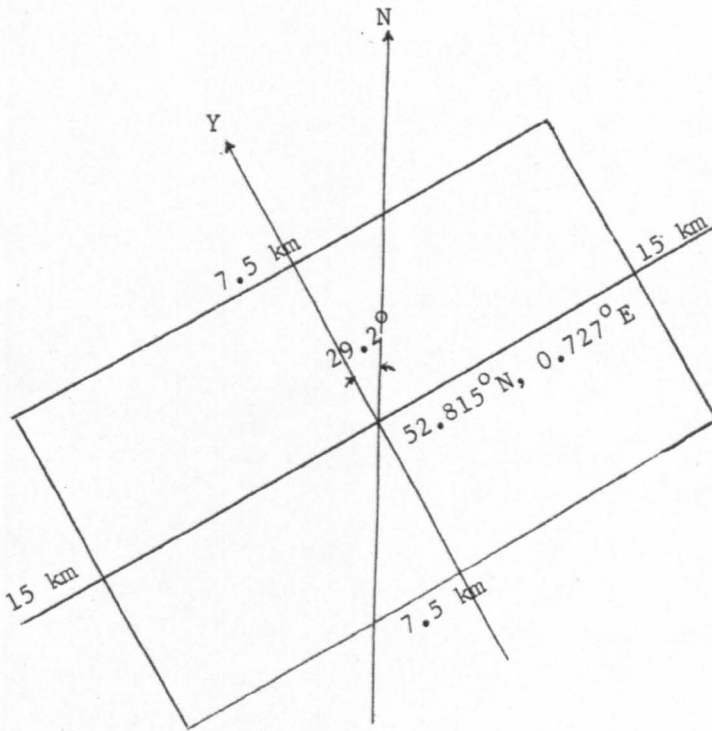


Fig 8.4a Geographic boundary of East Anglia test area



Grid origin $52.815^{\circ} N, 0.727^{\circ} E$

Grid orientation (Y-axis) -29.2 from true North

Image parameters:

Xmax. = +15 km, Xmin. = -15 km
 Ymax. = +7.5 km, Ymin. = -7.5 km
 pixel size = 12m x 12m
 Azimuth resolution = 20 m

Fig 8.4b Processing details of East Anglia SEASAT-A image
 (source RAE, Farnborough)

The image (Fig 8.5) had been processed digitally by the R.A.E. Experimental SAR Processing Facility (ESPF) as described in section 5.2.3.1 and was supplied in the form of a positive film transparency at approximately 1:150,000 scale produced by the Linoscan 204D precision raster drum plotter of R.A.E.

8.2.3 Milford Haven Test Area

The Milford Haven test area covers a 40 x 38 km area, from $04^{\circ}45.2'W$ to $05^{\circ}20.0W$ in longitude and from $51^{\circ}33.1'N$ in latitude (Fig 8.6). The area is very hilly with topography ranging from sea level to a height of around 800 m. There is relatively little developed agricultural land and few cultural features appear on the image. The image (Fig 8.7) was acquired on orbit 791 and, like the East Anglia image, it had also been processed digitally as a three-look image as part of the test program of the R.A.E. ESPF.

8.3 Selection of Ground Control Points

Many difficulties, some of them rather unexpected, were experienced in the selection of suitable control points for the tests of metric accuracy. These arise from the lack of certainty as to the exact positions of those features shown on the SAR images which were well defined on the map.

Road intersections are a natural and obvious type of feature to use in the testing of small-scale imagery. Yet they proved singularly difficult and elusive to identify with conviction and, where a number of intersections were located in a certain area, it was difficult to decide which one actually appeared on the image. Sometimes, there was a lack of resolution and contrast so that the road disappeared for a stretch. Much depended on the orientation of the road with respect

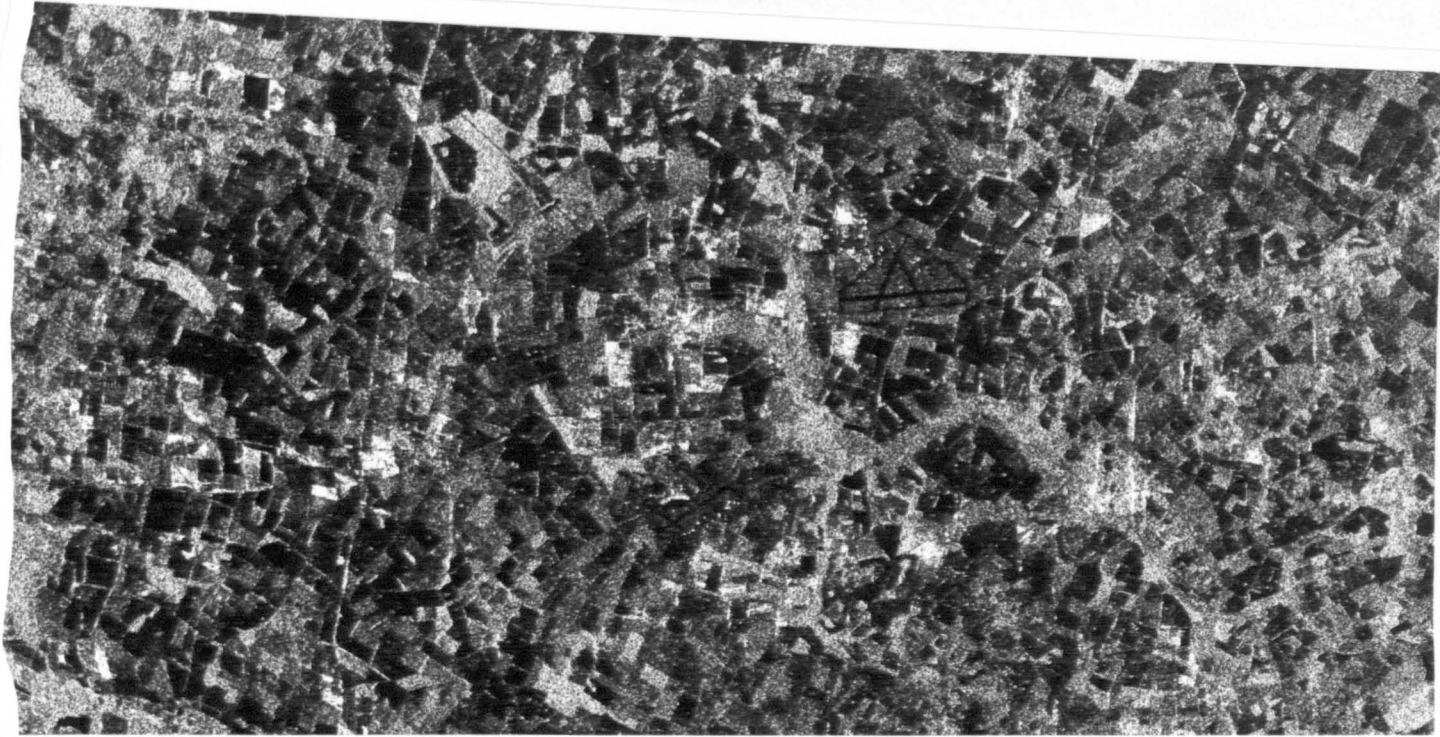


Fig 8.5 Seasat-A digitally processed image of East Anglia

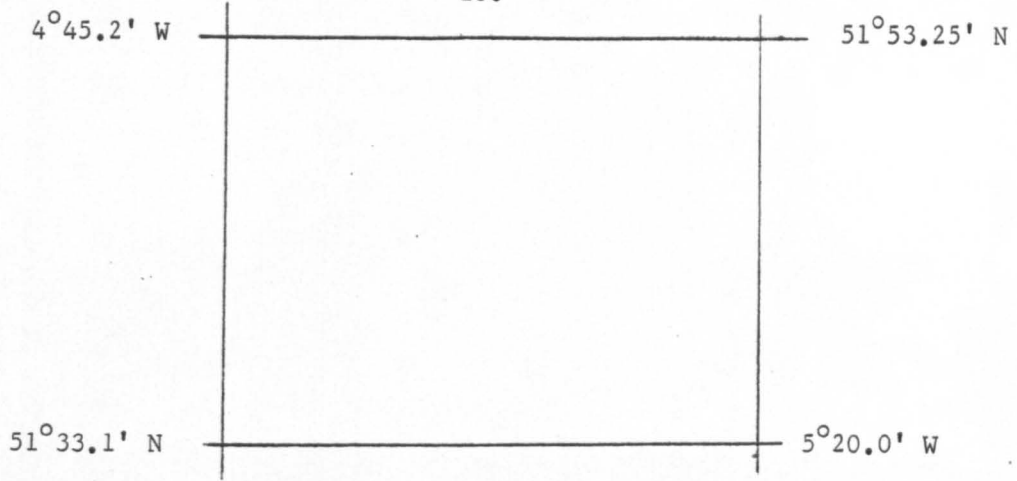
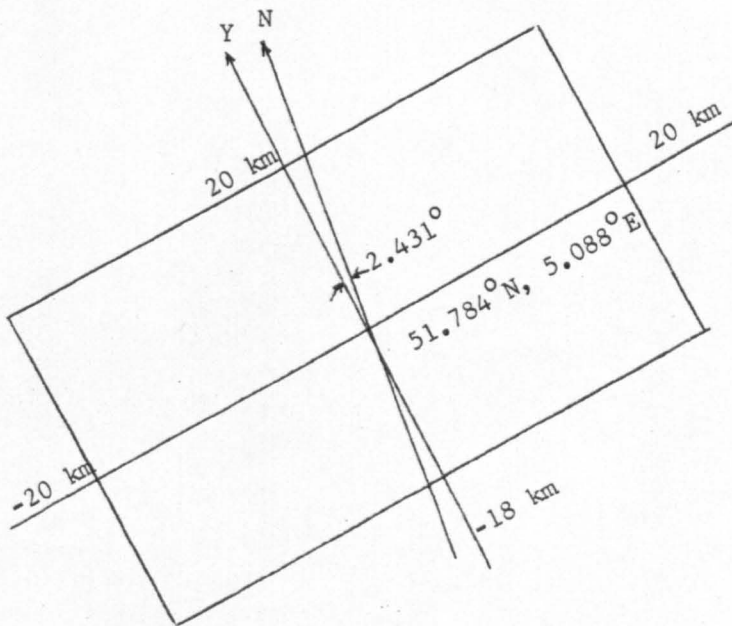


Fig 8.6a The geographic boundary of Milford Haven test area



Grid origin 51.784° N
 5.088° W

Rotation of Y-axis from true North = -2.431°

Image parameters:

Xmax. = 20 km, Xmin. = -20 km.
 Ymax. = 20 km, Ymin. = -18 km.
 pixel size = 20m x 20m

Fig 8.6b Processing details of Milford Haven SEASAT-A image
 (source RAE, Farnborough)

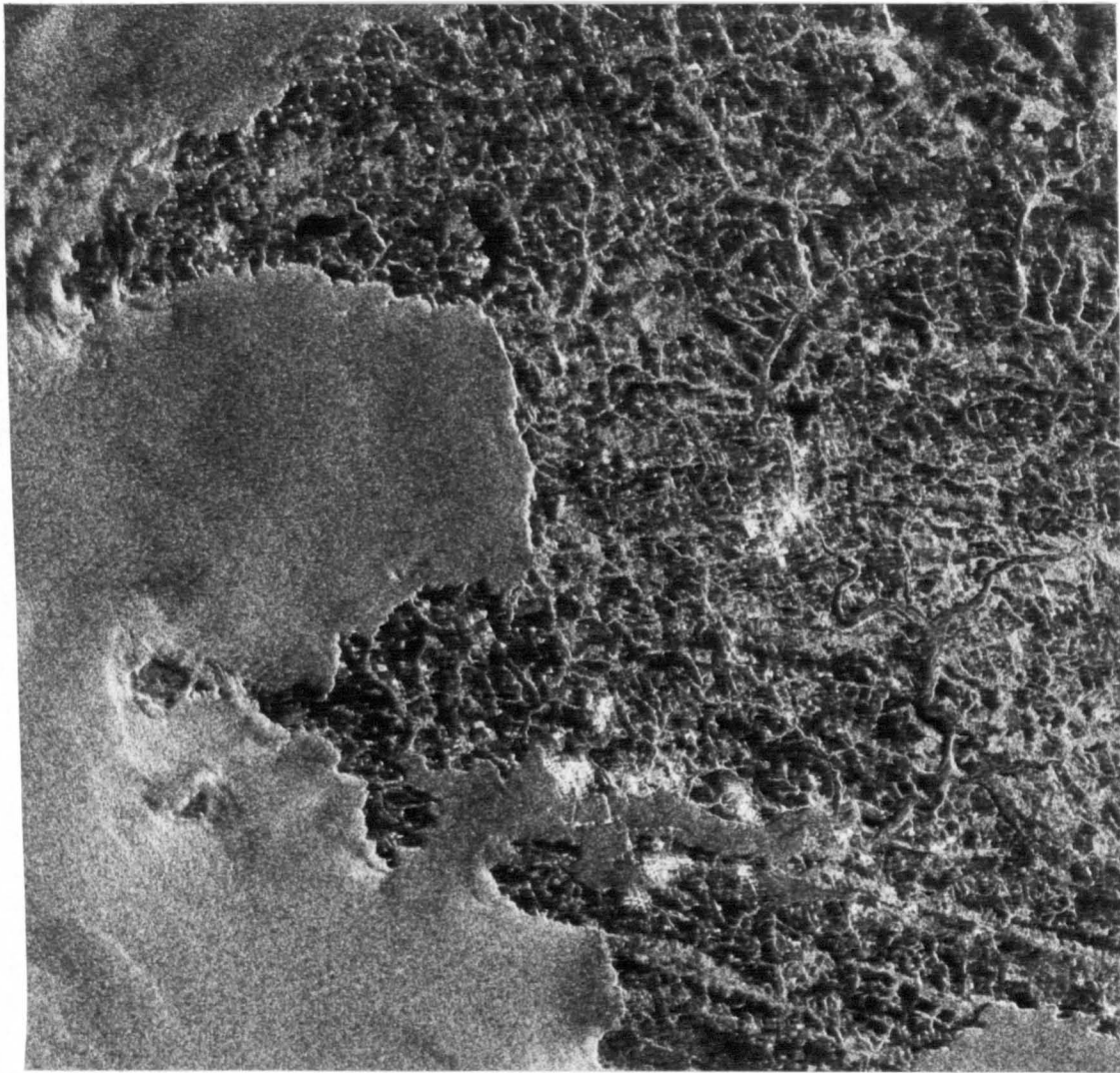


Fig 8.7 Seasat-A digitally processed image of Milford Haven test area

to the satellite track and the direction of the SAR beam. For example, rather twisting roads running transverse to the satellite track were easily confused with small streams. As a result of this experience, road intersections were avoided wherever possible and only a few definite and unambiguous examples were used.

The use of water features posed similar problems. Isolated lakes were mostly visible on the SAR imagery but their boundaries were very difficult to define exactly. Some lakes exhibited unusual characteristics due presumably to the prevailing weather conditions, especially wind, altering the back-scattering of the emitted signal. In coastal areas, sand banks often showed up prominently in an unexpected manner causing a great deal of uncertainty as to the position of the coast itself and where exactly a river enters a lake or an estuary. Rivers and streams were often ill-defined and discontinuous on the SAR image.

Wooded areas also exhibited their own special series of signatures, often confusing in nature. Sometimes, the image showed up as a very light area, indicating a strong return signal. This may be due to the type of trees, but it appears to be due also to the location and orientation of the forest with respect to the satellite antenna at the time of imaging. It would seem that, if a wood or forest lies on a slope dipping towards the antenna, a large amount of the incident microwave energy is returned. However, other wooded areas appear very dark, i.e. they exhibit little reflection. This may be due to the type of tree dominant in the forest though, sometimes, such an area was situated on a slope dipping away from the antenna.

For all these reasons, the ground control points selected for geometric testing were largely restricted to objects such as the centres

of small lakes and the corners of forests, plantations or woods. Only on rare occasions were road intersections or the junctions of two rivers used for the purpose. A further consequence of the difficulties described above was that on all images the pattern of identified ground control was sometimes rather irregular in its distribution. Within these limitations, the actual control points used on all strips were selected on the basis of being well-identified on both the SAR image and the map, reasonably well-distributed over the entire area of the image, and forming a mainly regular pattern so that the check points were located between the control points. In this way, the effects of the transformation in terms of the residual errors could be fully determined.

8.4 Measurement of Coordinates of Ground Control Points

The four areas selected for the test have plenty of topographic map coverage at a variety of scales (from 1:10,000 to 1:250,000). After preliminary inspection of the SAR images, it was decided to use medium-scale Ordnance Survey maps at 1:50,000 and 1:63,360 scale to derive terrain coordinates of the identified points. The accuracy with which coordinates could be scaled off appeared to be well in excess of that likely to be present in the Seasat SAR images. A distance of 1 mm on a map at 1:50,000 scale is equivalent to 50 metres on the ground. If the measuring accuracy on the map is 0.2 to 0.3 mm, this is equivalent to 10 to 17 metres in ground terms.

Each map was stretched out on a long smooth table with a flat surface. Each control or check point required to be coordinated is located on the map in the gross sense by the National Grid square in which it falls. By using a set square and an accurate scale (microrule), the distances in metres from each of the two grid lines to the actual

control or check point were measured and added to the grid line values. Since the actual measurements were carried out over very short distances, this procedure should minimize any possible effects of paper deformation in the actual map sheet.

8.4.1 River Tay Test Area

(i) Thirty two ground points were originally identified on the survey-processed image. Ten of these were intended for use as control points, giving a control density of approximately one point per 170 square kilometres.

(ii) On the precision-processed image, thirty six points were identified, thirteen of which were intended for use as ground control points. This gives a control density of about one point per 130 square kilometres.

8.4.2 East Anglia Test Area

By contrast with the River Tay area, it proved much easier to find suitable control and check points on the digitally processed image of East Anglia. Thus a total of 105 points were identified; thirty of these were chosen at the outset to serve as ground control points for the adjustment. This gives rise to a control density of one point per fifteen square kilometres.

8.4.3 Milford Haven Test Area

Forty seven points were identified on the digitally processed image of Milford Haven, eighteen of which were used as control points. A control density of one point per 85 square kilometres was therefore established.

The O.S. map used for the River Tay area was last revised in

1969, while those for East Anglia and Milford Haven were last revised in 1969 and 1974 respectively.

8.5 Measurement of Image Coordinates

The image coordinates of the control and check points located in all (four) test areas were measured using a Houston Hi-Pad tablet digitizer. This is an absolutely encoded digitizer with its grid positioning wires built into the tablet surface (Fig 8.8). The latter is translucent which allowed for back lighting of the SAR film transparencies over a light table. Normally, the coordinate origin can be located at any desired point on the tablet using the cursor to define it. However, in the examples used in the Department, the origin has been fixed at the bottom left corner of the active surface of the digitizer to allow all measured image coordinates to be positive. The measurements were made with the tablet in point mode, which is of course the only suitable mode for measuring the coordinates of discrete points. In this mode, measurements and recording occurs only when the cursor button is pressed. The x and y coordinates are continuously displayed on an LCD display which is connected to the output interface of the tablet.

The resolution of the instrument is of the order of 0.1 mm. To use an instrument of a higher resolution appeared to be unnecessary since the nominal best resolution of the actual images used in the experiment was of the order of 20 to 30 metres while the actual resolution was considerably poorer on the 1:250,000 scale image of the Milford Haven and River Tay areas. Thus the 0.1 mm (100 μ m) resolution of the digitizer corresponds to 25 metres on the ground which is of the same order as the very best resolution of the Seasat SAR images. Thus the use of the Hi-Pad digitizer as the image coordinate measuring device seems justified.



Fig 8.8 The Hipad Digitizer

The image coordinates of the control and check points were measured for each of the four test images using the Hi-Pad. Each point was measured twice independently and the mean calculated for each point. All the measurements were made using the 3X magnification of the instrument cursor. This magnification value seems to be an appropriate one, given the resolution and other characteristics of the Seasat SAR images.

The precision of measurement was then calculated via the differences of the observed values from the mean of the points measured. This ranged from $m_x = \pm 33 \mu\text{m}$ for the East Anglian image to $\pm 50 \mu\text{m}$ for the survey-processed River Tay image and from $m_y = \pm 36 \mu\text{m}$ for the East Anglian image to $\pm 56 \mu\text{m}$ for the precision processed River Tay image. This may be regarded as a satisfactory result considering the many problems encountered in picking out the ground control points and the actual resolution of the imagery and the accuracy of the measuring instrument.

8.6 Coordinate Transformations

Three different transformation algorithms have been used to convert the image coordinates of the measured points into the corresponding terrain values. In each case, the appropriate transformation parameters have been computed from the comparison of the image coordinates and the corresponding terrain coordinates of the control points.

(i) Linear Conformal Transformation

The first of these transformations is the simple four-term linear conformal (or similarity) transformation comprising a scale change, a rotation and two independent translations. This transformation has the form:

$$\left. \begin{aligned} N &= ax + by + c ; \text{ and} \\ E &= bx - ay + d \end{aligned} \right\} \text{----- 8.1}$$

where

- N = Northings of the point in the terrain system;
- E = Eastings of the point in the terrain system;
- x,y = measured image coordinates of the point;
- and a,b,c,d = transformation parameters.

In effect, this transformation does not change the basic relationship between image points. If the identification and measurement of the control points have been carried out well, the results obtained from this transformation show the geometric fidelity of the imagery in its original state.

This simple transformation can be applied in either of two modes. The first is to base the whole computation on the parameters obtained using two widely separated points on the SAR image. This is the minimum number of ground control points required to compute the four transformation parameters. These can then be used to compute the terrain coordinates of the remaining measured points and to determine the residual errors in the check points. This procedure has obvious limitations since any small error in measuring one of the two control points affects the values of the four parameters.

Therefore it is more sensible and usual to base the computation of the transformation parameters on a larger number of ground control points favourably distributed over the image area and to use a least squares technique to obtain their most probable values. This technique is of course more refined, since it calculates the optimum values of the transformation parameters based on a large number of control points. These parameters are then used to calculate the coordinates of the control and check points. Comparison of the known terrain coordinates

with the transformed values allows the errors to be calculated for each point. From these, the accuracy of the imagery can be determined by computing the root mean square errors (r.s.m.e. values) in the X and Y directions for both the control and check points.

The use of this transformation allows one to judge the effect of using more ground control points to cause an improvement in the accuracy of the direct image-map transformation which mathematically rectifies the image. In this way, one can establish the optimum number of control points which have to be provided for the rectification.

(ii) Affine Transformation

The second algorithm is a six-term affine transformation. Here, in addition to the two translations and the general rotation, two discrete scale factors are applied separately in the X and Y directions. Furthermore, one of the coordinate axes may be rotated by itself to account for the non-orthogonality of the axes. Certain of the obvious distortions present in SAR images such as the differential scale between the X and Y directions will be eliminated or reduced by using this particular transformation.

As employed in this series of tests, the transformation has not been uniquely programmed but is obtained by truncating the higher order terms in the polynomial transformation which will be mentioned below. In this respect it is simply the first three linear terms in both the X and Y directions. A minimum of three points is required to implement this transformation. As usual, the least squares method of adjustment may be employed to determine the parameters when more than this minimum number of points is available, as indeed is the case in this present work.

(iii) Polynomial Transformation

The third and most important transformation used in the tests is the polynomial transformation.

The actual form of polynomial employed in the tests is based on the analysis performed in Chapter Six and which resulted in the following eight-term polynomials:-

$$\left. \begin{aligned} X &= n_0 + n_1x + n_2y + n_3xy + n_4x^2 + n_5x^2y + n_6x^3 + n_7x^3y \\ Y &= m_0 + m_1x + m_2y + m_3xy + m_4x^2 + m_5x^2y + m_6x^3 + m_7x^3y \end{aligned} \right\} \dots\dots\dots 8.2$$

These equations attempt to correct further for the errors in the image left after the initial correction of systematic errors such as Earth curvature, atmospheric refraction, Earth rotation, range walk and synthetic beam pointing error applied during the image data processing. As in the previous two transformations, the parameters are determined from a large number of ground control points using the least squares adjustment technique.

8.7 Computer Programs

A large amount of repetitive computation work is involved in the test procedures described above - in the determination of the transformation parameters; the transformation of all the measured image points into the terrain coordinate system; the computation of the residual errors and their statistical analysis; the plotting of these errors in graphical form; etc. Since this had to be carried out using the three different transformations for each of the four test areas, the sheer volume of processing demanded the use of computer techniques. Since no suitable programs were available in the Department, these had to be written by the present author. These took a considerable time to write, de-bug and test.

These transformation programs were:-

- (i) LINCON, which employed the simple linear conformal transformation described above, including a version which allowed the implementation of the least squares technique when more than the minimum number of control points were available; and
- (ii) POLY, which was based on the polynomial transformation technique discussed above. Again this was implemented using the least squares adjustment technique.

Both of these programs were written in BASIC and implemented on the large ICL 2976 mainframe computer of the University of Glasgow. This machine has a very large (4 megabyte) core store and operates under the standard VME/B operating system. The machine can be accessed using VDU or teletype terminals located in the Department or in the University Computer Centre.

An additional program, PLOTIR, was written to allow the plotting of the vector errors in position at control and check points after transformation to provide a graphical representation of these errors. This program was written in FORTRAN IV in order to make use of the standard plotting routines of the GHOST graphics package available on the ICL 2976 machine. The actual plotting was carried out on the CIL Economist 2 plotter available in the University Computer Centre.

8.8 Description of the Computer Programs

8.8.1 Program LINCON

8.8.1.1 Definition of Variables

- D0 Planimetric errors in the control points;
- D1 Planimetric errors in the check points;
- D2,D3 RMSEs in Northings and Eastings respectively at the check points;

- D6,D7 RMSEs in Northings and Eastings at the control points;
- DEFFN A BASIC language statement for defining a variable function;
- I(k,1) Residual errors in the check points in the X-direction;
- T1 Matrix of the designation numbers of check points;
- T2 Residual errors in the check points in the Y-direction;
- U(n,1) Residual errors in Northings in the control points after transformation;
- X,Y Northings and Eastings respectively;
- Z2 Residual errors in Eastings in the control points after transformation.

8.8.1.2 Definition of Arrays

The same letters have been employed in these definitions as have been used in the explanation of least squares adjustment procedures given in Appendix "A".

- A Coefficient matrix of transformation parameters for control points;
- B Transpose matrix of $A (= A^T)$;
- C Matrix of transformation parameters to allow conversion from image to map coordinate system;
- F Matrix used in the least squares adjustment procedure (please see Appendix "A":- $F = A^T G^{-1} L \dots \dots \dots A.7)$);
- G Cofactor matrix, equal to unity in this case;
- H Coefficient matrix of transformation parameters for check points (equivalent to matrix A in this case);
- I Matrix of residual errors at the check points;
- J The matrix formed by the product $H * C$;
- L Array of the ground coordinates of the control points;
- M The matrix formed by N inversed;

- N Matrix used in the least squares adjustment procedure (please see Appendix "A": $N = A^T G^{-1} A \dots \dots A.7$);
- P Vector matrix for the designation numbers of the check points;
- Q Vector matrix for the designation numbers of the control points;
- T The matrix of the ground coordinates of the check points;
- W The matrix formed by the product $A * C$ equal to the array of transformed ground coordinates of the control points.

8.8.1.3 Explanation of Program LINCON

The program is listed in Fig 8.9. As indicated in the listing, the program has been broken up into a number of blocks to assist the explanation of the sequence of operations carried out by the program.

Block 1. In this first block, the arrays required for input data are dimensioned.

Block 2. The input array A (m,4) comprises the coordinates of the control points which act as the coefficients of the unknown transformation parameters. The first and second columns of this array are the image coordinate values, while the third and fourth columns are the coefficients of the two translations, i.e. either 1 or 0. This data is input by the operator in sequential order:- x - coordinate; y - coordinate; 1 ; 0 (or 0, 1 as the case may be) using the computer terminal. Any error in the input data can be edited using the terminal before computation begins. Once this data has been entered and checked, the program reads in the input array A, transposes it to form array B ($=A^T$) and then computes array N ($= A^T G^{-1} A$) which is needed for the least squares adjustment. It then inverses N to obtain array M ($=N^{-1}$) needed for the computation of the transformation parameters.

PULLOUTS

```
000110 REM THIS IS PROGRAM LINCON FOR TRANSFORMING RADAR IMAGE TO TERRAIN
(0002)110 REM USING THE ALGORITHM OF LINEAR CONFORMAL TRANSFORMATION
(0003)120 MAT A
(0004)20 MAT B
(0005)25 MAT C
(0006)40 REM A(56,1),B(4,56),L(56,1),C(4,1),N(4,4),M(4,4),U(56,1),U(56,1)
(0007)50 REM F(4,1),G(142,4),T(142,1),J(142,1),I(142,1),Q(28,1),P(71,1)
(0008)60 REM THIS PROGRAM SOLVES THE SYSTEM OF OBSERVATION EQNS BY
(0009)70 REM BY THE LEAST SQUARES TECHNIQUE IE SOLVING THE SYSTEM
(0010)80 REM V=A*X-L WHERE X IS THE MATRIX OF THE UNKNOWN
(0011)90 MAT READ A
(0012)100 REM A IS THE MATRIX OF COEFFICIENTS OF THE TRANSFORMATION PARAMETERS
(0013)105 REM FOR CONTROL POINTS
(0014)270 MAT B=TRN(A)
(0015)280 REM B IS THE TRANSPOSE MATRIX OF A
(0016)290 MAT N=B*A
(0017)300 MAT M=INV(N)
(0018)310 MAT READ L
(0019)320 REM L IS THE MATRIX OF CONTROL POINTS X COORDS IN METRES
(0020) 450 MAT F=B*M
CONTINUE(Y OR N)?
```

(1)

```
(0021) 460 REM COMPUTATION OF UNKNOWN TRANSFORMATION PARAMETERS BEGINS
(0022) 470 MAT C=M*F
(0023) 480 REM C IS THE MATRIX OF TRANSFORMATION PARAMETERS FROM IMAGE TO MAP
(0024)485 PRINT"VECTOR MATRIX C OF TRANSFORMATION PARAMETERS FROM IMAGE TO TERRA
IN"
(0025)500 PRINT
(0026)505 PRINT
(0027)505 MAT PRINT C
(0028)520 MAT READ H
(0029)530 REM H IS THE MATRIX OF COEFFICIENTS OF TRANSFORMATION PARAMETERS
(0030)535 REM FOR CHECK POINTS
(0031)920 MAT J=H*C
(0032)930 MAT READ T
(0033)940 REM T IS THE MATRIX OF CHECK POINTS MAP COORDS
(0034)1160 REM COMPUTATION OF CHECK POINTS RESIDUALS BEGINS
(0035)1170 MAT I=J-T
(0036)1180 REM I IS THE MATRIX OF RESIDUALS IN CHECK POINTS
(0037)1190 MAT W=A*C
(0038)1210 MAT U=W-L
(0039)1220 REM U IS MATRIX OF RESIDUALS IN CONTROL POINTS
(0040)1250 PRINT"PT NO","N(N)","E(N)","DN(N)","DE(N)","DO(N)"
CONTINUE(Y OR N)?
```

(2)

(3)

(4)

```
(0041)1253 PRINT
(0042)1255 REM DO IS THE RESIDUAL PLANIMETRIC ERROR IN CONTROL POINTS
(0043)1260 MAT READ P
(0044)1270 REM P IS THE MATRIX OF CHECK POINTS DESIGNATION NUMBERS
(0045)1340 MAT READ Q
(0046)1350 REM Q IS THE MATRIX OF CONTROL POINTS DESIGNATION NUMBERS
(0047)1380 PRINT"ACCURACY OF CONTROL POINTS"
(0048)1385 PRINT
(0049)1390 PRINT
(0050)1400 FOR N=1 TO N1 STEP 2
(0051)1410 Z1=Q(FNY(N),1)
(0052)1420 DEFFNY(N)=(N+1)/2
(0053)1422 Z3=L(FNW(N),1)
(0054)1425 DEFFNW(N)=N+1
(0055)1430 Z2=U(FND(N),1)
(0056) 1440 DEFFND(N)=N+1
(0057)1444 D0=SQR(U(N,1)**2+Z2**2)
(0058)1450 PRINT Z1,L(N,1),Z3,U(N,1),Z2,INT(D0+.50)
(0059)1460 NEXT N
(0060)1470 REM RMSE OF CONTROL POINTS
CONTINUE(Y OR N)?
```

(5)

(6)

```
(0061)1480 S4=0
(0062)1490 S5=0
(0063)1510 FOR L=1 TO N1 STEP 2
(0064)1520 A1=U(FNR(L),1)
(0065)1530 DEFFNR(L)=L+1
(0066)1540 S4=S4+ABS(U(L,1))
(0067)1550 S5=S5+ABS(A1)
(0068)1560 NEXT L
(0069)1570 M4=S4/(N1/2)
(0070)1580 M5=S5/(N1/2)
(0071)1590 PRINT"MEAN IN METRES IN X COORDS RESIDUALS=";M4
(0072)1600
(0073)1610 PRINT"MEAN IN METRES OF Y COORDS RESIDUALS=";M5
(0074)1620 S6=0
(0075)1630 S7=0
(0076)1650 FOR B=1 TO N1 STEP 2
(0077)1660 A2=U(FNT(B),1)
(0078)1670 DEFFNT(B)=B+1
(0079)1680 W2=(M4-ABS(U(B,1)))**2
(0080)1690 W5=(M5-ABS(A2))**2
CONTINUE(Y OR N)?
```

(7)

```
(0081)1700 S6=S6+W2
(0082)1710 S7=S7+W5
(0083)1720 NEXT B
(0084)1725 N3=((N1/2)-2)
(0085)1730 D6=SQR(S6/N3)
(0086)1740 D7=SQR(S7/N3)
(0087) 1750 PRINT"RMSE IN X COORDS OF CONTROL POINTS=";D6
(0088)1760
```

(8)

```
(0089)1770 PRINT"RMSE IN Y COORDS OF CONTROL POINTS=";D7
(0090)1780 PRINT
(0091)1785 PRINT
(0092)1788 PRINT
(0093)1790 PRINT"ACCURACY OF CHECK POINTS"
(0094)1820 PRINT"PT NO","N(N)","E(N)","DN(N)","DE(N)","DI(N)"
(0095) 1830 FOR K=1 TO N2 STEP 2
(0096)1840 T1=P(FNC(K),1)
(0097)1850 DEFFNC(K)=(K+1)/2
(0098)1855 T4=T(FNV(K),1)
(0099)1857 DEFFNV(K)=K+1
(0100)1860 T2=I(FNS(K),1)
CONTINUE(Y OR N)?
```

(9)

(10)

```
(0101)1870 DEFFNS(K)=K+1
(0102) 1880 D1=SQR(T2**2+I(K,1)**2)
(0103)1890 PRINT T1,T(K,1),T4,I(K,1),T2,INT(D1+.50)
(0104)1900 NEXT K
(0105)1910 REM COMPUTATION OF RMSE
(0106)1920 S1=0
(0107)1930 S2=0
(0108) 1950 FOR L=1 TO N2 STEP 2
(0109)1960 T3=I(FNZ(L),1)
(0110)1970 DEFFNZ(L)=L+1
(0111)1980 S1=S1+ABS(I(L,1))
(0112)1990 S2=S2+ABS(T3)
(0113)2000 NEXT L
(0114)2005 N6=N2/2
(0115)2010 M1=S1/N6
(0116)2020 M2=S2/N6
(0117) 2030 PRINT"MEAN IN X COORDS RESIDUALS=";M1
(0118)2040
(0119)2050 PRINT"MEAN IN Y COORDS RESIDUALS=";M2
(0120)2060 S3=0
CONTINUE(Y OR N)?
```

(11)

```
(0121)2070 S4=0
(0122)2090 FOR U=1 TO N2 STEP 2
(0123)2100 T4=I(FNG(U),1)
(0124)2110 DEFFNG(U)=U+1
(0125)2120 W3=(M1-ABS(I(U,1)))**2
(0126)2130 W4=(M2-ABS(T4))**2
(0127)2140 S3=S3+W3
(0128)2150 S4=S4+W4
(0129)2160 NEXT U
(0130)2170 D2=SQR(S3/N6)
(0131)2180 D3=SQR(S4/N6)
(0132)2190 PRINT"RMSE IN X COORDINATES=";D2
(0133)2200
(0134)2210 PRINT"RMSE IN Y COORDINATES=";D3
(0135)2220 END
(0136)**END**
```

Next, the operator inputs in sequential order the coordinates (Northing followed by Easting) of each of the control points used for the determination of the transformation parameters. This forms the input array L (m,1) used to compute array $F (= A^T G^{-1} L)$. The transformation parameters are then computed and stored in array C.

Block 3. The operator next enters the image coordinates of the check points in the form:- x - coordinate; y - coordinate; 1 ; 0 (or 0, 1) in the same manner as was done for the input array A in Block 2. This data forms the input array H (n,1) which comprises the coefficients of the transformation parameters required to compute the coordinates of the check points. Array J which comprises the ground coordinates of the check points is then obtained by multiplying array H by array C containing the transformation parameters already obtained in Block 2.

Next, the operator enters the given ground coordinates of the check points in the order Northing followed by Easting to form the input array T (n,1) which is then read into the computer memory and subtracted from array J containing the transformed image coordinates of the same points to give the values of the residual errors in the check points. These are stored in array I. Similarly, the residual errors in the control points themselves are computed by subtraction of array H from array W, the results being stored in array U.

Block 4. This prints out the words "Point Number"; "N(m)" which is the Northings in metres of a control point; "E(m)", which is the Easting of a control point; "DX in metres", which is the residual error in the Northings of a control point; "DY in metres", which is the residual error in the Eastings of a control point; and "Do in metres", which is the vector error in planimetry. All of these headings are set out in tabular form under which the actual numerical values of the residual errors will be listed.

Block 5. The operator first enters the designation numbers of the check points and the control points which comprise the input arrays P and Q respectively. Once formed, these two arrays are stored in the computer memory.

Block 6. In this block, the number of each control point from array Q above is printed out, followed by its Northings in metres, its Eastings in metres, its residual errors in Northings, Eastings and planimetry in the tabular form already set out in Block 4 above.

Block 7. Next, the root mean square errors (RMSE) of the residual errors in the control points are computed.

Block 8. In this block, the headings to be used for the listings of the RMSEs in the X and Y directions for the control points are printed out.

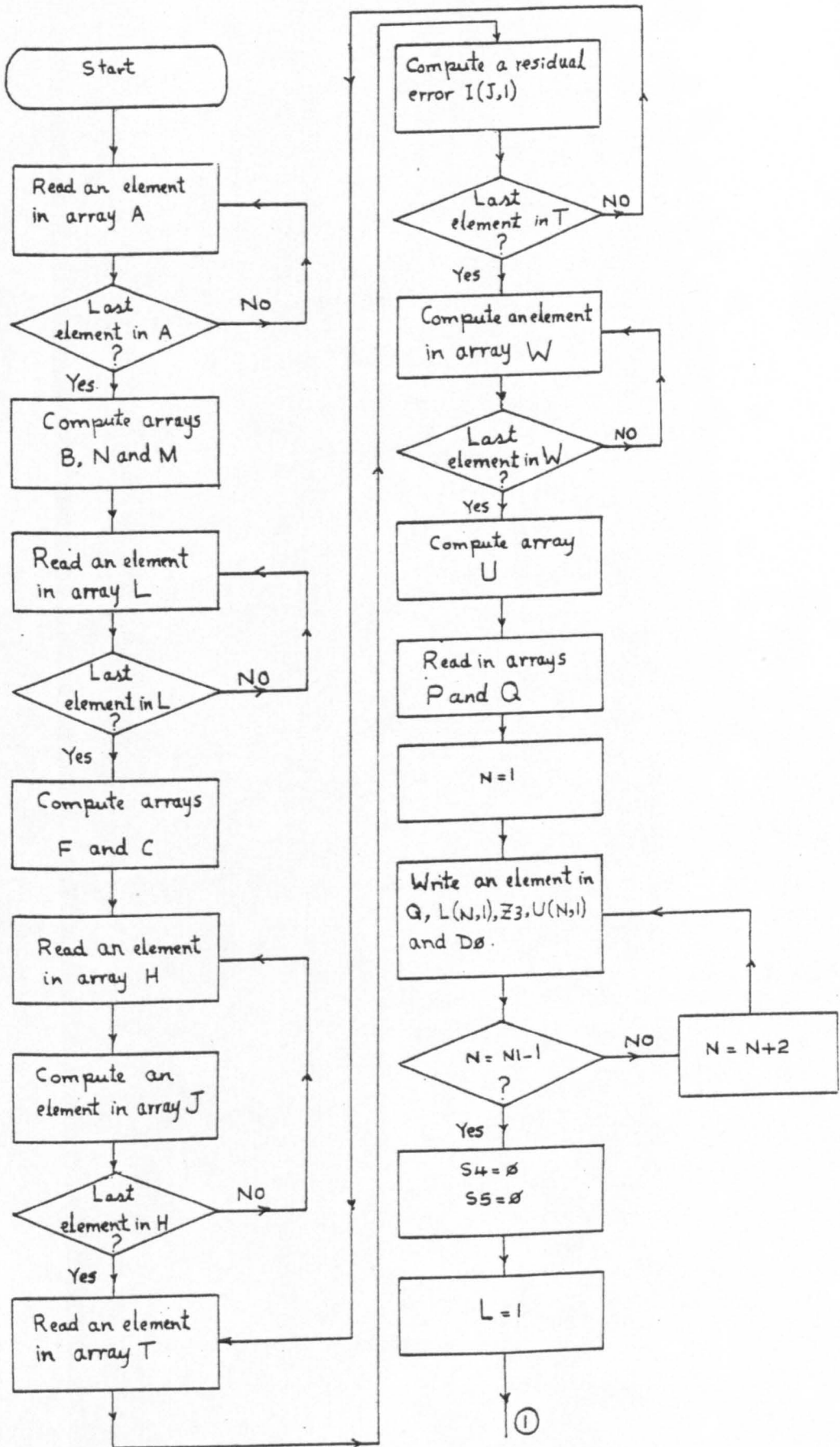
Block 9. This short block simply prints the headings for the table showing the residual errors in the individual check points in the same manner as has been done for the control points in Block 4.

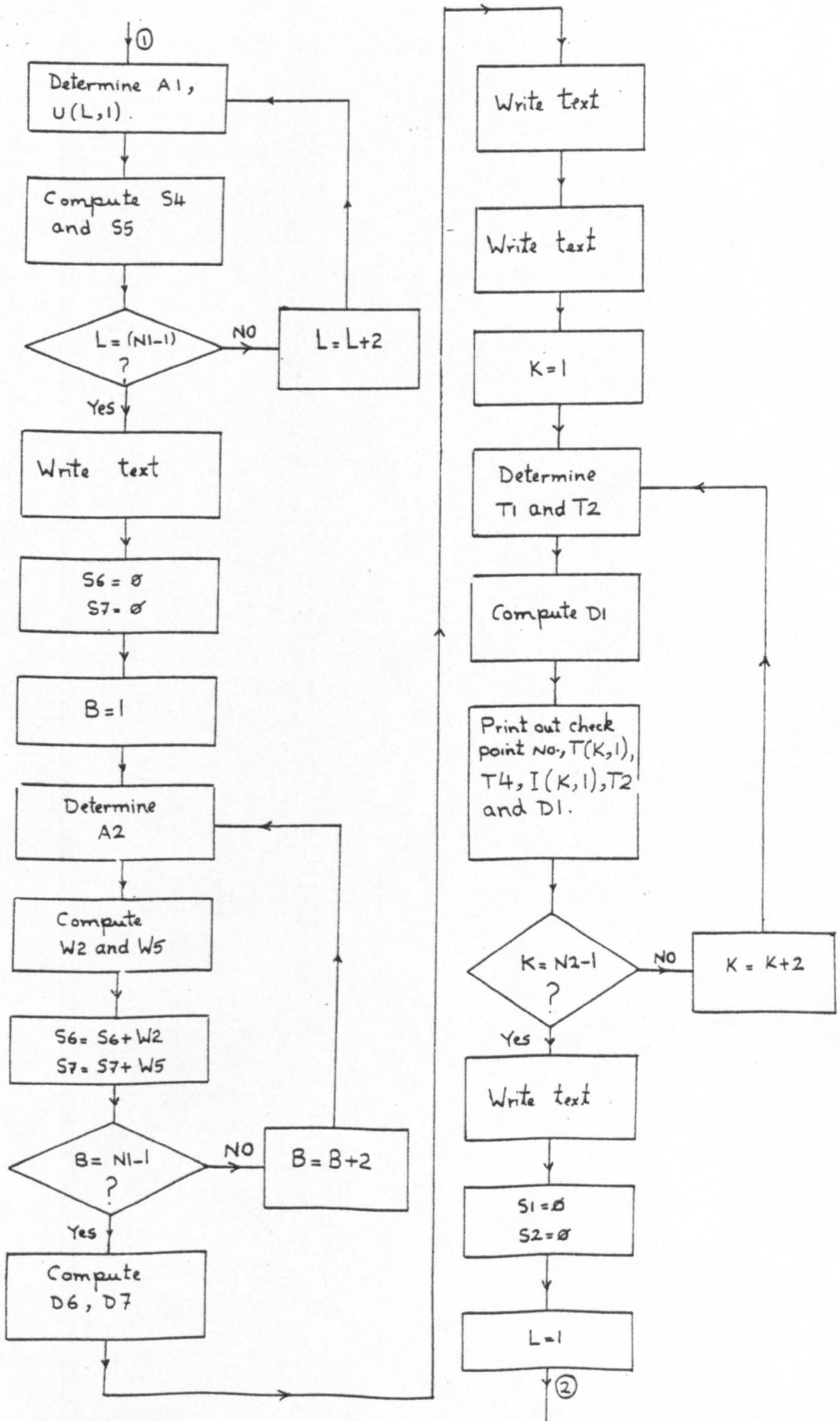
Block 10. This particular block writes out the individual residual errors in the coordinates of the check points.

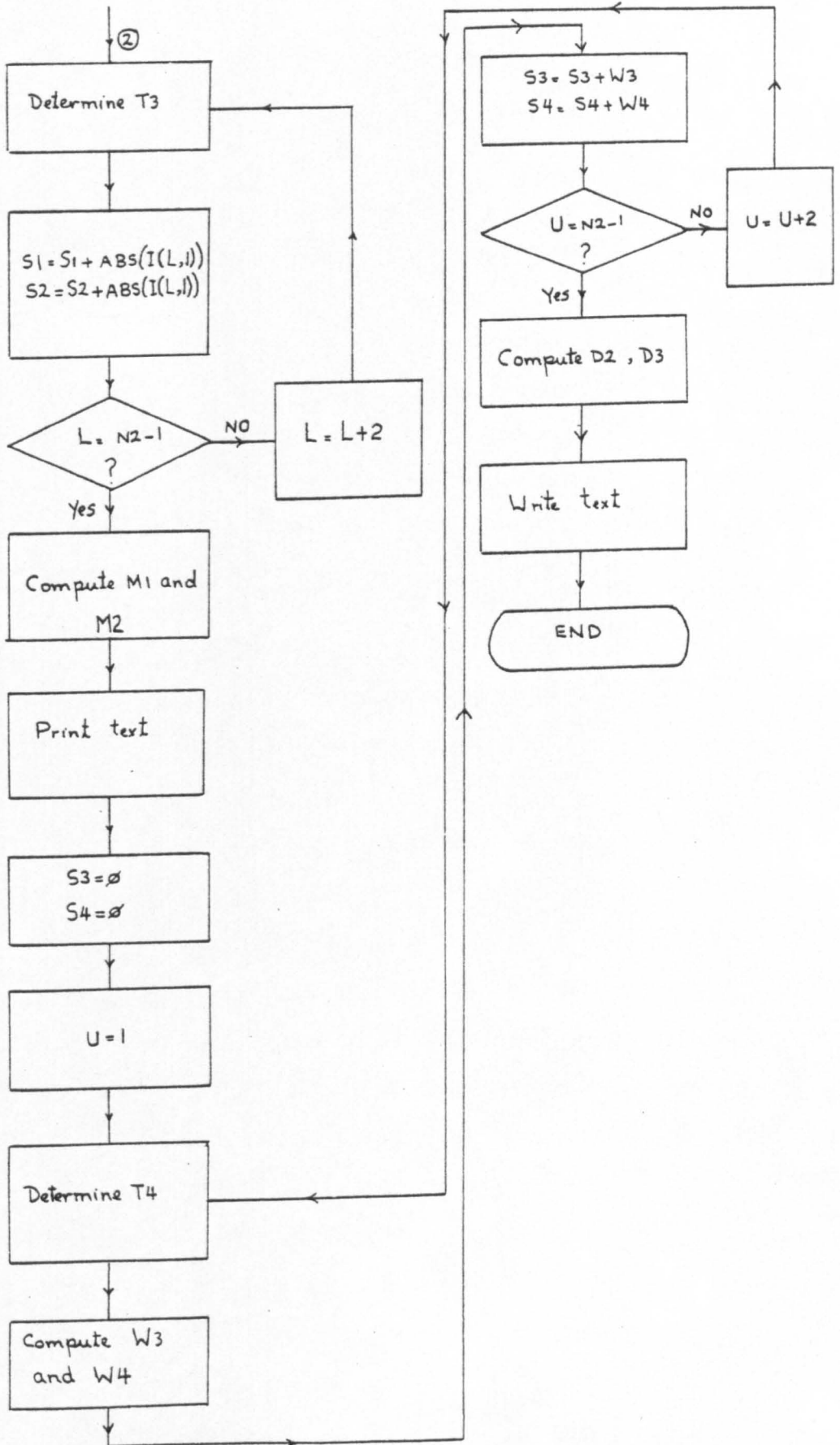
Block 11. Finally, this block computes the RMSEs in the X and Y directions and in planimetry for all the check points and prints them out in the same manner as was carried out for the control points in Blocks 7 and 8 above.

8.8.1.5. Detailed explanation of the Program

<u>Statement No.</u>	<u>Comments</u>
10 and 15	Name of Program.
20 and 25	Number of coordinate values for control points (N_1) and check points (N_2) respectively.
40 and 50	Dimensions of arrays.
60 - 80	Purpose of the program.







<u>Statement No.</u>	<u>Comments</u>
90	Read array A.
100 and 105	Explain array A.
110 - 250	Input data for array A.
270	Transpose array A to obtain array B.
280	Explain array B.
290	Multiply array B by array A to obtain array N.
300	Inverse array N to obtain array M.
310	Read input array L.
320	Explain array L.
350 - 440	Input data of array L.
450	Compute array F by multiplying array B by array L.
470	Multiply array M by array F to get array C.
510	Print out transformation matrix C.
520	Read data for input array H.
540 - 890	Input data for array H.
920	Obtain array J by multiplying array H by array C.
930	Read data for input array T.
950 - 1130	Input data for array T.
1170	Compute array of residual errors in the check points by subtracting array T from array J.
1190 - 1210	Compute array W from which array U of residual errors in control points can be obtained by subtracting array L from array W.
1250 - 1255	Print text as shown to prepare for the table of residual errors in the control points.
1260	Read input array P.
1270	Explain array P.

<u>Statement No.</u>	<u>Comments</u>
1280 - 1310	Input data for array P.
1340	Read input array Q.
1350	Explain array Q.
1360 - 1370	Input data for array Q.
1400 - 1460	Print out the individual control point number and its residual errors in the X- and Y-directions and the resulting planimetric error.
1470 - 1740	Compute mean errors and RMSEs for the control points.
1750 - 1770	Print out the RMSEs in Northings and Eastings for the control points.
1790 - 1820	Print headers for the table of the residual errors in the individual check points.
1830 - 1900	Print out the residual errors in the check points.
1910 - 2180	Compute the mean errors and RMSEs in Northings and Eastings of the check points.
2190 - 2210	Print out the values of the RMSEs for check points.

8.8.1.6 Program and Sample Input and Output Listings

Fig 8.9 is the actual listing of the program LINCON while a sample of input data to the program is given in Fig 8.10 with the corresponding output data in Fig 8.11.

8.8.2 Program POLY

This program was written in such a manner that the x-coordinates and y-coordinates were computed and transformed as two quite separate operations (originally termed X-POLY and Y-POLY). This solution was adopted with the idea that various alternative polynomials could be used for the correction of the y (cross-track) coordinates. In fact

PULLOUTS

MEASURED IMAGE COORDINATES OF CONTROL POINTS				
PT NO	X(MM)	Y(MM)	COEFF. OF C	COEFF. OF D
3	64	18.5	1	0
	-18.5	64	0	1
4	35.8	31	1	0
	-31	35.8	0	1
8	120.1	33.6	1	0
	-33.6	120.1	0	1
12	24.8	33.1	1	0
	-33.1	24.8	0	1
13	21.4	61.7	1	0
	-61.7	21.4	0	1
15	20.3	15.3	1	0
	-15.3	20.3	0	1
PRESS RETURN TO CONTINUE				
17	29.2	5	1	0
	-5	29.2	0	1
18	5.6	0.93	1	0
	-0.93	5.6	0	1
21	53.6	7.9	1	0
	-7.9	53.6	0	1
27	88.7	1.7	1	0
	-1.7	88.7	0	1
29	119.4	11.5	1	0
	-11.5	119.4	0	1
30	169.6	17.5	1	0
	-17.5	169.6	0	1
35	73.3	49.8	1	0
	-49.8	73.3	0	1
37	56.8	86.9	1	0
	-86.9	56.8	0	1
38	182.1	71.1	1	0
	-71.1	182.1	0	1
40	73	84.4	1	0
PRESS RETURN TO CONTINUE				

211

49	-84.4	73	0	1
	90	86.4	1	0
	-86.4	90	0	1
54	105.6	80.6	1	0
	-80.6	105.6	0	1
57	108	98.8	1	0
	-98.8	108	0	1
59	118.1	63.8	1	0
	-63.8	118.1	0	1
64	141.9	63.3	1	0
	-63.3	141.9	0	1
69	148.5	80.7	1	0
	-80.7	148.5	0	1
71	152.1	96.3	1	0
	-96.3	152.1	0	1
72	156.9	97	1	0
	-97	156.9	0	1
82	3	98	1	0
	-98	3	0	1
PRESS RETURN TO CONTINUE				
84	42.2	96.5	1	0
	-96.5	42.2	0	1
86	42.6	59.7	1	0
	-59.7	42.6	0	1
99	26.8	6.9	1	0
	-6.9	26.8	0	1

212

GROUND COORDINATES OF THE CONTROL POINTS

PT NO	NORTHINGS	EASTINGS
3	320526	582000
4	319890	577418
8	326729	587919
12	319285	575789
13	322691	573253
15	316760	576729
17	316146	578659
18	313446	575792
PRESS RETURN TO CONTINUE		
21	318377	581497
27	320279	586425
29	323855	589507
30	328507	595380
35	325190	580836
37	328523	575855
38	336336	592824
40	329539	578101
49	331120	580032
54	331577	582475
57	334051	581339
59	330396	585292
64	332190	588425
69	334912	587893
71	337158	587108
72	337596	587678
82	325788	568040
84	328725	573275
86	324100	576185
PRESS RETURN TO CONTINUE		
99	316170	578210

MEASURED IMAGE COORDINATES OF THE CHECK POINTS

PT NO	X(MM)	Y(MM)	COEFF. OF C	COEFF. OF D
1	36.2	27.7	1	0
	-27.7	36.2	0	1
2	41.8	23.6	1	0
	-23.6	41.8	0	1
5	177.5	74.3	1	0
	-74.3	177.5	0	1
6	179	70.9	1	0
	-70.9	179	0	1
7	160.7	23.9	1	0
	-23.9	160.7	0	1
9	163.5	16.6	1	0
	-16.6	163.5	0	1
10	27.8	32.1	1	0
PRESS RETURN TO CONTINUE				
11	-32.1	27.8	0	1
	31.1	23.8	1	0
	-23.8	31.1	0	1
14	24.9	28.2	1	0
	-28.2	24.9	0	1
16	29.1	12.2	1	0
	-12.2	29.1	0	1
19	63.5	11	1	0
	-11	63.5	0	1
20	62.6	13.8	1	0
	-13.8	62.6	0	1
22	46.6	12.1	1	0
	-12.1	46.6	0	1
23	47.3	19.4	1	0
	-19.4	47.3	0	1
24	75.4	10.1	1	0
	-10.1	75.4	0	1
25	75	4.7	1	0
	-4.7	75	0	1
PRESS RETURN TO CONTINUE				
26	80.6	6.2	1	0
	-6.2	80.6	0	1
28	111.3	12.4	1	0
	-12.4	111.3	0	1
31	101.4	36.3	1	0
	-36.3	101.4	0	1
32	93.9	30.8	1	0
	-30.8	93.9	0	1
33	85	34.6	1	0
	-34.6	85	0	1
34	68.8	42	1	0
	-42	68.8	0	1
36	60.8	83	1	0
	-83	60.8	0	1
39	65.1	88.6	1	0
	-88.6	65.1	0	1
41	68.5	83.3	1	0
	-83.3	68.5	0	1
42	69.6	91.2	1	0
PRESS RETURN TO CONTINUE				
43	-91.2	69.6	0	1
	79.9	98	1	0
	-98	79.9	0	1
44	77.7	91.8	1	0
	-91.8	77.7	0	1
45	80.4	88.4	1	0
	-88.4	80.4	0	1
46	82.9	86.1	1	0
	-86.1	82.9	0	1
47	87.6	81.6	1	0
	-81.6	87.6	0	1
48	92.3	83.2	1	0
	-83.2	92.3	0	1
50	96.4	87	1	0
	-87	96.4	0	1
52	99.9	80.2	1	0
	-80.2	99.9	0	1
53	103.6	80.9	1	0
	-80.9	103.6	0	1
PRESS RETURN TO CONTINUE				
55	104.3	86.5	1	0
	-86.5	104.3	0	1
56	101.1	95.8	1	0
	-95.8	101.1	0	1
58	111.6	90.9	1	0
	-90.9	111.6	0	1
60	123.1	64.3	1	0
	-64.3	123.1	0	1
61	128.6	65	1	0
	-65	128.6	0	1
62	126.7	73.2	1	0
	-73.2	126.7	0	1

213

214

13	31.1	23.8	1	0
	-23.8	31.1	0	1
14	24.9	28.2	1	0
	-28.2	24.9	0	1
16	29.1	12.2	1	0
	-12.2	29.1	0	1
19	63.5	11	1	0
	-11	63.5	0	1
20	62.6	13.8	1	0
	-13.8	62.6	0	1
22	46.6	12.1	1	0
	-12.1	46.6	0	1
23	47.3	19.4	1	0
	-19.4	47.3	0	1
24	75.4	10.1	1	0
	-10.1	75.4	0	1
25	75	4.7	1	0
	-4.7	75	0	1

PRESS RETURN TO CONTINUE

26	80.6	6.2	1	0
	-6.2	80.6	0	1
28	111.3	12.4	1	0
	-12.4	111.3	0	1
31	101.4	36.3	1	0
	-36.3	101.4	0	1
32	93.9	30.8	1	0
	-30.8	93.9	0	1
33	85	34.6	1	0
	-34.6	85	0	1
34	68.8	42	1	0
	-42	68.8	0	1
36	60.8	83	1	0
	-83	60.8	0	1
39	65.1	88.6	1	0
	-88.6	65.1	0	1
41	68.5	83.3	1	0
	-83.3	68.5	0	1
42	69.6	91.2	1	0

PRESS RETURN TO CONTINUE

43	-91.2	69.6	0	1
	79.9	98	1	0
	-98	79.9	0	1
44	77.7	91.8	1	0
	-91.8	77.7	0	1
45	80.4	88.4	1	0
	-88.4	80.4	0	1
46	82.9	86.1	1	0
	-86.1	82.9	0	1
47	87.6	81.6	1	0
	-81.6	87.6	0	1
48	92.3	83.2	1	0
	-83.2	92.3	0	1
50	96.4	87	1	0
	-87	96.4	0	1
52	99.9	80.2	1	0
	-80.2	99.9	0	1
53	103.6	80.9	1	0
	-80.9	103.6	0	1

PRESS RETURN TO CONTINUE

55	104.3	86.5	1	0
	-86.5	104.3	0	1
56	101.1	95.8	1	0
	-95.8	101.1	0	1
58	111.6	90.9	1	0
	-90.9	111.6	0	1
60	123.1	64.3	1	0
	-64.3	123.1	0	1
61	128.6	65	1	0
	-65	128.6	0	1
62	126.7	73.2	1	0
	-73.2	126.7	0	1
63	135.7	65.6	1	0
	-65.6	135.7	0	1
65	140.4	69.6	1	0
	-69.6	140.4	0	1
66	134.6	73.5	1	0
	-73.5	134.6	0	1
67	134.6	76.6	1	0

PRESS RETURN TO CONTINUE

68	-76.6	134.6	0	1
	143.5	77.3	1	0
	-77.3	143.5	0	1
70	152.5	85.1	1	0
	-85.1	152.5	0	1
74	69.6	76.6	1	0
	-76.6	69.6	0	1
75	86	89.2	1	0
	-89.2	86	0	1
76	125.4	70.2	1	0
	-70.2	125.4	0	1
77	31.7	19.2	1	0
	-19.2	31.7	0	1
78	30.1	11.7	1	0
	-11.7	30.1	0	1
79	52.2	93.6	1	0
	-93.6	52.2	0	1
80	8.3	82.6	1	0
	-82.6	8.3	0	1

PRESS RETURN TO CONTINUE

81	9	94.1	1	0
	-94.1	9	0	1
83	14.9	96.2	1	0
	-96.2	14.9	0	1
87	41.7	70	1	0
	-70	41.7	0	1
88	29.8	80.4	1	0
	-80.4	29.8	0	1
89	26.1	69.4	1	0
	-69.4	26.1	0	1
92	177.5	3.4	1	0
	-3.4	177.5	0	1
93	195.3	33.2	1	0
	-33.2	195.3	0	1
94	176.7	88.3	1	0
	-88.3	176.7	0	1
96	158.2	75.8	1	0
	-75.8	158.2	0	1
97	178.5	72.6	1	0

PRESS RETURN TO CONTINUE

98	-72.6	178.5	0	1
	10	2.8	1	0
	-2.8	10	0	1
100	24.6	20.6	1	0
	-20.6	24.6	0	1
101	116.3	15.8	1	0
	-15.8	116.3	0	1
102	90.2	37.9	1	0
	-37.9	90.2	0	1
103	80.5	92.9	1	0
	-92.9	80.5	0	1
104	86.6	87.2	1	0
	-87.2	86.6	0	1
105	76.4	81.9	1	0
	-81.9	76.4	0	1

GROUND COORDINATES OF THE CHECK POINTS

PT. NO	NORTHINGS	EASTINGS
PRESS RETURN TO CONTINUE		
1	319545	577760
2	319513	578868
5	336325	591965
6	336079	592475
7	328589	593722
9	327925	594672
14	318722	576330
16	317032	578070
19	319507	582494
20	319741	582171
22	318361	580323
23	319361	579849
24	320364	584158
25	319634	584507
26	320228	585076
28	323349	588469
PRESS RETURN TO CONTINUE		
31	325602	585418
32	324349	584855
33	324165	583368
34	323836	580836
36	328428	576646
39	329437	576722
41	329108	577634
42	330215	577101
43	331805	577855
44	330925	578139
45	330615	578748
46	330545	579209
47	330361	580127
48	330925	580570
50	331691	580824
52	331143	581843
53	331456	582206
55	332177	581808
56	333152	580684
PRESS RETURN TO CONTINUE		
58	333333	582399
60	330912	585963
61	331406	586592
62	332330	585722
63	332051	587399
65	332735	587716
66	332925	586672
67	333317	586425
68	334127	587507
70	335735	588016
74	328333	578269
75	331190	579304
76	331824	585824
77	318127	577862
78	317045	578250
79	329110	574725
80	324275	569875
81	325800	569065
83	326560	569660
PRESS RETURN TO CONTINUE		
87	325360	575100
88	325725	572825
89	324050	573200
92	327375	597575
93	332505	597470
94	338055	590850
96	335000	589469
97	336241	592317
98	314228	576330
100	317760	576849
101	324152	588792
102	324982	583798
103	331158	578349
104	330963	579602
105	329539	578691
* 4.649 SECONDS USED		
		12:37:16

this did not have to be implemented. Thus, in retrospect, the separate computation of each set of coordinates now appears as a clumsy and much less efficient procedure computationally than one where the two sets of coordinates would have been transformed at the same time. While the solution of separate computation of the X and Y coordinates is less efficient from the computational point of view, the final results are identical to those which would result from the use of the alternative and more efficient procedure.

8.8.2.1 Definition of Variables

- D3 RMSE in Northings (Eastings) at the check points;
 D4 RMSE in the Northings (Eastings) at the control points;
 D0 Vector error at the control points;
 D1 Vector error at the check points;
 I(u,1) Residual errors in Northings (Eastings) at the check points after transformation;
 U(a,1) Residual errors in Northings in the control points after the transformation;
 X(m),Y(m) Image coordinates of measured points.

8.8.2.2 Definition of Arrays

As in the previous program LINCON, the same letters have been used as have been used in Appendix "A" in the explanation of the least squares procedure.

- A Array of coefficients of the polynomial transformation parameters from the image coordinate system to the terrain system for the control points;
 B Transpose matrix of A;
 C Vector array of polynomial transformation parameters;

- E Array comprising x- and y-image coordinates of all measured points;
- F Array used in the least squares adjustment procedure
(= $A^T G^{-1} L$, i.e. $BG^{-1}L$ - see equation A.7, Appendix "A");
- G Cofactor matrix used in the least squares procedure (= unity in this case);
- H Array of coefficients of polynomial transformation parameters for check points;
- I Array of residual errors at the check points;
- J Array of transformed ground coordinates of check points (= $H*C$);
- L Array comprising the Northings (Eastings) of the control points;
- M Inverse matrix of array N;
- N Array used in the least squares procedure (= $A^T G^{-1} A$, i.e. $BG^{-1}A$ in this case - see equation A.7 in Appendix "A");
- P Array comprising the designation numbers of all measured points on the image;
- T Array comprising the Northings (Eastings) of the check points;
- U Array of residual errors in Northings (Eastings) at the control points;
- W Array of transformed ground coordinates (Northings or Eastings) of control points (= $A*C$);
- X(m6),Y(m6) Arrays comprising image x- and y-coordinates respectively.

There are two additional arrays. The first is Array D (m,2) which comprises the Eastings values and the residual errors in these Eastings for control points. The second is Array Q (n,2) which comprises the Eastings and the residual errors in these Eastings for check points. These two arrays are computed separately by program POLY and are merely introduced here as data to allow the computation of the residual vector errors at both the control and check points (i.e. D0 and D1).

8.8.2.3 Explanation of the Program

The program is listed in Fig 8.12. As in the case of program LINCON, this program has also broken up into various blocks to make it easy to explain the sequence of operations performed by the program.

Block 1. Gives the name and function of the program.

Block 2. Gives the number of control points ($M4 = 28$), the check point ($M5 = 71$) and the total number of points (99) used in the particular computations.

Block 3. Dimensions all the arrays to be used in the computations.

Block 4. In this block, the operator begins by inputting the image coordinates (x and y) of all the measured points in a sequential order. Once these are input, a small FOR-NEXT loop reads the input data in pairs, i.e. the x and y image coordinates for each increment of the loop. This allows array E ($M6, 2$) ($M6 = M4 + M5$) to be formed. This comprises the image coordinates of all the measured points, and which is later used to form arrays A and H for the control points and check points respectively.

Block 5. Here the operator starts by inputting the designation numbers of all measured image points. Once this is complete, the data is read into array P, in the order control points first, followed by the check points.

Block 6. This particular block is an explanatory one, giving some details about the technique and function of the program.

Block 7. In this block, the matrix A of the coefficients of the polynomial transformation parameters is formed inside a FOR-NEXT loop from array E. The eight columns which are created by the loop consist of 1, x, y, xy, x^2 , x^2y , x^3 and x^3y respectively for each control point. These are 1, E(I,1), E(I,2), E(I,1)*E(I,2), E(I,1)**2, (E(I,1)**2*E(I,2)),

PULLOUTS

$E(I,1)**3$, $(E(I,1)**3)*E(I,2)$ respectively.

Block 8. First of all, array A is transposed to give array B. Next, arrays N ($= BG^{-1}A$) and M ($= INV(N)$) required in the least squares adjustment procedure are then computed.

Block 9. In this block, the operator begins by inputting the values of the Northings (or Eastings) of the control points in sequential order. These are then read into array L which is used to compute array F ($= B*L$). The vector matrix of the polynomial transformation parameters C is then computed ($C = M*F$) and printed out.

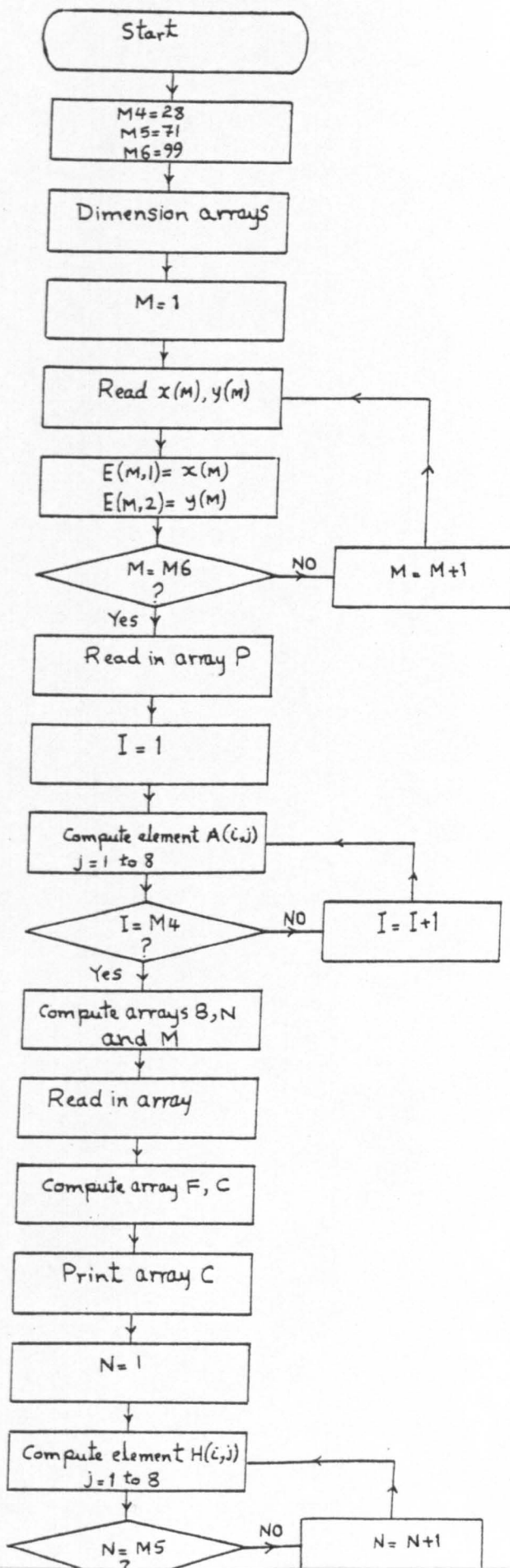
Block 10. Here, the array H comprising the coefficients of the polynomial transformation parameters required to compute the coordinates of the check points, is formed inside a FOR-NEXT loop using array E in the same manner as for control points in Block 7 above. Once this loop is exhausted, array J of the transformed ground coordinates of the check points is computed ($J = H*C$).

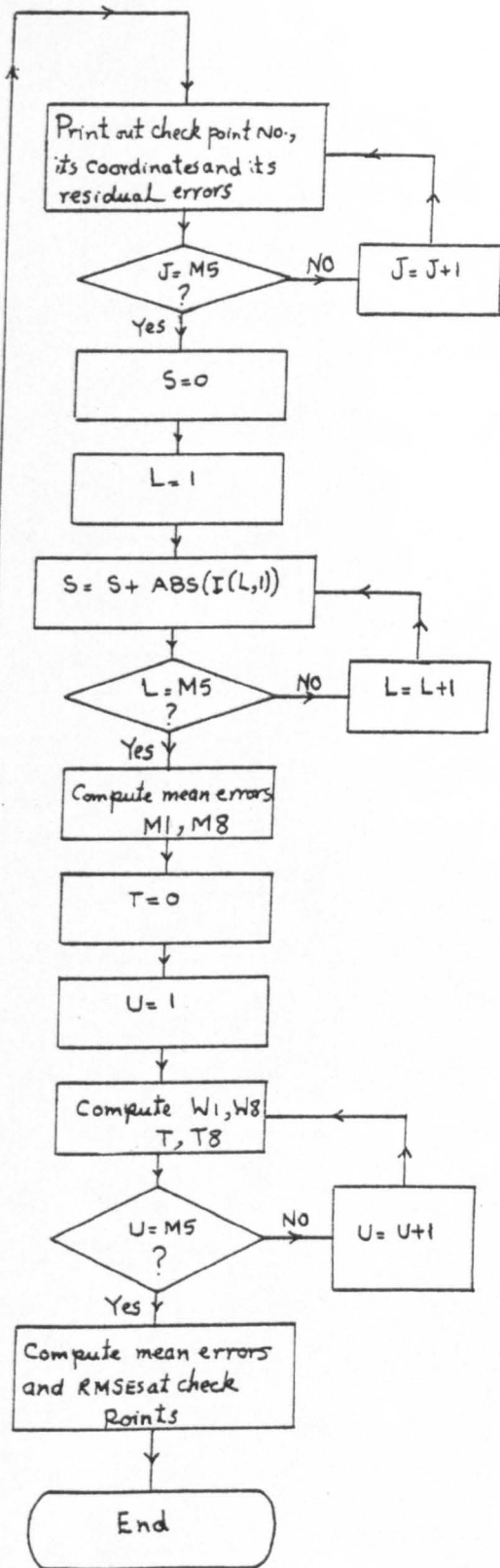
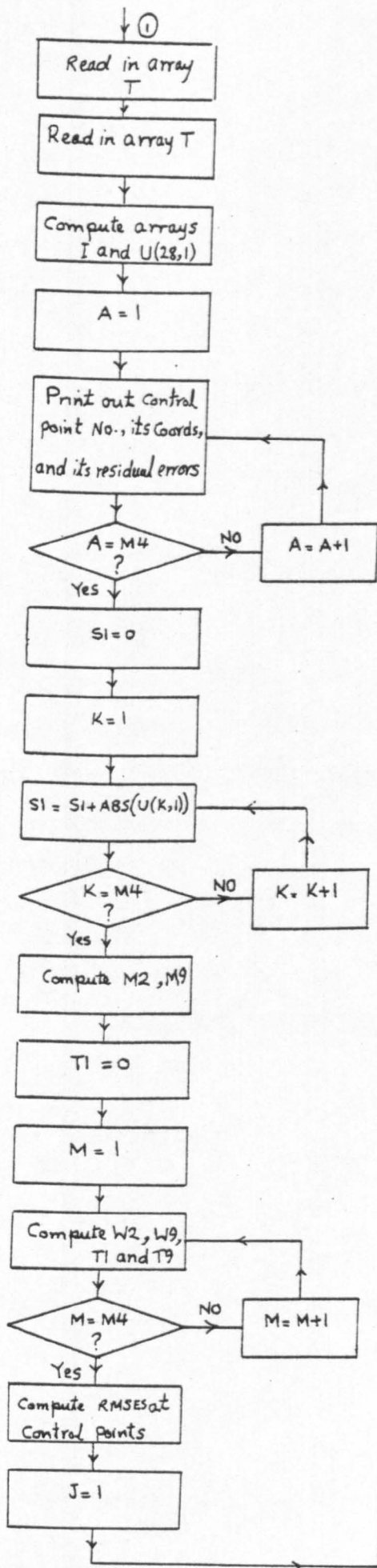
Block 11. As is the case in Block 9, in this block, the operator begins by inputting the Northings (Eastings) of all check points sequentially. When this is completed, the data is read into array T. This allows the program to compute array I ($= J-T$) of the residual errors in the check points later in Block 13.

Block 12. In this block, the array D containing the Eastings and the residual errors in Eastings of control points is read in the computer memory. This data was obtained by Program POLY separately.

Next, the Eastings followed by the residual errors in Eastings for each check point in Array Q is then read into the computer memory. The purpose of so doing is to merge the Easting data with the corresponding data obtained in the Northing direction stored in Arrays T and I. This will produce a unified output giving the Northing and Easting information for each control and check point.

Flow Diagram for Program POLY





Block 13. actually computes the residual errors in Northings of the check points (see Block 11). These are placed in Array I.

Block 14. In this block, array W containing the transformed coordinates of the control points is computed ($W=A*C$). This allows the computation of array U which gives the residual errors in Northings at the control points ($U=W-L$)

Block 15. This block simply prints out the headings under which the output for control points will be set out.

Block 16. The block prints out the point number, its Northings, Eastings and the residual errors ($\Delta N, \Delta E$) for each control point.

Block 17. Next, the mean errors and RMSEs at the control points are computed.

Block 18. Prints out the headings under which the output for check points will be set out in the same manner as has been done for the control points in Block 15.

Block 19. Prints out the point number, its Northings, Eastings and residual errors (DN and DE) for each check point.

Block 20. The block computes the mean errors and RMSEs at the check points.

8.8.2.5 Detailed Explanation of Program

<u>Statement No.</u>	<u>Comments</u>
10 & 15	Gives name and function of the program.
20 - 27	Defines the number of control and check points used in the computations.
30 - 37	Dimensions all the arrays.
40 - 90	A loop reading the input x,y data (arrays X(99), Y(99)) and forms array E from it.
530 - 540	Reads the input array P.
700 - 770	Explains the function and technique of the program.
780 - 870	Computes array A from array E.

<u>Statement No.</u>	<u>Comments</u>
880 - 885	Explains array A.
890	Transposes array A to obtain array B.
900	Explains array B.
910	Multiplies B by A to give array N.
920	Inverses N to produce M.
930	Reads the input array L.
940	Explains L.
990	Computes array F.
1010	Computes array C.
1022	Prints the text as shown.
1025	Prints the array C.
1030 - 1120	Computes array H.
1130 - 1135	Explains array H.
1140	Computes array J.
1150	Reads in the input matrix T.
1160	Explains T.
1280	Computes array I.
1290	Explains I.
1300 - 1330	Computes arrays W and U.
1340 - 1360	Prints the text as shown to prepare for the output for the control points in a table.
1370 - 1400	Prints out point No., Northing, Easting, DN, DE and vector error for each control point.
1410 - 1570	Computes mean errors and RMSEs for control points.
1580 - 1600	Prints text shown to prepare to set out output data in a table for check points.
1620 - 1640	Prints point No., Northing, Easting, DN, DE and the resulting vector error for each check point.

<u>Statement No.</u>	<u>Comments</u>
1650 - 1830	Computes the mean errors and RMSEs for each check point.

8.8.2.6 List of program and Sample of Output Data

Fig 8.12 is a listing of the program POLY together with a sample of input (Fig 8.13) and output data (Fig 8.14). To obtain the sample of output data, the data computed by program POLY in the Y-direction was merged inside the computer core with the corresponding data from the X-direction. The merged data was then output as a single data set.

8.8.3 Program PLOTIR

This program plots the residual errors at all the test points (including the control points and the check points). This plot takes place after the transformation of the image coordinates of the measured points into terrain coordinates and their comparison with the given terrain coordinates of these points. By offering a graphical presentation of the results, it is possible to detect any tendency towards systematic errors over the whole or part of the image and, in this way, help the analysis of the effectiveness of different procedures as revealed by the extent and distribution of the residual errors.

8.8.3.1 Definition of Variables

N Number of points to be plotted.

8.8.3.2 Definition of Arrays

M Array containing the designation numbers of the test points, their terrain coordinates and the residual errors at these points.

PULLOUTS

MEASURED IMAGE COORDINATES OF ALL POINTS

(A) MEASURED IMAGE COORDINATES OF THE CONTROL POINTS

POINT NO.	X(MM)	Y(MM)
3	107.1	115.5
4	79.2	128.5
8	163.3	129.5
12	68.3	130.8
13	65.4	159.4
15	63.5	113.1
17	72.1	102.6
18	48.5	99
21	96.5	105.1
27	131.4	98.2
29	162.1	107.4
30	212.3	112.5

PRESS RETURN TO CONTINUE

35	116.9	146.5
37	101.2	183.9
38	225.8	165.8
40	117.3	181.1
49	134.3	182.8
54	149.7	176.7
57	152.4	194.8
59	161.8	159.73
64	185.5	158.7
69	192.5	176
71	196.3	191.5
72	201.1	192.1
82	47.8	196
84	86.8	193.7
86	86.5	157
99	69.8	104.6

(B) MEASURED IMAGE COORDINATES OF THE CHECK POINTS

PRESS RETURN TO CONTINUE

POINT NUMBER	X(MM)	Y(MM)
1	79.5	125.2
2	65	121
5	221.2	169.1
6	222.7	165.6
7	203.5	119.1
9	206.2	111.7
10	71.3	129.7
11	74.4	121.4
14	68.3	125.9
16	72.2	109.8
19	106.4	108
20	105.6	110.8
22	89.6	109.4
23	90.4	116.7
24	118.3	106.9
25	117.8	101.5
26	123.4	102.9
28	154.1	108.5

PRESS RETURN TO CONTINUE

31	144.7	132.5
32	137.1	127.2
33	128.3	131.1
34	112.3	138.8
36	105.1	179.9
39	109.5	185.4
41	112.8	180.1
42	114	187.9
43	124.4	194.5
44	122.1	188.4
45	124.7	184.9
46	127.2	182.6
47	131.8	178
48	136.5	179.5
50	140.7	183.3
52	144	176.4
53	147.7	177
55	148.5	182.6
56	145.5	192

PRESS RETURN TO CONTINUE

58	155.9	186.9
60	166.8	160.1
61	172.3	160.7
62	170.6	168.9
63	179.4	161.2
65	184.2	165.1
66	178.5	169.1
67	178.5	172.2
68	187.4	172.7
70	196.5	180.3
74	113.7	173.4
75	130.3	185.6
76	169.2	165.9
77	74.9	116.8
78	73.2	109.3
79	96.7	190.7
80	52.8	180.5
81	53.7	192
83	59.6	194

PRESS RETURN TO CONTINUE

87	85.8	167.3
88	74.2	177.9
89	70.3	167
92	219.9	98.3
93	238.2	127.7
94	220.7	183.1
96	202	170.9
97	222.2	167.3
98	53	100.8
100	67.8	118.3
101	159.1	111.8
102	133.6	134.3
103	124.9	189.4
104	130.9	183.6
105	120.6	178.5

GROUND COORDINATES OF THE CONTROL POINTS

PT NO. NORTHINGS(M) EASTINGS(M)
PRESS RETURN TO CONTINUE

3	320526	582000
4	319890	577418
8	326729	587919
12	319285	575798
13	322691	573253
15	316760	576729
17	316146	578659
18	313646	575792
21	318377	581497
27	320279	586425
29	323855	589507
30	328507	595380
35	325190	580836
37	328523	575855
38	336336	592887
40	329539	578101
49	331120	580032
54	331577	582475

PRESS RETURN TO CONTINUE

57	334051	581339
59	330396	585292
64	332190	588425
69	334912	587893
71	337158	587108
72	337596	587678
82	325788	568040
84	328725	573275
86	324100	576185
99	316170	578210

GROUND COORDINATES OF THE CHECK POINTS

PT. NO. NORTHINGS(M) EASTINGS(M)

1	319545	577760
2	319513	578868
5	336325	591965
6	336079	592475

PRESS RETURN TO CONTINUE

7	328589	593722
9	327925	594672
10	319406	576292
11	318634	577425
14	318722	576330
16	317032	578070
19	319507	582494

101	159.1	111.8
102	133.6	134.3
103	124.9	189.4
104	130.9	183.6
105	120.6	178.5

GROUND COORDINATES OF THE CONTROL POINTS

PT. NO. NORTHINGS(M) EASTINGS(M)
PRESS RETURN TO CONTINUE

3	320526	582000
4	319890	577418
8	326729	587919
12	319285	575798
13	322691	573253
15	316760	576729
17	316146	578659
18	313646	575792
21	318377	581497
27	320279	586425
29	323855	589507
30	328507	595380
35	325190	580836
37	328523	575855
38	336336	592887
40	329539	578101
49	331120	580032
54	331577	582475

PRESS RETURN TO CONTINUE

57	334051	581339
59	330396	585292
64	332190	588425
69	334912	587893
71	337158	587108
72	337596	587678
82	325788	568040
84	328725	573275
86	324100	576185
99	316170	578210

GROUND COORDINATES OF THE CHECK POINTS

PT. NO. NORTHINGS(M) EASTINGS(M)

1	319545	577760
2	319513	578868
5	336325	591965
6	336079	592475

PRESS RETURN TO CONTINUE

7	328589	593722
9	327925	594672
10	319406	576292
11	318634	577425
14	318722	576330
16	317032	578070
19	319507	582494
20	319741	582171
22	318361	580323
23	319361	579849
24	320364	584158
25	319634	584507
26	320228	585076
28	323349	588469
31	325602	585418
32	324349	584855
33	324165	583368
34	323836	580836
36	328428	576646

PRESS RETURN TO CONTINUE

39	329437	576722
41	329108	577634
42	330215	577101
43	331805	577855
44	330925	578139
45	330615	578748
46	330545	579209
47	330361	580127
48	330925	580570
50	331691	580824
52	331143	581843
53	331456	582206
55	332177	581808
56	333152	580684
58	333333	582387
60	330912	585950
61	331406	586592
62	332330	585722
63	332051	587399

PRESS RETURN TO CONTINUE

65	332735	587716
66	332925	586672
67	333317	586425
68	334127	587507
70	335735	588016
74	328333	578269
75	331190	579304
76	331824	585824
77	318127	577862
78	317045	578250
79	329110	574725
80	324275	569875
81	325800	569065
83	326560	569660
87	325360	575100
88	325725	572825
89	324050	573200
92	327375	597575
93	332505	597470

PRESS RETURN TO CONTINUE

94	338055	590850
96	335000	589469
97	336241	592317
98	314228	576330
100	317760	576849
101	324152	588792
102	324982	583798
103	331158	578349
104	330963	579602
105	329539	578691

* 4.175 SECONDS USED 20:59:49

296526.
 166.269
 129.161
 -0.112074
 -0.208649
 8.94859 E-4
 4.90152 E-4
 -2.0851 E-6
 ACCURACY OF CONTROL POINTS

PT NO. N(M) E(M) DN(M) DE(M) DO(M)
 3 320526 582000 11.6643 30.8 33
 4 319870 577418 31.9821 50.5 60
 8 326729 567919 -8.13862 -11.3 14
 PRESS RETURN TO CONTINUE

12	319285	575758	34.1506	88.5	95
13	322691	573253	-33.2824	-10.8	35
15	316760	576729	-50.8374	-58.6	78
17	316146	578659	-39.0104	-44.1	59
18	313666	575792	32.7941	34.9	48
21	318377	581497	18.4447	27.1	33
22	320279	586425	10.403	12.2	16
29	323855	589507	-5.34803	5.8	8
30	328507	595360	12.6177	6.5	14
35	325190	580836	-3.19513	-43.3	43
37	328523	575955	83.47	-1.4	83
38	336336	592887	-5.92686	19.1	20
40	329539	578101	3.22066	-8.7	9
49	331120	580032	-11.7135	41.97	44
54	331577	582475	-8.34796	-3.5	9
57	334051	581339	3.62267	30.1	30
59	330376	585292	3.85845	32.3	33
64	332190	588425	-29.0102	-67.1	73
69	334912	587893	-10.8623	-27	29

PRESS RETURN TO CONTINUE

71	337158	587108	0.503354	9.6	10
72	337596	587678	25.6272	-1.2	26
82	325788	568040	16.1393	6.5	17
83	328725	573275	-50.3223	-17.9	53
86	324100	576185	-30.0772	-50.6	59
99	318170	578210	-2.46655	-50.1	50

RESIDUALS IN CONTROL POINTS AS STANDARD DEVIATION
 MEAN ERROR IN NORTHINGS OF CONTROL POINTS= 20.6099
 MEAN ERROR IN EASTINGS= 28.2668
 RMSE AT NORTHINGS OF CONTROL POINTS= 22.3627
 RMSE AT EASTINGS OF CONTROL POINTS= 24.036

ACCURACY OF CHECK POINTS

PT NO.	N(M)	E(M)	DN(M)	DE(M)	DI(M)
1	319545	577760	-10.6941	8.9	14
2	319513	-578868	-57.4603	-64.3	86
5	336325	591965	40.53	89.6	96

PRESS RETURN TO CONTINUE

6	336079	592475	-29.6093	48.2	57
7	328589	593722	40.3675	30.8	51
9	327925	594672	-6.52099	6.3	9
10	319406	576292	21.6921	68.4	72
11	318634	577425	10.2748	-7.3	13
14	318722	576330	-15.432	-54.5	57
16	317632	578070	-17.1503	-13.9	22
19	319507	582494	38.6881	45.1	59
20	319741	582171	90.7866	45.2	101
22	318361	580323	17.6809	-13.5	22
23	317861	577849	-6.90857	-18.1	19
24	319634	584158	-15.2011	-42.8	45
25	320364	584507	0.57665	-24.99	25
26	320228	585076	21.7578	-7.3	23
28	323349	588469	9.80586	-35.2	37
31	325602	585418	28.0653	-55.8	62
32	324349	584855	18.5812	-14.7	24
33	324165	583368	-2.35361	69	69
34	323636	580836	23.9921	-6	25

PRESS RETURN TO CONTINUE

36	328428	576646	-9.0323	15.3	18
39	329437	576722	20.1664	53.5	57
41	329108	577634	-49.4393	-24.3	55
42	330215	577101	-86.3367	38.7	95
43	331805	577855	-21.5896	57.4	61
44	330925	578139	-87.7615	-28.3	92
45	330615	578748	-8.2069	-35.2	36
46	330545	579209	-26.8057	-2	27
47	330361	580127	-52.4304	17.7	55
48	330925	580570	-54.9253	39.6	68
50	331691	580824	-10.8077	5.5	12
52	331143	581843	-65.1092	-55.5	86
53	331456	582206	-8.75018	-6.7	11
55	332177	581608	36.2339	45.8	58
56	333152	580684	0.987693	50.4	50
58	333333	582387	9.35256	44.5	45
60	330912	585950	-68.1494	-35.8	77
61	331406	586592	-48.6893	-40.8	64
62	332330	585722	-77.1675	-33.1	84

PRESS RETURN TO CONTINUE

63	332051	587399	-63.9096	-2	64
65	332735	587716	127.194	-27.9	130
66	332925	586672	-15.9713	-13.6	21
67	333317	586425	-17.9616	-12.4	22
68	334127	587507	-51.474	-20.2	55
70	335735	588016	29.0825	13.3	33
74	338333	578269	-39.6525	-14.3	42
75	331190	579304	-49.6479	50.1	71
76	331824	585824	-59.9648	-71.4	93
77	318127	577842	-16.4694	-14.9	22
78	317045	578250	-10.5637	-25.7	28
79	329110	574725	-15.1589	21.8	27
80	324275	589875	-7.17313	55.5	56
81	325800	589065	-16.2755	71.4	73
83	325560	589660	-45.3247	85.9	97
87	325360	575100	-60.8598	127.3	141
88	325225	572825	-39.0618	81	90
89	324050	573200	-42.4557	71	83
92	327375	577575	-9.83374	-102.8	103

PRESS RETURN TO CONTINUE

93	332505	597470	90.1192	38.9	98
94	338055	570850	27.8524	36	46
96	335000	589469	26.3691	-2	26
97	336241	592317	-19.3059	7.9	21
98	314228	576330	59.876	-53.7	80
100	317760	576849	-44.7621	-34.0	57
101	324152	588792	14.1738	-1	14
102	324982	583798	-1.05578	43.5	44
103	331158	578349	27.4962	31	41
104	330963	579602	-25.1653	-14.3	29
105	339539	578691	-58.8894	19.6	62

MEAN IN METRES OF CHECK POINTS RESIDUALS= 33.5235
 RMSE OF CHECK POINTS AFTER POLYNOMIAL FIT
 AND LEAST SQUARES INTERPOLATION= 26.0549
 RMSE IN THE EASTINGS OF CHECK POINTS= 26.183

B Array containing the designation numbers of the test points, their terrain coordinates and the scaled residual errors required for plotting.

8.8.3.3 Explanation of Program PLOTIR

Block 1. This gives the name of the program and explains its function.

Block 2. This block dimensions the arrays M (5,m) and B(5,m) where m is the number of test points to be plotted.

Block 3. In this block, the number of points whose vector errors are to be plotted is read.

Block 4. Reads the elements of the integer array M from a standard data file in which the five columns are as follows: Point Number; Northings; Eastings; Residual error in Northings; and Residual error in Eastings respectively. (See input data sample attached.)

Block 5. Derives the real array B from the integer array M by scaling the residual errors in Northings and Eastings.

Block 6. This block calls the appropriate GHOST routines to prepare for the plotting.

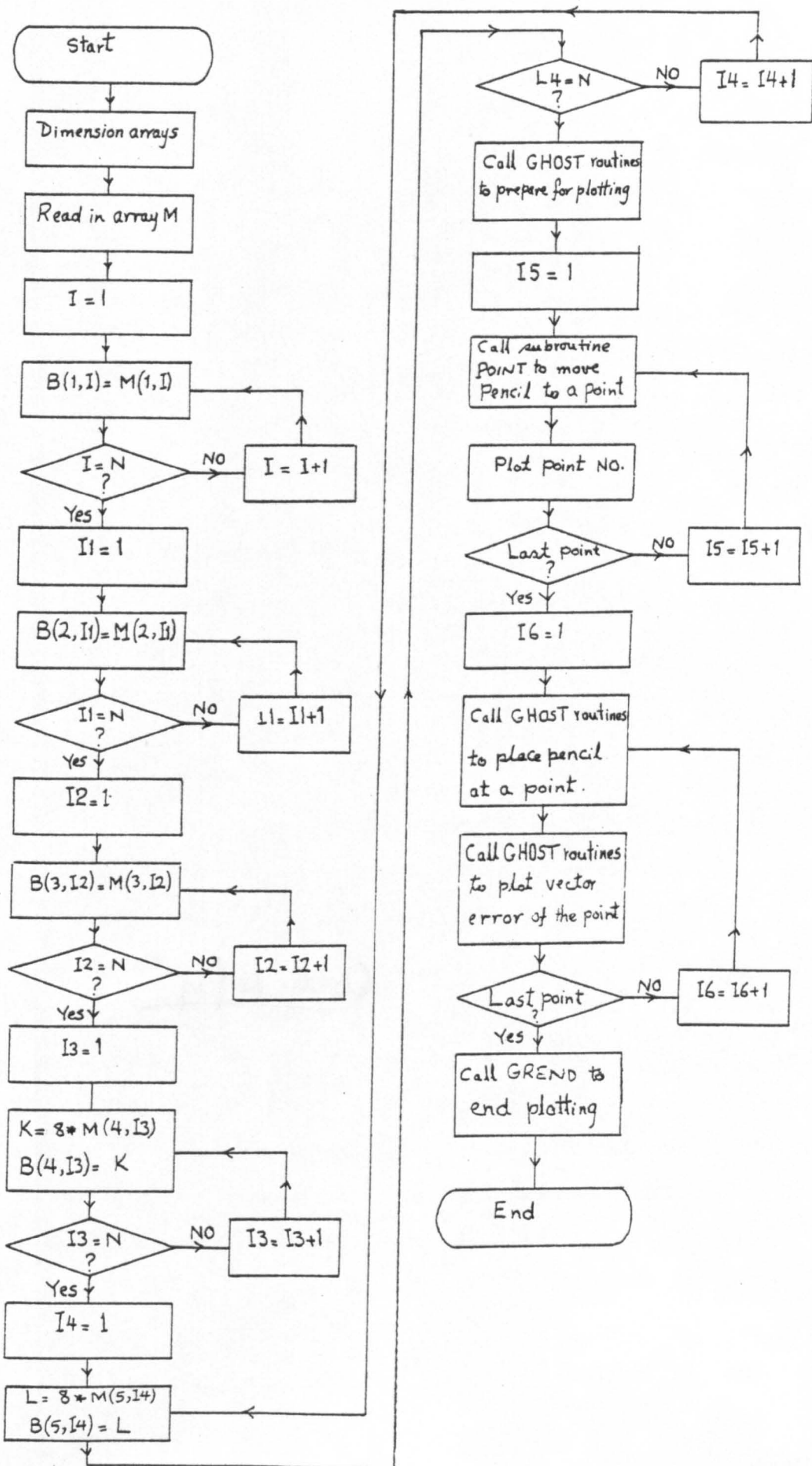
Block 7. Plots and writes the designation number of each point in its correct planimetric position.

Block 8. Plots the vector errors for all points.

Block 9. Calls the GHOST routine GREND to end the plotting.

8.8.3.5 Detailed description of Program

<u>Statement No.</u>	<u>Comments</u>
1	Procedure of program
2 - 5	Explains the function and input of program
6 - 7	Dimensions the arrays
8 - 9	Reads the number of points to be plotted and the corresponding format;



<u>Statement No.</u>	<u>Comments</u>
10 - 11	Reads the array M; and the corresponding format;
12 - 28	Derives the real array B from the integer array M;
29 - 44	Calls certain GHOST routines to prepare for plotting;
45 - 48	Plots the point numbers in their correct planimetric positions;
48 - 52	Plots vector errors
53	Calls the subroutine GREND to end plotting
54 - 55	End of the program.

8.8.3.6 Listing of Program

Fig 8.15 is a Listing of the program PLOTIR. Fig 8.16 is a sample input data for the program and Fig 8.17 is a sample output data from program PLOTIR.

8.9 Conclusion

The test work carried out in this study could never have been achieved without the availability of a digital computer. The time and effort involved in developing, debugging, testing and running the programs for purpose were considerable. Since they are the author's first programs they are less well designed than those written by an experienced programmer. Undoubtedly, they could be made more efficient and quicker in performance. However, this would have resulted in the expenditure of much more time and effort than was available during the present study. Nevertheless since they appeared to be effective, a serious attempt has been made in the preceding pages to document them thoroughly so that they may be utilized by other experimenters. Certainly the present author has gained much experience in this field, which was previously unfamiliar to him.

BEST COPY

AVAILABLE

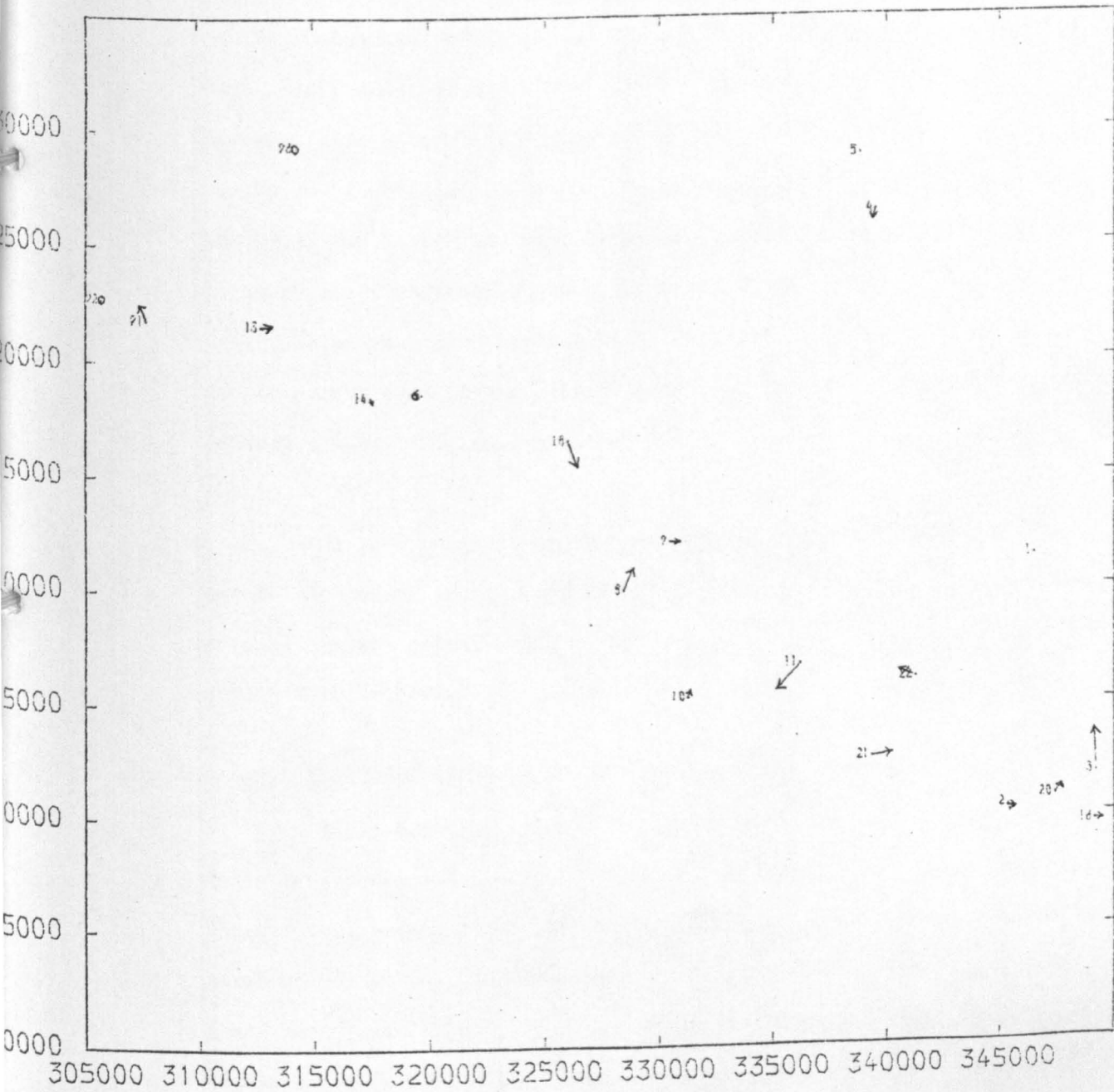
Variable print quality

(0001)	PROGRAM PLOTIR	
(0002)C	THE PROGRAM PLOTS RESIDUALS ERRORS OBTAINED FROM TAY RIVER SURVEY	(1)
(0003)C	PROCESSED AREA	
(0004)C	ARRAY M COMPRISES THE COORDINATES OF POINTS,THE POINTS,NUMBERS &	
(0005)C	THE RESIDUALS	
(0006)	INTEGER M(5,20),J	(2)
(0007)	REAL B(5,20),K,L	
(0008)	READ(5,100) N	(3)
(0009) 100	FORMAT(I2)	
(0010)	READ(5,110) M	(4)
(0011) 110	FORMAT(I2,1X,I6,1X,I6,1X,I4,1X,I5)	
(0012)	DO 120 I=1,N	
(0013)	B(1,I)=M(1,I)	
(0014) 120	CONTINUE	
(0015)	DO 130 I1=1,N	
(0016)	B(2,I1)=M(2,I1)	
(0017) 130	CONTINUE	
(0018)	DO 140 I2=1,N	
(0019)	B(3,I2)=M(3,I2)	
(0020) 140	CONTINUE	(5)
	CONTINUE(Y OR N)?Y	
(0021)	DO 150 I3=1,N	
(0022)	K=8*M(4,I3)	
(0023)	B(4,I3)=K	
(0024) 150	CONTINUE	
(0025)	DO 160 I4=1,N	
(0026)	L=8*M(5,I4)	
(0027)	B(5,I4)=L	
(0028) 160	CONTINUE	
(0029)	CALL PAPER(1)	
(0030)	CALL PSPACE(0.10,0.75,0.10,0.75)	
(0031)	CALL MAP(690000.,735000.,305000.,350000.)	
(0032)	CALL SCALES	
(0033)	CALL BORDER	
(0034)	CALL ITALIC(0)	
(0035)	CALL PLACE(12,3)	
(0036)	CALL TYPECS('VECTOR MAP OF POSITION ERRORS OF RIVER TAY AREA',47)	
(0037)	CALL CTRMAG(5)	(6)
(0038)	CALL ITALIC(0)	
(0039)	CALL PLACE(12,2)	
(0040)	CALL TYPECS('MAP SCALE 1/250000,VECTOR SCALE 1/20000',39)	
	CONTINUE(Y OR N)?Y	
(0041)	CALL ITALIC(0)	
(0042)	CALL PLACE(12,1)	
(0043)	CALL TYPECS('AFTER LINEAR CONFORMAL',22)	
(0044)	CALL CTRMAG(5)	
(0045)	DO 170 I5=1,N	
(0046)	J=B(1,I5)	
(0047)	CALL PLOTNI(B(2,I5),B(3,I5),J)	(7)
(0048) 170	CONTINUE	
(0049)	DO 180 I6=1,N	
(0050)	CALL POINT(B(2,I6),B(3,I6))	(8)
(0051)	CALL LINE(B(4,I6),B(5,I6))	
(0052) 180	CONTINUE	
(0053)	CALL GEND	(9)
(0054)	STOP	
(0055)	END	
(0056)**END**		

**TEXT
BOUND INTO THE
SPINE**

UNIT COORDINATE TRANSFORM
SCALE 1:25000, VECTOR SCALE 1:25000

VECTOR MAP OF POSITION ERRORS OF RIVER TAY AREA



CHAPTER IX

RESULTS OF ACCURACY TESTS

9.1 Results from the River Tay Test Area

It soon became apparent from the results of the accuracy tests on the River Tay area that, in spite of the care taken in the selection of the control and check points (see Section 8.3), quite a number had been poorly identified. This showed up in the shape of very large residual errors in these points after transformation. Out of the thirty two identified points on the survey-optimally processed image of the River Tay test area, only twenty gave good or acceptable results in terms of their residual errors. Thus 37.5% of the points originally selected for test purposes had to be rejected. The final distribution of the points used in the test is shown on Fig 9.1. Nine were used as control points, the remaining eleven points being employed as check points.

On the precision processed imagery of the same area, twenty two points proved to be acceptable for the accuracy analysis. Ten were used as control points and the remaining twelve as check points. The final distribution of the control and check points is shown on Fig 9.2.

9.1.1 Overall Results from the Survey Processed Image

Table 9.1 summarises the results obtained from the tests of the survey processed image of the River Tay test area. The r.m.s.e. of the residual errors obtained at the control and check points was first computed using the polynomial transformation with the full eight terms. These terms were then dropped one by one in order to judge their significance for the along-track and cross-track coordinate accuracies.

At the control points, the smallest residual errors were obtained

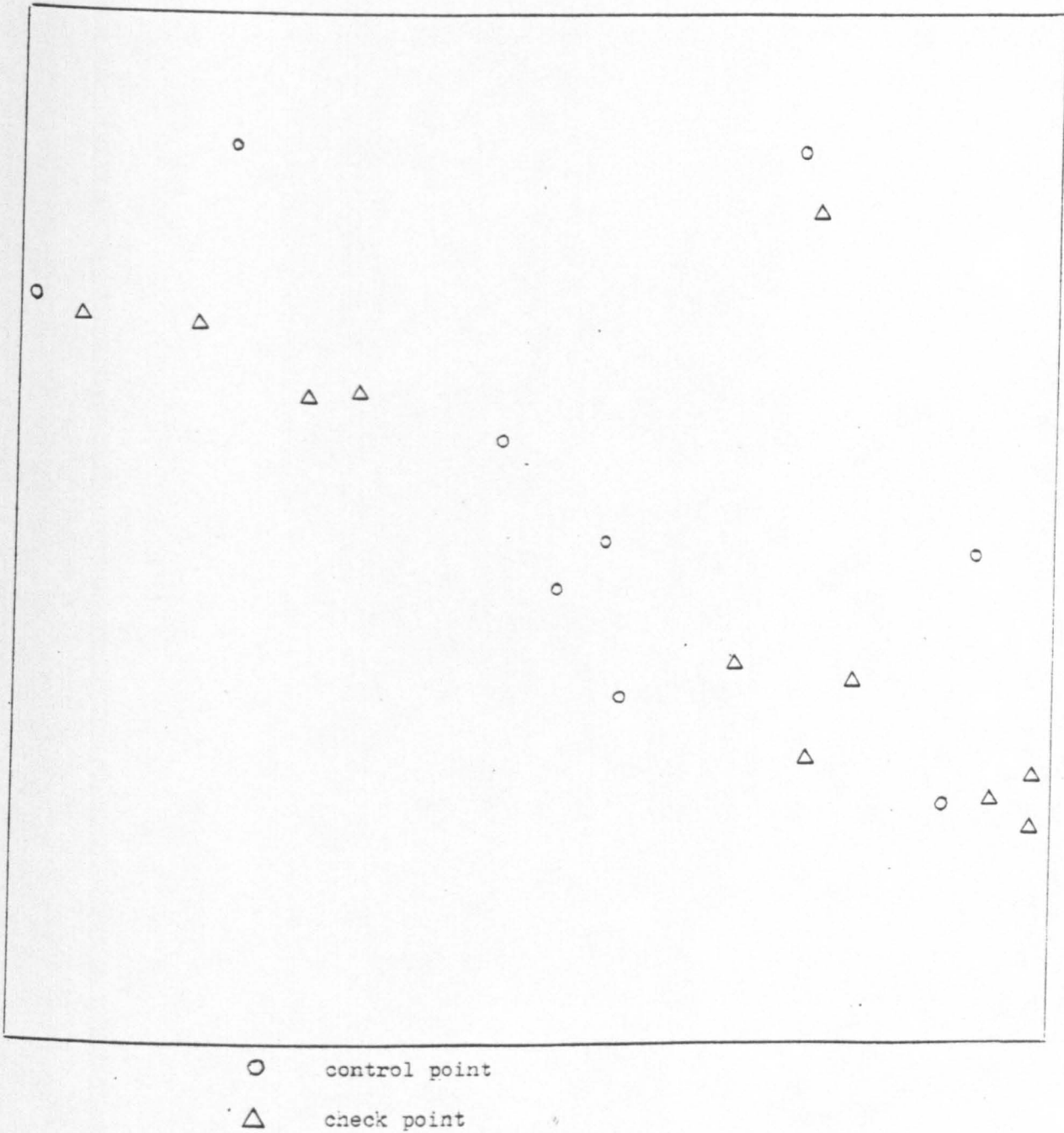


Fig. 9.1 Control distribution pattern on the survey optically processed image of the River Tay test area

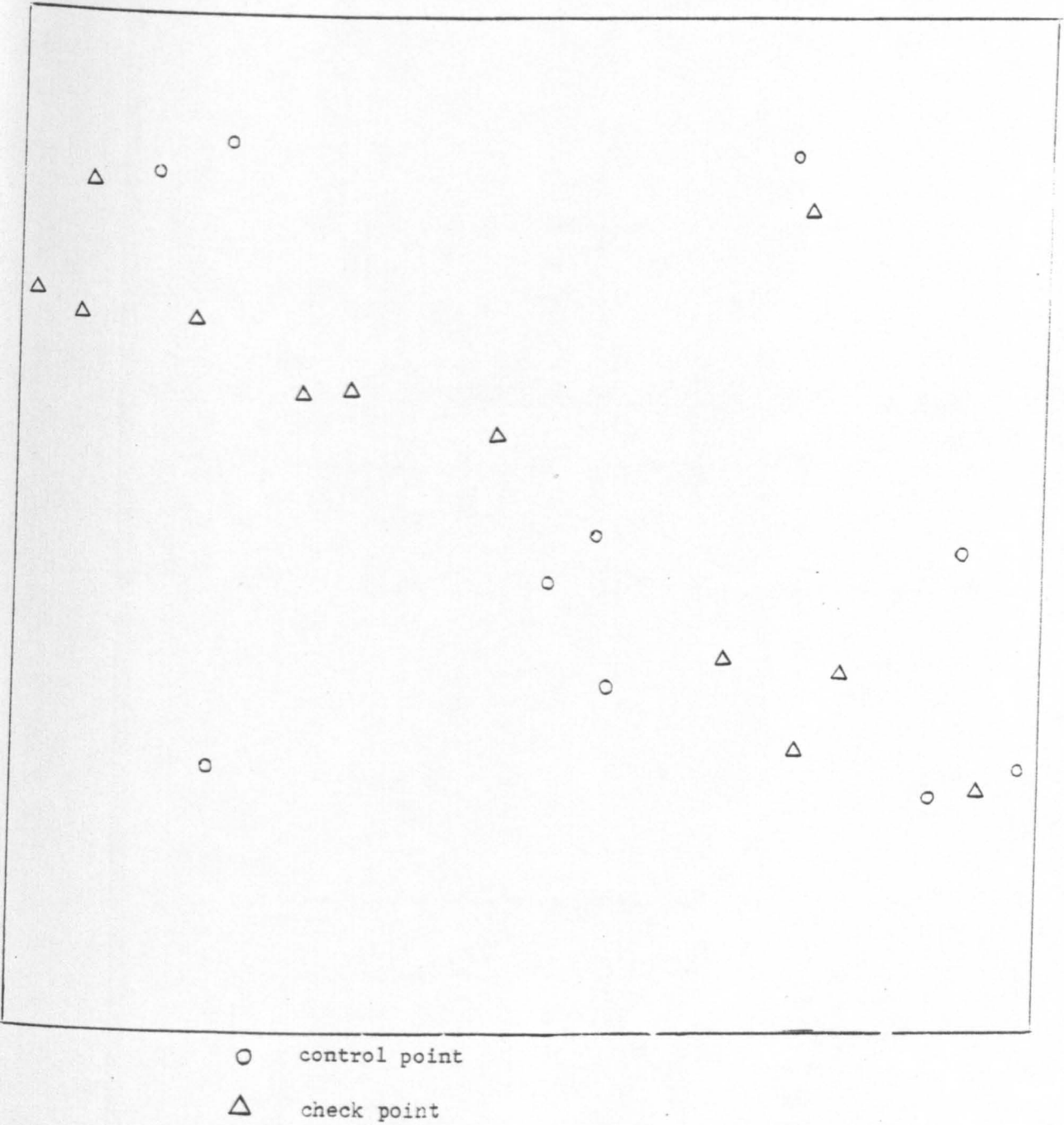


Fig. 9.2 Control distribution on the precision processed image of the River Tay test area

TABLE 9.1 RESULTS OF SURVEY-PROCESSED IMAGE - RIVER TAY TEST AREA

No. of terms in polynomial	Control Points (n=9)			Check Points (n = 11)		
	$\sigma_X(m)$	$\sigma_Y(m)$	$\sigma_P(m)$	$\sigma_X(m)$	$\sigma_Y(m)$	$\sigma_P(m)$
8	7	34	35	75	43	87
7	12	27	30	80	44	91
6	83	111	139	68	60	91
5	69	86	110	70	72	100
4	67	78	103	70	71	100
3	58	75	95	88	78	118
Linear Conformal Transformation	97	271	288	132	226	262
	-	(n=2)	-	115	480	494

TABLE 9.2 RESULTS OF PRECISION-PROCESSED IMAGE - RIVER TAY TEST AREA

No. of terms in polynomial	Control Points (n=10)			Check Points (n = 12)		
	$\sigma_X(m)$	$\sigma_Y(m)$	$\sigma_P(m)$	$\sigma_X(m)$	$\sigma_Y(m)$	$\sigma_P(m)$
8	26	90	94	79	74	108
7	59	105	120	173	110	205
6	51	103	115	172	156	232
5	81	147	168	67	86	109
4	79	126	149	63	84	105
3	69	124	142	63	86	107
Linear Conformal Transformation	134	517	534	240	247	344
	-	(n=2)	-	148	474	497

when the full polynomial was used. This is true for both the X and Y directions. With the full polynomial having all eight terms, the r.m.s.e. values in the X and Y directions were ± 7 m and ± 34 m respectively, giving rise to a vector error of only ± 35 m. When the eighth term was removed, the resulting values using the remaining seven terms were $\sigma_X = \pm 12$ m and $\sigma_Y = \pm 27$ m with a vector positional error of ± 30 m.

There is, however, a sudden and dramatic drop in the accuracy of fit at the control points when these two highest-order terms are truncated. The error in the X-direction rose to ± 83 m while that in the Y-direction was ± 111 m. Curiously, the use of the five-term polynomial seemed to produce better results than those produced with the six-term polynomial. Thus, the errors reduced to ± 69 m and ± 86 m respectively when the sixth term was removed. Then a plateau appears to have been reached, since elimination of the fifth and fourth terms seemed to have no serious effect on the accuracy. When the polynomial was restricted to the three linear terms only (i.e. to the affine transformation case), the r.m.s.e. became ± 58 m in the X-direction and ± 75 m in the Y-direction, with a positional accuracy of ± 95 m.

At the check points, the best planimetric accuracies were again obtained when the highest-order terms were retained in the polynomial. However, the accuracy encountered at these check points was overall much lower (2.5 to 3x) than that achieved at the control points. In particular, the results in the X-coordinate direction were strikingly poorer. With the subsequent elimination of the two highest order polynomial terms, the vector error (± 91 m) remained the same though the ratio between the X and Y errors altered from 2:1 to nearly equal with the use of the six-term polynomial. As further terms were dropped, there are further slight deteriorations in the r.m.s.e. values

encountered at the check points. The planimetric error (σ_p) in the check points finally increased to ± 118 m when the polynomial is restricted to three terms, i.e. to the affine transformation case.

The simple linear conformal transformation using only two well-defined and widely separated points for the computation of the transformation parameters gave positional accuracies of ± 115 m and ± 480 m in the along-track and cross-track directions respectively. The resulting positional error in this case is of the order of ± 494 m. This indicates the existence of substantial errors in scale in the cross-track direction for the survey processed image.

When a larger number of points - nine (giving seven redundancies) was used for the determination of the transformation parameters, the along-track accuracy improved slightly to ± 97 m and the cross-track accuracy to ± 271 m for control points. At the check points, there was a substantial improvement in the Y-direction (i.e. from ± 480 m to ± 226 m) while a slight degradation in accuracy occurred in the X-direction (from ± 115 m to ± 132 m). The corresponding positional errors improved to ± 288 m at the control points and ± 262 m at the check points with the use of the large number of control points.

9.1.2 Overall Results from the Precision Processed Image

Table 9.2 presents the accuracies achieved with the tests carried out on the precision processed image of the River Tay area.

Regarding the fit to the control points, as with the survey processed image, the best results were obtained (both in X and Y directions) when the three highest degree terms are present in the polynomial solution. When all eight terms are employed, the r.m.s.e. values at the control points were ± 26 m, ± 90 m and ± 94 m in X, Y and plan respectively. Elimination of the eighth term sharply reduced the

accuracy to ± 59 m, ± 105 m and ± 120 m respectively. Further elimination of the seventh term did not alter the results significantly. However, when the sixth, seventh and eighth terms are all truncated leaving only five terms, the errors increased markedly to ± 81 m in the X-direction, and to ± 147 m in the Y-direction corresponding to ± 168 m in planimetry. Curiously, the accuracy started to improve again when the polynomial solution was restricted to four terms and three terms (i.e. to an affine transformation).

At the check points, the use of the full eight term polynomial gave the following r.m.s.e. values:- $\sigma_X = \pm 79$ m; $\sigma_Y = \pm 74$ m; and $\sigma_P = \pm 108$ m. Surprisingly, a sudden two-fold drop in accuracy occurred when the eighth term was removed. In the X-direction, the accuracy dropped from ± 79 m to ± 173 m and in the Y-direction from ± 74 m to ± 110 m, giving rise to a drop in positional accuracy from ± 108 m to ± 205 m. Elimination of the seventh term resulting in the restriction of the polynomial to six terms only did not alter this situation significantly. However, a sudden and significant improvement in accuracy took place when the sixth, seventh and eighth terms were truncated. The X-accuracy improved from ± 172 m to ± 67 m and the Y-accuracy from ± 156 m to ± 86 m giving rise to a position r.m.s.e. improvement from ± 232 m to ± 109 m.

Further elimination of the fifth and fourth terms seemed to have no effect on the r.m.s.e. values at the check points. Even when the polynomial is restricted to three terms, corresponding to an affine transformation, virtually the same results were obtained as when the polynomial has five terms.

The simple linear conformal transformation based on only two well-defined control points gave the following results:- $\sigma_X = \pm 148$ m; $\sigma_Y = \pm 474$ m; and $\sigma_P = \pm 497$ m. With the use of ten control points

and a least squares adjustment, the simple linear conformal transformation gave considerably smaller values in the overall planimetric accuracy.

9.1.3 Detailed Analysis of Results from the Survey Processed Image

Besides the overall impression given by the summary tables, all the individual vector errors at each control point and check point have been plotted out graphically for each transformation applied to the measured data using the PLOTIR program. This allows a much more effective analysis of the error patterns than simple tabular listing of the individual residual errors, since the distribution, direction and extent of these errors can be appreciated readily and any systematic pattern to these errors can be discerned.

Figs 9.3 to 9.9 are the plotted residual positional errors at both the control points (shown in red) and the check points (shown in black) after the various transformation solutions have been applied to the survey processed image of the River Tay area.

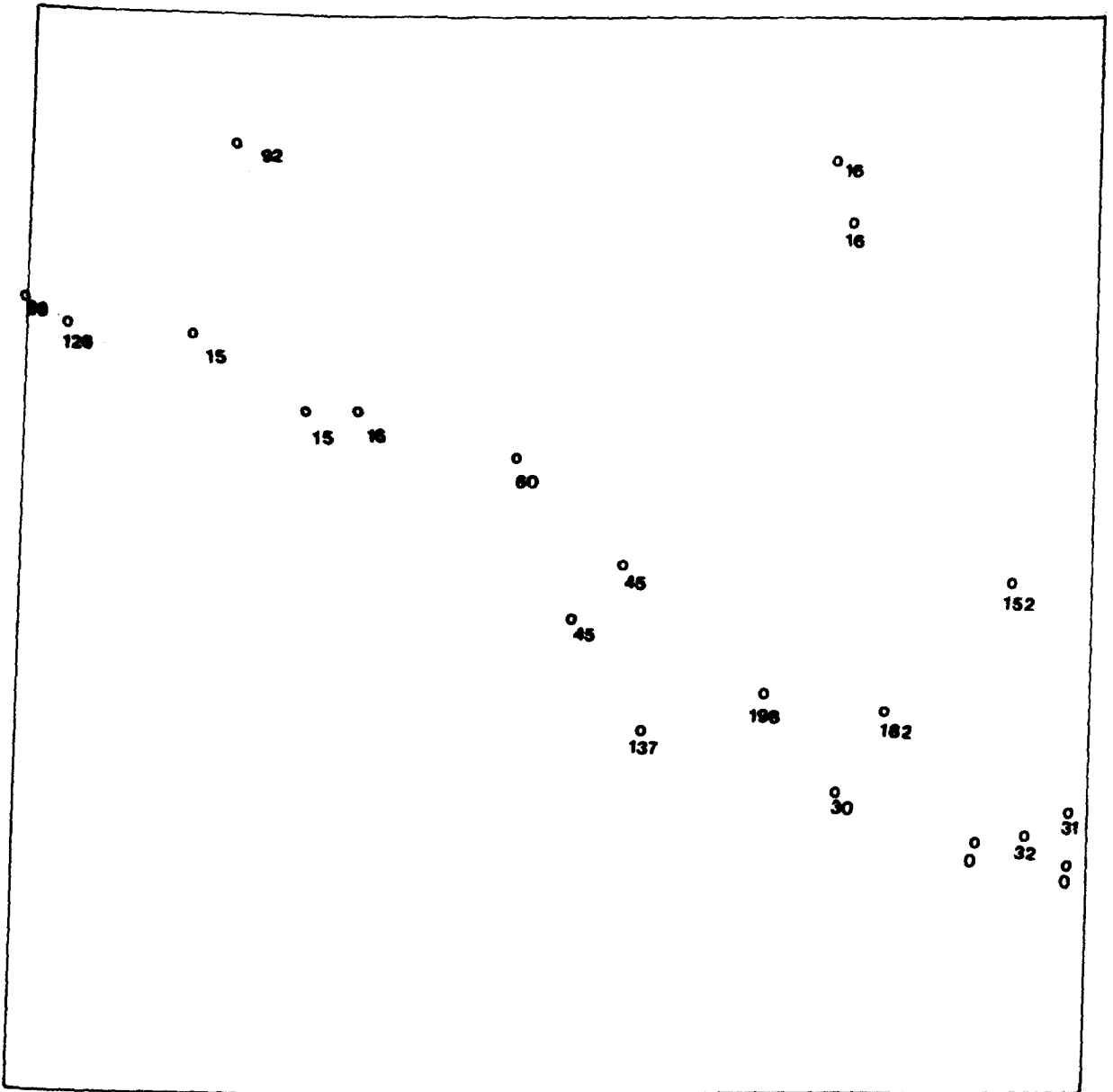
As can be seen from Fig 9.3, substantial residual errors occurred at most of the test points after the application of the simple linear conformal transformation. The largest components of these errors lie in the along-track direction. Since this type of transformation merely relates the radar image to the terrain without any geometric rectification, this suggests that large differential scale errors are present in this image. Since the affine transformation caters for the removal of any differential scaling between the along-track and cross-track directions, inspection of Fig 9.4, which represents the residual errors after the application of the affine transformation, further confirms the presence of substantial scale differences between the two directions in this survey processed image. Obviously, the

**VOLUME CONTAINS
CLEAR OVERLAYS**

**OVERLAYS HAVE
BEEN SCANNED
SEPERATELY
AND
THEN AGAIN OVER
THE RELEVANT PAGE**

Heights of Points (metres) above Mean-Sea-Level

Average Ground Height = 75m



**TEXT
BOUND INTO THE
SPINE**

VECTOR MAP OF EIGHTY-TWO ERRORS OF RIVER TAY AREA

(Survey Processed Image)

After the application of the Linear Conformal Transformation
with Least Squares Solution.
Heights of Points (metres) above Mean-Sea-Level

Average Ground Height = 75m

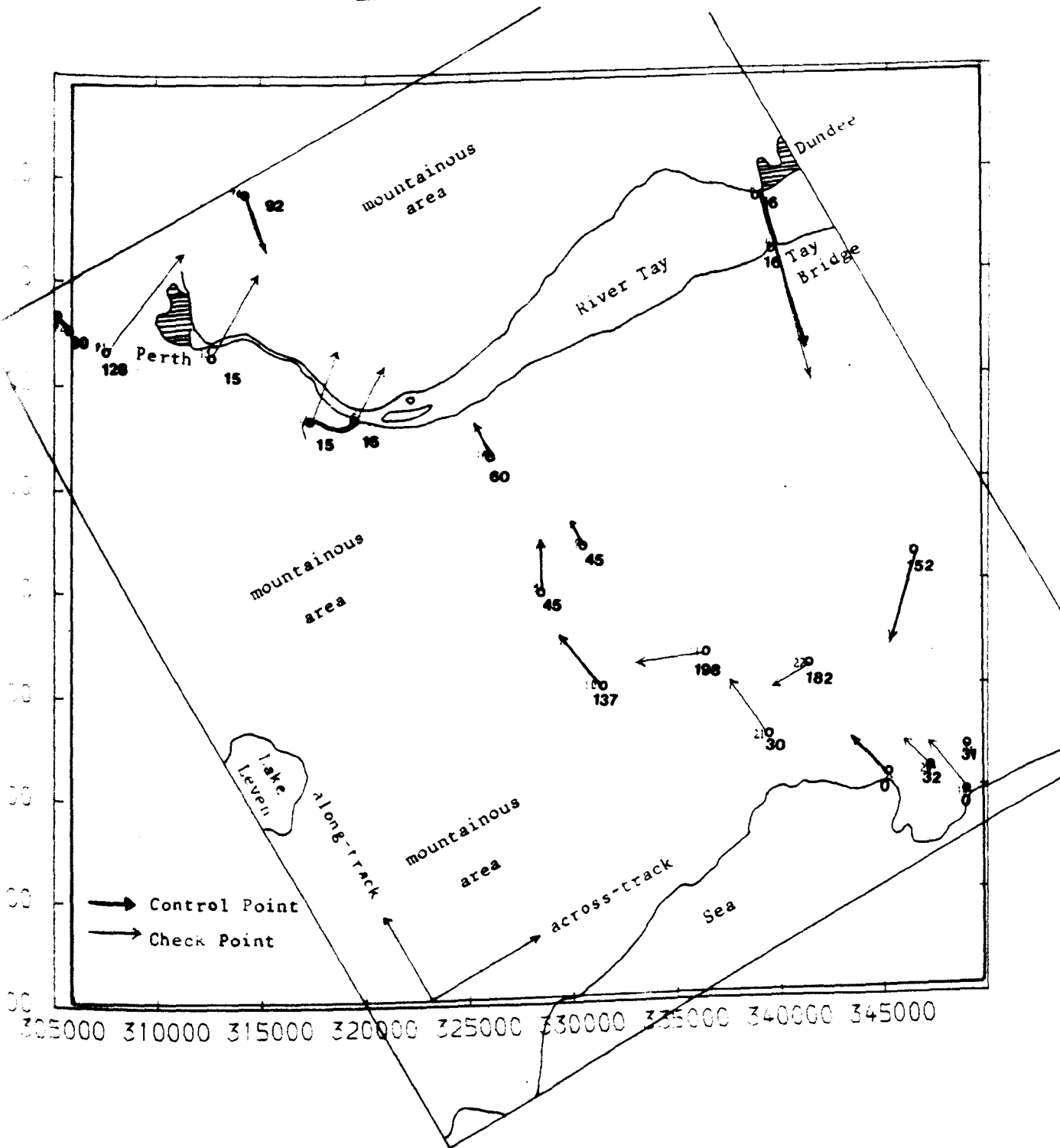


Fig 9.3

VECTOR MAP OF POSITION ERRORS OF RIVER TAY AREA

(Survey Processed Image)

After the application of the Linear Conformal Transformation with Least Squares Solution.

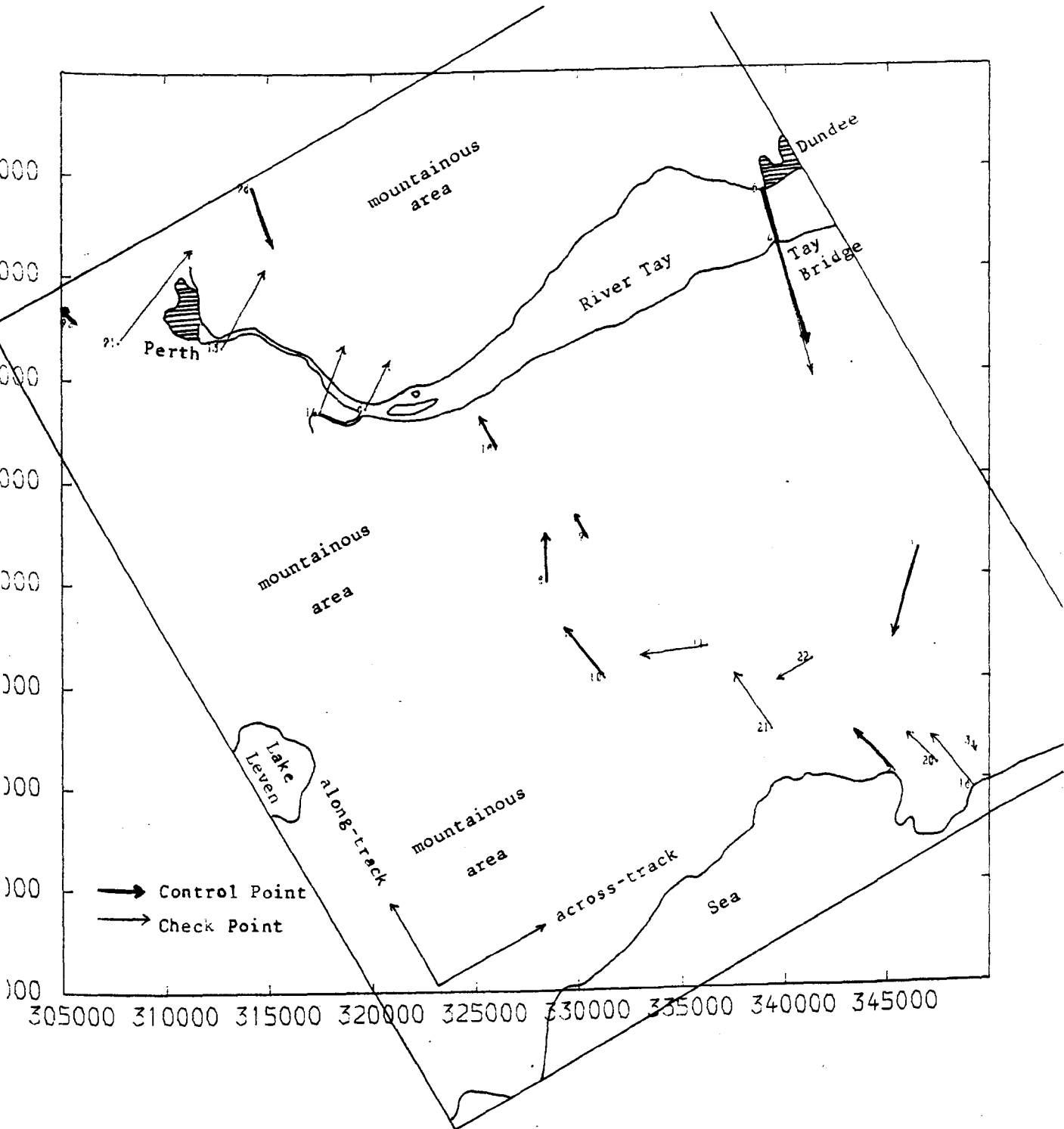


Fig 9.5

VECTOR MAP OF POSITION ERRORS OF RIVER TAY AREA

(Survey Processed Image)

After the application of the 4-term Polynomial Solution



Fig 9.6

VECTOR MAP OF POSITION ERRORS OF RIVER TAY AREA

(Survey Processed Image)
After the application of the 5-term Polynomial Solution

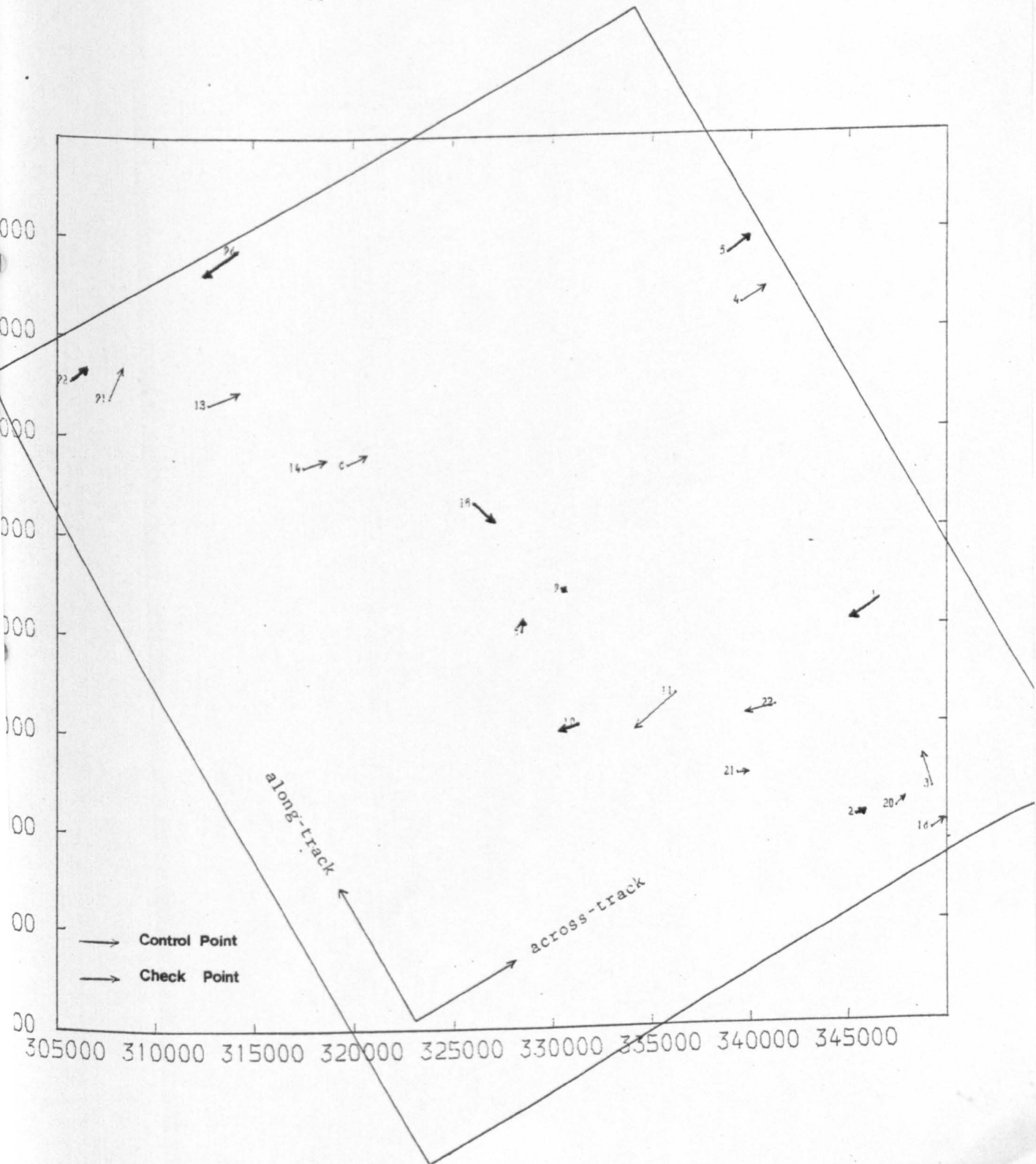


Fig 9.7

VECTOR MAP OF POSITION ERRORS OF RIVER TAY AREA

(Survey Processed Image)

After the application of the 6-term Polynomial Solution

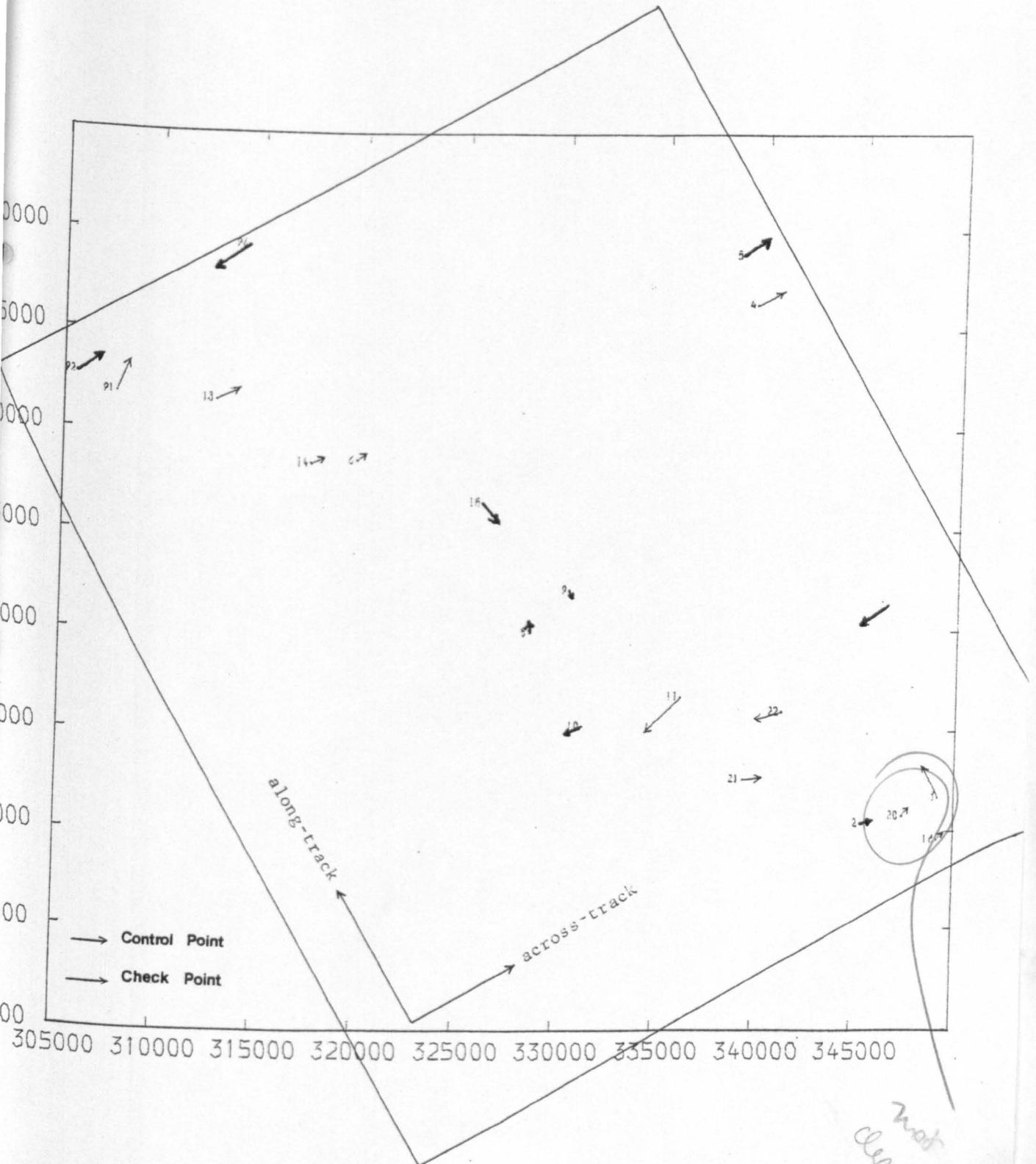


Fig 9.8

VECTOR MAP OF POSITION ERRORS OF RIVER TAY AREA

(Survey Processed Image)
After the application of
the 7-term Polynomial Solution

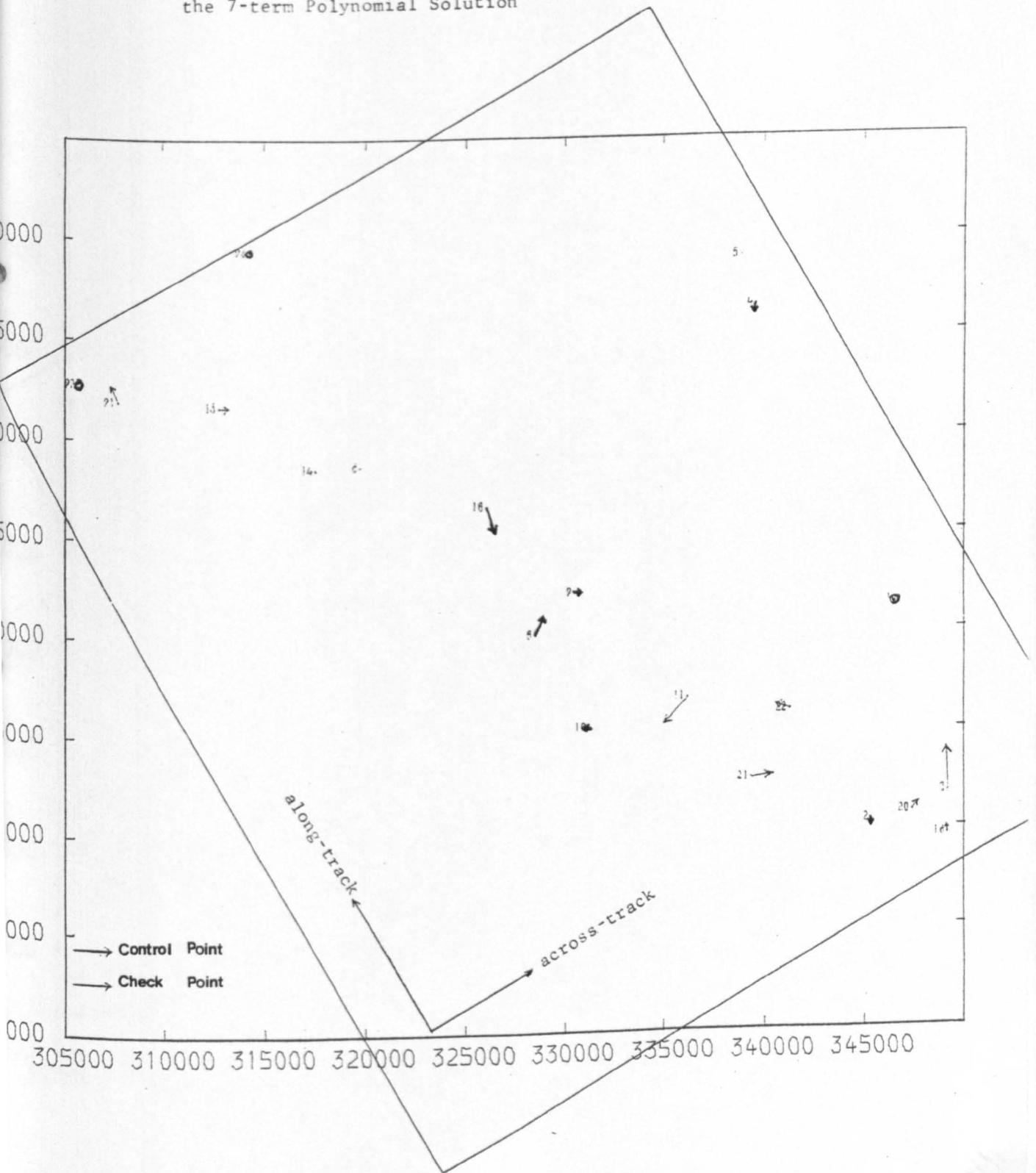
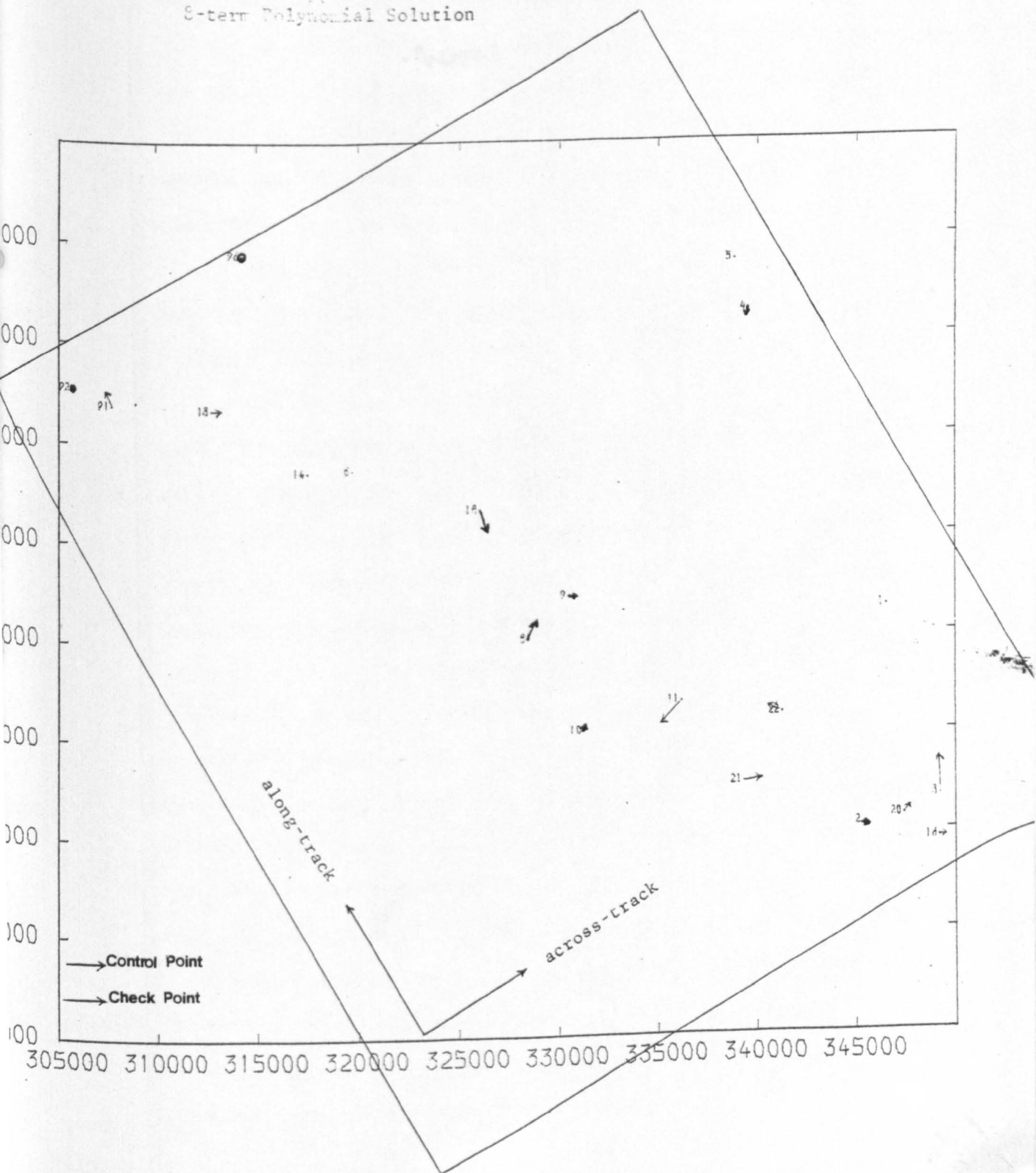


Fig 9.9

VECTOR MAP OF POSITION ERRORS OF RIVER TAY AREA

(Survey Processed Image)
After the application of the
8-term Polynomial Solution



errors present in Fig 9.4 are quite considerably smaller than those in Fig 9.3 and furthermore, the main component of the remaining errors has been changed in direction to across-track (either inwards or outwards) after the application of the affine transformation.

Inspection of Fig 9.4 shows that most of these residual errors are again of a systematic nature. From the overlay placed over Fig 9.4, it will be seen that the average ground height of the points on this image is of the order of 75 m so that half of the points lie above this level while the others lie below it. Further inspection of Fig 9.4 and its overlay shows that the majority of points lying below the 75 m level have vector errors pointing outwards in the cross-track direction while the points having heights above this level have vector errors pointing inwards in the cross-track direction. This clearly points to the effect of the terrain topography on the overall accuracy of this image. There appears to be a strong correlation between the accuracy of individual points as measured on the survey processed imagery and their topographic heights. From inspection of the further series of diagrams (Figs 9.5 to 9.9), it is apparent that the use of polynomials of varying degrees removes the effects of topography to a considerable extent, provided always that a suitable density of well-distributed control points is available for the determination of the transformation parameters. The most effective of all are those polynomials which have the highest number of terms - as can be seen from inspection of Figs 9.8 and 9.9. In these, the pattern of residual errors is quite random. Taking into account the relatively unsophisticated method of optical processing by which this survey processed image has been produced, and the rather poor resolution, the results of applying a geometric rectification through the use of polynomial transformations can be regarded as satisfactory.

9.1.4 Detailed Analysis of Results from the Precision Processed Image

The vector plots of the positional errors obtained after testing this image are shown as Figs 9.10 to 9.16. A very similar sequence to that of the survey-processed image can be traced. After the application of the simple linear conformal transformation (Fig 9.10), relatively large residual errors still remained at most points. Most of these errors appeared to have substantial components lying either in the direction of the satellite track or at right angles to it. When an affine transformation was applied, the errors were again substantially reduced (Fig 9.11) and most of the individual errors still present in the image were oriented in the direction perpendicular to that of the satellite track. Again, this points to the occurrence of differential scale errors in the original unrectified image and their effective removal through the application of the affine transformation. An overlay which shows the heights of the individual test points has been placed on top of Fig 9.11. The average height of the test points is of the order of 73 m. Inspecting Fig 9.11, it can be seen that the majority of these points lying below this level again have positional vector errors pointing away from the antenna in the cross-track direction while those points with elevations higher than this value have vectors pointing towards the satellite, as would be expected from relief layover. This is again an indication of the effects of the ground topography on the accuracy of the positions of the test points.

Further inspection of Figs 9.12 and 9.13 reveals that the test points still exhibit the same systematic pattern of residual errors in the cross-track direction after the application of the four-term and five-term polynomial transformations. Examination of Figs 9.14, 9.15 and 9.16 shows that, after the application of the six-

Heights of Points (metres) above Mean-Sea-Level

Average Ground Height = 73m

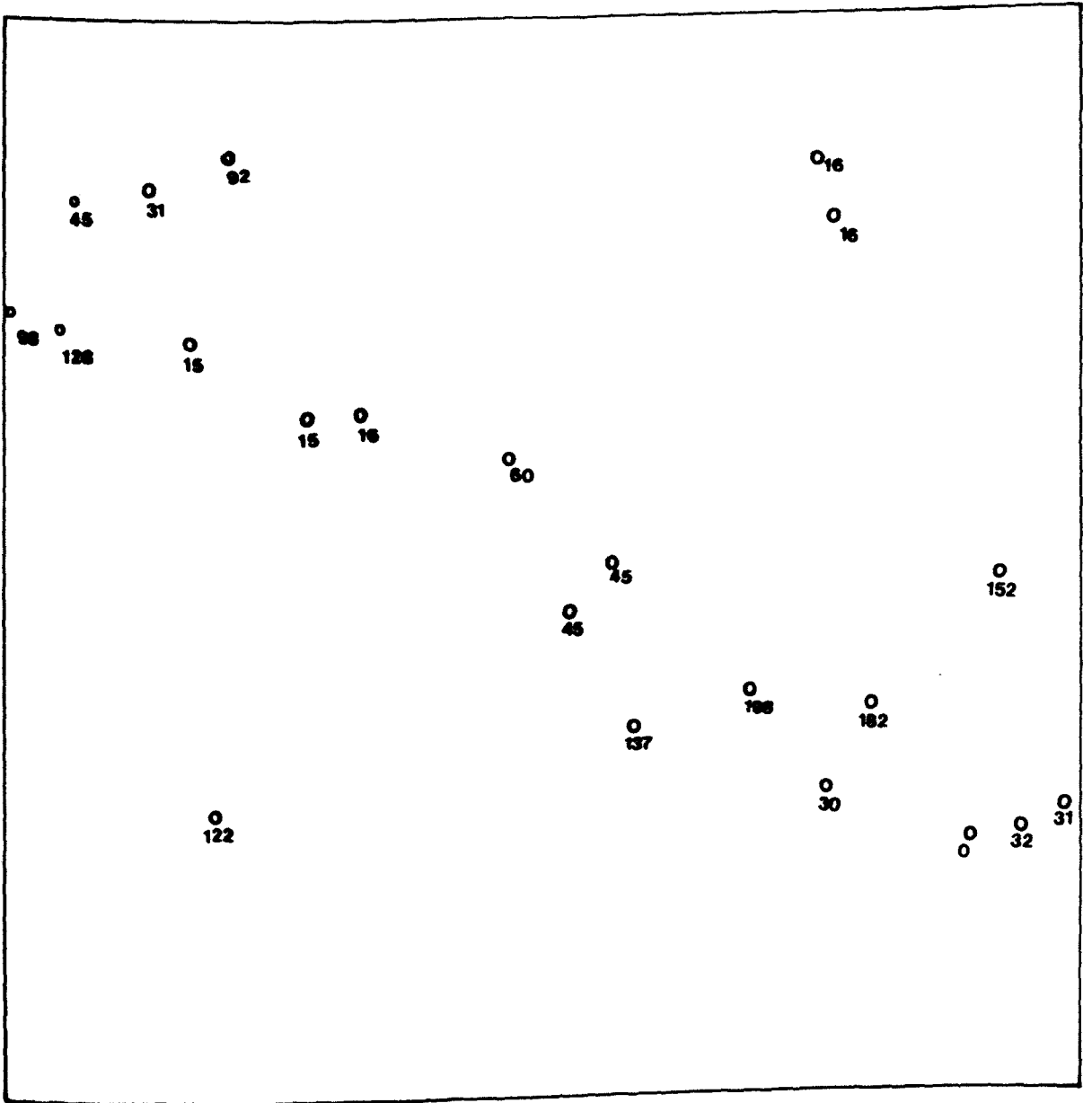
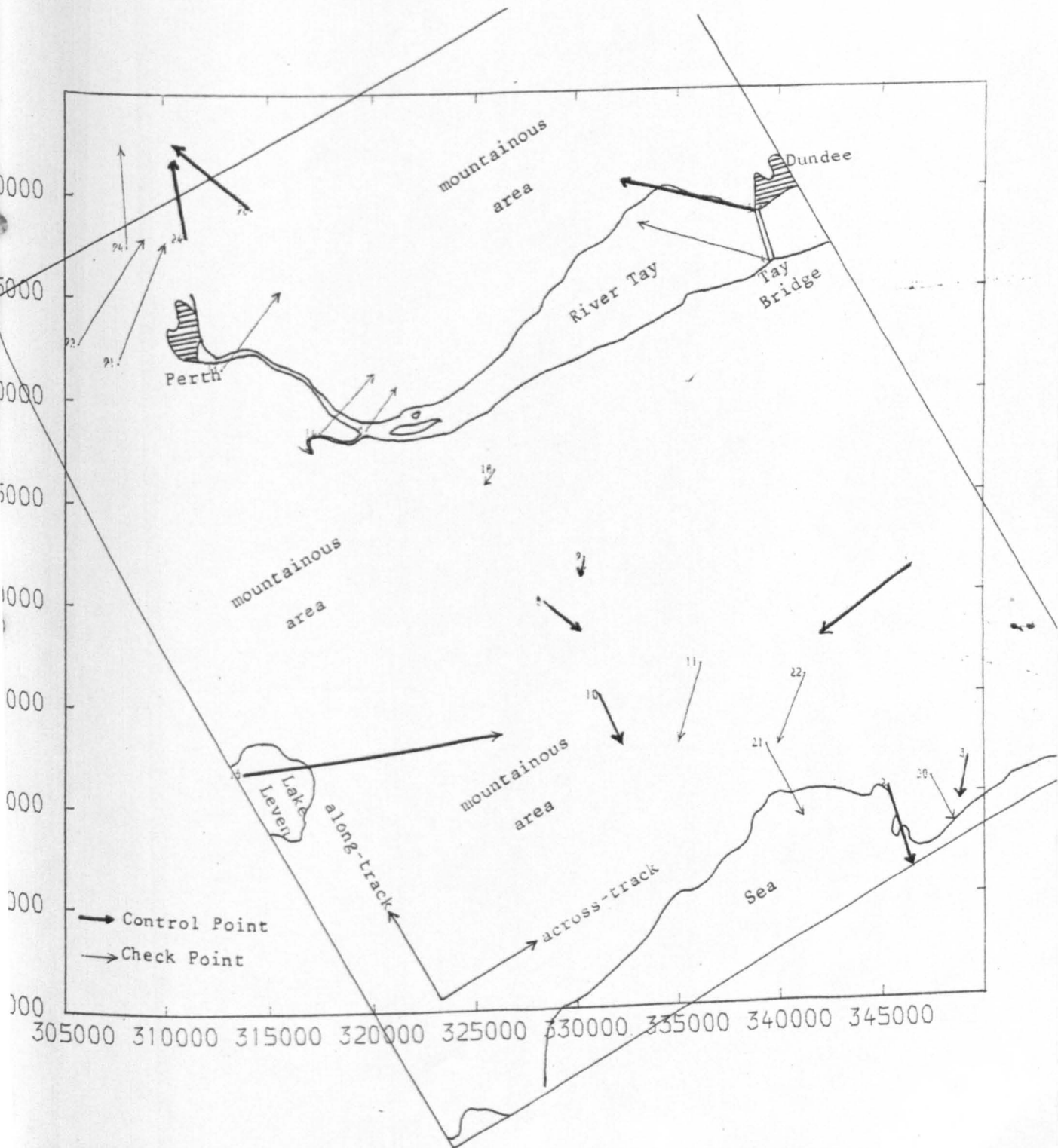


Fig 9.10

VECTOR MAP OF POSITION ERRORS OF RIVER TAY AREA

(Precision Processed Image)

After the application of the Linear Conformal Transformation with Least Squares Solution



VECTOR MAP OF POSITION ERRORS OF RIVER TAY AREA

Heights of Points (metres) above Mean-Sea-Level

After the application of the Linear Conformal Transformation with Least Squares Average Ground Height = 73m

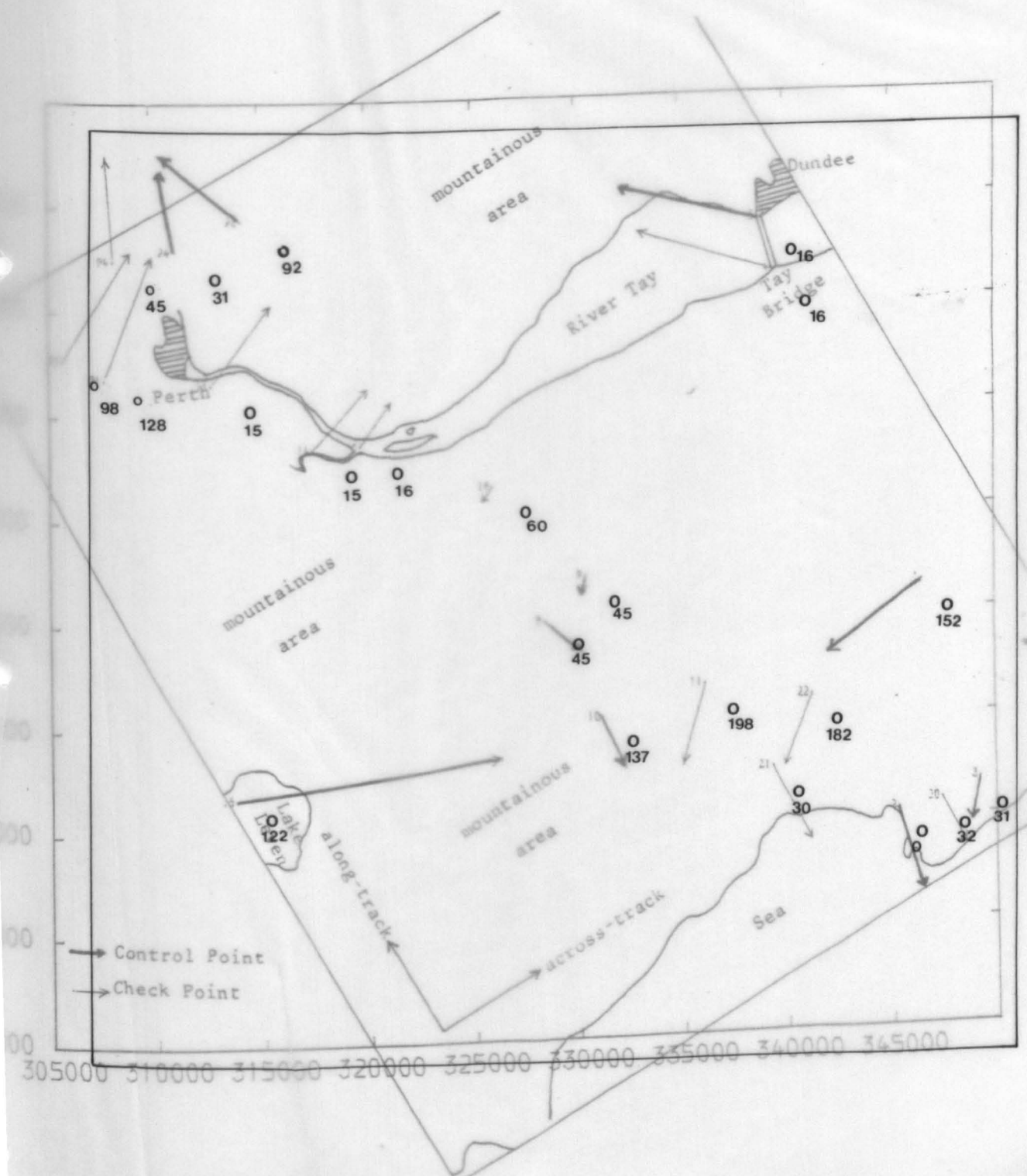


Fig 9.11

VECTOR MAP OF POSITION ERRORS OF RIVER TAY AREA

(Precision Processed Image)
After the application of the 3-term Polynomial Solution
(Affine Transformation)

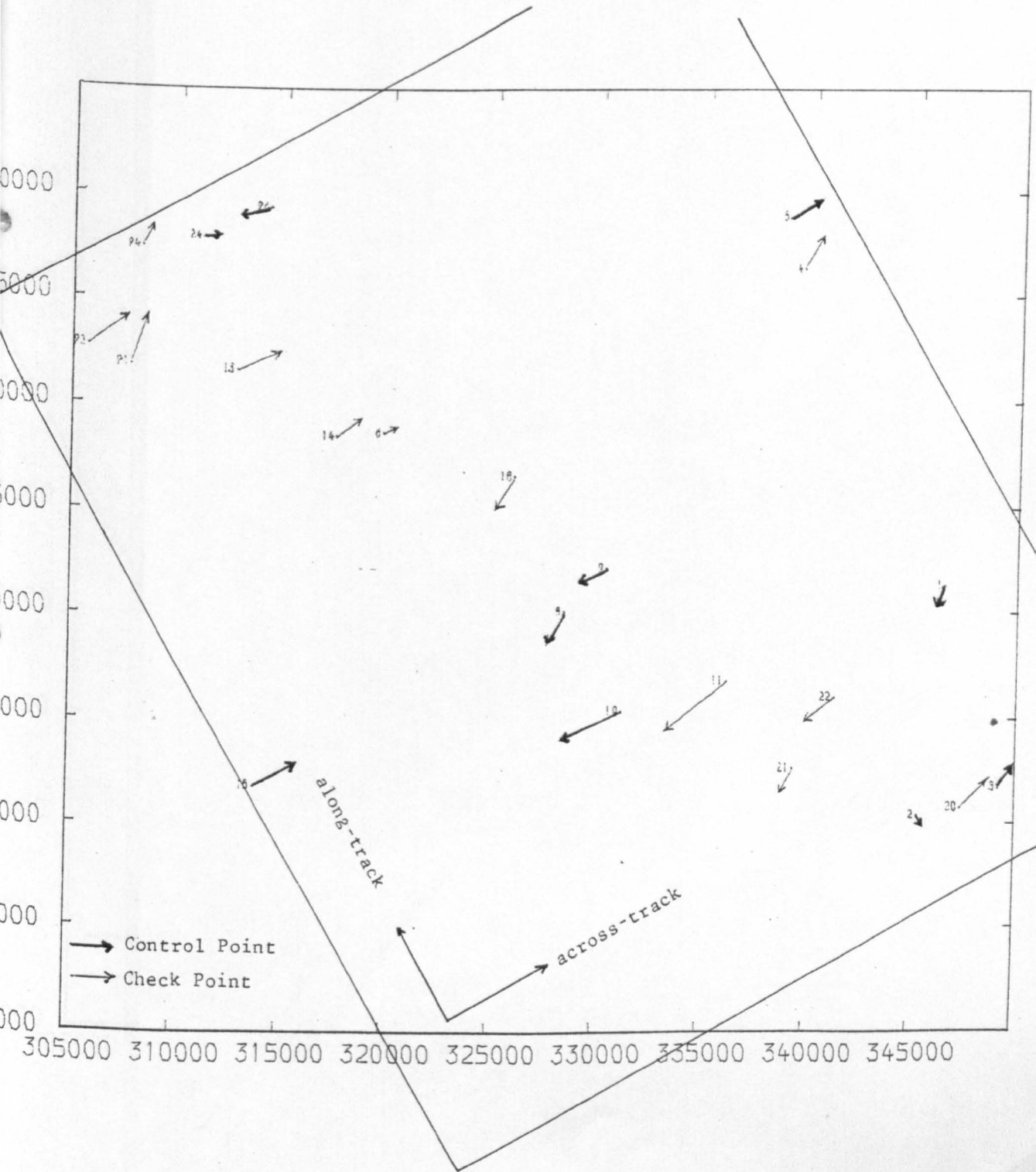


Fig 9.12

VECTOR MAP OF POSITION ERRORS OF RIVER TAY AREA

(Precision Processed Image)

After the application of the 4-term Polynomial Solution

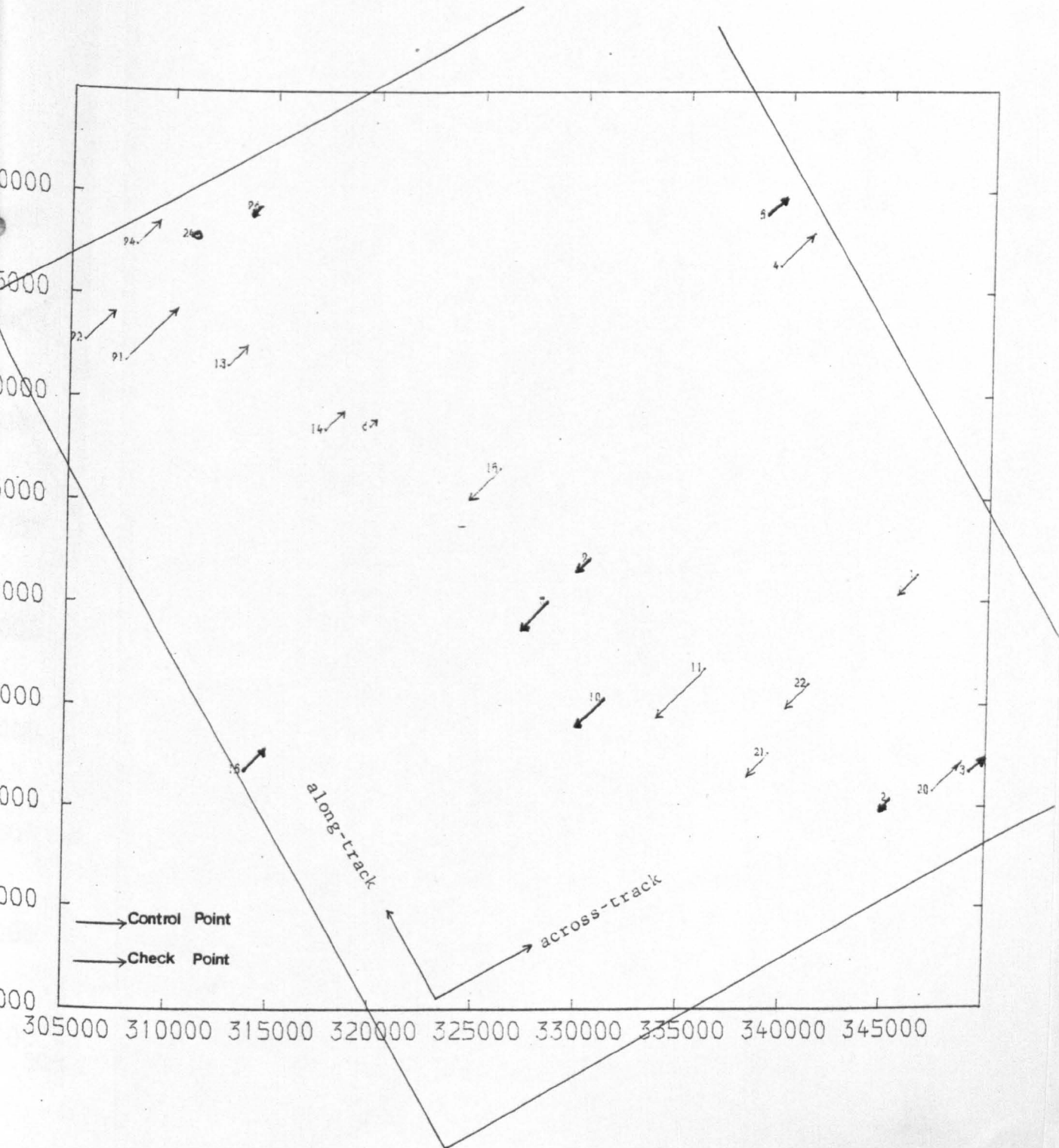


Fig 9.13

VECTOR MAP OF POSITION ERRORS OF RIVER TAY AREA

(Precision Processed Image)
After the application of the 5-term Polynomial Solution

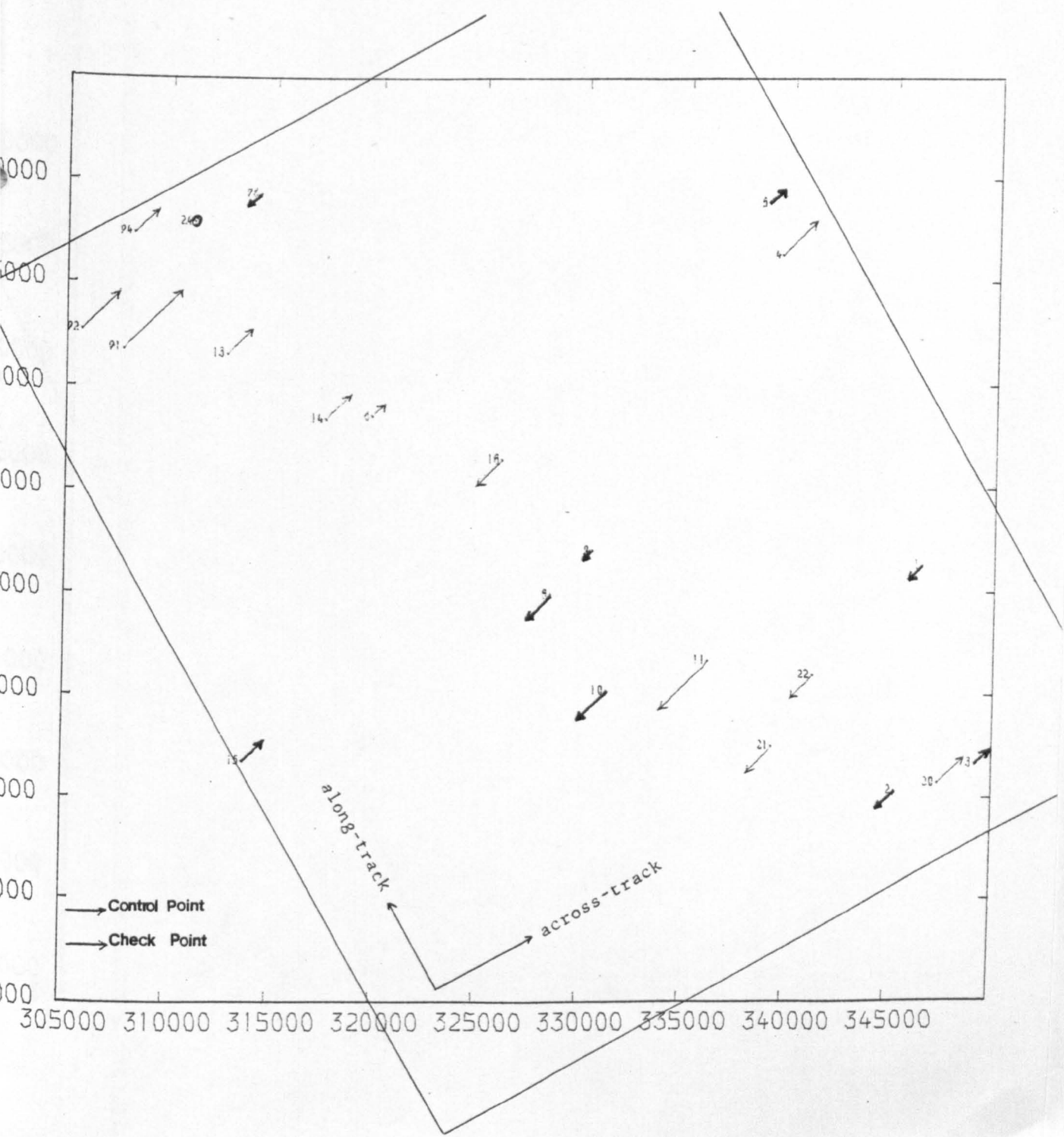


Fig 9.14

VECTOR MAP OF POSITION ERRORS OF RIVER TAY AREA

(Precision Processed Image)

After the application of the 6-term Polynomial Solution

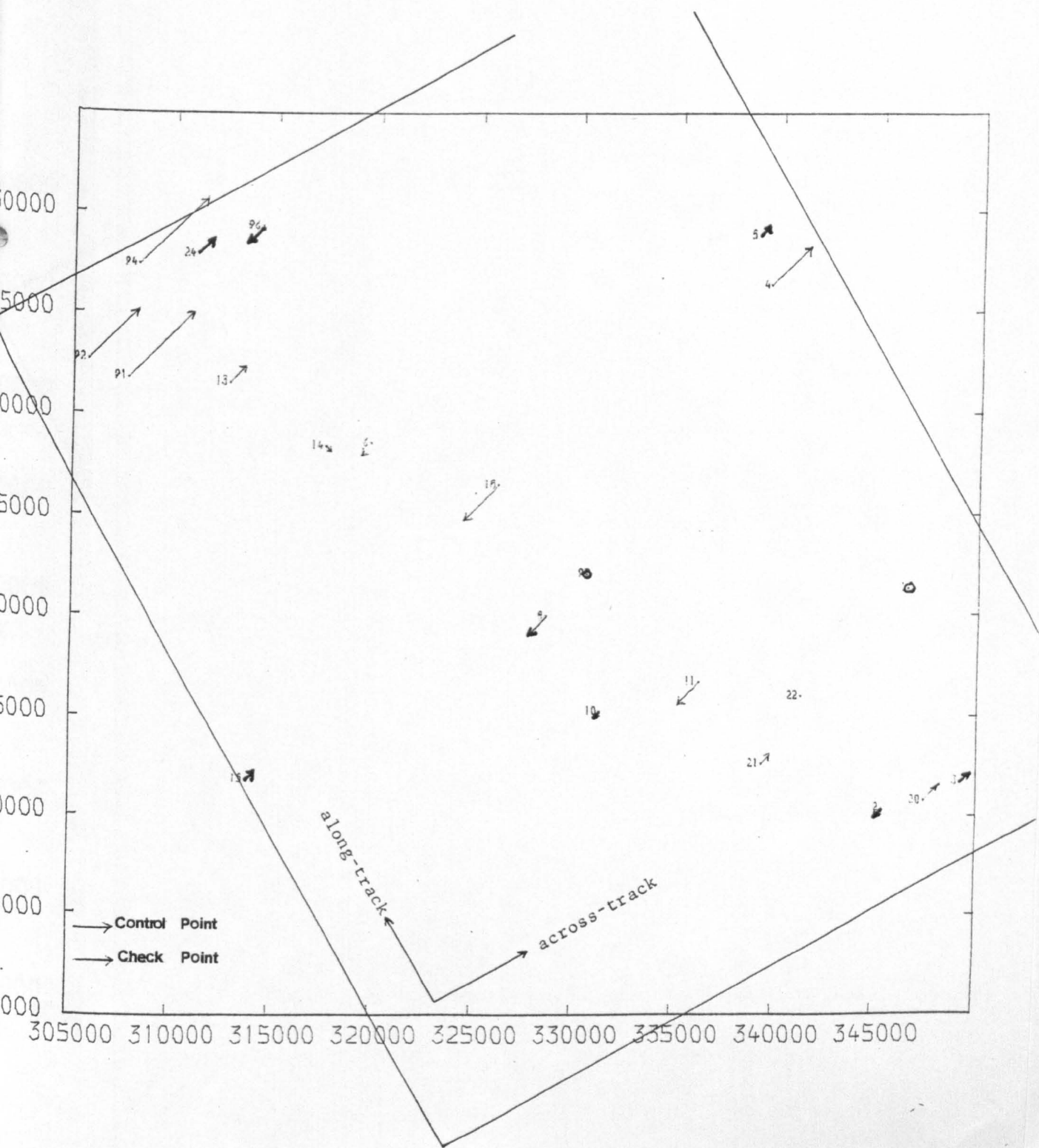


Fig 9.15

VECTOR MAP OF POSITION ERRORS OF RIVER TAY AREA

(Precision Processed Image)
After the application of the 7-term Polynomial Solution

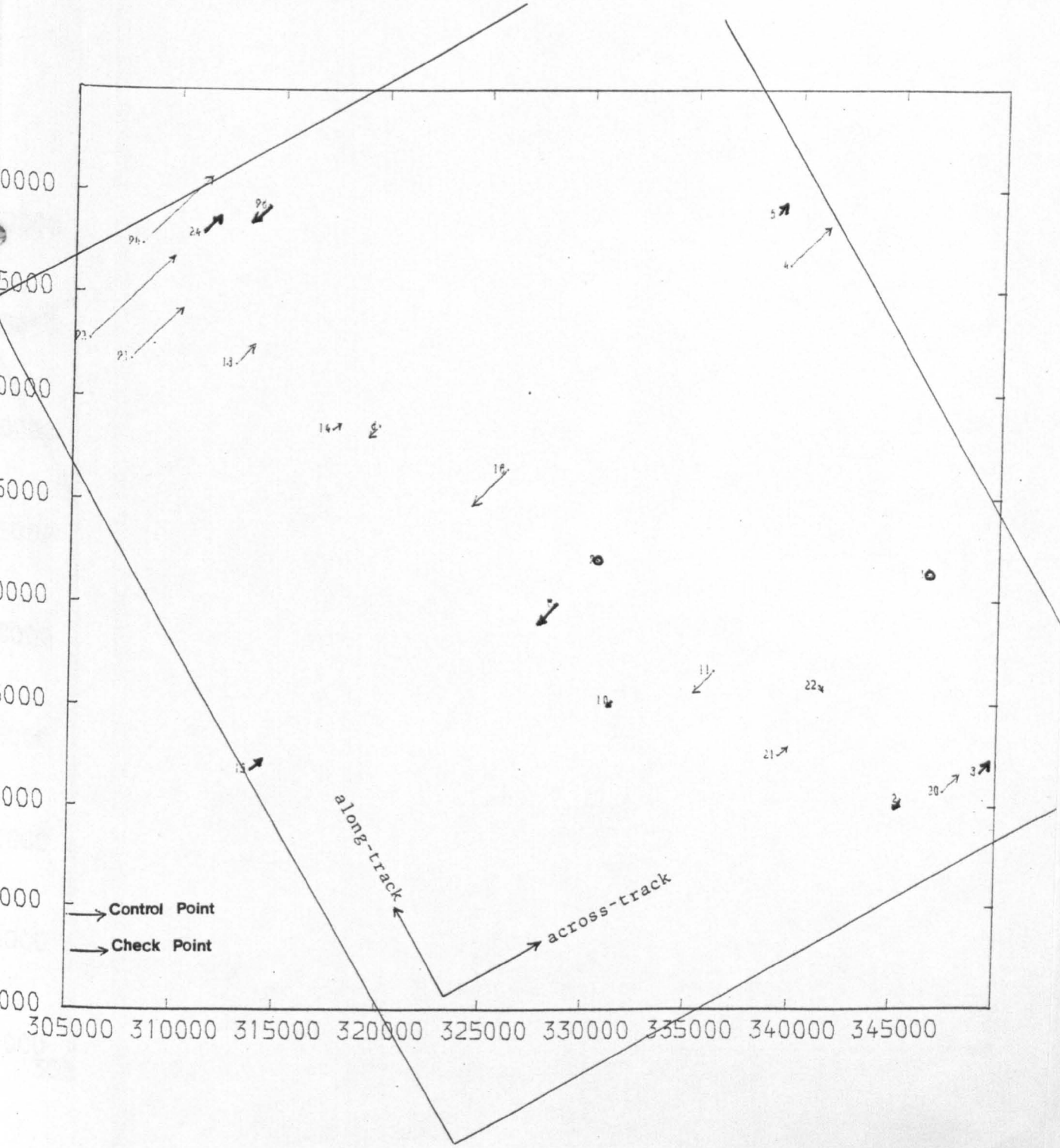
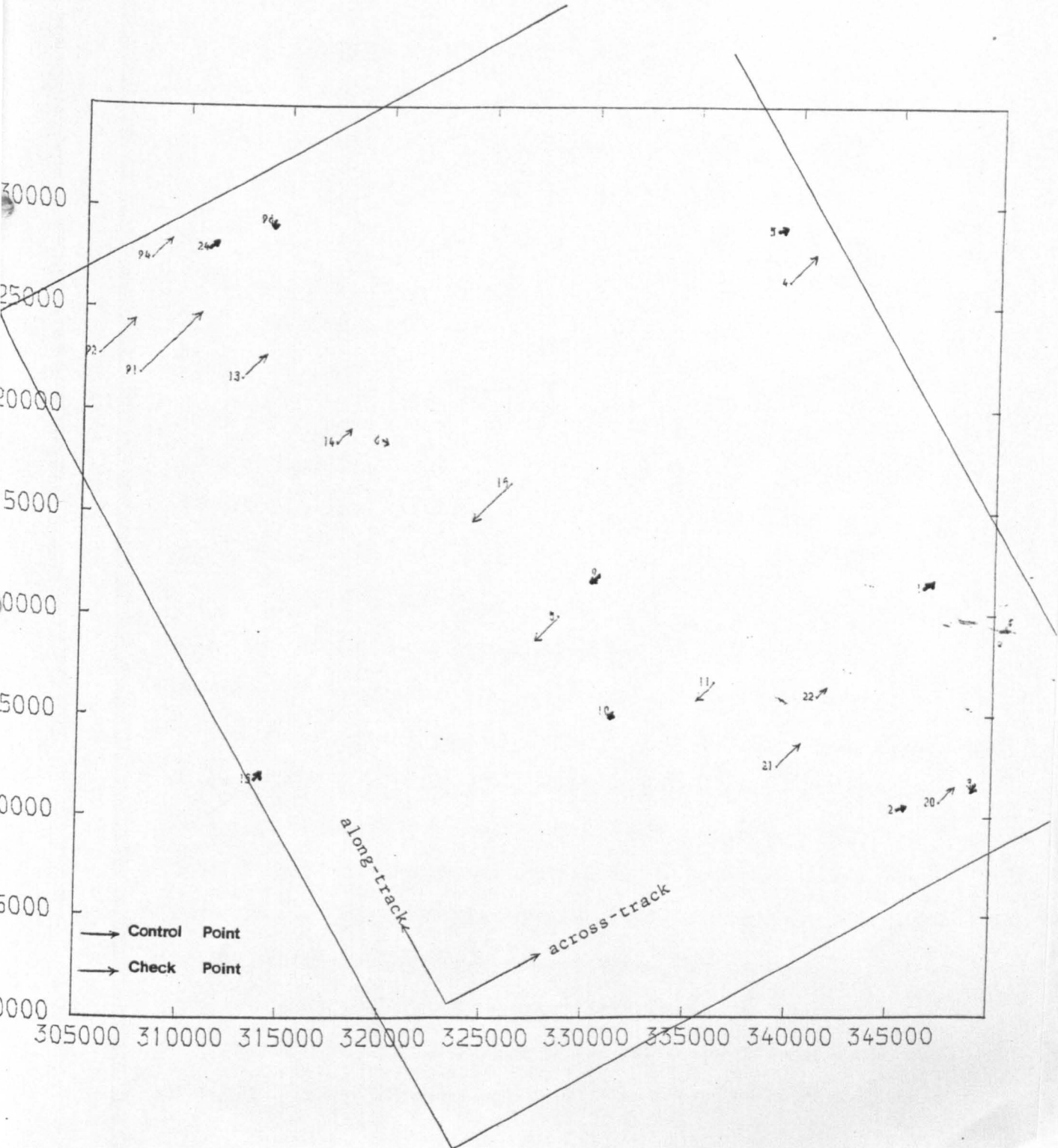


Fig 9.16

VECTOR MAP OF POSITION ERRORS OF RIVER TAY AREA

(Precision Processed Image)
After the application of the
8-term Polynomial Solution



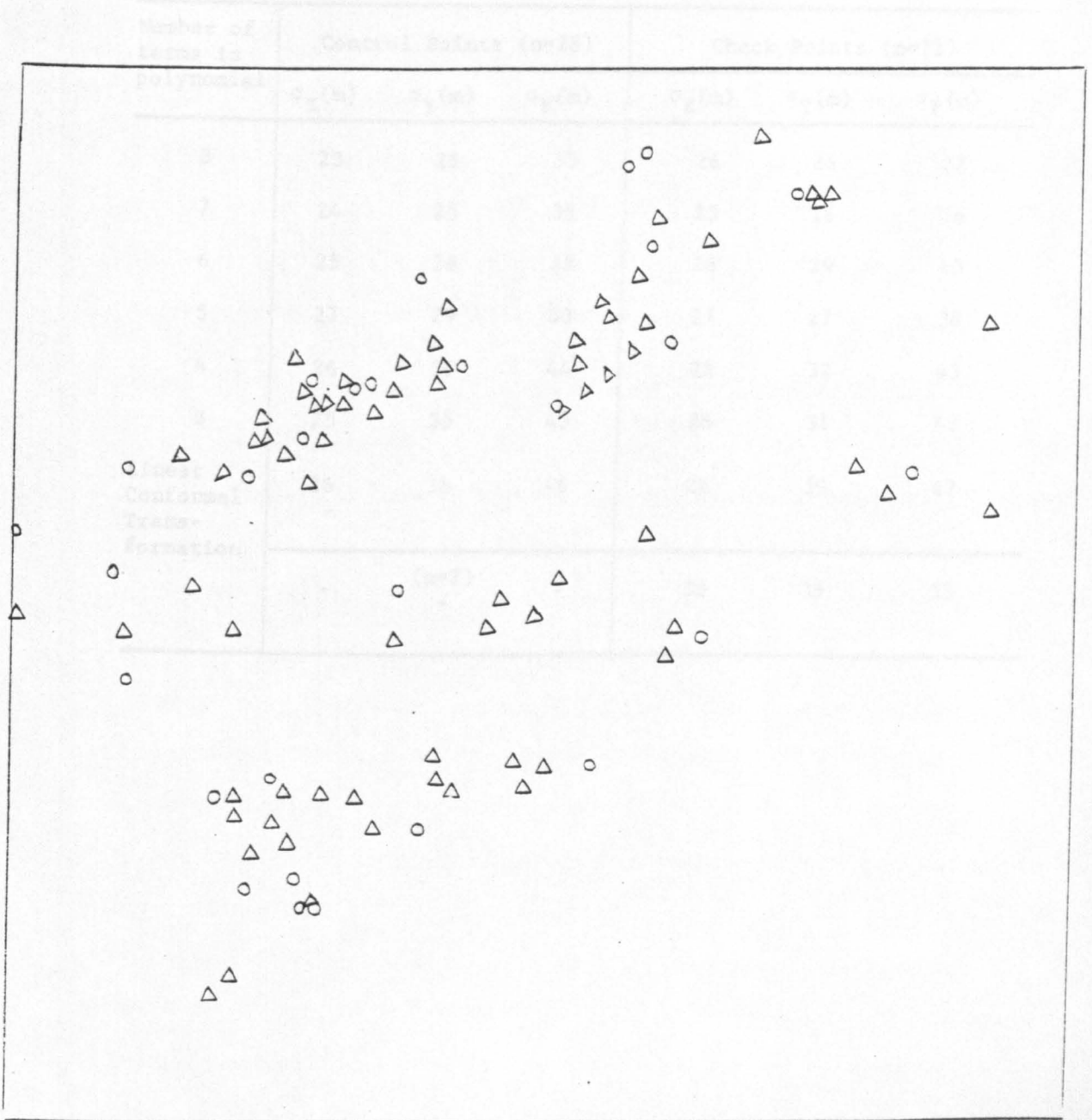
term, the seven-term and the eight-term polynomial solutions, the overall extent of the residual errors is reduced considerably, although quite a number of the test points still retain the systematic pattern of errors in the cross-track direction.

9.2 Results from the East Anglia Test Area

The digital processing carried out by the RAE resulted in a noticeably higher resolution and quality of the East Anglian image as compared with the two optically processed images of the River Tay test area. This factor, combined with the much larger number of points exhibiting a definite and interpretable character, allowed a far greater number of points (105) to be identified for accuracy testing. Of these, no less than 99 were retained after initial testing. Twenty-eight of these points were used as control points for the determination of the transformation parameters, leaving seventy-one points available for use as check points. The distribution of these points is shown in Fig 9.17.

As before, Table 9.3 summarises the root mean square errors (r.m.s.e. values) of the discrepancies at the control and check points in metres at the ground scale. The table is largely self-explanatory, but some brief comments may be made about the results. The discrepancies at the control points were small overall. In the X-direction, there was a small insignificant range in the residual values of only four metres between the results using different combinations of polynomial terms. In the lateral (Y) direction, there is a slight but perceptible rise in the error values as successive terms were truncated. When the polynomial was restricted to three or four terms, the cross-track accuracy had reduced by less than half a resolution element where one resolution element is equivalent to 20 m at ground scale in the case of

TABLE 9.1 RESULTS OF DIGITALLY PROCESSED IMAGE OF THE EAST ANGLIA TEST AREA



- control point
- △ check point

Fig 9.17 Control distribution pattern on East Anglia test area image

TABLE 9.3 RESULTS OF DIGITALLY PROCESSED IMAGE OF THE EAST ANGLIA
TEST AREA

Number of terms in polynomial	Control Points (n=28)			Check Points (n=71)		
	$\sigma_X(m)$	$\sigma_Y(m)$	$\sigma_P(m)$	$\sigma_X(m)$	$\sigma_Y(m)$	$\sigma_P(m)$
8	23	26	35	26	26	37
7	24	25	35	25	26	36
6	25	28	38	28	29	40
5	27	29	40	27	27	38
4	26	36	44	28	32	43
3	25	35	43	28	31	42
Linear Conformal Trans- formation	26	38	46	26	39	47
	-	(n=2) -	-	36	38	52

this digitally processed imagery. The vector planimetric error ranged from ± 35 m to ± 44 m. Even when using the simple linear conformal transformation, the residual errors at the control points were of the same order as those using three or four terms.

At the check points, again the along-track accuracy remained nearly the same for every case tested and so did the across-track accuracy. The planimetric point accuracy ranged from ± 36 m with the polynomial having seven or eight terms to ± 43 m with the polynomial restricted to three terms only. As the table shows, the errors at the check points hardly varied at all from those which were obtained at the corresponding group of control points.

9.2.1 Detailed Analysis of Results from the East Anglia Digitally Processed Image

Figs 9.18 to 9.24 are the vector diagrams of the individual errors obtained after applying the series of polynomial transformations to the test points of the East Anglian image. It should be noted that, since the overall magnitude of these errors is smaller, the scale at which they have been represented is five times larger (1:7,000 scale versus 1:35,000) than the scale used to represent the errors on the River Tay images.

As can be seen from the diagrams, for each solution, the magnitudes of the residual errors at all points are small but continuously and slowly reducing as the degree of the polynomial transformation increases. Starting with Fig 9.18 which represents a linear conformal transformation, although most of the errors point in the cross-track direction (either inwards or outwards), these errors are relatively higher in magnitude than those obtained in the other solutions. Inspection of Fig 9.19, which represents the pattern of residual errors

VECTOR MAP OF POSITION ERRORS OF EAST ANGLIA AREA

After the application of the Linear Conformal Transformation with Least Squares Solution.

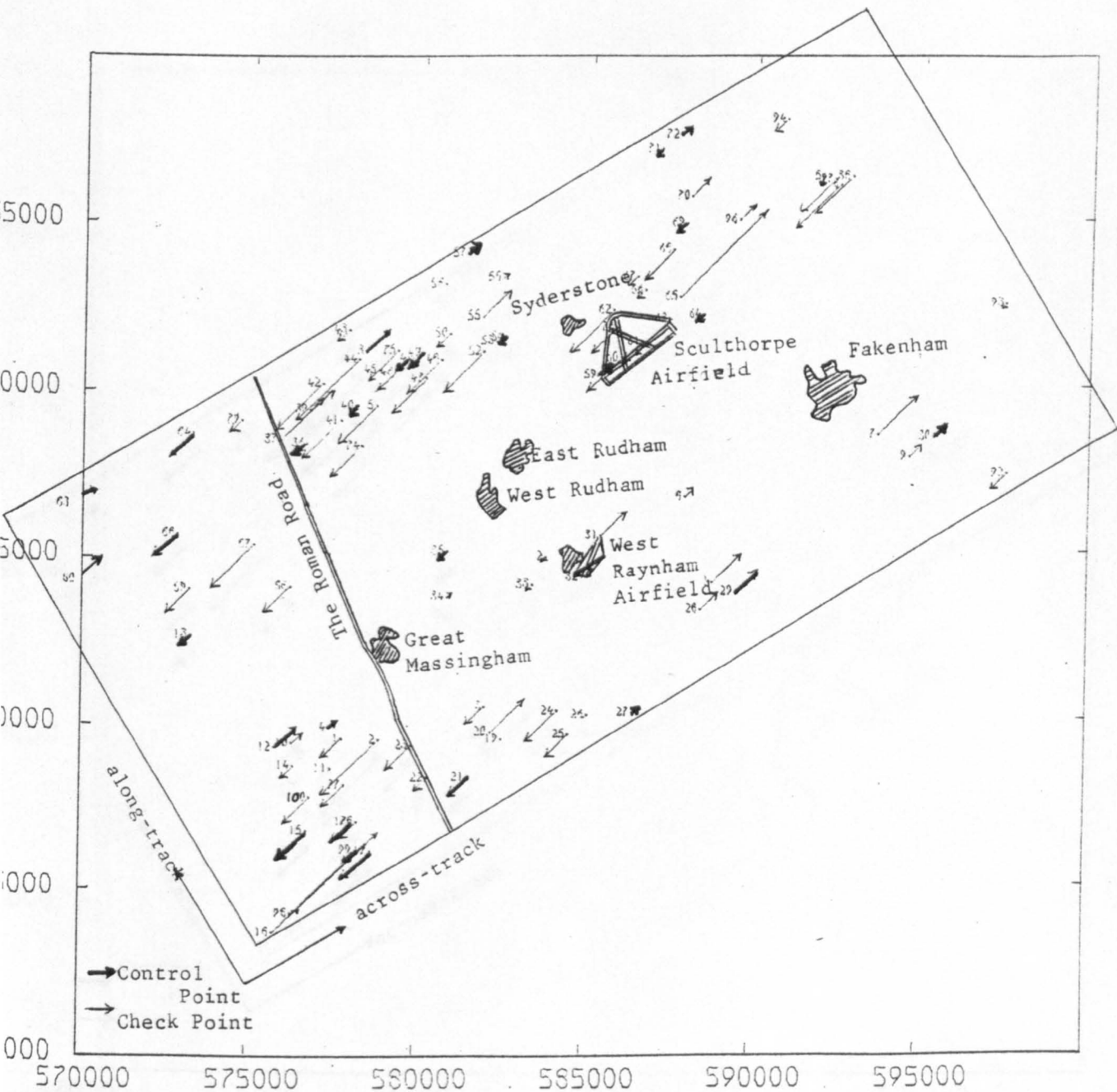


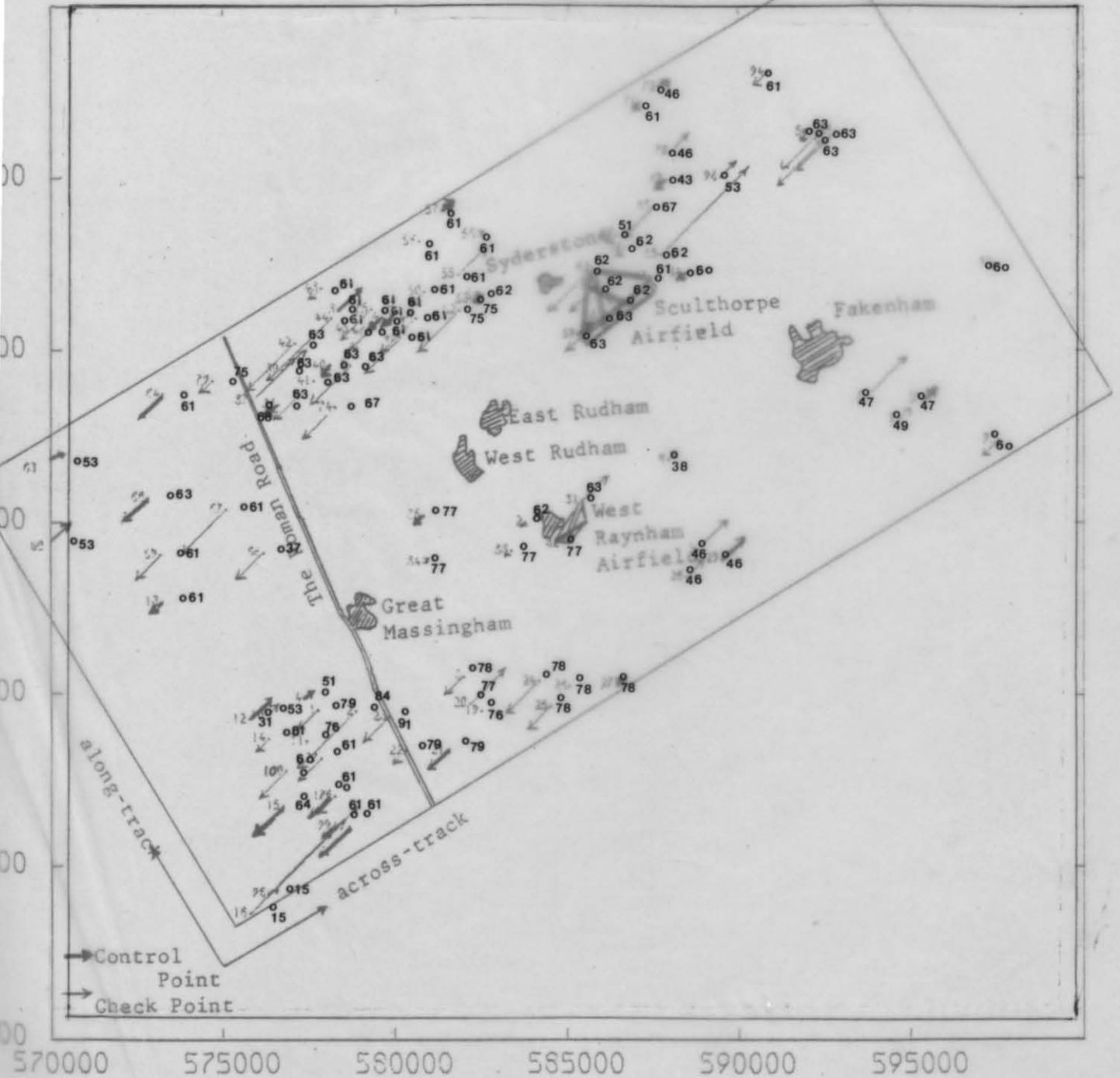
Fig 9.18

VECTOR MAP OF POSITION ERRORS OF EAST ANGLIA AREA

After the application of the Linear Conformal Transformation with Least Squares Solution.

Heights of Points (metres) above Mean-Sea-Level

Average Terrain Elevation = 55m



VECTOR MAP OF POSITION ERRORS OF EAST ANGLIA AREA

After the application of the 3-term Polynomial Solution
(Affine Transformation)

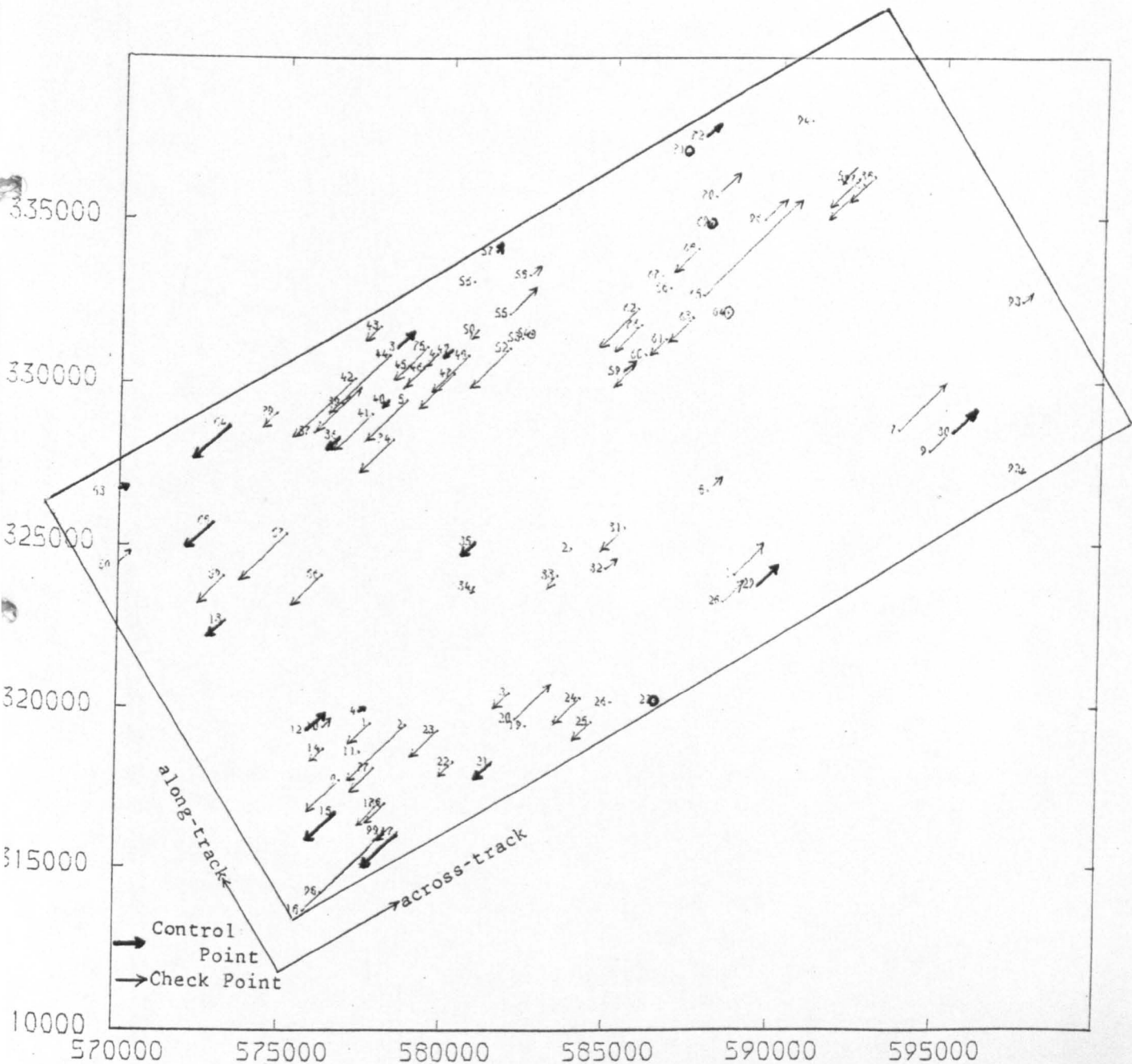


Fig 9.20

VECTOR MAP OF POSITION ERRORS OF EAST ANGLIA AREA

After the application of the 4-term Polynomial Solution

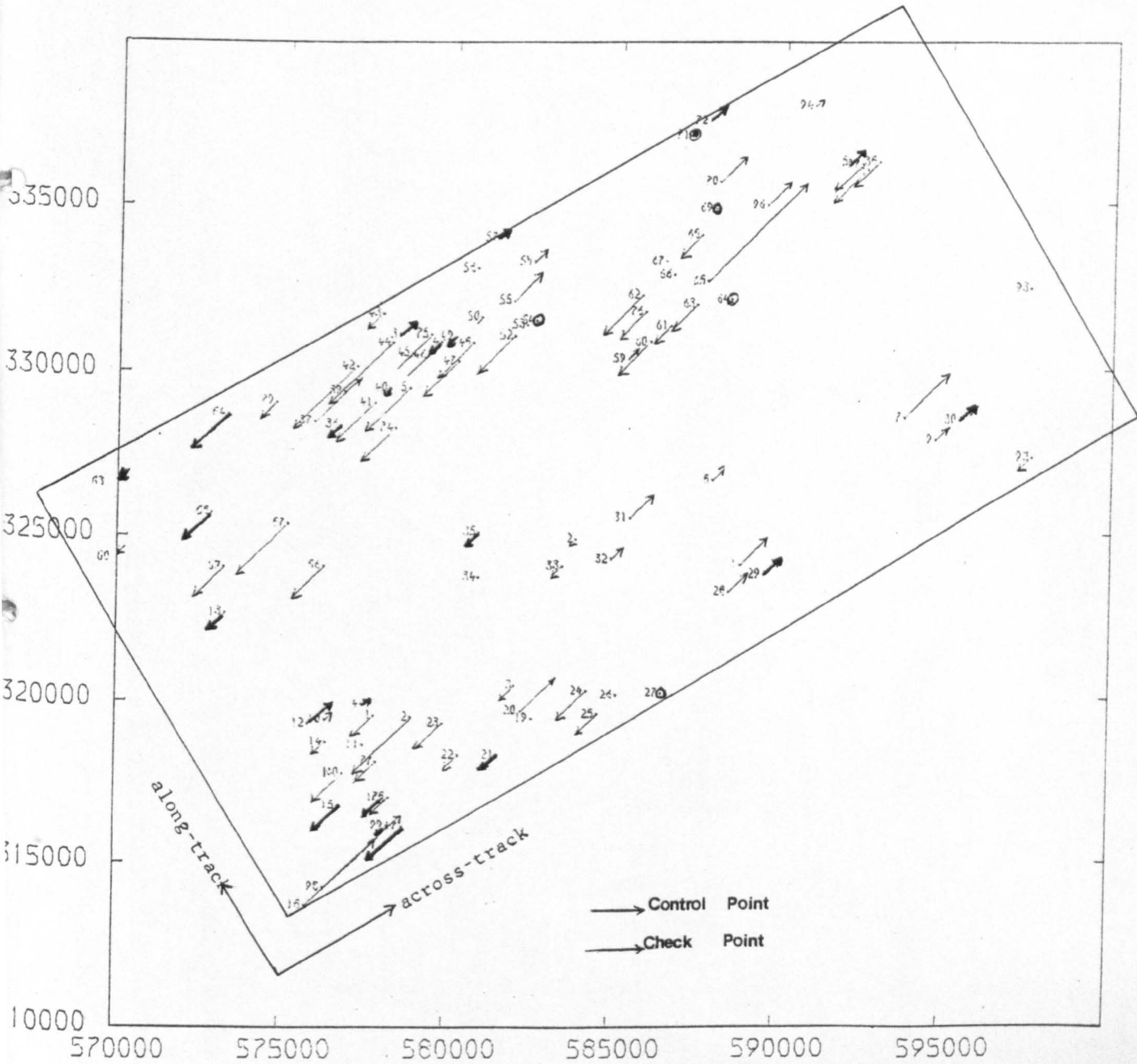


Fig 9.21

VECTOR MAP OF POSITION ERRORS OF EAST ANGLIA AREA

After the application of the 5-term Polynomial Solution

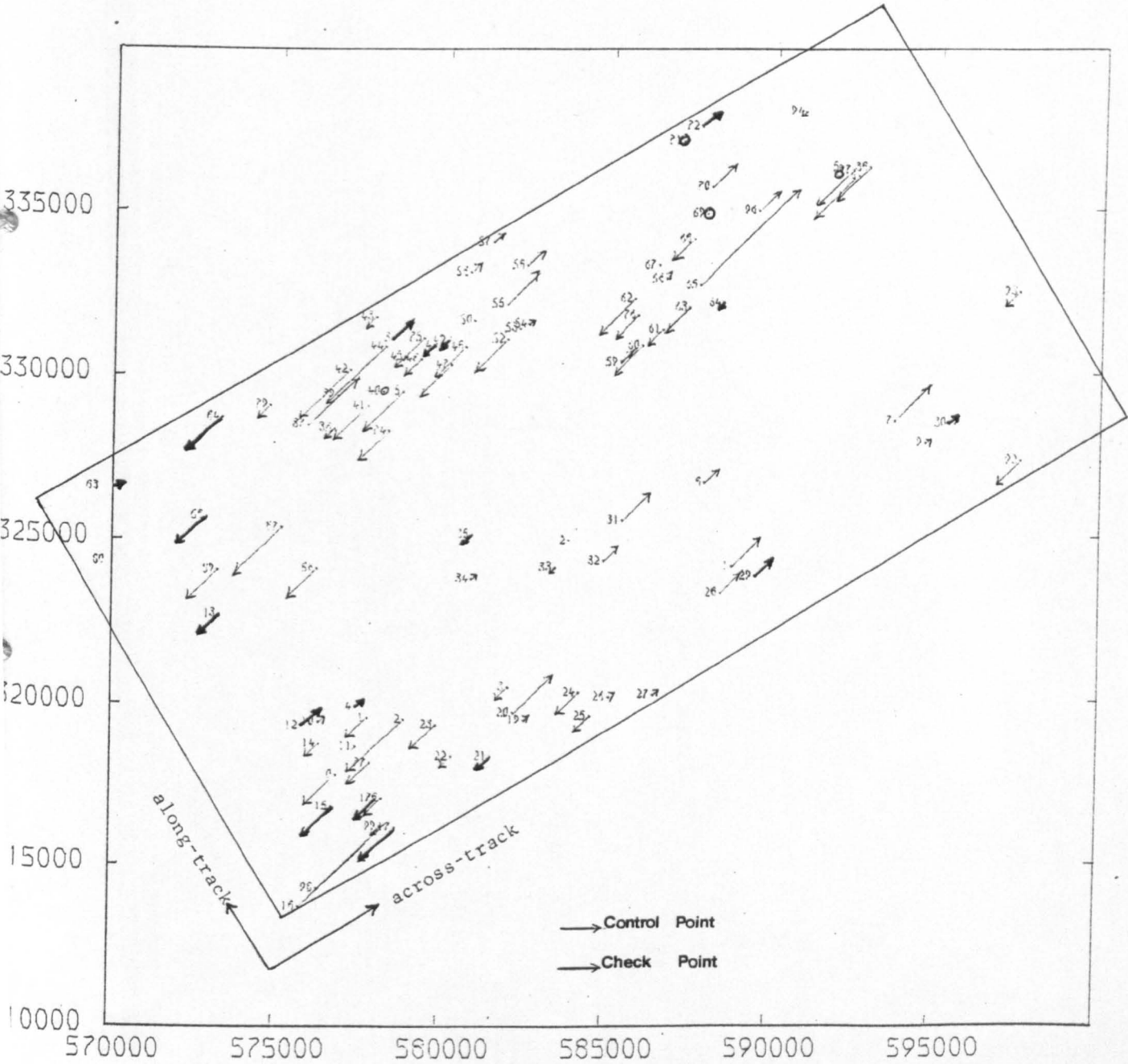


Fig 9.22

VECTOR MAP OF POSITION ERRORS OF EAST ANGLIA AREA

After the application of the 6-term Polynomial Solution

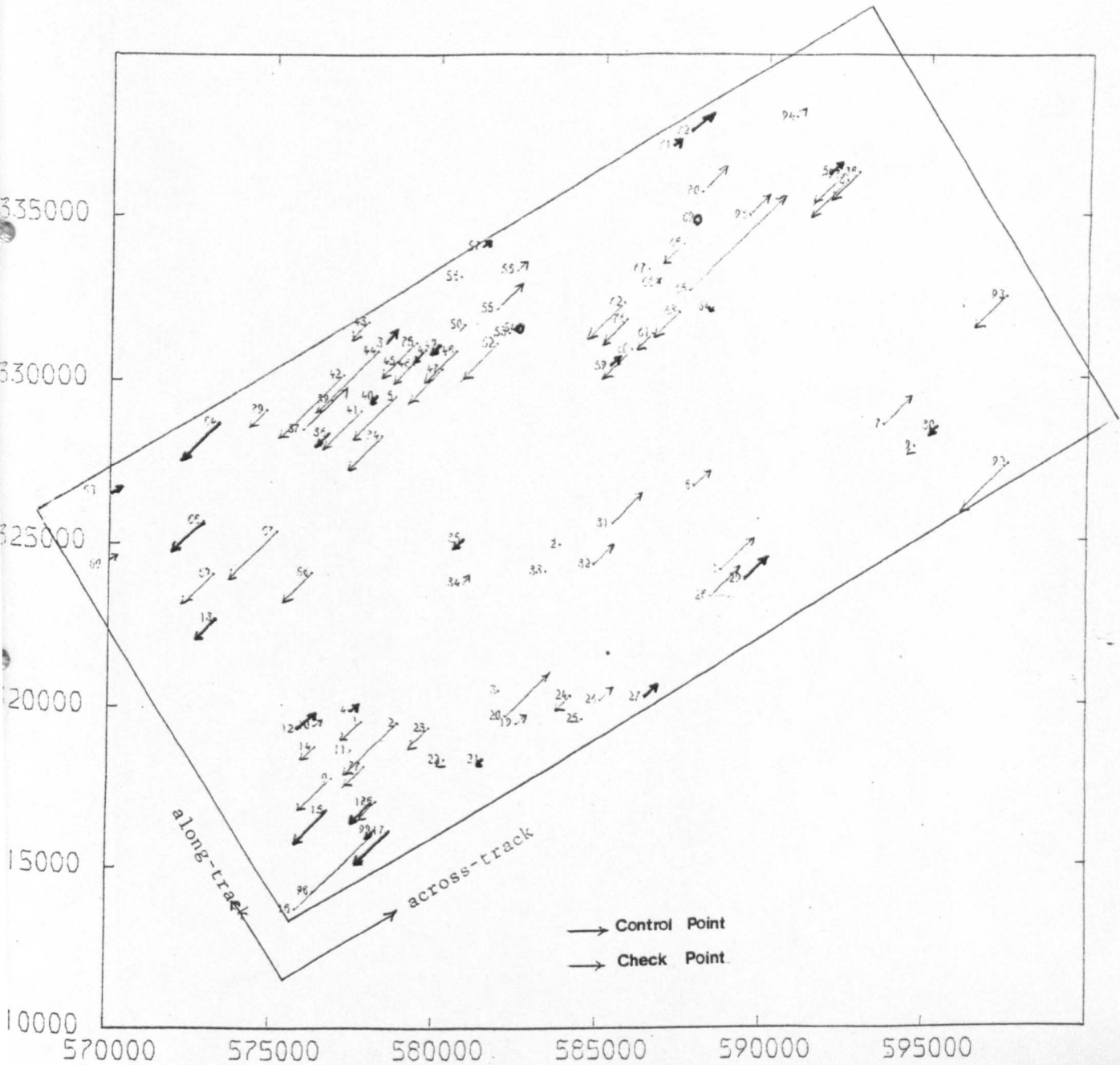


Fig 9.23

VECTOR MAP OF POSITION ERRORS OF EAST ANGLIA AREA

After the application of the 7-term Polynomial Solution

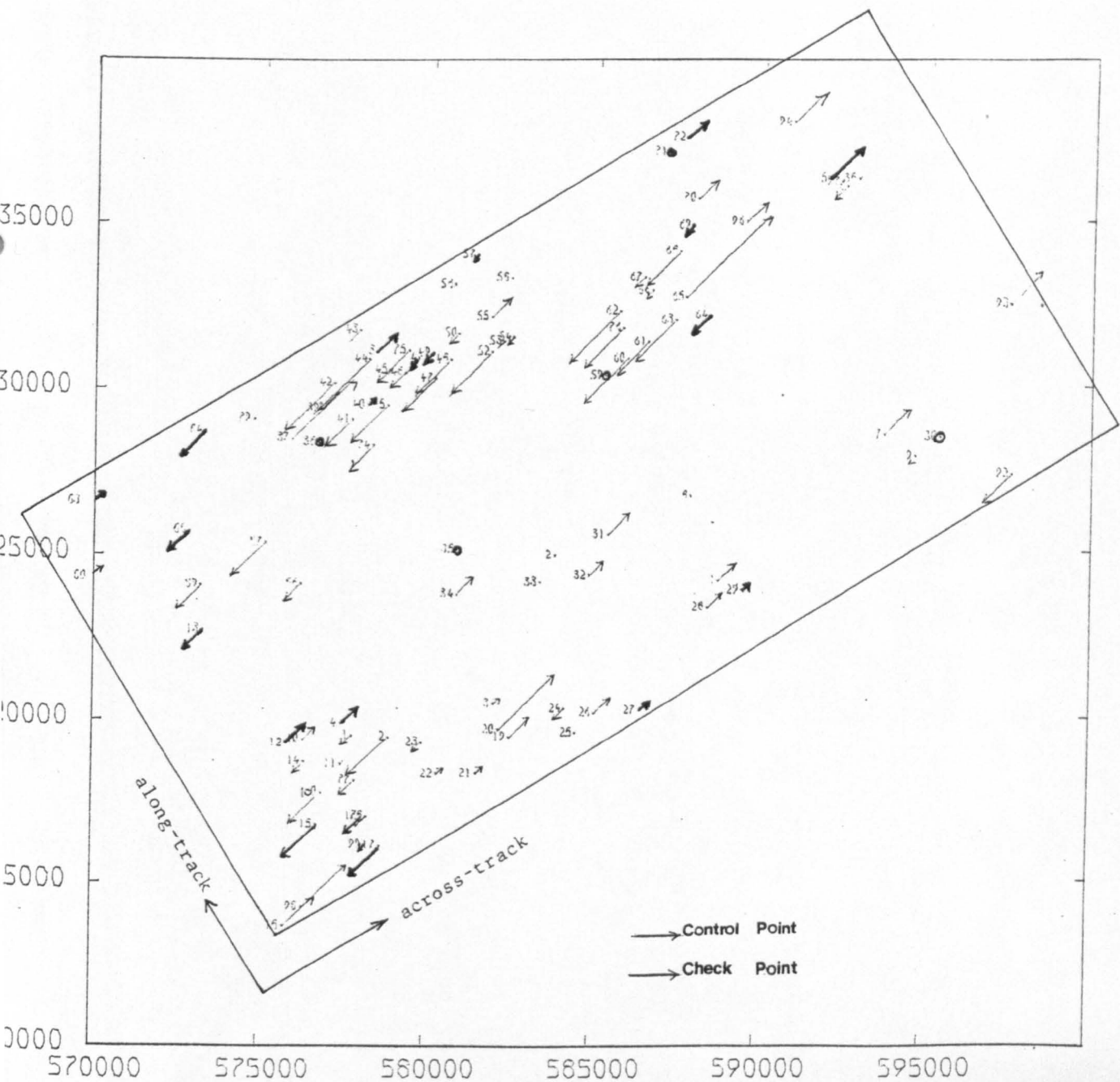


Fig 9.24

VECTOR MAP OF POSITION ERRORS OF EAST ANGLIA AREA

After the application of the 8-term Polynomial Solution



obtained after the application of the affine transformation, shows that the magnitudes of the errors are smaller compared with those obtained after the linear conformal transformation. This indicates that a very small residual error in scale was present in the image after the application of the linear conformal transformation solution. However the most obvious and striking pattern of errors present after applying the affine transformation is that they point almost uniformly in the across-track direction of the image, either outwards or inwards. This clearly indicates the presence of a systematic error present all over the image area.

Inspection of the overlay on top of Fig 9.18 enables one to identify those image points which lie at levels either above or below the average terrain elevation of 55 metres. Most points with elevations less than 55 m have vector errors pointing away from the satellite track (e.g. points no. 10, 12, 18, 98, 1, 28, 29, 7, 9, 30, etc). Similarly most of those points (e.g. 64, 66, 69, 74, etc) which lie at elevations greater than 55 m have their vector errors pointing towards the satellite antenna, which once again highlights the effect of topographic relief on this image. Therefore, although the overall magnitude of the residual errors is small, the effects of relief displacement appear to be present and are significant in this image just as they were in the River Tay area examples.

However, one characteristic which proved very worrying when the pattern of the residual errors was plotted out after the application of the affine transformation, was that there appears to be a slight but discernible lack of compensation of the scale in the cross-track direction. This may be seen by inspecting the pattern of the errors present in the control points (marked in red) in Fig 9.19. Those

b/w
in this copy!

lying in the western half of the image are virtually all pointing to the left, i.e. south-westwards from the mid line of the image. Similarly, the pattern of errors present at those control points located in the eastern half of the image point to the right, i.e. north-eastwards from the mid line - though to a lesser extent. This pattern cannot be explained entirely by the topographic heights of these control points, which therefore called into question the effectiveness or the correctness of the author's transformation program.

A considerable time was spent on checking the input data, the program, etc, but no errors were discovered. Furthermore, a completely independent check of the computation was applied through the use of a general purpose least-squares solution of simultaneous equations written in ALGOL by Mr. Methley of the Department of Geography. When the same input data was used in this program, the solution gave values for the six parameters (n_0 , n_1 , n_2 , m_0 , m_1 and m_2) of the affine transformation which are identical to those obtained by the author's program in BASIC. The results from program POLY and from Mr. Methley's program are included as Figs 9.25 and 9.26 respectively. The figures for the individual errors, the transformation parameters, the r.m.s.e. values, etc, are identical.

A similar check was made using the data for the Milford Haven test area (see later) since a similar pattern was visible in the plotted results there too. The magnitude of this error pattern is really quite small but it does in fact appear throughout the solutions no matter which polynomial is applied. The reasons for this tendency and its source are not apparent.

Inspecting the rest of the diagrams for the East Anglian area (Figs 9.20 to 9.24), one notices that there is a slow but continuous

* RADAR.TEST 09 DEC 81 20:56:45
 VECTOR MATRIX OF POLYNOMIAL TRANSFORMATION PARAMETERS

297470.
 79.9825
 125.244

TRANS. PARAMETERS IN Y DIRECTION

577702.
 125.546
 -79.3948

ACCURACY OF CONTROL POINTS

PT NO.	N(M)	E(M)	DN(M)	DE(M)	DO(M)
3	320526	582000	-24.2068	-22.053	33
4	319890	577418	8.44751	25.0945	26
8	326729	587919	21.2225	3.07924	21
12	319285	575798	29.6982	94.0402	99
13	322691	573253	-26.2835	4.26767	27
15	316760	576729	-46.0301	-34.2908	57
17	316146	578659	-59.2384	-50.9541	78
18	313646	575792	102.297	138.992	173
21	318377	581497	-25.5554	-24.13	35
27	320279	586425	-0.34588	-22.7669	23
29	323855	589507	31.3594	19.0491	37
30	328507	595380	33.2252	43.5216	55
35	325190	580836	-21.8256	-88.9447	92
37	328523	575855	73.5602	-48.3741	88
38	336336	592887	-40.5253	-0.355126	41
40	329539	578101	-5.40315	-50.7857	51
49	331120	580032	-13.7859	17.5173	22
54	331577	582475	-3.04089	-7.77334	8
57	331051	581770	5.82157	36.1549	71

PRESS RETURN TO CONTINUE

59	330396	585292	20.3635	41.6569	46
64	332190	588425	-7.05131	-34.1373	35
69	334912	587893	-2.45883	3.15188	4
71	337158	587108	-3.24901	34.6059	35
72	337596	587678	17.8133	19.5876	26
82	325788	568040	52.9405	101.818	115
84	328725	573275	-52.8009	-54.2986	76
86	324100	576185	-48.2367	-88.1741	101
99	316170	578210	-16.711	-49.4984	52

RESIDUALS IN CONTROL POINTS AS STANDARD DEVIATION
 MEAN ERROR IN NORTHINGS OF CONTROL POINTS= 28.3392
 MEAN ERROR IN EASTINGS= 41.1812
 RMSE AT NORTHINGS OF CONTROL POINTS= 25.1505
 RMSE AT EASTINGS OF CONTROL POINTS= 35.2647

ACCURACY OF CHECK POINTS

PT NO.	N(M)	E(M)	DN(M)	DE(M)	D1(M)
PRESS RETURN TO CONTINUE					
1	319545	577760	-35.8617	-17.239	40
2	319513	578868	-89.981	-101.281	135
5	336325	591965	15.859	82.1327	84
6	336079	592475	-56.5199	38.3327	68
7	328589	593722	73.9868	72.7154	104
9	327925	594672	27.1368	49.2096	56
10	319406	576292	10.8778	64.0111	65
11	318634	577425	-8.6984	-20.8211	23
14	318722	576330	-20.9956	-48.9254	53
16	317032	578070	-35.486	-21.0419	41
19	319507	582494	-0.521786	-8.47405	8
20	319741	582171	52.1743	-8.21585	53
22	318361	580323	-22.8873	-57.7917	62
23	319361	579849	-44.6228	-62.9371	77
24	320364	584158	-43.4976	-91.1479	101
25	319634	584507	-29.8044	-74.1889	80
26	320228	585076	-0.56114	-51.2866	51
28	323349	588469	35.2671	-34.6494	49
31	325602	585418	36.2782	-69.252	78
PRESS RETURN TO CONTINUE					
32	324349	584855	17.6197	-39.6058	43
33	324165	583368	-13.7765	32.9539	36
34	323836	580836	-0.121169	-55.1144	55
34	329829	571181	-76.8978	-79.1178	70

39	329437	576722	11.2806	7.56163	14
41	329108	577634	-59.5682	-69.3458	91
42	330215	577101	-93.6889	-4.97039	94
43	331805	577855	-25.2626	22.6977	34
44	330925	578139	-93.2085	-65.749	114
45	330615	578748	-13.6066	-70.4489	72
46	330545	579209	-31.7106	-34.977	47
47	330361	580127	-55.9116	-10.2516	57
48	330925	580570	-56.1282	17.7202	59
50	331691	580824	-10.2758	-10.6887	15
52	331143	581843	-62.5144	-67.5645	92
53	331456	582206	-4.43288	-13.6828	14
55	332177	581808	39.9175	40.1429	57
56	333152	580684	2.25991	41.1954	41
58	333333	582387	14.3358	48.7823	51

PRESS RETURN TO CONTINUE

60	330912	585950	-49.3837	-17.9915	53
61	331406	586592	-28.3335	-17.1279	33
62	332330	585722	-61.3061	-11.5924	62
63	332051	587399	-42.8357	27.548	51
65	332735	587716	145.531	3.52697	146
66	332925	586672	0.604632	14.3383	14
67	333317	586425	-3.14013	15.2145	16
68	334127	587507	-38.6737	10.8724	40
70	335735	588016	33.0189	40.9365	53
74	328333	578269	-51.7162	-59.4098	79
75	331190	579304	-53.0339	21.0298	57
76	331824	585824	-43.0126	-51.1719	67
77	318127	577862	-37.8278	-29.8324	48
78	317045	578250	-31.1253	-35.799	47
79	329110	574725	-21.7046	-23.2135	32
80	324275	569875	24.577	125.164	128
81	325800	569065	11.863	135.115	136
83	326560	569660	-25.7528	122.044	125
87	325360	575100	-74.2151	91.1779	118

PRESS RETURN TO CONTINUE

88	325725	572825	-39.4301	68.2651	79
89	324050	573200	-41.5175	69.0405	81
92	327375	597575	-5.36697	-69.9266	70
93	332505	597470	10.476	-1.64963	11
94	338055	590850	-0.721547	22.8331	23
96	335000	589469	30.6328	24.7478	39
97	336241	592317	-45.597	-1.41121	46
98	314228	576330	105.657	23.0368	108
100	317760	576849	-50.8384	-27.2979	58
101	324150	599700	85.8277	0.07548	46

102	324982	583798	-6.08944	14.2819	16
103	331158	578349	22.9862	-3.61623	23
104	330963	579602	-28.5316	-42.8533	51
105	329539	578691	-67.0942	-20.059	70

MEAN IN METRES OF CHECK POINTS RESIDUALS= 35.8478

RMSE OF CHECK POINTS AFTER POLYNOMIAL FIT

AND LEAST SQUARES INTERPOLATION= 27.6145

RMSE IN THE EASTINGS OF CHECK POINTS= 30.8455

PRESS RETURN TO CONTINUE

MEASURED IMAGE COORDINATES OF ALL POINTS

MEASURED IMAGE COORDINATES OF THE CONTROL POINTS

POINT NO.	X(MM)	Y(MM)
3	107.1	115.5
4	79.2	128.5
8	163.3	129.5
12	68.3	130.8
13	65.4	159.4
15	63.5	113.1
17	72.1	102.6
18	48.5	99
21	96.5	105.1

PRESS RETURN TO CONTINUE

27	131.4	98.2
29	162.1	107.4
30	212.3	112.5
35	116.9	146.5
37	101.2	183.9
38	225.8	165.8
40	117.3	181.1
49	134.3	182.8
54	149.7	176.7
57	152.4	194.8
59	161.8	159.73
64	185.5	158.7
69	192.5	176
71	196.3	191.5
72	201.1	192.1
92	47.0	196

77 67.8
PRESS RETURN TO CONTINUE

101.5

MEASURED IMAGE COORDINATES OF THE CHECK POINTS

POINT NUMBER	X(MM)	Y(MM)
1	79.5	125.2
2	85	121
5	221.2	169.1
6	222.7	165.6
7	203.5	119.1
9	206.2	111.7
10	71.3	129.7
11	74.4	121.4
14	68.3	125.9
16	72.2	109.8
19	106.4	108
20	105.6	110.8
22	89.6	109.4
23	90.4	116.7
24	118.3	106.9

PRESS RETURN TO CONTINUE

25	117.8	101.5
26	123.4	102.9
28	154.1	108.5
31	144.7	132.5
32	137.1	127.2
33	128.3	131.1
34	112.3	138.8
36	105.1	179.9
39	109.5	185.4
41	112.8	180.1
42	114	187.9
43	124.4	194.5
44	122.1	188.4
45	124.7	184.9
46	127.2	182.6
47	131.8	178
48	136.5	179.5
50	140.7	183.3
52	144	176.4

PRESS RETURN TO CONTINUE

53	147.7	177
4	319890	577418
8	326729	587919
27	310711	570040

56	145.5	192
58	155.9	186.9
60	166.8	160.1
61	172.3	160.7
62	170.6	168.9
63	179.4	161.2
65	184.2	165.1
66	178.5	169.1
67	178.5	172.2
68	187.4	172.7
70	196.5	180.3
74	113.7	173.4
75	130.3	185.6
76	169.2	165.9
77	74.9	116.8
78	73.2	109.3
79	96.7	190.7

PRESS RETURN TO CONTINUE

80	52.8	180.5
81	53.7	192
83	59.6	194
87	85.8	167.3
88	74.2	177.9
89	70.3	167
92	219.9	98.3
93	238.2	127.7
94	220.7	183.1
96	202	170.9
97	222.2	167.3
98	53	100.8
100	67.8	118.3
101	159.1	111.8
102	133.6	134.3
103	124.9	189.4
104	130.9	183.6
105	120.6	178.5

PRESS RETURN TO CONTINUE

GROUND COORDINATES OF THE CONTROL POINTS

PT NO.	NORTHINGS(M)	EASTINGS(M)
3	320526	582000
4	319890	577418
B	326729	587919

13	322691	573253
15	316760	576729
17	316146	578659
18	313646	575792
21	318377	581497
27	320279	586425
29	323855	589507
30	328507	595380
35	325190	580836
37	328523	575855
38	336336	592887

PRESS RETURN TO CONTINUE

40	329539	578101
49	331120	580032
54	331577	582475
57	334051	581339
59	330396	585292
64	332190	588425
69	334912	587893
71	337158	587108
72	337596	587678
82	325788	568040
84	328725	573275
86	324100	576185
99	316170	578210

GROUND COORDINATES OF THE CHECK POINTS

PT. NO.	NORTHINGS(M)	EASTINGS(M)
---------	--------------	-------------

1	319545	577760
---	--------	--------

PRESS RETURN TO CONTINUE

2	319513	578868
5	336325	591965
6	336079	592475
7	328589	593722
9	327925	594672
10	319406	576292
11	318634	577425
14	318722	576330
16	317032	578070
19	319507	582494
20	319741	582171
22	318361	580323
23	319361	579849

25	319634	584507
26	320228	585076
28	323349	588469
31	325602	585418
32	324349	584855

PRESS RETURN TO CONTINUE

33	324165	583368
34	323836	580836
36	328428	576646
39	329437	576722
41	329108	577634
42	330215	577101
43	331805	577855
44	330925	578139
45	330615	578748
46	330545	579209
47	330361	580127
48	330925	580570
50	331691	580824
52	331143	581843
53	331456	582206
55	332177	581808
56	333152	580684
58	333333	582387
60	330912	585950

PRESS RETURN TO CONTINUE

61	331406	586592
62	332330	585722
63	332051	587399
65	332735	587716
66	332925	586672
67	333317	586425
68	334127	587507
70	335735	588016
74	328333	578269
75	331190	579304
76	331824	585824
77	318127	577862
78	317045	578250
79	329110	574725
80	324275	569875
81	325800	569065
83	326560	569660
87	325360	575100
88	325725	572825

PRESS RETURN TO CONTINUE

89	324050	573200
92	327375	597575
93	332505	597470
94	338055	590850
96	335000	589469
97	336241	592317
98	314228	576330
100	317760	576849
101	324152	588792
102	324982	583798
103	331158	578349
104	330963	579602
105	329539	578691

* 4.203 SECONDS USED 21:09:05

300

300

PULLOUTS

* SEASAT.BDFM 06 MAY 82 22:20:50
 VECTOR MATRIX OF POLYNOMIAL TRANSFORMATION PARAMETERS

ACCURACY OF CONTROL POINTS

TRANSFORMATION PARAMETERS IN X DIRECTION

297470.
 79.9825
 125.244

TRANSFORMATION PARAMETERS IN Y DIRECTION

577702.
 125.546
 -79.3948

PRESS RETURN TO CONTINUE

PT NO.	N(M)	E(M)	DN(M)	DE(M)	DO(M)
3	320526	582000	-24.2137	-22.0598	33
4	319890	577418	8.4414	25.0884	26
8	326729	587919	21.2132	3.07015	21
12	319285	575798	29.6924	94.0344	99
13	322691	573253	-26.2899	4.26118	27
15	316760	576729	-46.0353	-34.296	57
17	316146	578659	-59.2436	-50.9593	78
18	313646	575792	102.292	138.988	173
21	318377	581497	-25.5616	-24.1361	35
27	320279	586425	-0.35318	-22.7741	23
29	323855	589507	31.3507	19.0406	37
30	328507	595380	33.2145	43.5112	55
35	325190	580836	-21.8336	-88.9527	92
37	328523	575855	73.5518	-48.3825	88
38	336336	592887	-40.5378	-0.36734	41
40	329539	578101	-5.41199	-50.7945	51
49	331120	580032	-13.7954	17.5078	22

PRESS RETURN TO CONTINUE

54	331577	582475	-3.05083	-7.78321	8
57	334051	581339	5.81108	30.1438	31
59	330396	585292	20.3535	41.6471	46
64	332190	588425	-7.06213	-34.1479	35
69	334912	587893	-2.47035	3.14055	4
71	337158	587108	-3.26105	34.594	35
72	337594	587678	17.8011	19.5754	26
82	325788	568040	52.9339	101.811	115
84	328725	573275	-52.8089	-54.3048	76
86	324100	576185	-48.2438	-88.1813	101
99	316170	578210	-16.7161	-49.5036	52

RESIDUALS IN CONTROL POINTS AS STANDARD DEVIATION
 MEAN ERROR IN NORTHINGS OF CONTROL POINTS= 28.3409
 MEAN ERROR IN EASTINGS= 41.1807
 RMSE AT NORTHINGS OF CONTROL POINTS= 25.1483
 RMSE AT EASTINGS OF CONTROL POINTS= 35.2653

ACCURACY OF CHECK POINTS

PRESS RETURN TO CONTINUE

PT NO.	N(M)	E(M)	DN(M)	DE(M)	DO(M)
1	319545	577260	-35.8677	-17.2451	40
2	319513	578848	-89.9871	-101.287	135
5	334325	591965	15.8466	82.1205	84
6	336079	592475	-56.5323	38.3206	68
7	328589	593222	73.9763	72.7052	104
9	327925	594672	27.1264	49.1995	56
10	319406	576292	10.872	64.0052	65
11	318434	577425	-8.70416	-20.8269	23
14	318722	576330	-21.0012	-48.9311	53
16	317032	578070	-35.4914	-21.0473	41
19	319507	582494	-0.5284	-8.4806	8
20	319741	582121	52.1677	-8.22244	53
22	318361	580323	-22.8934	-57.7977	62
23	319361	579849	-44.6291	-62.9434	77
24	320364	584158	-43.5046	-91.1549	101
25	319634	584507	-29.8113	-74.1957	80
26	320228	585076	-0.56826	-51.2936	51

PRESS RETURN TO CONTINUE

28	323349	588469	35.2586	-34.6577	49
31	325602	585418	36.2695	-69.2606	78
32	324349	584855	17.6115	-39.6139	43
33	324165	583368	-13.7845	32.946	36
34	323836	580836	-0.12877	-55.122	55
36	328428	576646	-20.4908	-32.1759	38
39	329437	576722	11.272	7.55293	14
41	329108	577634	-59.5768	-69.3545	91
42	330215	577101	-93.6978	-4.97932	94
43	331805	577855	-25.272	22.6882	34
44	330925	578139	-93.2177	-65.7582	114
45	330615	578748	-13.6158	-70.4581	72
46	330545	579209	-31.7198	-34.9863	47
47	330361	580127	-55.9209	-10.2609	57
48	330925	580570	-56.1378	17.7107	59
50	331691	580824	-10.2856	-10.6984	15
52	331143	581843	-62.5242	-67.5741	92
53	331456	582206	-4.44275	-13.6927	14
55	332177	581808	39.9074	40.1329	57

PRESS RETURN TO CONTINUE

56	333152	580684	2.24975	41.1852	41
58	333333	582387	14.3254	48.7719	51
60	330912	585950	-49.3938	-18.0015	53
61	331406	586592	-28.3439	-17.1381	33
62	332330	585722	-61.3167	-11.6028	62
63	332051	587399	-42.8464	27.5375	51
65	332735	587716	145.52	3.51622	146
66	332925	586672	0.59381	14.3277	14
67	333317	586425	-3.15103	15.2038	16
68	334127	587507	-38.685	10.8613	40
70	335735	588016	33.0071	40.9249	53
74	328333	578269	-51.7247	-59.4184	79
75	331190	579304	-53.0433	21.0204	57
76	331824	585824	-43.023	-51.1821	67
77	318127	577862	-37.8335	-29.8381	48
78	317045	578250	-31.1307	-35.8044	47
79	329110	574725	-21.7129	-23.2219	32
80	324275	569875	24.5706	125.158	128
81	325800	569065	11.8562	135.108	136

PRESS RETURN TO CONTINUE

83	326560	569660	-25.7598	122.037	125
87	325360	575100	-74.2224	91.1705	118
88	325725	572825	-39.4373	68.2578	79
89	324050	573200	-41.5243	69.0336	81
92	327375	597575	-5.37757	-69.9368	70
93	332505	597470	10.464	-1.66126	11
94	338055	590850	-0.73429	22.8206	23
96	335000	589469	30.621	24.7363	39
97	336241	592317	-45.6094	-1.42334	46
98	314228	576330	105.652	23.0323	108
100	317260	576849	-50.8438	-27.3033	58
101	324152	588792	45.475	8.06701	46
102	324982	583798	-6.09772	14.2738	16
103	331158	578349	22.9769	-3.62557	23
104	330963	579602	-28.541	-42.8627	51
105	329539	578691	-67.1031	-20.0679	70

MEAN IN METRES OF CHECK POINTS RESIDUALS= 35.8508
 RMSE OF CHECK POINTS AFTER POLYNOMIAL FIT
 AND LEAST SQUARES INTERPOLATION= 27.6148
 PRESS RETURN TO CONTINUE

RMSE IN THE EASTINGS OF CHECK POINTS= 30.8447

MEASURED IMAGE COORDINATES OF ALL POINTS

MEASURED IMAGE COORDINATES OF THE CONTROL POINTS

POINT NO.	X(MM)	Y(MM)
3	107.1	115.5
4	79.2	128.5
8	163.3	129.5
12	68.3	130.8
13	65.4	159.4
15	63.5	113.1
17	72.1	102.6

PRESS RETURN TO CONTINUE

18	48.5	99
21	96.5	105.1
27	131.4	98.2
29	162.1	107.4
30	212.3	112.5
35	116.9	146.5
37	101.2	183.9
38	225.8	165.8
40	117.3	181.1
49	134.3	182.8
54	149.7	176.7
57	152.4	194.8
59	161.8	159.73
64	185.5	158.7
69	192.5	176
71	196.3	191.5
72	201.1	192.1
82	47.8	196
84	86.8	193.7

PRESS RETURN TO CONTINUE

86	86.5	157
99	69.8	104.6

MEASURED IMAGE COORDINATES OF THE CHECK POINTS

POINT NUMBER	X(MM)	Y(MM)
1	79.5	125.2
2	85	121
5	221.2	169.1
6	222.7	165.6
7	203.5	119.1
9	206.2	111.7
10	71.3	129.7
11	74.4	121.4
14	68.3	125.9
16	72.2	109.8
19	106.4	108
20	105.6	110.8
22	89.6	109.4

PRESS RETURN TO CONTINUE

23	90.4	116.7
24	118.3	106.9
25	117.8	101.5
26	123.4	102.9
28	154.1	108.5
31	144.7	132.5
32	137.1	127.2
33	128.3	131.1
34	112.3	138.8
36	105.1	179.9
39	109.5	185.4
41	112.8	180.1
42	114	187.9
43	124.4	194.5
44	122.1	188.4
45	124.7	184.9
46	127.2	182.6
47	131.8	178
48	134.5	179.5

18	48.5	99
21	96.5	105.1
27	131.4	98.2
29	162.1	107.4
30	212.3	112.5
35	116.9	146.5
37	101.2	183.9
38	225.8	165.8
40	117.3	181.1
49	134.3	182.8
54	149.7	176.7
57	152.4	194.8
59	161.8	159.73
64	185.5	158.7
69	192.5	176
71	196.3	191.5
72	201.1	192.1
82	47.8	196
84	86.8	193.7

PRESS RETURN TO CONTINUE

86	86.5	157
99	69.8	104.6

MEASURED IMAGE COORDINATES OF THE CHECK POINTS

POINT NUMBER	X(MM)	Y(MM)
1	79.5	125.2
2	85	121
5	221.2	169.1
6	222.7	165.6
7	203.5	119.1
9	206.2	111.7
10	71.3	129.7
11	74.4	121.4
14	68.3	125.9
16	72.2	109.8
19	106.4	108
20	105.6	110.8
22	89.6	109.4

PRESS RETURN TO CONTINUE

23	90.4	116.7
24	118.3	106.9
25	117.8	101.5
26	123.4	102.9
28	154.1	108.5
31	144.7	132.5
32	137.1	127.2
33	128.3	131.1
34	112.3	138.8
36	105.1	179.9
39	109.5	185.4
41	112.8	180.1
42	114	187.9
43	124.4	194.5
44	122.1	188.4
45	124.7	184.9
46	127.2	182.6
47	131.8	178
48	136.5	179.5

PRESS RETURN TO CONTINUE

50	140.7	183.3
52	144	176.4
53	147.7	177
55	148.5	182.6
56	145.5	192
58	155.9	186.9
60	166.8	160.1
61	172.3	160.7
62	170.6	168.9
63	179.4	161.2
65	184.2	165.1
66	178.5	169.1
67	178.5	172.2
68	187.4	172.7
70	196.5	180.3
74	113.7	173.4
75	130.3	185.6
76	169.2	165.9
77	74.9	116.8

PRESS RETURN TO CONTINUE

78	73.2	109.3
79	96.7	190.7
80	52.8	180.5
81	53.7	192
83	59.6	194
87	85.8	167.3
88	74.2	177.9
89	70.3	167
92	219.9	98.3
93	238.2	127.7
94	220.7	183.1
96	202	170.9
97	222.2	167.3
98	53	100.8
100	67.8	118.3
101	159.1	111.8
102	133.6	134.3
103	124.9	189.4
104	130.9	183.6

PRESS RETURN TO CONTINUE

105	120.6	178.5
-----	-------	-------

GROUND COORDINATES OF THE CONTROL POINTS

PT. NO.	NORTHINGS(M)	EASTINGS(M)
3	320526	582000
4	319890	577418
8	326729	587919
12	319285	575798
13	322691	573253
15	316760	576729
17	316146	578659
18	313646	575792
21	318377	581497
27	320279	586425
29	323855	589507
30	328507	595380
35	325190	580336

PRESS RETURN TO CONTINUE

37	328523	575855
38	336336	592887
40	329539	578101
49	331120	580032
54	331577	582475
57	334051	581339
59	330396	585292
64	332190	588425
69	334912	587893
71	337158	587108
72	337596	587678
82	325788	568040
84	328725	573275
86	324100	576185
99	316170	578210

GROUND COORDINATES OF THE CHECK POINTS

PT. NO.	NORTHINGS(M)	EASTINGS(M)
---------	--------------	-------------

PRESS RETURN TO CONTINUE

1	319545	577760
2	319513	578868
5	336325	591965
6	336079	592475
7	328589	593722
9	327925	594672
10	319406	576292
11	318634	577425
14	318722	576330
16	317032	578070
19	319507	582494
20	319741	582171
22	318361	580323
23	319361	579849
24	320364	584158
25	319634	584507
26	320228	585076
28	323349	588469

PRESS RETURN TO CONTINUE

31	325602	585418
32	324349	584855
33	324165	583368
34	323836	580836
36	328428	576646
39	329437	576722
41	329108	577634
42	330215	577101
43	331805	577855
44	330925	578139
45	330615	578748
46	330545	579209
47	330361	580127
48	330925	580570
50	331691	580824
52	331143	581843
53	331456	582206
55	332177	581808
56	333152	580684

PRESS RETURN TO CONTINUE

58	333333	582387
60	330912	585950
61	331406	586592
62	332330	585722
63	332051	587399
65	332735	587716
66	332925	586672
67	333317	586425
68	334127	587507
70	335735	588016
74	328333	578269
75	331190	579304
76	331824	585824
77	318127	577362
78	317045	578750
79	329110	574725
80	324275	569875
81	325800	569065
83	326560	569460

PRESS RETURN TO CONTINUE

87	329360	575100
88	325725	572825
89	324050	573200
92	327375	592575
93	332505	592470
94	338055	590850
96	335000	589469
97	336241	592317
98	314228	576330
100	317760	576849
101	324152	588792
102	324982	583798
103	331158	578349
104	330963	579602
105	329539	578691

* 3.929 SECONDS USED 22:33:06

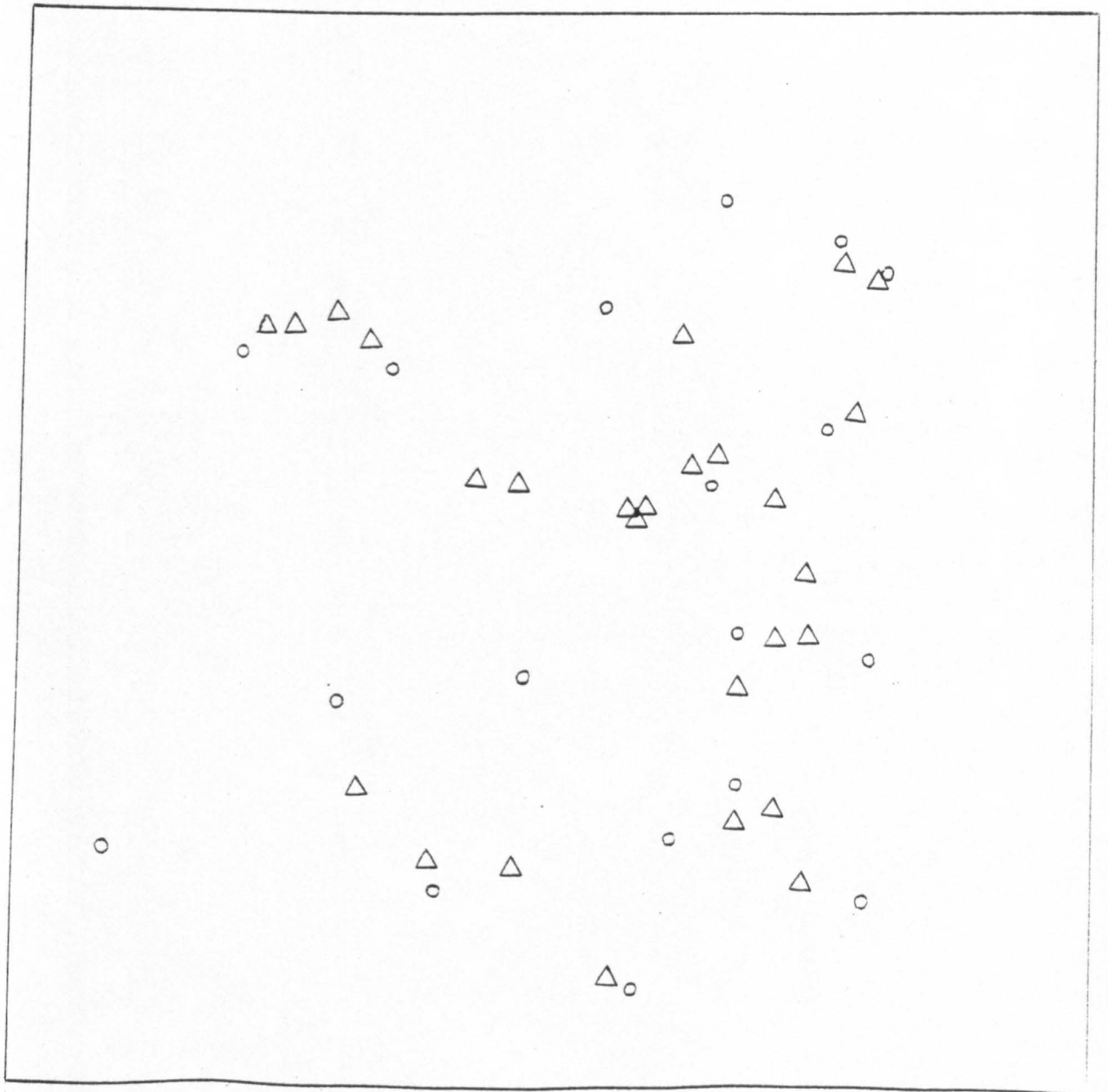
decrease in the overall magnitude of the vector errors, although most points still exhibited the systematic nature of their individual errors. This suggests that the use of the polynomials does compensate partially for the effect of topography on this type of digitally processed SAR imagery.

In essence, therefore, although the relief displacement errors are generally small on this digitally processed image of a fairly flat piece of terrain, there is strong evidence to suggest that the variations in terrain elevation are still the major source of error affecting the geometric accuracy of this particular image.

9.3 Results from the Milford Haven Test Area

On the digitally processed image of Milford Haven test area, 47 points were first identified. Of these, 45 were retained after initial testing. Eighteen of these points were used as the control points on which the computation of the transformation parameters was based. The remaining 27 points were employed as check points. The final distribution of these points is shown on Fig 9.27. A summary of the results obtained from the geometrical test of the digitally processed image of this area is presented in Table 9.4. At the ground control points, the full eight terms of the polynomial provided r.m.s.e. values as follows:- $\sigma_X = \pm 74$ m; $\sigma_Y = \pm 85$ m; and $\sigma_P = \pm 113$ m. With the subsequent truncation of terms, the r.m.s.e. values then decrease gradually but slowly and rather insignificantly in both the X and the Y directions. The best results were obtained when the polynomial was restricted to represent an affine transformation.

At the check points, the r.m.s.e. values in both the X and the Y directions remain virtually the same irrespective of the number of the terms used in the polynomial transformation. The three-term



○ control point

△ check point

Fig 9.27 Control distribution pattern on Milford Haven test area image

TABLE 9.4 RESULTS OF THE DIGITALLY PROCESSED IMAGE OF THE MILFORD
HAVEN AREA

Number of terms in polynomial	Control Points (n=18)			Check Points (n=27)		
	$\sigma_X(m)$	$\sigma_Y(m)$	$\sigma_P(m)$	$\sigma_X(m)$	$\sigma_Y(m)$	$\sigma_P(m)$
8	74	85	113	79	86	117
7	70	81	107	79	86	117
6	66	79	103	80	86	118
5	68	73	100	81	88	120
4	62	70	94	79	88	118
3	57	70	90	82	89	121
Linear Conformal Transform- ation	72	77	105	89	102	135
	-	(n=2) -	-	128	132	184

polynomial, therefore, performed as well as the eight-term polynomial transformation. The simple linear conformal transformation, based on the use of only two well-defined points gave:- $\sigma_X = \pm 128$ m; $\sigma_Y = \pm 132$ m and a corresponding planimetric error (σ_p) of ± 184 m. However, when this transformation was applied in its least squares form with 16 redundant points, the values of the errors were as follows:- $\sigma_X = \pm 72$ m; $\sigma_Y = \pm 77$ m; and $\sigma_p = \pm 105$ m for the control points; and $\sigma_p = \pm 135$ m for the check points. As would be expected, the planimetric accuracy of this image was improved considerably for both the control and the check points when the redundant points are available for the determination of the transformation parameters.

Comparing the overall results for the Milford Haven area with the results for the other digitally processed image of East Anglia given in Table 9.3, they are very poor - almost exactly three times larger on average for each transformation tested. While this is very disappointing, the reasons for the very different results appear to lie in the totally different topographic character of each of the two areas - the East Anglian area being fairly flat and the area around Milford Haven being quite mountainous. This became apparent when the detailed analysis of the results was undertaken below.

9.3.1 Detailed Analysis of Results obtained from the Milford Haven Area

Figs 9.28 to 9.34 are the vector diagrams of the individual positional errors of the control points and the check points obtained after application of the various polynomial transformations to the measured numerical coordinates of the test points on the image of the Milford Haven area. It should be noted that, because of the much larger errors present in this image, the scale of their representation is much

Heights of Points (metres) above Mean-Sea-Level

Average Ground Height = 95m

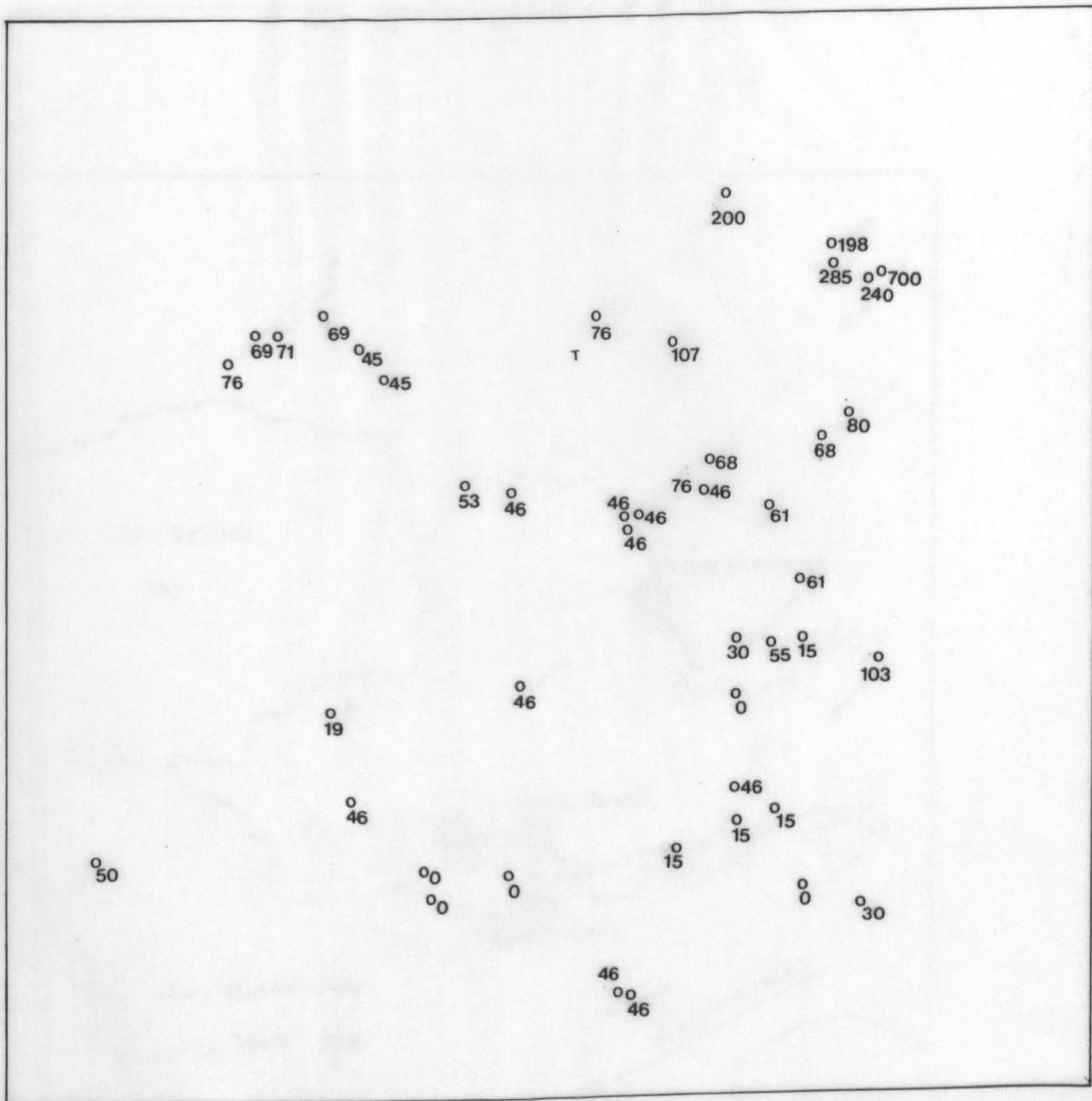


Fig 9.28

VECTOR MAP OF POSITION ERRORS OF MILFORD HAVEN AREA

After the application of the Linear Conformal Transformation with Least Squares Solution

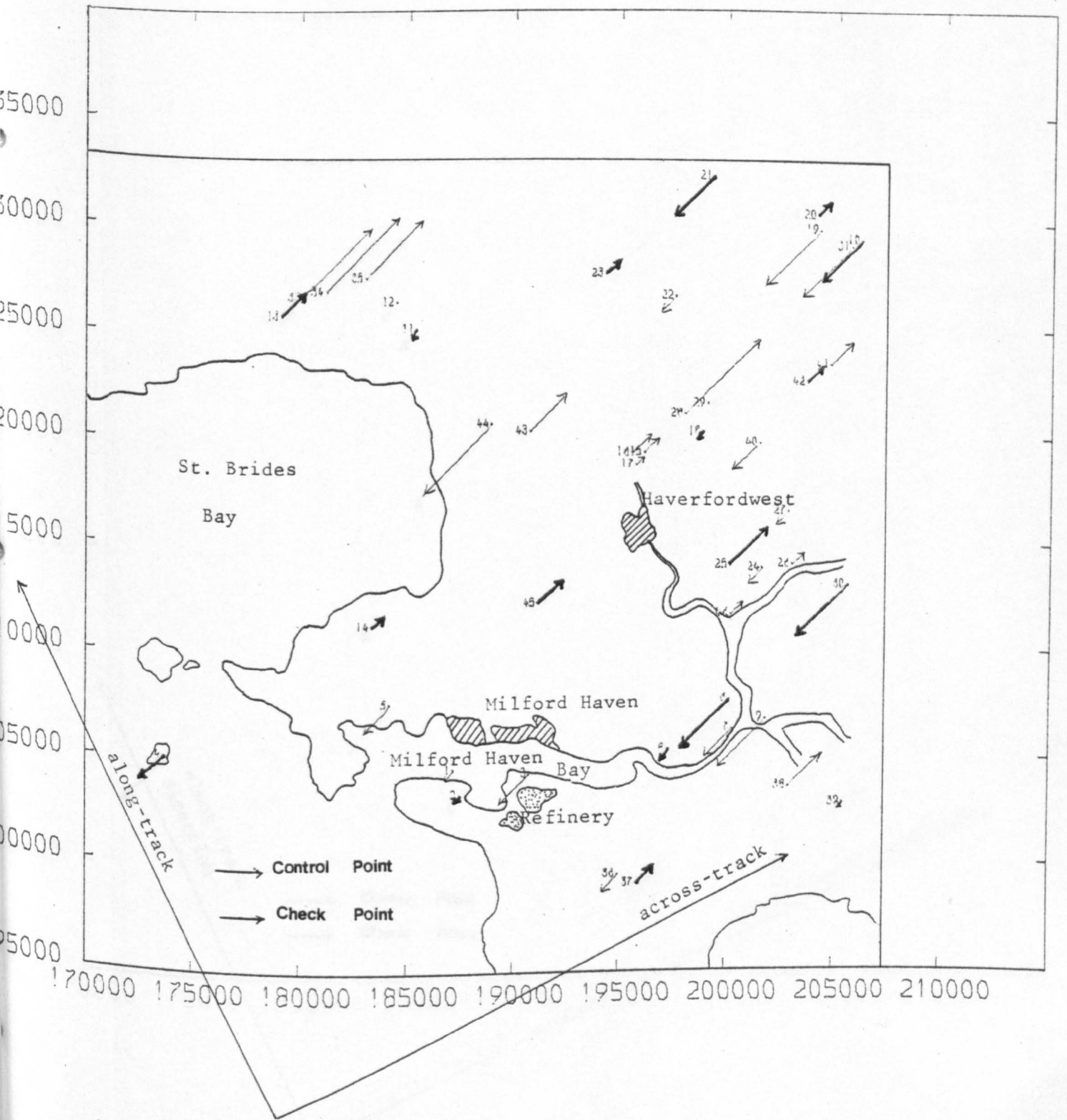


Fig 9.29

VECTOR MAP OF POSITION ERRORS OF MILFORD HAVEN AREA

After the application of the 3-term Polynomial Solution
(Affine Transformation)

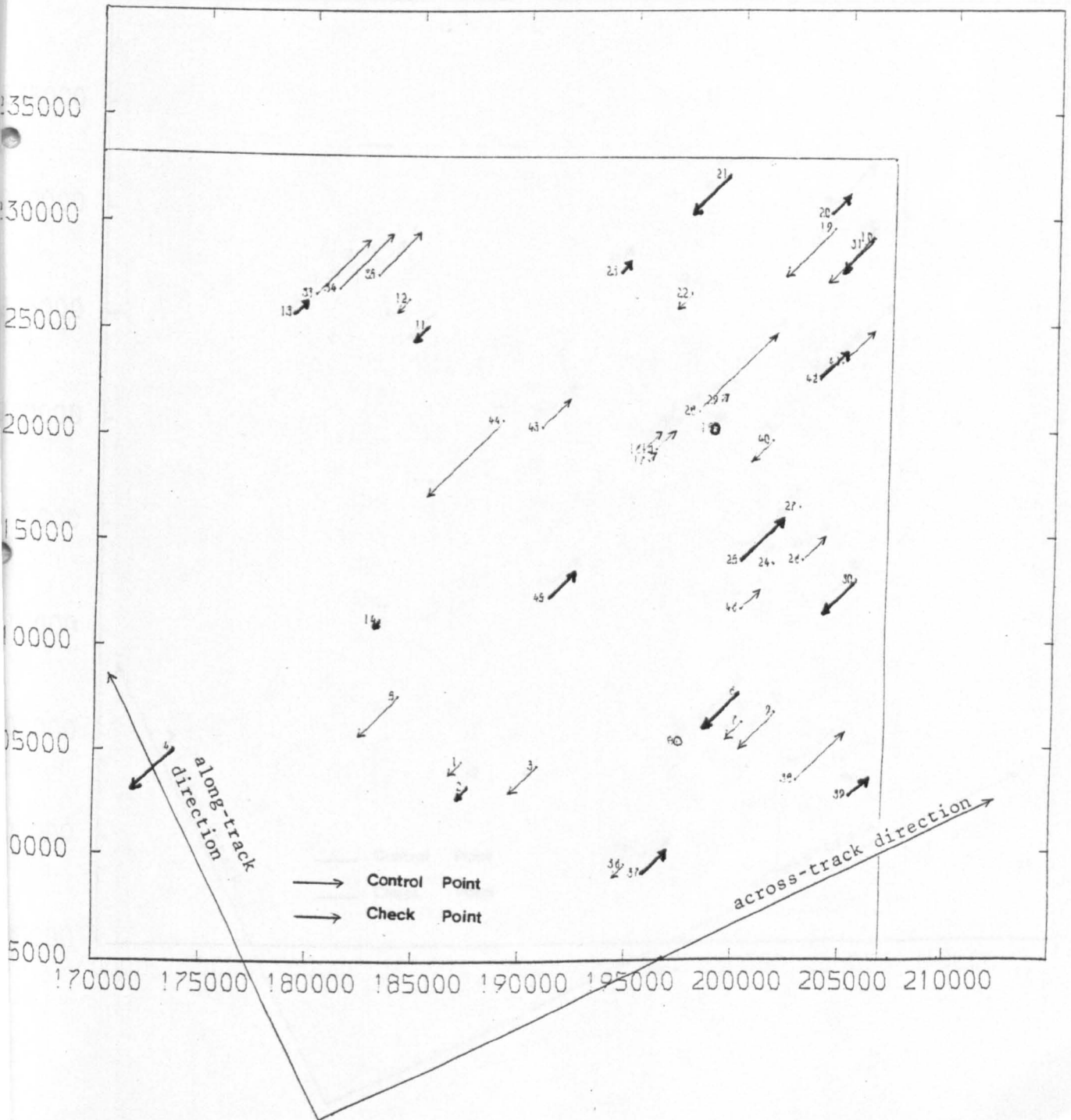


Fig 9.30

VECTOR MAP OF POSITION ERRORS OF MILFORD HAVEN AREA

After the application of the 4-term Polynomial Solution

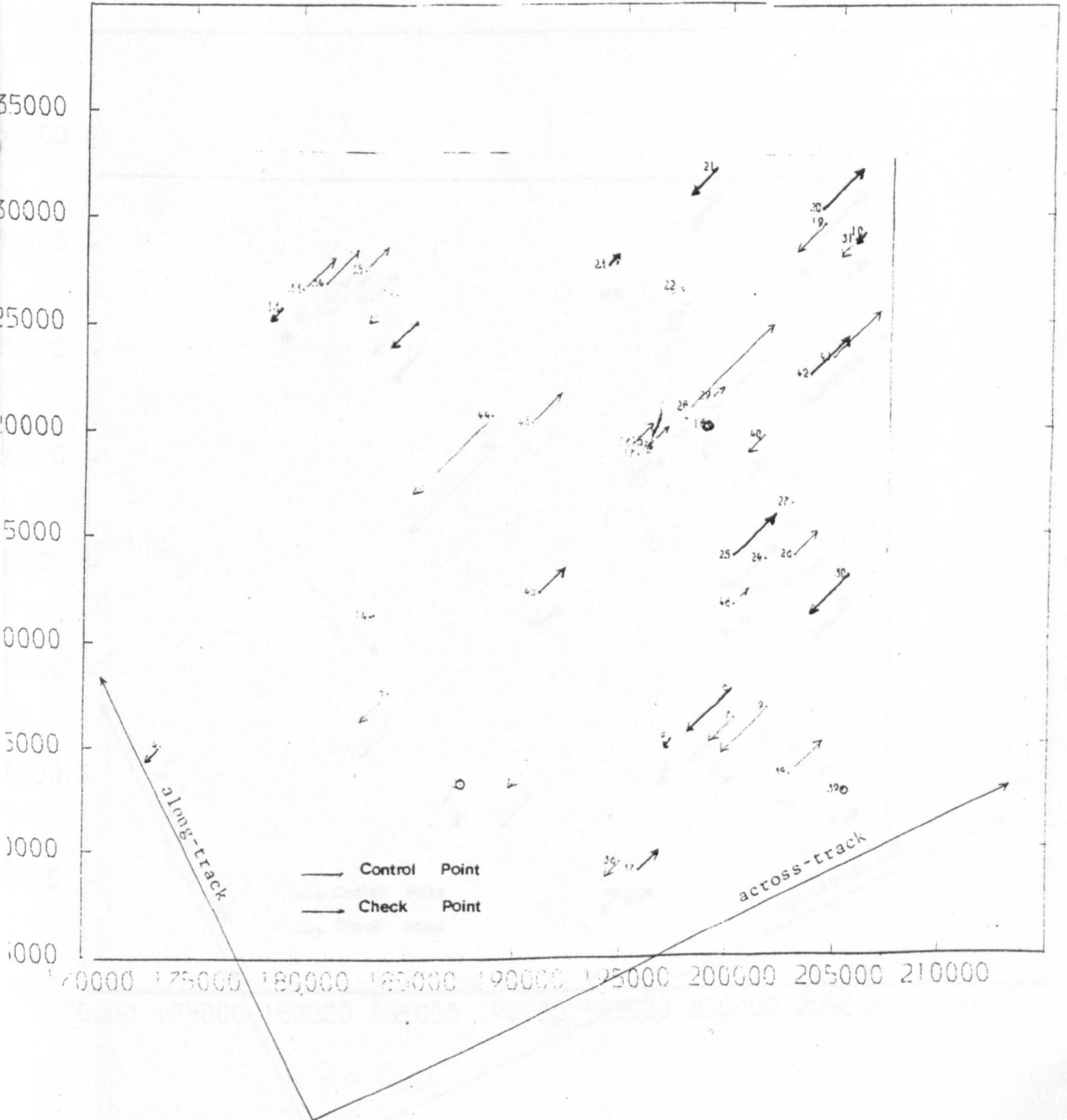


Fig 9.31

VECTOR MAP OF POSITION ERRORS OF MILFORD HAVEN AREA

After the application of the 5-term Polynomial Solution

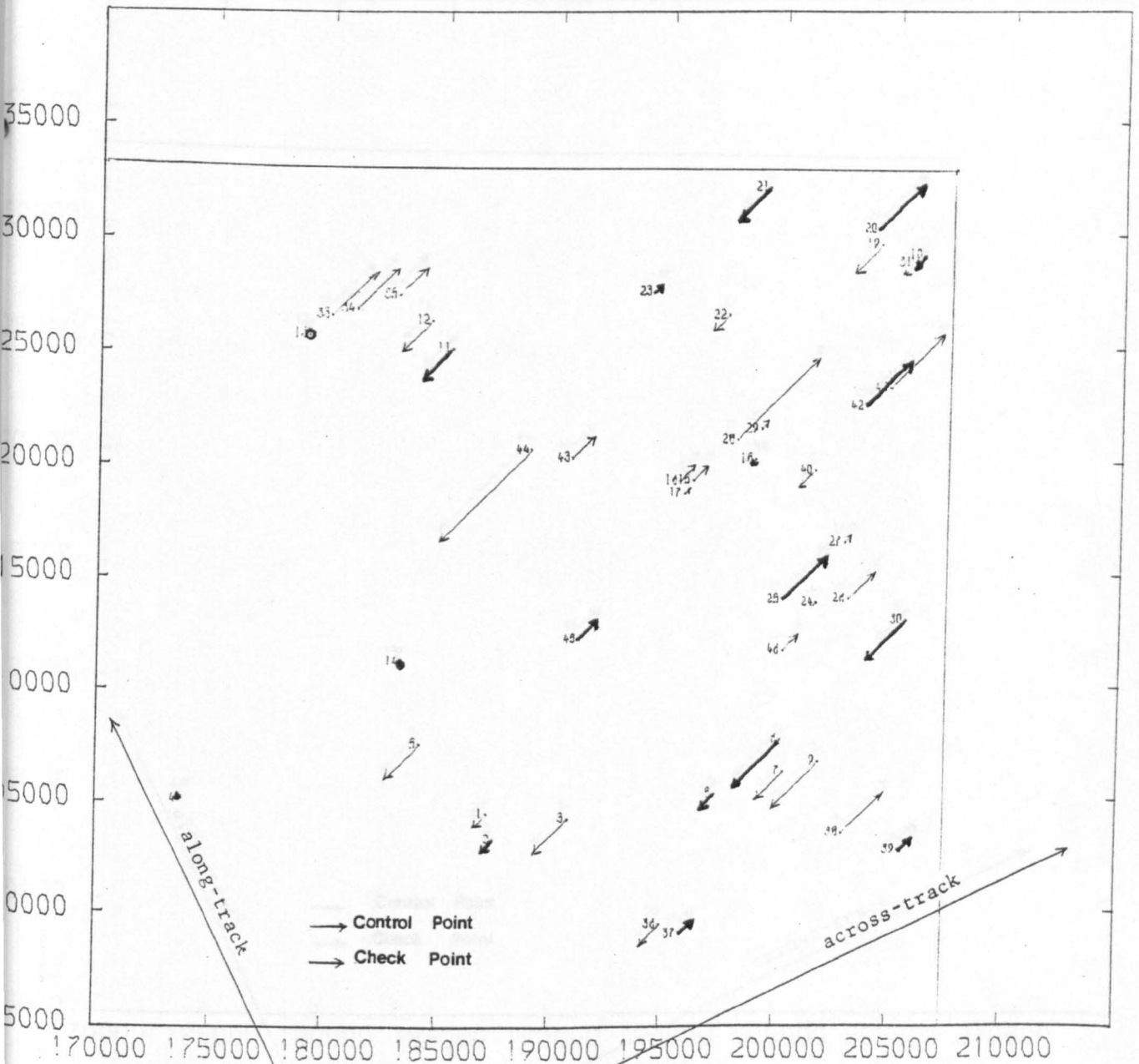


Fig 9.32

VECTOR MAP OF POSITION ERRORS OF MILFORD HAVEN AREA

After the application of the 6-term Polynomial Solution

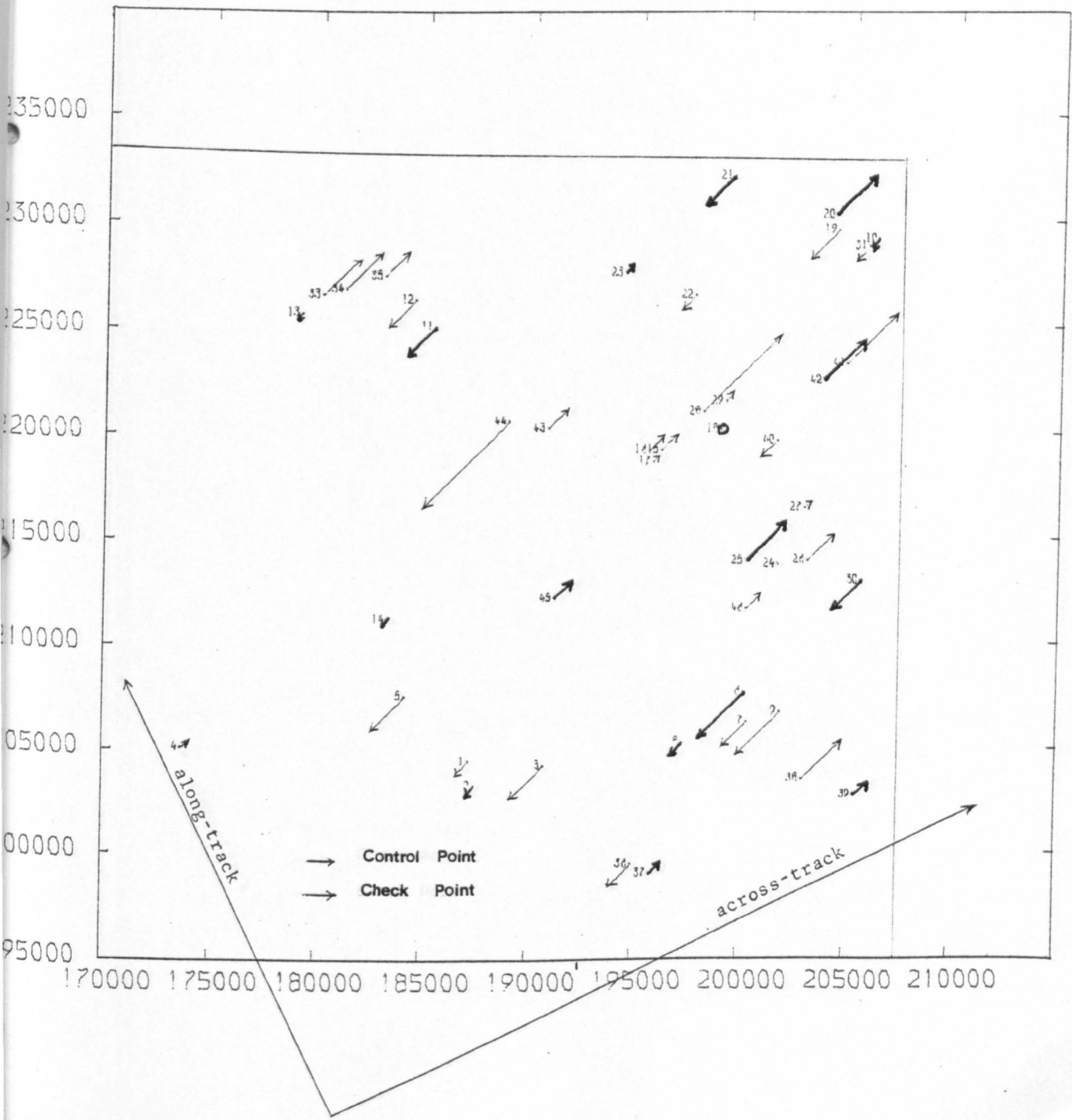


Fig 9.33

VECTOR MAP OF POSITION ERRORS OF MILFORD HAVEN AREA

After the application of the 7-term Polynomial Solution

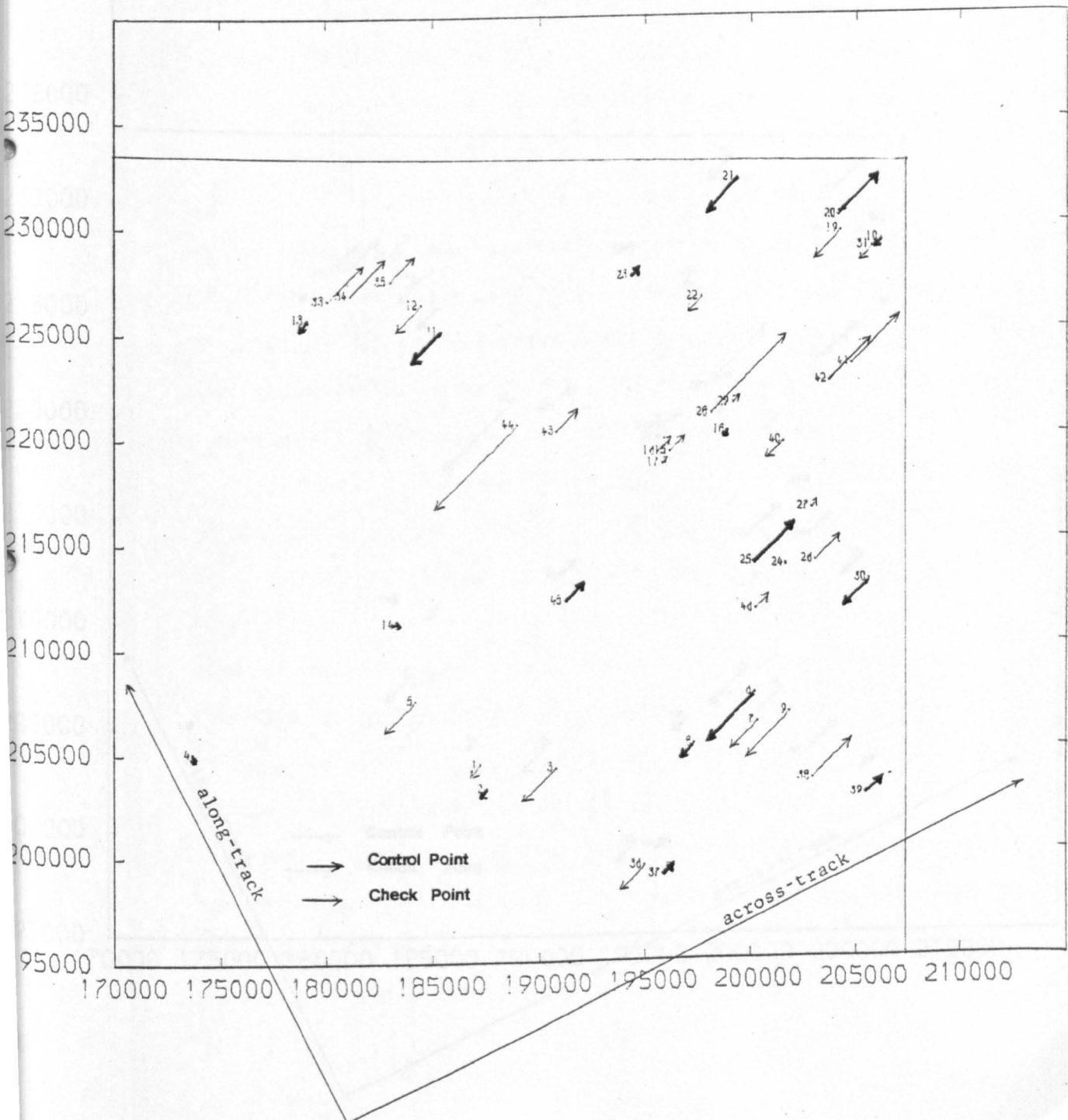
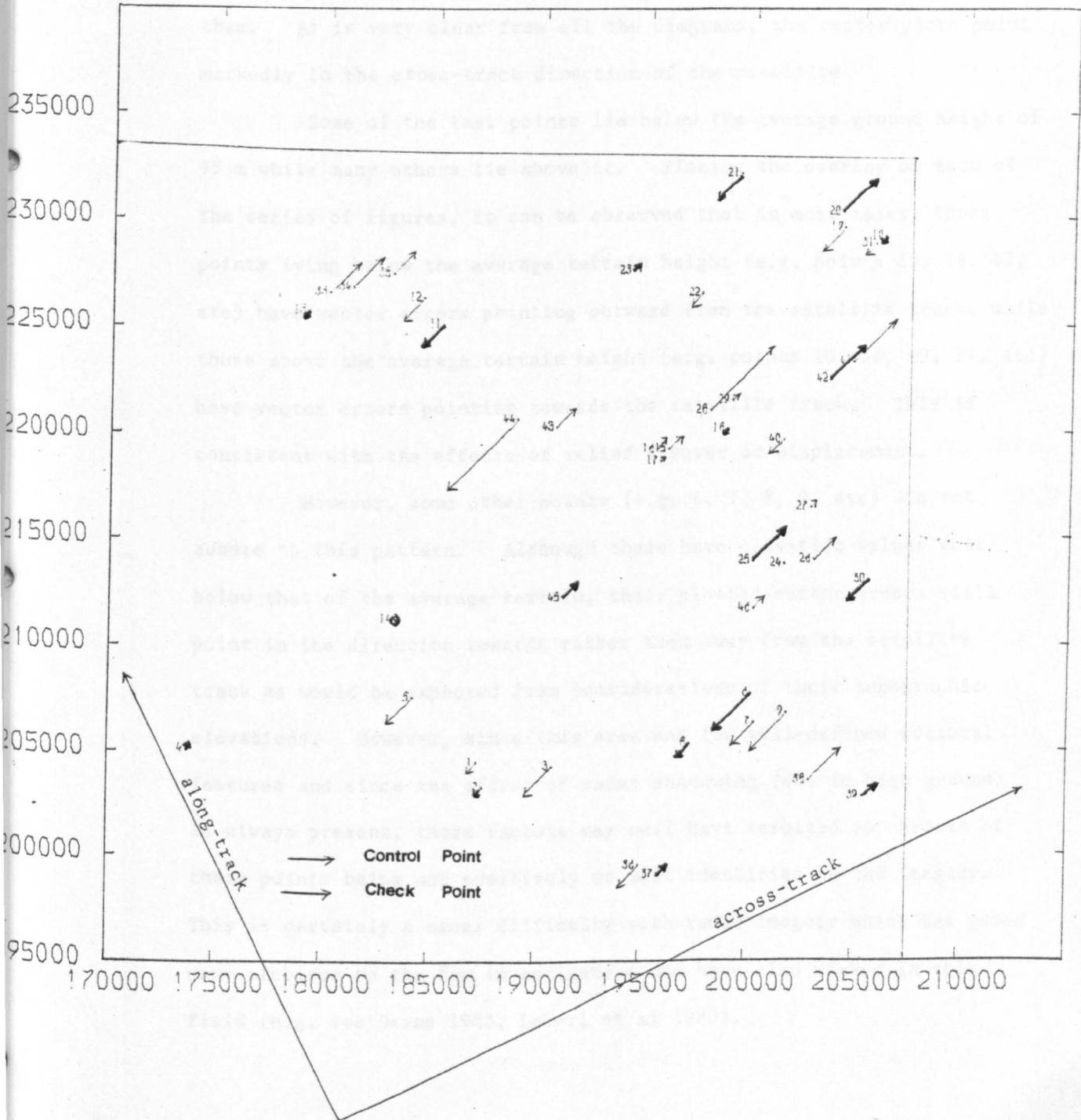


Fig 9.34

VECTOR MAP OF POSITION ERRORS OF MILFORD HAVEN AREA

After the application of the 8-term Polynomial Solution



smaller than for the East Anglia test area. Thorough inspection of these figures discloses that, although the patterns of the errors present in some very few points (e.g. points number 4, 13, 14, etc) are fairly random in character from one solution to another, the error patterns present in the majority of the points are consistent and systematic in character irrespective of the transformation applied to them. As is very clear from all the diagrams, the vector plots point markedly in the cross-track direction of the satellite.

Some of the test points lie below the average ground height of 95 m while many others lie above it. Placing the overlay on each of the series of figures, it can be observed that in most cases, those points lying below the average terrain height (e.g. points 15, 16, 17, etc) have vector errors pointing outward from the satellite track, while those above the average terrain height (e.g. points 10, 31, 19, 21, etc) have vector errors pointing towards the satellite track. This is consistent with the effects of relief layover or displacement.

However, some other points (e.g. 6, 7, 8, 9, etc) did not adhere to this pattern. Although these have elevation values well below that of the average terrain, their plotted vector errors still point in the direction towards rather than away from the satellite track as would be expected from considerations of their topographic elevations. However, since this area has few well-defined cultural features and since the effect of radar shadowing (due to high ground) is always present, these factors may well have resulted in certain of these points being not positively or well identified on the imagery. This is certainly a usual difficulty with radar imagery which has posed many problems to the few investigators who have also worked in this field (e.g. see Deane 1980, Leberl et al 1980).

Taking into account the poor resolution of the imagery and the mountainous nature of the area, the size and characteristics of the vector errors obtained from this test appear to be explicable.

9.4 Discussion of the Results from the Four Test Areas

9.4.1 Comparison of the Results from the Optically Processed Images

(i) Clearly, the results of testing the survey optically processed image showed its superiority over the precision processed image in terms of its geometrical accuracy, both before and after the application of the geometric rectification procedures. This is apparent from both the overall magnitude and the patterns of the individual vector errors. This is somewhat surprising in view of the fact that the two images cover the same area, were processed in the same optical processor at ERIM and that a larger number of ground control points were available for the testing of the precision processed image. Thus the planimetric accuracy (σ_p) at the control points ranged from slightly better (± 35 m) than a resolution element i.e. at sub-pixel level to more than two times (± 139 m) the resolution element for the survey processed image. The corresponding values for the precision processed image were ± 90 m and ± 147 m respectively. At the check points, the planimetric accuracy ranged from more than a resolution element (± 87 m) to more than twice the resolution (± 118 m) for the survey processed image while the corresponding figures were ± 105 m and ± 232 m for the precision processed image. The effects of the topography and elevation of individual test points above and below the average terrain level were apparent in both images, but these affected both images more or less equally.

(ii) It is apparent that both two optically processed images fit

quite poorly to the ground after the simple linear conformal transformation. This shows that the basic geometric fidelity of each of the two optically processed images analysed in this study was rather low in the original, uncorrected state as delivered to the user.

(iii) For both optical processing methods, the application of an affine transformation gives much superior results to those of a simple linear conformal transformation in the process of relating orbital radar images to the ground. This is because affine transformation employs two different scale correction terms in the directions of the satellite track and that normal to it. This effectively eliminates the differential scale errors present in the original image as a result of the optical processing, as is clear from the patterns shown in Figs 9.3 and 9.4 for the survey processed image and Figs 9.10 and 9.11 for the precision processed image. An obvious point to make is that the application of this affine correction could readily be made in the optical processor with evident benefit to the users from the geometric point of view.

(iv) For both the survey optically processed and the precision optically processed images, provided that a sufficient number of well placed control points are available, the highest order terms of the correction polynomial are effective in both reducing the magnitude of the errors and in rendering their patterns somewhat more random.

(v) Relief displacement or layover appears to make a significant contribution to the magnitude of the discrepancies as observed at the test points on both images. This is noticeable from the vector plots of the errors which are well correlated both with cross-track direction of the image and with the heights above or below the average terrain level on both the survey and the precision processed images.

9.4.2 Discussion of the Results from the Digitally Processed Images

The results obtained from the East Anglian image are much superior in both qualitative and quantitative terms to those obtained from both the optically processed images and from the digitally processed Milford Haven image. The reasons may include:-

(i) Image interpretability and target detection on the River Tay and Milford Haven images were rather difficult as compared with the East Anglian image. This may be due to the effect of radar shadowing and the lack of sufficient tonal variations due to the shortage of definite cultural features appearing on these images, both of which had substantial areas of hilly and moorland. In turn, this would result in a lack of positive identification in a number of the features being used as test points. In making comparisons between the two digitally processed images, it should be remembered also that differences between the two images will also result from differences in the orbital and processing parameters and values, since the two images were selected from two completely different satellite orbits.

(ii) Turning specifically to the Milford Haven image, the effect of relief displacement is obviously much greater than on the East Anglian image. This can be perceived from a comparison of the magnitude and pattern of the vector errors in all the plots for the two test areas.

(iii) Due to lack of well-defined planimetric detail on the Milford Haven image, the number of ground control points available for rectification was significantly less than on the East Anglian image. This also added to the difficulties since the computed values of the transformation parameters were less likely to be well determined as compared with the situation where a larger number of ground control points is available. However, this is a much less significant point than the effects of topography and interpretation discussed above.

(iv) For both digitally processed images, even taking into account the effects of topography, there still seems to be some kind of systematic pattern in the residual errors at the test points which is so far unexplained.

9.4.3 Comparison of Optically and Digitally Processed Images

Comparing the overall results from both the optically and digitally processed images, it is noticeable that, while the optically processed images fit quite poorly to the ground after the linear conformal transformation, with the two digitally processed images this simple type of transformation produces results which are not too different from those obtained from the other more complex polynomial transformations, including those with the highest degree terms. This confirms what has been mentioned in Section 3.6, that digital processing techniques have the advantages of increased flexibility in handling geometric and radiometric corrections, in controlling image sidelobes and in producing a better quality image.

While the highest order polynomial solutions offer little advantage over an affine transformation on the two digitally processed images, these polynomials do provide far superior results than the affine transformation for the optically processed images as far as geometric accuracy is concerned. Furthermore, while the application of these highest order polynomials resulted in the patterns of the residual errors being fairly random on the optically processed images, this is actually not generally the case with the two digitally processed images. In spite of much effort on the part of the present writer, small systematic effects could not be eliminated on the two digitally processed images.

9.5 Comparison with Other Tests of Geometric Accuracy of Seasat SAR Imagery

The only published work of a similar nature to that of the present project is that of Leberl (1980) carried out at the Technical University of Graz in Austria. The lack of other results may stem from any one or a combination of the following reasons:-

- (i) The very disappointing resolution of the Seasat SAR images even when produced by digital processing is a highly inhibiting factor. The nominal resolution of 20 to 30 metres has certainly not been realized for most areas: indeed, the resolution of digitally processed Landsat MSS and RBV imagery of much poorer nominal resolution (79 m in the case of the MSS) over the test areas is obviously superior to that of the Seasat SAR. Thus experimenters are inhibited from putting effort into the testing of this obviously fuzzy imagery which is extremely difficult to interpret and therefore to use as a basis for mapping. The problems encountered in the present test in getting a suitable number of individual test points are a pointer to the image quality.
- (ii) The early failure of the satellite could also be a reason for the apparent lack of interest, but in fact, because of the all-weather capability of the SAR, a great deal of coverage has been obtained over North America and Western Europe where most of the laboratories interested in mapping from remote sensing imagery are located. However, a more inhibiting factor has been the great delay in the supply of imagery for experimentation, especially digitally processed imagery. It has taken a great deal of time, energy and expense to provide

even the rather limited number of images available from the R.A.E. and D.F.V.L.R. facilities.

The methodology used by Leberl in his tests follows the general lines followed in this present study though with a smaller number of transformations which were limited to the simpler linear forms as follows:-

	<u>Leberl</u>		<u>Ali</u>
(i)	<u>Linear Conformal</u> (E=a+bx+cy; and ((N=d-cx+by	<u>2 parameter</u> as used in present tests.
(ii)	<u>Linear 5-parameter</u> (E=a+bc+cy+ex; and ((N=d-cx+by	not used.
(iii)	<u>Linear 6-parameter</u> (E=a+bx+cy) (and (N=d+ex+fy)	<u>3 parameter affine</u> as used in present tests.
(iv)	<u>Bilinear 8-parameter</u> (E=a+bx+cy+gxy) (and (N=d+ex+fy+hxy)	<u>4-parameter</u> as used in present tests.
(v)	<u>Moving average interpolative method</u>	not used.

where the point to be interpolated is considered a new point so that its interpolated coordinates can be evaluated against map values.

The area used by Leberl for his tests is that of the Imperial Valley adjacent to the Salton Sea in the far south west of the United States near the Mexican border. The area consists of a large block of irrigated fields set in a semi-desert area. The pattern of large rectangular fields coupled with the almost flat character of the

terrain makes it near ideal for test purposes. Maps at scales of 1:250,000, 1:62,500 and 1:24,000 were available for the selection and the measurement of coordinates of the control points. From the diagram in Leberl's paper about 50 points were used in his tests. The image coordinates of the points were measured using a monocomparator. The results of his tests of geometric accuracy expressed in r.m.s.e. values were as follows:-

Transformation	Optically Processed			Digitally Processed (by J.P.L.)		
	$\sigma_X(m)$	$\sigma_Y(m)$	$\sigma_P(m)$	$\sigma_X(m)$	$\sigma_Y(m)$	$\sigma_P(m)$
Moving Average	120	113	165	170	208	269
Bilinear 8-parameter	220	349	413	155	188	244
Linear 6-parameter	284	241	372	119	198	231
Linear 5-parameter	292	243	380	535	222	579
Linear Conformal	300	273	406	502	574	763

It would appear that Leberl has used all the available measured points as control points, since no distinction between control and check points is made in his paper. Making a comparison of his results for the digitally processed image of the Salton Sea area (produced by J.P.L.) with those of the present study for the relatively flat East Anglian area (produced by R.A.E.), the following results are obtained. (It should be noted that the order of terms used in this table - 8 parameter, 7 parameter, etc. - are those used previously in the author's tests already described.)

Transformation	ALI			LEBERL		
	$\sigma_X(m)$	$\sigma_Y(m)$	$\sigma_P(m)$	$\sigma_X(m)$	$\sigma_Y(m)$	$\sigma_P(m)$
8-parameter	23	26	35	-	-	-
7-parameter	24	25	35	-	-	-
6-parameter	25	28	38	-	-	-
5-parameter	27	29	40	-	-	-
Moving Average	-	-	-	170	208	269
4-parameter	26	36	44	155	188	244
3-parameter	25	35	43	119	198	231
Leberl's 5-parameter	-	-	-	535	222	579
2-parameter	26	38	46	502	574	763

There is such a wide discrepancy in the results as to virtually defy comparison. However, the first point to be made is that the R.A.E. digitally processed image appears to have been processed to much higher standards geometrically than the J.P.L. image. This is shown by the very small improvement in the results obtained when an affine (3-parameter) and a bi-linear (4-parameter) transformations are applied, as compared with those achieved with the simple linear conformal (2-parameter) transformation. By contrast, there is dramatic improvement in the r.m.s.e. values obtained by Leberl when using the affine and bi-linear transformations over those obtained with the linear conformal transformation which points to large residual differential scale errors between the X and Y directions in the Salton Sea image.

Even when this affine scale error is eliminated, there still remains the obvious point that the r.m.s.e. values obtained with the Salton Sea image are over five times larger than those of the East

Anglian image for the same transformations. The possibility of gross error in either the East Anglian data or measurements has been considered by the present author, but after an exhaustive check no such errors came to light. Further comparison of two such different sets of results seems quite pointless.

In his report, Leberl mentions the difficulties experienced in the selection and accurate identification of features which could be used as control points and gives some excellent illustrations of these difficulties. This parallels the present author's experiences in all the test imagery. Leberl also makes the observation that, although there is a great difference in quality between the optically and digitally processed images, the accuracies obtained with each are nearly equal. Apparently those points which could be identified in both images could be measured equally well. The advantage of the digitally processed image is that more points could be identified and measured than on the optically processed image - again a similar experience to that in the present study.

It is of course possible to make comparisons with previous geometric tests of airborne side-looking radar (SLR) imagery discussed in Chapter VII. However, in view of the fact that these have utilised such different systems with resolutions, look-angles, processing methods, terrain, ground control, etc, that are so very different to those of the present study, comparisons of this kind would be close to meaningless. However, the single point can be made that, for the East Anglian area where topographic effects were minimal, the results obtained ($\sigma_X = \sigma_Y = \pm 26$ m) are comparable to the very best obtained by an airborne SAR - those of Derenyi (1975) over the Pheonix test area using the GEMS-1000 system where $\sigma_X = \pm 30$ m and $\sigma_Y = \pm 28$ m were obtained.

9.6 An Assessment of the Geometric Accuracy of Seasat SAR Imagery for Planimetric Mapping at Small Scales

A matter of some interest to the Topographic Mapping Community is to assess the scales at which mapping from Seasat SAR imagery might be attempted from the standpoint of the geometric accuracy as revealed by the present tests. A convenient set of standards to use in such an assessment is the NATO specifications for topographic mapping. For maps at 1:600,000 scale and larger, the planimetric accuracy for class A maps is given as $\sigma_p = \pm 0.3$ mm (Petrie, 1974). On this basis, the required accuracies over the whole range of map scales from 1:50,000 to 1:600,000 scale are plotted in Fig 9.35. At 1:100,000 scale, the σ_p value is ± 30 m; at 1:150,000 scale, $\sigma_p = \pm 45$ m; at 1:250,000 scale, $\sigma_p = \pm 75$ m; at 1:300,000 scale, $\sigma_p = \pm 90$ m; and at 1:500,000 scale, $\sigma_p = \pm 150$ m.

It can be seen that, for flat ground and a dense network of control (as represented by the East Anglia area), and using the transformation techniques described above, the geometrical accuracy of the SAR imagery is compatible with mapping at the scale of 1:150,000. However, when there is considerable relief present (as represented by the River Tay and Milford Haven images), the geometric accuracy attainable with the Seasat SAR imagery is markedly lower and lies in the scale range 1:350,000 to 1:500,000 depending on the extent and character of the relief; the density and distribution of the available control points; and the transformation procedure employed. Thus, in purely geometric terms, the Seasat SAR imagery definitely has some possibilities for small-scale topographic mapping.

However, the discussion of the accuracy side cannot be conducted in isolation from the matter of the resolution of the imagery

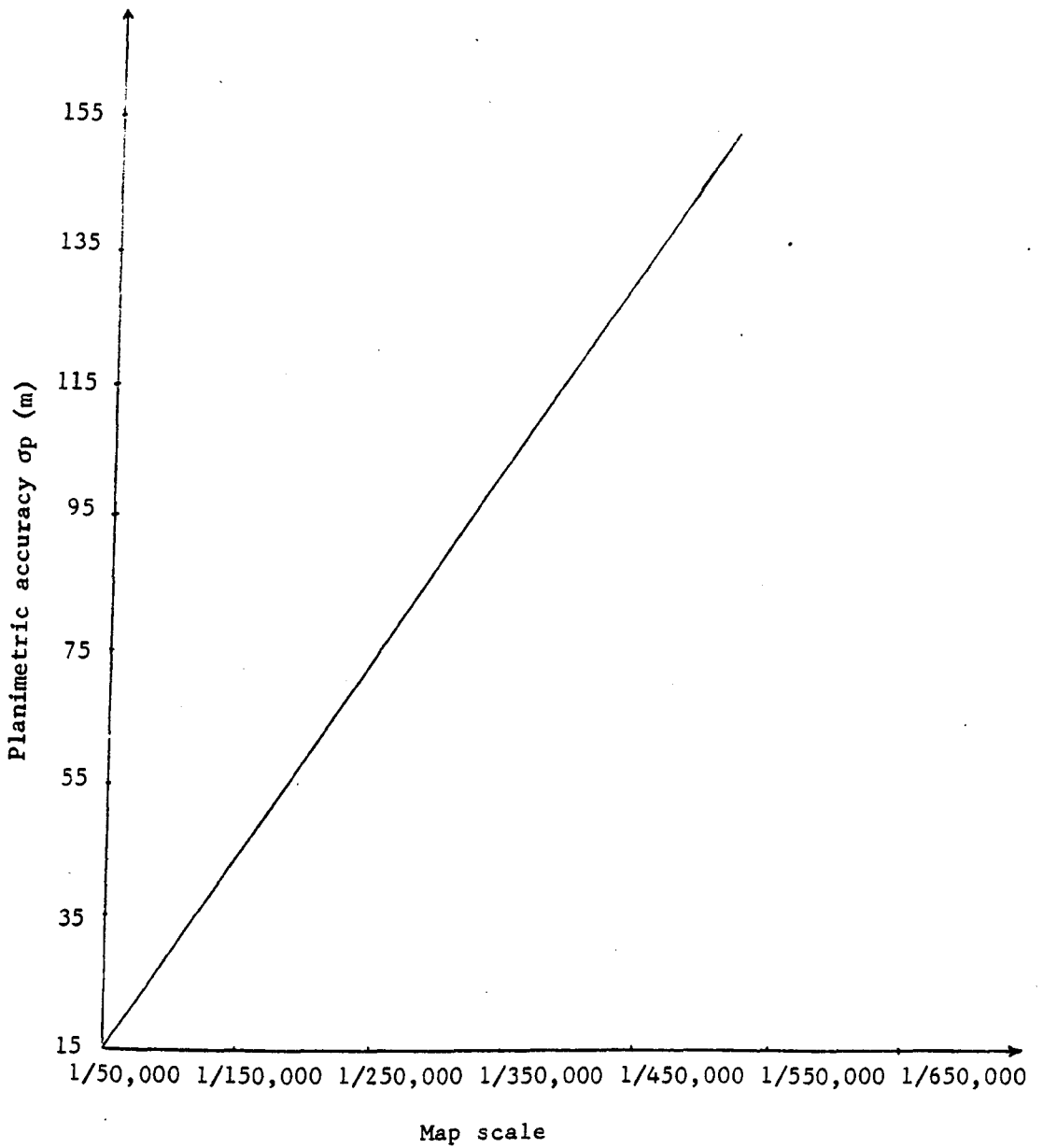


Fig 9.35 Planimetric detail accuracy at different scales
(Petrie, 1974)

and, in particular, the detection and interpretability of the objects present on the terrain which need to be mapped. The difficulties encountered by the present author in the selection, identification and measurement of the ground control points were extremely sobering in this respect. Therefore, the next area of research in the present study was to investigate in a systematic manner the suitability of the Seasat SAR images from the interpretational point of view. This has been carried out and the results are presented in Chapter XI.

Since the other major finding of the geometric tests was the considerable effects of relief on the accuracy of the imagery, it was decided to explore methods of compensating for these effects on the basis of continuous plotting. The attempts to do this employing digital monoplotting techniques are described in Chapter X.

CHAPTER XDIGITAL MONOPLOTTING FROM SEASAT SAR IMAGERY10.1 Introduction

As the name implies, digital monoplotting entails the measurement of the image coordinates of a single image and their transformation and rectification to ground coordinates. As applied to conventional photogrammetric work, the method usually requires a knowledge of the exterior orientation parameters of the photograph (derived from space-resection or aerial triangulation) and the ground relief (obtained from a digital terrain model (DTM)). This concept of utilizing a DTM for the digital planimetric mapping of terrain features from single conventional photographs has been the subject of research and development at only a few institutes, notably at the I.T.C. in the Netherlands (Makarovic, 1973, Besenicar, 1976a,b) and at the various military mapping research laboratories in the United States, i.e. the Rome Air Development Center (RADC) and the Engineer Topographic Laboratories (E.T.L.). The primary aim of all these efforts has been the development of a system which can be utilized for map revision - for cadastral and topographic mapping respectively.

Basically, a digital monoplotting system consists of three components (Fig 10.1). These are:

- (i) a measuring unit which generates image (x,y) coordinates in digital form, e.g. a monocomparator or a cartographic digitizer;
- (ii) a digital computer; and
- (iii) a digitally-controlled x/y plotting device e.g. a flat-bed or drum plotter.

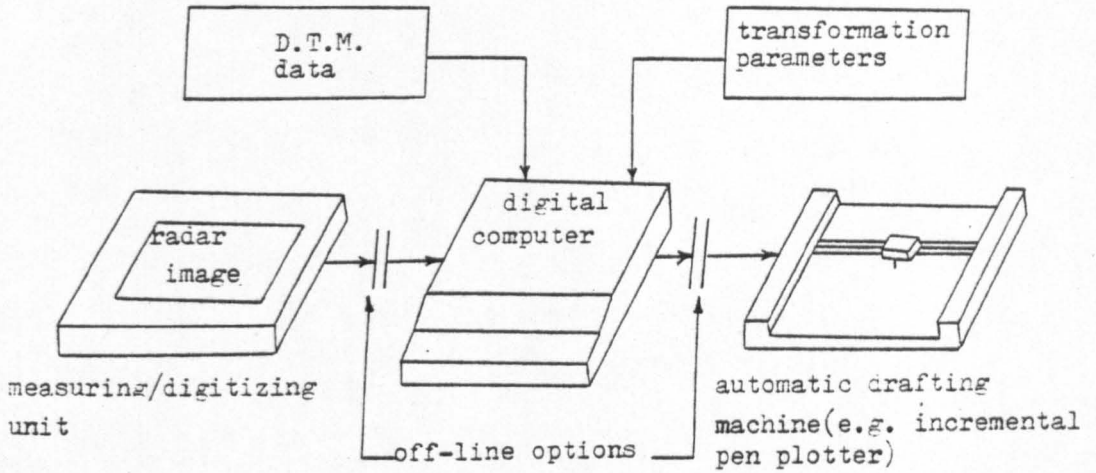


Fig 10.1 Atypical digital monoplotting system structure

Such a digital monoplotting system can be operated either on-line or off-line. While the on-line mode of operation has the advantage of immediate availability of the final product in digital or graphical analogue form, it may however have operational disadvantages in terms of programming and computational requirements, computer constraints, etc. Provided that immediate (i.e. real-time) results are not required, the off-line mode has much to offer in terms of somewhat more relaxed requirements on the computing side.

Since it appears unlikely that, in those countries with good topographic map coverage, SLR imagery will be used for basic topographic mapping, interest is likely to be concentrated on map revision, i.e. on the updating of existing maps. Given the geometrical characteristics of SLR imagery which almost invariably is monoscopic in character, the concept of digital monoplotting from SLR images is one which needs to be fully investigated for this application. The results of such an investigation are reported in this chapter. In particular, experimental work has been carried out to produce and update line-maps using individual Seasat SAR images. The procedures which have been followed, the programs which have been written and developed and the results obtained are described in detail.

10.2 Digital Monoplotting Systems

An early example of a digitally-based rectification system designed to plot detail from single images is the Bendix Line-Rectifier. Two different models of this instrument, the LR-1 (Forrest and Hattaway, 1968) and the LR-2 (Forrest, 1972), have been produced for the U.S. Navy. Each has a tracing device which allows the measurement of points, features, lines, etc. on a photograph on a point-to-point basis. On

the LR-1 this measuring device comprises a two-arm arrangement which measures the distance and angle, i.e. the polar coordinates, of each point. These are converted to rectangular coordinates. On the LR-2, the measuring/tracing device is a Bendix Datagrid tablet digitizer with a translucent surface which measures rectangular coordinates directly.

Empirical rectification procedures similar to those of optical rectification were employed on the LR-1 using electronic analogue computers. The orientation parameters were dialed into the device. Once this had been done, the path traced out by the measuring device was rectified, scaled and plotted using an analogue-based x/y plotter. On the LR-2 device, digital technology and procedures were introduced to give improved accuracy, greater range and simplified operation (Forrest, 1972). A specially-built hard-wired digital computer carried out the rectification on a point-to-point basis, the final plotting being carried out on a digitally-driven x/y coordinatograph. Forrest (1972) mentions specifically that the instruments were designed to accommodate infrared linescan and SLR imagery as well as frame and panoramic photography. However, the effect of terrain relief is not accounted for so that the generated terrain coordinates of image features will still contain errors of relief displacement. Still, it will be apparent that, apart from this feature, the LR-1 and LR-2 instruments contain all the other elements required for a digital monoplotting system.

Another extremely interesting and well-executed development in this field has been that carried out at the Rome Air Development Center (RADC) of the U.S.A.F. (Hall, 1974). Various digital monoplotting techniques were implemented, based on the use of a Calma 303

cross-slide digitizer and a Concord Cartographic Digitizer Plotter (CDP) attached to a PDP-9 computer.

The input data to the system are the digitized measurements made on the photograph. From the comparison of the measured image and the known terrain coordinates of the control points, the camera orientation parameters are computed using space resection. A DTM is also generated from existing topographic material, e.g. by tracing contours on maps and interpolating the heights into the rectangular array of the DTM. To obtain the height of any other point, a further interpolation is carried out based on the DTM elevations. Thus, if a feature has to be plotted from a new photograph to update the existing map, then as it is traced on the photograph, its position is continually rectified for tilt and relief using the camera orientation parameters and the height interpolated from the DTM. The result is a tape containing digital information on the new cartographic features which can be processed and edited interactively on the CDP device prior to its final plotting. While the software used in this system was designed specifically to handle reconnaissance panoramic photography, the general concept could be applied also to frame photography. Obviously, it represented an advanced and sophisticated implementation of the digital monoplotting technique at an early date.

In the I.T.C., the digital monoplotting concept was applied by Besenicar (1976b), the principal aim being the investigation of the possibility of revising cadastral maps from aerial photographs. The input data are again the digitized measurements of the cadastral features required to be updated made on the photograph with a d-Mac digitizer. The orientation parameters of the camera at the moment of exposure are computed using space resection and the photo and

terrain coordinates of the control points. A dense and homogeneous square grid DTM from which the heights of the measured cadastral features are to be interpolated, is formed from the digitized contour lines on the existing topographic map of the area. Thus, a measured point on the photograph is transformed to the terrain system using the orientation parameters and the interpolated heights of the terrain point which are related to one another through the use of the collinearity transformation.

The actual process seems to be somewhat complex. The height of the particular point can be interpolated from the DTM by first entering an initial approximate height which allows the generation of the initial (X,Y) coordinates of the point. These are used to re-define the point in the DTM. This allows the interpolation of a more accurate height value from which another set of planimetric coordinates (X,Y) are generated. Thus an iterative process takes place in which the difference between any two successive sets of planimetric coordinates (X,Y) can be compared with a pre-set value or threshold to decide whether the point has been satisfactorily rectified or not. If the difference exceeds the threshold value, another iteration of the process takes place. This procedure is carried out for all measured points as an off-line process. The resulting set of coordinate values can then be plotted out using an automatic drafting machine.

The extension of the digital monoplottting concept to remote sensing imagery was first carried out by Raytheon Autometric, under contract to the U.S.A.E.T.L. The outcome was a procedure which could perform digital rectification of side-looking radar imagery taken with the AN/APQ-152 (TOPO II) X-band imaging radar system (Greve and Cooney,

1974). The test imagery was flown with simultaneous HIRAN tracking and the operation of a laser altimeter to give the air station coordinates of a series of positions along the flight track together with the coordinates of specific range marks generated on the SLR strip image. A series of transformations were performed to convert the measured image coordinates into the terrain system after the flight path had been modelled using piece-wise polynomials to enable interpolation between the individual HIRAN-fixed positions. The DTM was represented by a rectangular grid of spot heights at 250 m interval.

The terrain itself was modelled by a simple polynomial of the form $h = a_0 + a_1x + a_2y + a_3x^2 + a_4y^2$ based on a five-point control pattern in the space of a cross. The solution for terrain intersection was accomplished by solving simultaneously, through linearization and iteration the following equations:-

$$\left. \begin{aligned} \text{(i) } \underline{\text{the range equation:}} S &= \left[(X_I - X_P)^2 + (Y_I - Y_P)^2 + (Z_I - Z_P)^2 \right]^{1/2}; \\ \text{(ii) } \underline{\text{the SLR beam yaw condition:}} \cos Q &= V_x(X_I - X_P) + V_y(Y_I - Y_P) + \\ & \quad V_z(Z_I - Z_P); \text{ and} \\ \text{(iii) } \underline{\text{the DTM interpolation:}} h &= a_0 + a_1x + a_2y + a_3x^2 + a_4y^2 \end{aligned} \right\} 10.1$$

where X_I, Y_I, Z_I represent the position of the aircraft;

V_x, V_y, V_z are the velocity vector components;

X_P, Y_P, Z_P are the ground coordinates of a point P;

Q is the yaw angle of the radar beam;

S slant range to ground point P; and

h is the mathematical surface representing the terrain.

After the rectification had been completed, a tape was produced which made the data available in digital form which was used to drive an x/y

plotter for graphical output or for entry of the data to a digital mapping system.

The method is extremely complex and wholly dependent on the special circumstances of the test in which the aircraft positions and velocity and the time and range marks on the SLR imagery were all available. With most SLR imagery, this type and range of auxiliary information is simply not available (as indeed is the situation with the Seasat SAR data).

10.3 Digital Monoplotting Procedure for Seasat SAR Imagery

In the case of conventional aerial photography, the X and Y terrain coordinates of a point on the photograph are related to the x and y photo coordinates by the collinearity equations (6.12). However, as discussed in Chapter VI, since SLR imagery is geometrically quite different in character, these equations cannot be used here. If the position and attitude of the SLR sensor are available and the image contains range and time marks, then the procedure for digital monoplotting of the Seasat SAR images could have been similar to that followed by Greve and Cooney (1974) described above. However, this information was not available nor were the values of the imaging parameters of equation 10.1 available for Seasat. Thus an alternative approach had to be developed for digital monoplotting from Seasat SAR imagery.

With this method, the digital image data is first transformed into the terrain system using the polynomial equations 8.2, namely:-

$$X = n_0 + n_1x + n_2y + n_3xy + n_4x^2 + n_5x^2y + n_6x^3 + n_7x^3y ; \text{ and}$$

$$Y = m_0 + m_1x + m_2y + m_3xy + m_4x^2 + m_5x^2y + m_6x^3 + m_7x^3y.$$

In a single radar image, these transformed coordinates must contain certain planimetric errors due to changes in the topographic relief. The error at each point is given by equation 6.28, i.e.

$$S = \frac{-Hh}{S_g} \text{ (the (-) sign is for points above average ground level)}$$

where H = the flying height;

h = the height of a point above the average ground level; and

S_g = the ground range measured from the ground track to the point in question.

So, if the value of the ground range (S_g) is available and a value for the height (h) of the point can be derived from a DTM, then, knowing the average flying height (H), the correction for the relief error can be computed. This can be resolved into its easting and northing components if the angle between the flight direction and the National Grid is known. This will result in corrected planimetric coordinates for each measured point with the relief displacement errors either eliminated or considerably reduced.

10.3.1 Measurement and Transformation of the Contour Data to form a DTM.

The DTM has to be generated from an existing topographic map of the area in question at a suitable scale. For this particular experiment, the East Anglian test area was used since, of the three test areas available, it had the largest number of interpretable and plottable features available.

The first step in the process of generating the DTM was the measurement of the contour lines shown on the existing 1:63,360 Ordnance Survey (O.S.) topographic map of the area. This operation

was carried out on the large-format 36" x 48" (92 cm x 122 cm) GTCO cartographic digitizer belonging to the Department of Geography (Fig 10.2). This device has a resolution or least count of 0.1 mm and is equipped with a dot matrix coordinate display and a keyboard for the entry of header codes, height values or other information. For this particular operation, the GTCO digitizer was interfaced to a Lear Siegler ADM-3A video terminal which allowed the display and checking of coordinates and header codes and to an MFE2500 digital cassette drive which acted as the data recorder for the storage of the digitized contour data (Fig 10.2).

First of all, the corner points of the area of the map to be digitized were measured on the GTCO digitizer. Comparison of their digitizer coordinates and the corresponding map coordinates generated the transformation parameters which could be used to transform all the measured planimetric data to the terrain system. Next, a series of points located along each of the contour lines were measured in point mode using a sampling interval of 2-3 mm between points to form the basic input data for the construction of the DTM. The actual value of each measured contour was input using the menu technique, i.e. each was assigned a height value corresponding to its position (or coordinate value) in a series of boxes located outside the area of the map being digitized. On completion of the digitizing of the contours, the positions of all the points lying on the digitized contour lines were transformed to the map system using the already determined transformation parameters.

In most DTMs, the next stage is the interpolation of the actual DTM heights from the measured contour values such that the DTM values form a regular square, rectangular or triangular grid which

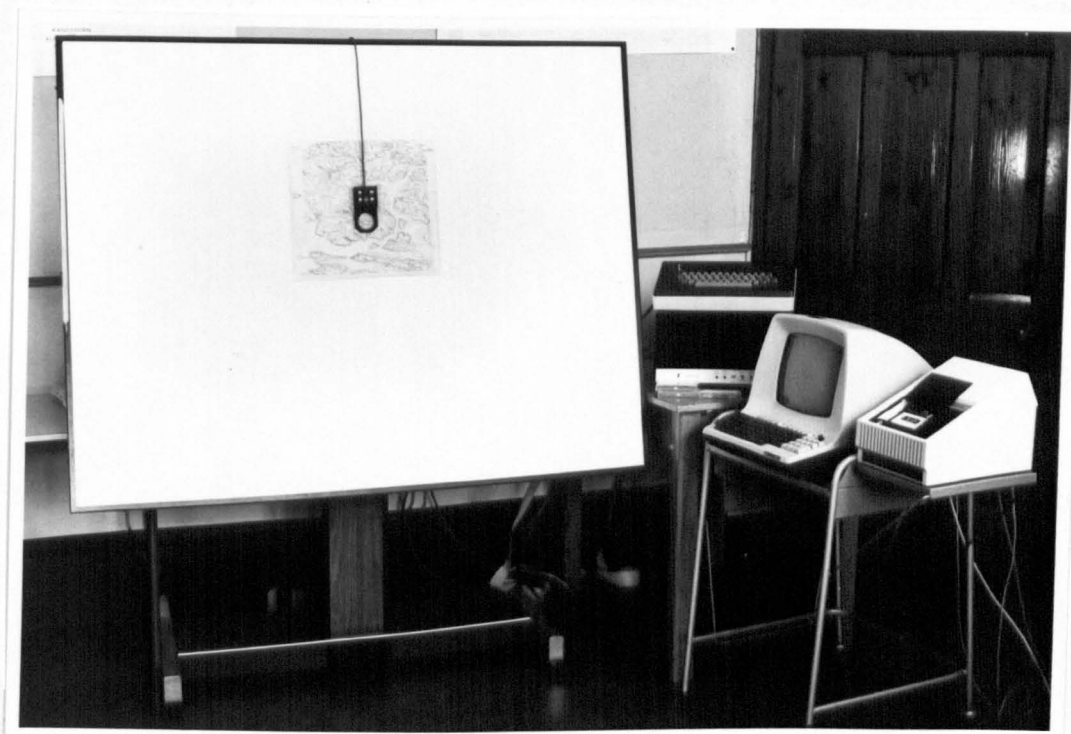


Fig 10.2 The GTCO Cartographic digitizer with its display unit connected to an MFE data recorder and a VDU (the contour map is on top of the active surface of the digitizer)

is often a prior condition of the DTM. This has not been carried out on this occasion. Instead, the measured points lying along the contours actually form the basic DTM itself and do not correspond to some pre-determined pattern. Such an arrangement is usually termed a string DTM. This cuts out the requirement for the interpolation of a DTM from the contour information but at the cost of more complex search and interpolation routines when direct interpolation of the height of a specific location from the string DTM is required for the purposes of rectification.

10.3.2 Measurement and Transformation of SLR Image Data

A positive film transparency of the digitally processed East Anglian image was first mounted on the 11" x 11" (28 cm x 28 cm) format Houston Hi-Pad digitizer which has a translucent surface and could be back-lit. The Lear Siegler ADM-3A video terminal and the MFE2500 digital cassette drive were again attached to the digitizer for the display and logging of the coordinate data respectively. A prior interpretation of all the image features to be plotted in the northern half of the test area was carried out with the help of the topographic map of the area and a 4x enlarged print of the image. The interpreted features were then measured and recorded in digital form, suitable header codes for feature identification being introduced during the digitizing.

As already mentioned above, the measured digital image coordinate data could then be transformed into the corresponding terrain values. The transformation parameters of equations 8.2 were derived from the comparison of image and terrain coordinates of 12 control points using Program POLY. The result of this stage

is that now both the DTM data and the measured image data are expressed in terms of terrain, (i.e. National Grid) coordinates.

10.3.3 Rectification of Measured SLR Image Data

The next stage is to generate corrected planimetric coordinates for the features measured on the SLR imagery by applying the height values interpolated from the DTM and correcting for relief displacement. For each image point, a corresponding height value is interpolated. Different algorithms exist for interpolating the height values for specific locations from DTMs, e.g. see Leberl (1975d), Allam (1978), Leberl (1975d) and Masry et al (1977) have come to the general conclusion that simple linear interpolation is quite suitable for nearly flat areas; the weighted arithmetic mean method suits areas of moderate relief; bi-linear interpolation usually suits hilly terrain; while higher order polynomial interpolation may be appropriate in areas having considerable relief. From this experience gained elsewhere, the weighted arithmetic mean method would be expected to give satisfactory results for height interpolation in this area of moderate relief and has therefore been adopted in the present study.

The actual procedure is as follows:-

- (i) The transformed image point P_j is first located horizontally within the DTM and a search zone of radius $R_c = 500$ m around this point is defined so that all the measured DTM points lying within this zone may be identified (Fig 10.3).
- (ii) Leg g_i ($i = 1, N$) be the N points of the DTM with known elevation values h_i that lie within this zone.

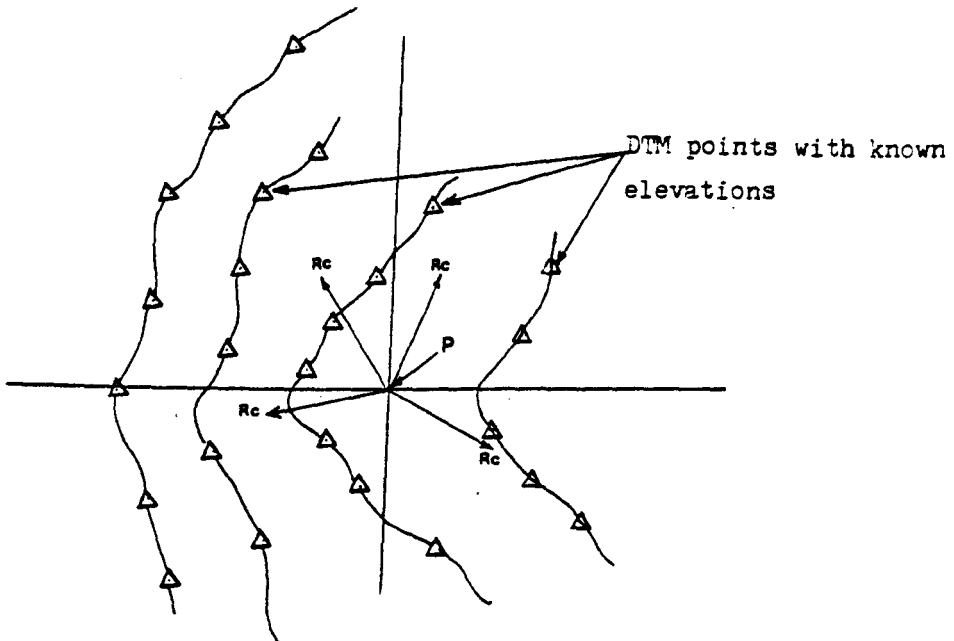


Fig 10.3 Height interpolation from a DTM file

(iii) If the horizontal distance between g_i and P_j is designated by D_{ij} , then the elevation of point P_j can be obtained by the weighted arithmetic mean interpolation method as set out in equation 7.2.

This is carried out for all N points. If it is required to speed up the interpolation process, N can be limited to the 3 or 4 points nearest to P_j .

Once the interpolated height of the measured image point P_j has been determined, it is then used to compute the value of the relief displacement error (procedure HCAL in Program FRECT) using the average ground elevation (procedure HAVERAGE in Program FRECT) and the angle between the Grid North and the across-track direction (THETA) which is a given parameter. This is repeated for all the measured image points to be plotted on the map. The final result of this operation is a file containing the X and Y terrain coordinates of all the digitized image features corrected for terrain relief. This file then serves as input to the plotting program to generate the planimetric line map. This is executed by a plotting program (PLOTTER) which calls the appropriate GHOST routines from the ICL 2976 mainframe machine and controls the plotting on a CIL incremental drum plotter.

10.4 Description of the Software

In this section, the suite of computer programs developed specifically for the purpose of digital monoplotting from Seasat SAR imagery will be described in detail. There are three such programs, all written in FORTRAN IV computer language. These have been compiled and run using the FORTRAN F1 compiler of the ICL 2976

mainframe computer of the Glasgow University Computing Service.

These programs are:-

- (i) Program DTM: which produces terrain coordinates from the measured coordinate data of the contours;
- (ii) Program FRECT: A feature rectification program which merges the measured image data, the image-to-terrain transformation parameters and the DTM in order to generate terrain coordinates with reduced relief displacement errors; and
- (iii) Program PLOTTER: This program provides instructions for the automatic plotting of the rectified coordinate data and the generation of the digital map of the area.

10.4.1 Program DTM

This program is designed to compute the terrain (National Grid) coordinate values of all the points lying along the contours which have been measured on the map using the digitizer, thus forming the string DTM. It utilizes transformation parameters determined in a prior operation using Program POLY.

10.4.1.1 Definition of Variables

G1 (1,i), G1 (2,i)	Digitizer (x,y) coordinates of a point on the map;
G2 (1,j)	Transformed Eastings value of a point;
G2 (3,j)	Elevation of a point above O.S. Datum;
N	Number of digitized points on the map;
X31, Y31)	Digitizer planimetric coordinates of all points measured on the map whose contour values are 31 m, 46 m, 61 m, 76 m and 91 m (100, 150, 200, 250 and 300 ft) respectively.
X46, Y46)	
X61, Y61)	
X76, Y76)	
X91, Y91)	

T1, T2,, T6 The six affine transformation parameters (as computed by program POLY) for the digitizer-terrain transformation.

10.4.1.2 Definition of Arrays

G1 (2,n) Array comprising the digitizer (x,y) coordinates of all points measured along the map contours together with the five headers (corresponding to the five contour values actually encountered in the East Anglian test area);

G2 (3,M) Array comprising the Eastings, Northings and elevation values which form the DTM of the area. N.B. $m = (n-5)$ since there are five headers in array G1 corresponding to the five measured contours.

10.4.1.3 Explanation of the Program

The program is listed in Fig 10.4. The program listing has been divided into a number of blocks to aid the explanation of the successive operations which it performs.

Block 1. In this initial block, the procedure of the program is given and the arrays G1 and G2 are dimensioned.

Block 2. This block is of an explanatory nature. It explains the purpose of arrays G1 and G2 and provides the information that the next block comprises the values of the parameters required for the transformation from digitizer to terrain coordinates.

Block 3. In this block, the values of the six parameters allowing an affine transformation between the digitizer coordinate system and the map system are given. These have been computed separately in a prior operation using program POLY of Section 8.8.2. The

(0001)	PROGRAM DTM	(1)
(0002)	REAL G1(2,903),G2(3,898)	
(0003)C	G1 IS THE ARRAY CONTAINING THE DIGITIZED CONTOUR DATA	
(0004)C	G2 IS THE ARRAY CONTAINING THE XYZ TERRAIN COORDINATES	
(0005)C	OF THE AREA IE THE DIGITAL TERRAIN MODEL OF THE AREA	(2)
(0006)C	INPUT VALUES OF TRANSFORMATION PARAMETERS FROM DIGITIZER	
(0007)C	TO TERRAIN	
(0008)	T1=544258.	
(0009)	T2=63.4755	
(0010)	T3=-3.61992	
(0011)	T4=302133.	(3)
(0012)	T5=3.55814	
(0013)	T6=63.4281	
(0014)	N=903	
(0015)	READ (5,100) G1	(4)
(0016) 100	FORMAT(1X,F5.1,1X,F5.1)	
(0017)C	NO. OF ROWS OF ARRAY G2>THAN THOSE OF ARRAY G1 BY 5 THE NO. OF HEADERS	(5)
(0018)C	THE FORMATION OF THE DIGITAL TERRAIN MODEL BEGINS	
(0019)	J=1	
(0020) 110	X31=G1(1,J)	
	CONTINUE(Y OR N)?Y	
(0021)	Y31=G1(2,J)	
(0022)	IF(X31.EQ.1013.3.AND.Y31.EQ.948.7)GOTO 120	(6)
(0023)	G2(1,J)=T1+T2*X31+T3*Y31	
(0024)	G2(2,J)=T4+T5*X31+T6*Y31	
(0025)	G2(3,J)=31.0	
(0026)	IF(J.GT.N)GOTO 170	
(0027)	J=J+1	
(0028)	GOTO 110	
(0029) 120	IF(J.GT.N) GOTO 170	
(0030)	J=J+1	
(0031)	X46=G1(1,J)	
(0032)	Y46=G1(2,J)	(7)
(0033)	IF(X46.EQ.895.9.AND.Y46.EQ.949.8)GOTO 130	
(0034)	G2(1,J-1)=T1+T2*X46+T3*Y46	
(0035)	G2(2,J-1)=T4+T5*X46+T6*Y46	
(0036)	G2(3,J-1)=46.00	
(0037)	GOTO 120	
(0038) 130	IF(J.GT.N)GOTO 170	
(0039)	J=J+1	
(0040)	X61=G1(1,J)	
	CONTINUE(Y OR N)?Y	
(0041)	Y61=G1(2,J)	(8)
(0042)	IF(X61.EQ.693.9.AND.Y61.EQ.947.5)GOTO 140	
(0043)	G2(1,J-2)=T1+T2*X61+T3*Y61	
(0044)	G2(2,J-2)=T4+T5*X61+T6*Y61	
(0045)	G2(3,J-2)=61.0	
(0046)	GOTO 130	
(0047) 140	IF(J.GT.N)GOTO 170	
(0048)	J=J+1	
(0049)	X76=G1(1,J)	
(0050)	Y76=G1(2,J)	(9)
(0051)	IF(X76.EQ.505.8.AND.Y76.EQ.950.6)GOTO 150	
(0052)	G2(1,J-3)=T1+T2*X76+T3*Y76	
(0053)	G2(2,J-3)=T4+T5*X76+T6*Y76	
(0054)	G2(3,J-3)=76.00	
(0055)	GOTO 140	
(0056) 150	IF(J.GT.N) GOTO 170	
(0057)	J=J+1	
(0058)	X91=G1(1,J)	
(0059)	Y91=G1(2,J)	
(0060)	IF(X91.EQ.7.00.AND.Y91.EQ.7.00)GOTO 170	(10)
	CONTINUE(Y OR N)?Y	
(0061)	G2(1,J-4)=T1+T2*X91+T3*Y91	
(0062)	G2(2,J-4)=T4+T5*X91+T6*Y91	
(0063)	G2(3,J-4)=91.00	
(0064)	GOTO 150	
(0065) 170	WRITE(6,180)G2	
(0066) 180	FORMAT(1X,F9.2,1X,F9.2,1X,F4.1)	(11)
(0067)	STOP	
(0068)	END	
(0069)**END**		(12)

352

353

block also gives the number of records that have been digitized, in this particular case, $N = 903$.

Block 4. In this block, the array $G1(2,n)$ is read into the computer memory from channel 5 using the format specified in statement 100.

Block 5. This block explains the difference in size between the arrays $G1$ and $G2$.

Block 6. This block begins by assigning the value of $j = 1$ to the first digitized record and gives it the local coordinates $X31, Y31$ since it has an elevation value of 31 m. It then checks whether these coordinates have values $x = 1013.3$ mm and $y = 948.7$ mm (which in this particular case, correspond to the starting values of a contour elevation value of 46 m and not 31 m). If this is not true, the program proceeds to transform the digitizer coordinates (i.e. $X31, Y31$) of this point into their terrain values using the transformation parameters already given. On completion of this operation, the program then stores these values together with the contour value of 31 m into array $G2$. It then increases the value of j by 1 and control is transferred to statement 110 for the next point and the same operation is repeated. If on the other hand, $X31, Y31$ are equal to 1013.3 mm and 948.7 mm (which are the header values of contour elevation of 46 m), control is transferred to statement 120 which means that the function of this block has now been exhausted and the program proceeds to Block 7.

Block 7. This block first checks whether the value of $N (= 903$ in this case) has been reached or not. If not, it increases the value of j it received from Block 6 by 1 and then executes the same set of operations as in Block 6 but on this occasion for all the

points with the elevation value of 46 m. This continues until the value $x = 895.9$ mm and $y = 949.8$ mm (corresponding to contour values of 61 m) is reached, in which case the program jumps to Block 8.

Blocks 8, 9, 10. The function of each of these Blocks is similar to that of Blocks 6 and 7 except that each carries out its operations on all points with elevation values of 61, 76 and 91 m respectively.

Block 11. This writes out array G2 into a pre-created data file in the format specified in statement 180.

Block 12. This ends the execution of the program.

10.4.1.4 Detailed Explanation of the Program

<u>Line Number</u>	<u>Comments</u>
1	Procedure of the Program.
2	Dimensions arrays.
3-7	Explains arrays G1 and G2 and comments on the transformation parameters.
8-14	Gives the values of the parameters used in the actual affine transformation and the number of digitized points.
15-16	Reads in array G1 in the specified format.
17-18	Comments on the sizes of arrays G1 and G2.
19	Put $j = 1$ for the first data point.
20-28	Transforms all those digitized points with contour elevation value of 31 m to terrain values and stores the transformed coordinates together with the elevation value of 31 m for each point in array G2 until all points with elevations = 31 m are transformed.
29-64	Transforms all digitized points with contour values

of 46 m (lines 29-37); 61 m (lines 38-46); 76 m (lines 47-55) and 91 m (lines 56-64) into terrain values and stores the transformed coordinates, together with the corresponding elevation values for each point, in array G2 until all points with elevations = 46, 61, 76 and 91 m have been transformed.

65-66 The array G2 (3,M) comprising the X, Y, Z coordinates of points (i.e. the DTM) is written in the specified format.

67-68 Ends the execution of the program.

10.4.1.5 Program and Sample Input and Output Listings

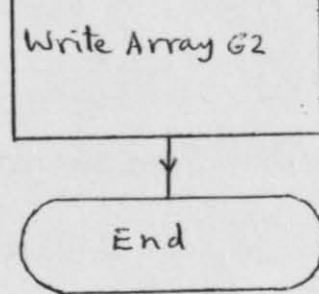
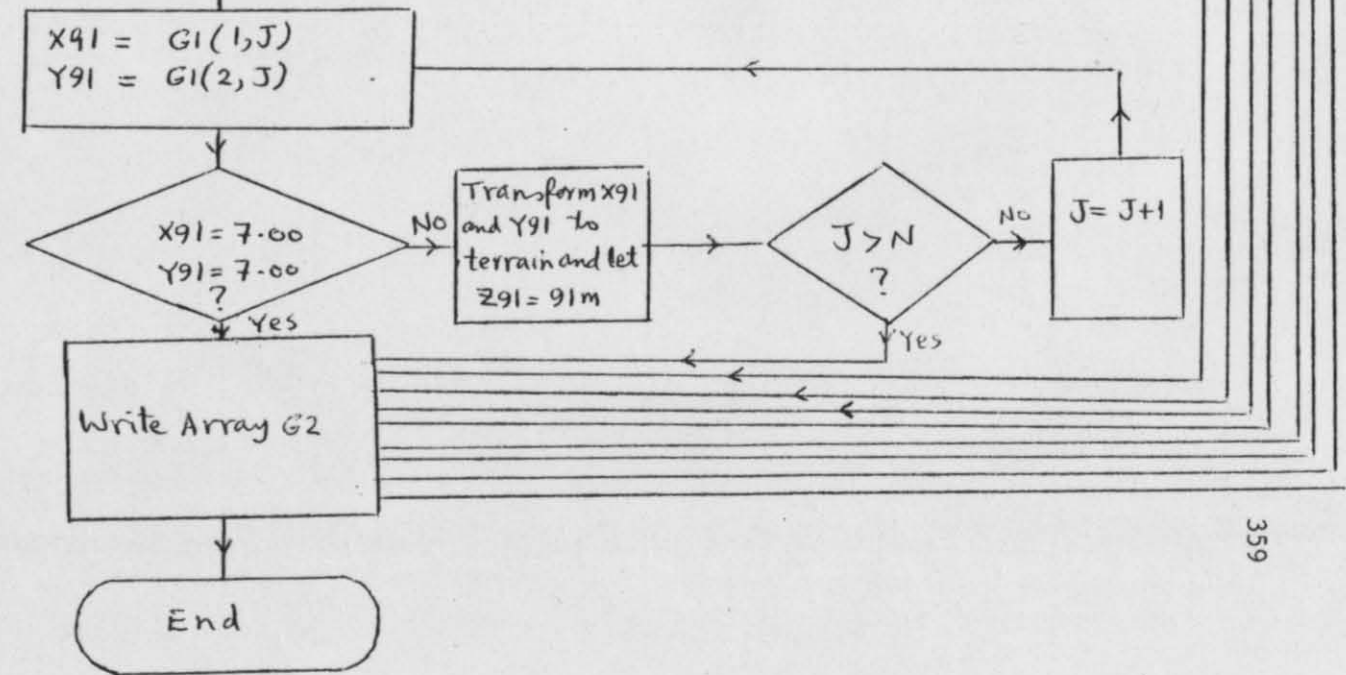
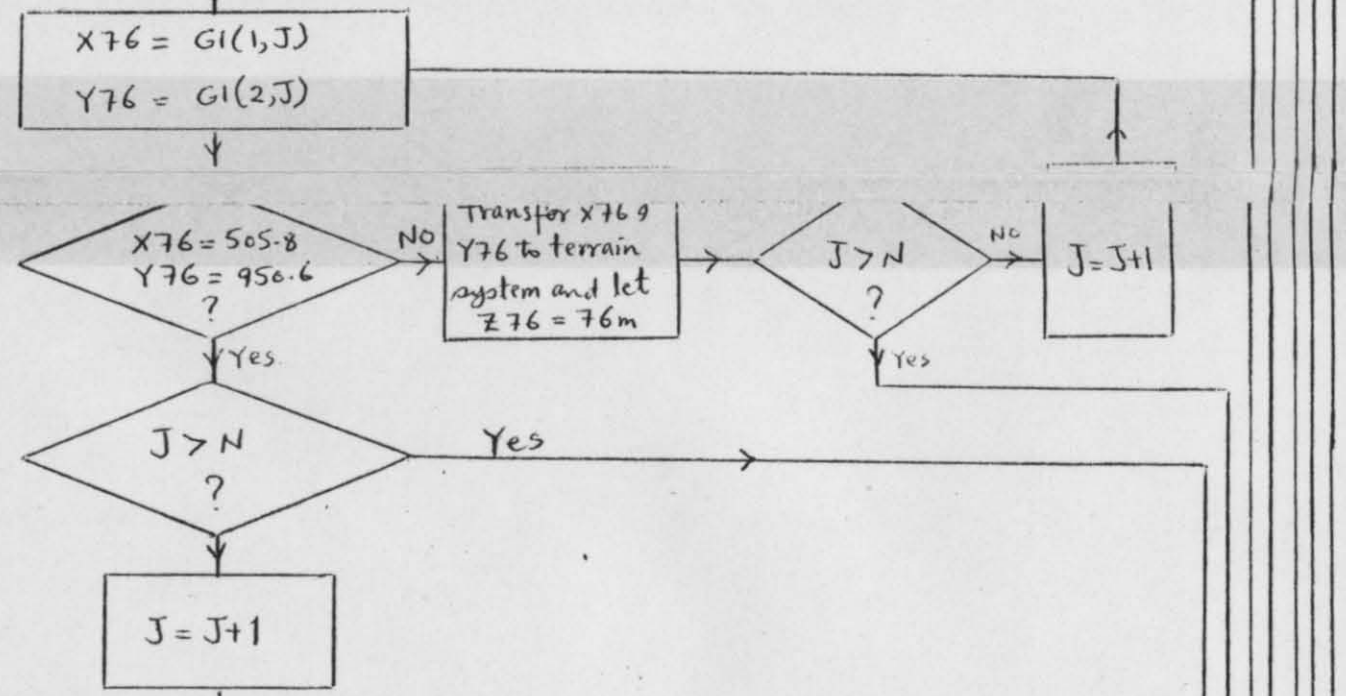
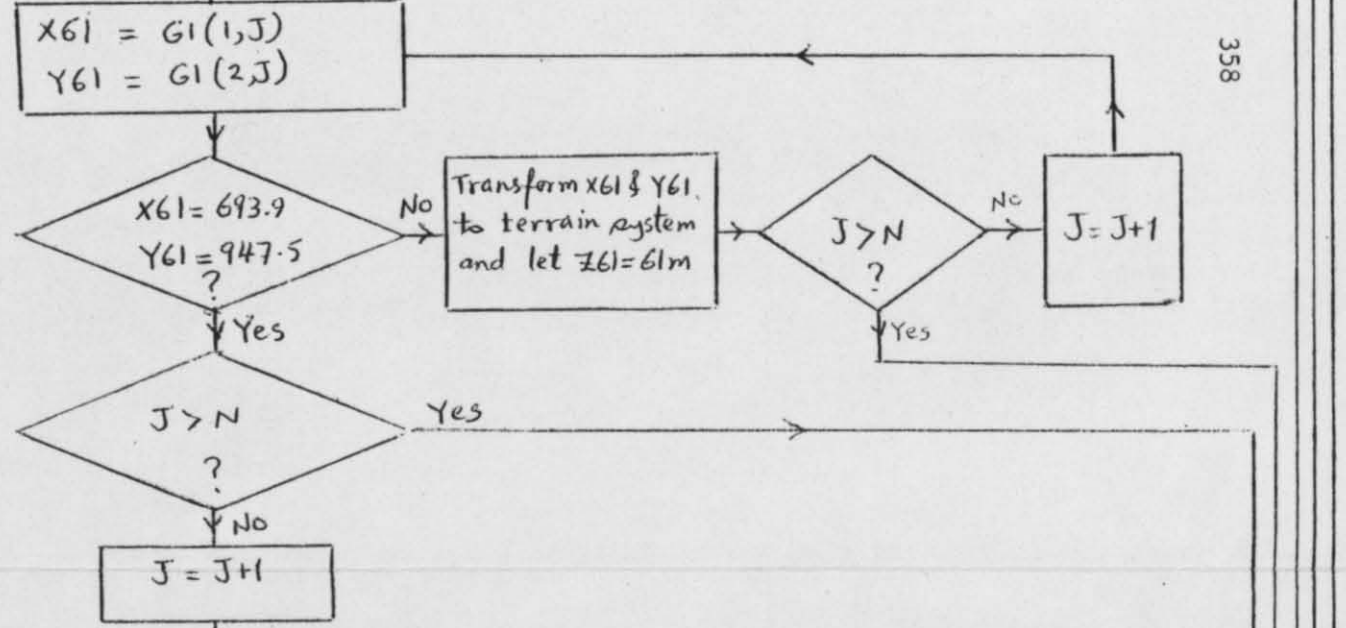
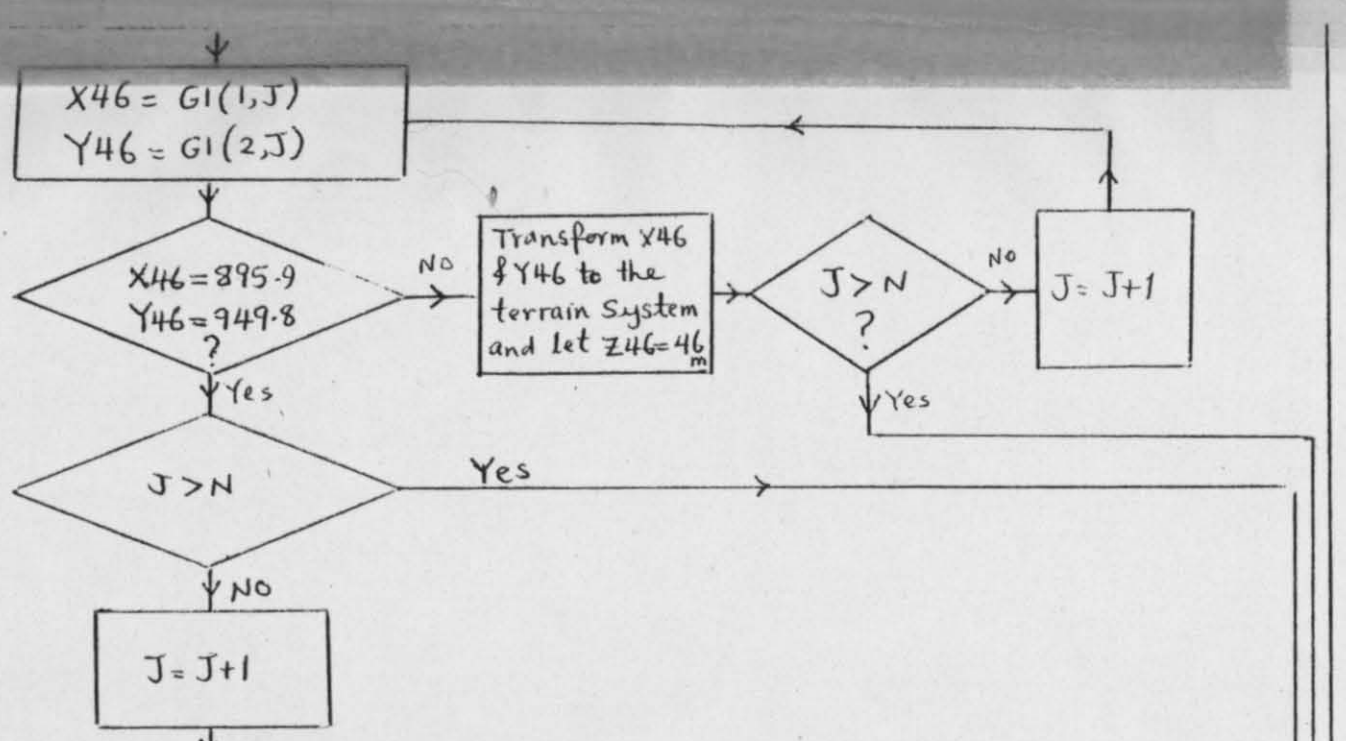
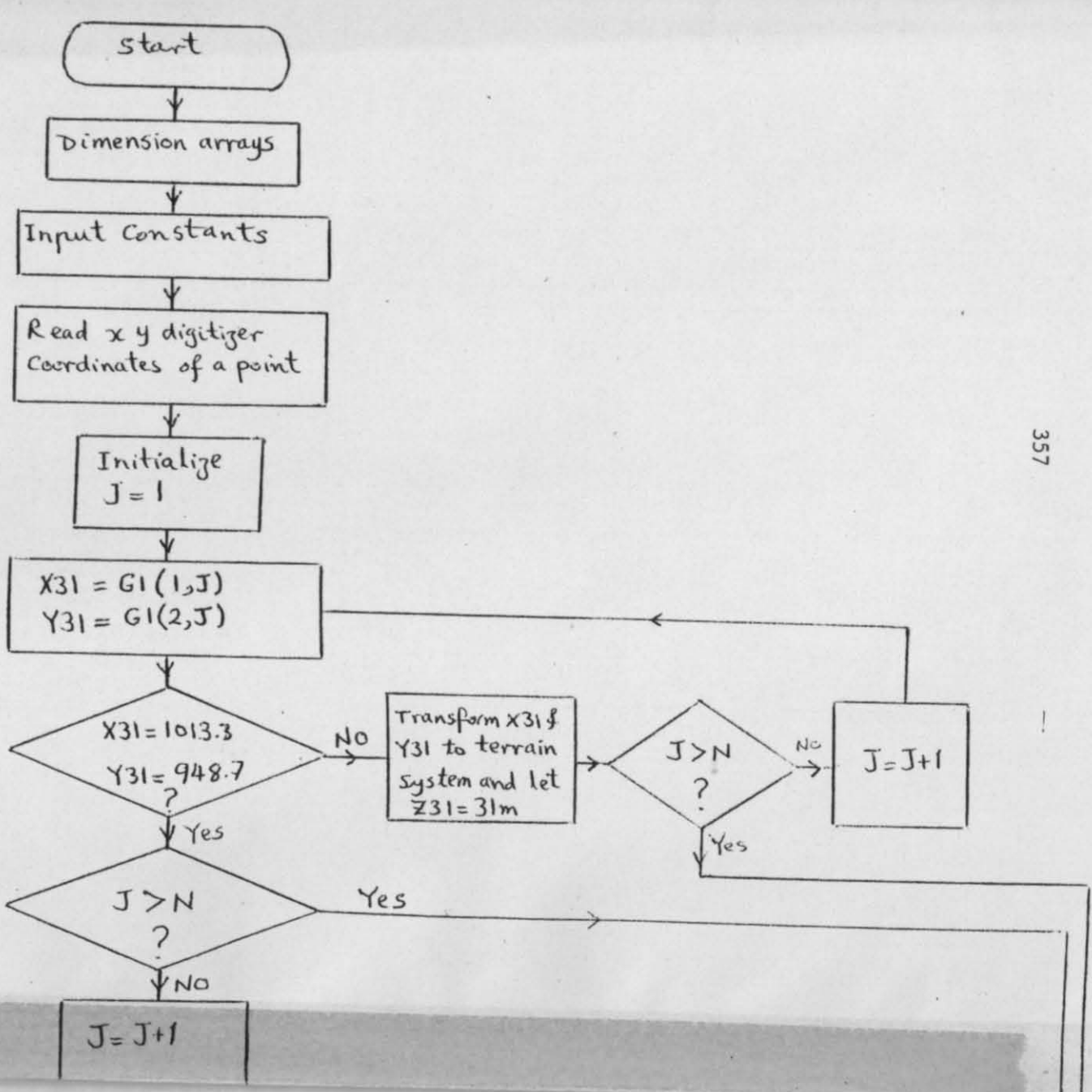
Fig 10.4 is the actual listing of the Program DTM supplemented by the flow diagram Fig 10.4.1. A sample of input data to the program is given in Fig 10.5 with a corresponding sample output data in Fig 10.6.

10.4.2 Program FRECT

This is the feature rectification program which transforms the digitized image coordinate data into the terrain system and then applies the necessary geometric corrections for relief displacement to the transformed data using the height values interpolated from the string DTM data generated by the previous Program DTM. In the same manner as the previous DTM program, the set of parameter values required for the image to terrain coordinate transformation are determined in a preliminary operation using Program POLY.

10.4.2.1 Definition of Variables

PULLOUTS



(0001) 06807 05150
 (0002) 06828 05109
 (0003) 06828 05080
 (0004) 06827 05028
 (0005) 06838 04979
 (0006) 06873 04935
 (0007) 06892 04902
 (0008) 06914 04883
 (0009) 06951 04872
 (0010) 06994 04862
 (0011) 07033 04855
 (0012) 07053 04850
 (0013) 07052 04835
 (0014) 07056 04834
 (0015) 07005 04831
 (0016) 06987 04824
 (0017) 06964 04753
 (0018) 06945 04822
 (0019) 06946 04818
 (0020) 06923 04842
 CONTINUE(Y OR N)?Y

(0021) 06881 04855
 (0022) 06847 04883
 (0023) 06818 04915
 (0024) 06818 04915
 (0025) 06782 04950
 (0026) 06769 04987
 (0027) 06748 05022
 (0028) 06747 05023
 (0029) 06724 05026
 (0030) 06723 05026
 (0031) 06690 05023
 (0032) 06716 05050
 (0033) 06731 05074
 (0034) 06743 05116

Header indicating the start of points with elevation=46m

(0035) 06920 05204
 (0037) 06917 05166
 (0038) 06946 05153
 (0039) 06965 05116
 (0040) 07002 05079
 CONTINUE(Y OR N)?Y

(0041) 07028 05039
 (0042) 07039 05005
 (0043) 07033 04961
 (0044) 07034 04928
 (0045) 07011 04926
 (0046) 07010 04927
 (0047) 06979 04955
 (0048) 06956 04951
 (0049) 06925 04931
 (0050) 06909 04942
 (0051) 06908 04970
 (0052) 06883 04992
 (0053) 06887 05042
 (0054) 06871 05076
 (0055) 06871 05073
 (0056) 06878 05110
 (0057) 06858 05119
 (0058) 06841 05141
 (0059) 06825 05144
 (0060) 06825 05161
 CONTINUE(Y OR N)?Y

(0061) 07131 05280
 (0062) 07121 05249
 (0063) 07095 05240
 (0064) 07071 05229
 (0065) 07064 05195
 (0066) 07049 05156
 (0067) 07064 05122
 (0068) 07090 05109
 (0069) 07090 05110
 (0070) 07059 05056
 (0071) 07065 05034
 (0072) 07109 05020
 (0073) 07110 04983
 (0074) 07118 04954
 (0075) 07132 04935
 (0076) 07136 04935
 (0077) 07152 04949
 (0078) 07183 04964
 (0079) 07195 04926
 (0080) 07234 04939
 CONTINUE(Y OR N)?Y

(0081) 07259 04964
 (0082) 07269 04969
 (0083) 07259 04923
 (0084) 07257 04895
 (0085) 07267 04878
 (0086) 07263 04854
 (0087) 07295 04825
 (0088) 07312 04801
 (0089) 07327 04763
 (0090) 07284 04795
 (0091) 07246 04825
 (0092) 07226 04845
 (0093) 07208 04859
 (0094) 07181 04866
 (0095) 07145 04853
 (0096) 07113 04863
 (0097) 07121 04831
 (0098) 07136 04799
 (0099) 07188 04791
 (0100) 07218 04778
 CONTINUE(Y OR N)?Y

(0101) 07192 04746
 (0102) 07192 04706
 (0103) 07195 04667
 (0104) 07194 04652
 (0105) 07207 04628
 (0106) 07186 04586
 (0107) 07216 04548
 (0108) 07255 04518
 (0109) 07278 04486
 (0110) 07278 04485
 (0111) 07321 04468
 (0112) 07347 04427
 (0113) 07375 04387
 (0114) 07410 04354
 (0115) 07452 04327
 (0116) 07456 04286
 (0117) 07476 04274
 (0118) 07505 04279
 (0119) 07512 04258
 (0120) 06582 05052
 CONTINUE(Y OR N)?Y

(0121) 07447 04308
 (0122) 07447 04299
 (0123) 07447 04276
 (0124) 07447 04257

	Eastings (metres)	Northings (metres)	Z (m)
(0001)	585601.50	337220.40	31.0
(0002)	585749.60	336967.90	31.0
(0003)	585760.10	336783.90	31.0
(0004)	585772.60	336453.80	31.0
(0005)	585860.10	336146.90	31.0
(0006)	586098.30	335880.30	31.0
(0007)	586230.80	335677.70	31.0
(0008)	586377.30	335565.00	31.0
(0009)	586616.20	335508.40	31.0
(0010)	586892.70	335460.30	31.0
(0011)	587142.80	335429.80	31.0
(0012)	587271.60	335405.10	31.0
(0013)	587270.60	335309.60	31.0
(0014)	587296.40	335304.80	31.0
(0015)	586973.80	335267.60	31.0
(0016)	586862.10	335216.80	31.0
(0017)	586741.80	334758.30	31.0
(0018)	586596.20	335189.10	31.0
(0019)	586604.00	335164.10	31.0
(0020)	586449.30	335308.10	31.0
CONTINUE(Y OR N)?Y			
(0021)	586178.00	335375.70	31.0
(0022)	585952.00	335541.20	31.0
(0023)	585756.40	335733.80	31.0
(0024)	585756.40	335733.80	31.0
(0025)	585515.20	335943.00	31.0
(0026)	585419.30	336173.10	31.0
(0027)	585273.30	336387.60	31.0
(0028)	585265.90	336406.30	31.0
(0029)	585119.50	336404.40	31.0
(0030)	585113.20	336404.10	31.0
(0031)	584904.80	336373.30	31.0
(0032)	585060.10	336553.80	31.0
(0033)	585146.60	336711.40	31.0
(0034)	585207.60	336982.10	31.0
(0035)	586299.20	337603.20	46.0
(0036)	586293.90	337361.10	46.0
(0037)	586482.70	337288.90	46.0
(0038)	586616.70	337061.10	46.0
(0039)	586864.90	336839.50	46.0
(0040)	587044.50	336595.10	46.0
CONTINUE(Y OR N)?Y			
(0041)	587126.60	336383.30	46.0
(0042)	587104.40	336102.10	46.0
(0043)	587122.80	335893.10	46.0
(0044)	586977.40	335872.30	46.0
(0045)	586970.80	335878.30	46.0
(0046)	586763.80	336044.80	46.0
(0047)	586619.30	336011.30	46.0
(0048)	586429.80	335873.40	46.0
(0049)	586324.20	335937.40	46.0
(0050)	586307.80	336114.70	46.0
(0051)	586141.10	336245.30	46.0
(0052)	586148.40	336563.90	46.0
(0053)	586034.50	336773.90	46.0
(0054)	586035.60	336754.90	46.0
(0055)	586066.60	336992.00	46.0
(0056)	585936.40	337042.00	46.0
(0057)	585820.60	337175.50	46.0
(0058)	585717.90	337188.80	46.0
(0059)	585711.80	337296.60	46.0
(0060)	587611.00	338160.30	46.0
CONTINUE(Y OR N)?Y			
(0061)	587558.80	337960.10	46.0
(0062)	587397.00	337893.80	46.0
(0063)	587248.60	337815.50	46.0
(0064)	587216.50	337597.30	46.0
(0065)	587135.40	337344.60	46.0
(0066)	587242.90	337134.30	46.0
(0067)	587412.70	337061.10	46.0
(0068)	587412.30	337067.40	46.0
(0069)	587235.10	336713.90	46.0
(0070)	587281.10	336576.50	46.0
(0071)	587565.50	336503.40	46.0
(0072)	587585.30	336269.00	46.0
(0073)	587646.50	336087.90	46.0
(0074)	587742.30	335972.40	46.0
(0075)	587767.60	335973.80	46.0
(0076)	587864.10	336068.30	46.0
(0077)	588055.50	336174.50	46.0
(0078)	588145.40	335937.80	46.0
(0079)	588388.30	336034.10	46.0
(0080)	588537.90	336201.50	46.0
CONTINUE(Y OR N)?Y			
(0081)	588599.60	336236.80	46.0
(0082)	588552.80	335941.50	46.0
(0083)	588550.20	335763.20	46.0
(0084)	588619.80	335658.90	46.0
(0085)	588603.10	335503.30	46.0
(0086)	588816.80	335332.70	46.0
(0087)	588933.30	335186.50	46.0
(0088)	589042.30	334950.80	46.0
(0089)	588757.80	335138.50	46.0
(0090)	588505.70	335315.30	46.0
(0091)	588371.50	335435.00	46.0
(0092)	588252.20	335517.40	46.0
(0093)	588078.30	335552.20	46.0
(0094)	587854.40	335456.90	46.0
(0095)	587647.80	335508.90	46.0
(0096)	587710.10	335308.80	46.0
(0097)	587816.90	335111.20	46.0
(0098)	588149.90	335078.90	46.0
(0099)	588345.00	335007.20	46.0
(0100)	588191.50	334794.90	46.0
CONTINUE(Y OR N)?Y			
(0101)	588206.00	334541.30	46.0
(0102)	588239.20	334294.90	46.0
(0103)	588238.30	334199.40	46.0
(0104)	588329.40	334051.90	46.0
(0105)	588211.40	333778.00	46.0
(0106)	588415.60	333547.60	46.0
(0107)	588673.90	333371.20	46.0
(0108)	588831.60	333176.40	46.0
(0109)	588831.90	333170.10	46.0
(0110)	589111.00	333077.60	46.0
(0111)	589290.90	332826.80	46.0
(0112)	589483.10	332583.00	46.0
(0113)	589717.20	332386.10	46.0
(0114)	589993.60	332229.80	46.0
(0115)	590033.80	331971.20	46.0
(0116)	590165.10	331902.20	46.0
(0117)	590347.40	331944.30	46.0
(0118)	590399.40	331813.50	46.0
(0119)	584208.80	336518.80	46.0
(0120)	584208.80	336518.80	46.0
CONTINUE(Y OR N)?Y			
(0121)	584476.30	336406.60	46.0
(0122)	584517.10	336249.80	46.0
(0123)	584565.80	336176.10	46.0
(0124)	584496.10	336057.70	46.0
(0125)	584654.90	336088.60	46.0
(0126)	584902.40	336080.40	46.0
(0127)	584889.70	336079.80	46.0
(0128)	585019.20	336042.40	46.0
(0129)	584934.80	335846.90	46.0
(0130)	584886.10	335697.80	46.0
(0131)	585085.70	335658.10	46.0
(0132)	585338.30	335583.10	46.0
(0133)	585419.40	335390.40	46.0
(0134)	585571.90	335284.40	46.0
(0135)	585680.30	335169.60	46.0
(0136)	585845.20	335070.70	46.0
(0137)	586054.10	334980.60	46.0
(0138)	586186.40	334892.60	46.0
(0139)	586359.40	334762.30	46.0
(0140)	586217.30	334576.10	46.0
CONTINUE(Y OR N)?Y			
(0141)	586102.80	334461.50	46.0
(0142)	585980.60	334371.90	46.0
(0143)	585831.40	334306.30	46.0
(0144)	585685.50	334298.10	46.0
(0145)	585897.60	334150.90	46.0
(0146)	585856.80	334085.10	46.0
(0147)	585656.10	334143.80	46.0
(0148)	585656.10	334143.80	46.0
(0149)	585455.70	334196.20	46.0
(0150)	585323.70	334277.90	46.0
(0151)	585217.40	334354.60	46.0
(0152)	585055.80	334396.50	46.0
(0153)	585142.90	334210.40	46.0
(0154)	585212.10	334112.60	46.0
(0155)	585199.90	333990.90	46.0
(0156)	585145.50	333828.80	46.0
(0157)	585105.60	333635.70	46.0
(0158)	585168.70	333645.60	46.0
(0159)	585246.90	333726.30	46.0
(0160)	585394.50	333817.30	46.0
CONTINUE(Y OR N)?Y			
(0161)	585604.50	333708.20	46.0
(0162)	585814.70	333707.30	46.0
(0163)	585931.90	333662.90	46.0
(0164)	586082.20	333595.00	46.0
(0165)	586176.90	333498.50	46.0
(0166)	586234.90	333374.50	46.0
(0167)	586415.40	333448.30	46.0
(0168)	586366.80	333630.00	46.0

A (1,j) Digitizer x-coordinate of point j;
 A (2,j) Digitizer y-coordinate of point j;
 D (1,m) Unrectified Eastings value of a point after transformation;
 D (2,m) Unrectified Northings value of a point after transformation;
 DRECT(1,j) Rectified Eastings value of point j;
 DRECT(2,j) Rectified Northings value of point j;
 G2 (1,m) Eastings of a point m in the DTM;
 G2 (2,m) Northings of a point m in the DTM;
 G2 (3,M) Height of a point as derived from the DTM;
 HCAL Calculated height of a point with respect to the
 average ground height;
 HP Height of a point with respect to the O.S. Datum;
 KCOUNT A counter which limits the number of points to be used
 in the height interpolation process to 4;
 SUM1, SUM2 Variables used in the process of height interpolation.

10.4.2.2 Definition of Arrays

A(2,a) Array comprising the measured image (x,y) coordinates
 of features and the corresponding feature identification
 codes (headers);
 D(2,a) Array containing Eastings and Northings of the trans-
 formed image coordinates before the application of the
 relief displacement correction, and the corresponding
 headers (untransformed);
 DRECT(2,a) Array containing the rectified coordinates of the
 transformed points and the headers required for plotting
 this data.
 G2(3,M) Array containing XYZ DTM data.

10.4.2.3 Explanation of Program FRECT

The program listing (see Fig 10.7) has again been divided into blocks so as to facilitate the explanation of the sequence of operations which it performs.

Block 1. This initial block gives the title of the program.

Block 2. This block dimensions the arrays A, D, DRECT and G2 used in the computations.

Block 3. This particular block outlines the function of the program.

Block 4. The x,y digitizer coordinates of the image points are read and input through channel 5. These are then stored in a data file in the format specified in statement 100 of line 8.

Block 5. This gives the number of pairs of coordinates in array A and the number of coordinate triplets in array G2 (see block 9 later).

Block 6. This sixth block simply lists the values of the sixteen transformation parameters which are to be used for the transformation of the digitizer coordinates into the terrain system - n_0, n_1, \dots, n_7 being the transformation parameters in the Easting direction and m_0, m_1, \dots, m_7 the corresponding transformation parameters in the Northing direction.

Block 7. In this block, the maximum and minimum coordinate limits of the DTM are given in order to check whether the digitized points fall within these limits.

Block 8. This particular block gives the values of (i) the multiplying constant $C9$ (= satellite orbital altitude (H) divided by the average satellite ground track distance Sg to the centre of the swath in this case, $\frac{800}{292.2}$) which is to be used for the calculation of relief displacement errors; (ii) the average terrain

PULLOUTS

(0001)	PROGRAM FRECT	(1)
(0002)	REAL A(2,639),D(2,639),DRECT(2,639),G2(3,898)	(2)
(0003)C	THE PROGRAM FIRST TRANSFORMS THE IMAGE DATA TO TERRAIN USING A	
(0004)C	POLYNOMIAL TRANSFORMATION, THEN THIS TRANSFORMED DATA IS MERGED	(3)
(0005)C	WITH ANOTHER SET OF DATA OBTAINED FROM A DTM	
(0006)C	TO PRODUCE AN OUTPUT WITH REDUCED RELIEF DISPLACEMENT ERRORS	
(0007)	READ(5,100) A	(4)
(0008) 100	FORMAT(2X,F5.1,1X,F5.1)	(5)
(0009)	I1=639	
(0010)	I2=898	
(0011)C	INPUT TRANSFORMATION PARAMETERS FROM IMAGE TO TERRAIN	
(0012)	N0=663582.0	
(0013)	N1=-1400.68	
(0014)	N2=-487.592	
(0015)	N3=7.37955	
(0016)	N4=9.08011	
(0017)	N5=-4.39113E-2	
(0018)	N6=-1.78013E-2	(6)
(0019)	N7=8.61387E-5	
(0020)	N0=239023.0	
	CONTINUE(Y OR N)?Y	
(0021)	M1=1055.27	
(0022)	M2=402.530	
(0023)	M3=-4.95087	
(0024)	M4=-5.64022	
(0025)	M5=2.87993E-2	
(0026)	M6=1.04419E-2	
(0027)	M7=-5.38999E-5	
(0028)C	INPUT MAXIMUM AND MINIMUM LIMITS OF DTM	
(0029)	X1=570000.	
(0030)	X2=595000.0	(7)
(0031)	Y1=320000.	
(0032)	Y2=340000.	
(0033)C	INPUT MULTIPLYING CONSTANT C9=H/Y	
(0034)	C9=2.737	
(0035)C	INPUT AVERAGE TERRAIN HEIGHT OF THE AREA	
(0036)	HAVEAVERAGE=60.0	(8)
(0037)C	INPUT ANGLE BETWEEN ACROSS-TRACK DIRECTION AND GRID NORTH	
(0038)	THETA=(63.5/180.0)*3.1429	
(0039)C	READ DTM DATA	
(0040)	READ(1,140) G2	
	CONTINUE(Y OR N)?Y	(9)
(0041) 140	FORMAT(1X,F9.2,1X,F9.2,1X,F4.1)	
(0042)	DO 180 J=1,I1	
(0043)	IF(A(1,J).LT.0.0.OR.A(2,J).LT.0.0) GOTO 160	
(0044)	P1=N0+N1*A(1,J)+N2*A(2,J)+N3*A(1,J)*A(2,J)+N4*A(1,J)**2	
(0045)	P2=N5*(A(1,J)**2*A(2,J))+N6*A(1,J)**3+N7*(A(1,J)**3*A(2,J))	
(0046)	D(1,J)= P1+P2	
(0047)	P3=N0+M1*A(1,J)+M2*A(2,J)+M3*A(1,J)*A(2,J)+M4*A(1,J)**2	
(0048)	P4=M5*(A(1,J)**2*A(2,J))+M6*A(1,J)**3+M7*(A(1,J)**3*A(2,J))	
(0049)	D(2,J)=P3+P4	
(0050)	X=D(1,J)	
(0051)	Y=D(2,J)	
(0052)C	CHECK IF POINT OUTSIDE DTM DOMAIN	
(0053)	IF(X.LT.X1.OR.X.GT.X2.OR.Y.LT.Y1.OR.Y.GT.Y2) GOTO 180	
(0054)	SUM1=0.0	
(0055)	SUM2=0.0	
(0056)	KCOUNT=0	
(0057)	DO 170 M=1,I2	
(0058)	IF(KCOUNT.GT.4) GOTO 175	
(0059)	DIST=SQRT((X-G2(1,M))**2+(Y-G2(2,M))**2)	
(0060)	IF(DIST.GT.500.0) GOTO 170	
	CONTINUE(Y OR N)?Y	
(0061)	KCOUNT=KCOUNT+1	(10)
(0062)	SUM1=SUM1+G2(3,M)/DIST**2	
(0063)	SUM2=SUM2+1/DIST**2	
(0064) 170	CONTINUE	
(0065) 175	IF(SUM1.EQ.0.0.OR.SUM2.EQ.0.0) GOTO 200	
(0066)	HP=SUM1/SUM2	
(0067)C	CALCULATE ELEVATION OF POINT WITH REFERENCE TO AVERAGE TERRAIN HT.	
(0068)	HCAL=(HP-HAVEAVERAGE)	
(0069)	IF(HCAL.GT.0.0) GOTO 165	
(0070)	DRECT(1,J)=X-C9*HCAL*SIN(THETA)	
(0071)	DRECT(2,J)=Y-C9*HCAL*COS(THETA)	
(0072)	GOTO 180	
(0073) 165	DRECT(1,J)=X+C9*HCAL*SIN(THETA)	
(0074)	DRECT(2,J)=Y+C9*HCAL*COS(THETA)	
(0075)	GOTO 180	
(0076) 160	D(1,J)=999999.99	
(0077)	D(2,J)=999999.99	
(0078)	DRECT(1,J)=999999.99	
(0079)	DRECT(2,J)=999999.99	
(0080)	GOTO 180	
	CONTINUE(Y OR N)?Y	
(0081) 200	DRECT(1,J)=X	
(0082)	DRECT(2,J)=Y	
(0083) 180	CONTINUE	
(0084)	WRITE(6,190) DRECT	
(0085) 190	FORMAT(1X,F9.2,1X,F9.2)	(11)
(0086)	STOP	
(0087)	END	(12)
(0088)**END**		

elevation of the area concerned (= 60 m for this test area); and (iii) the angle (THETA) between the across-track direction of the satellite and Grid North to allow the relief displacement errors (which are essentially in the cross-track direction of the satellite) to be resolved into their Easting and Northing components.

Block 9. In this block, the string DTM data is read from a data file into the computer memory through channel number 1. Once this is complete, the data is stored in array G2 for use in Block 10.

Block 10. This large block consists of two DO loops which actually transform the digitizer coordinates into the terrain coordinate system, carry out the corrections for relief displacement and then apply them to the transformed coordinates to produce the final set of terrain coordinates with reduced relief displacement errors. The block starts by transforming the first point from the digitizer (x,y) coordinate system into the terrain system using the given transformation parameters from the prior operation of program POLY. These transformed coordinates $D(1,j)$, $D(2,j)$ are then assigned values X and Y respectively and a check is applied as to whether they lie within the defined limits of the DTM. If a particular point does not, then the program simply rejects it and proceeds to the next point to be transformed. If, however, a point lies within the limits of the DTM, preparation is made to rectify its coordinates by eliminating the error arising from relief displacement (lines 54, 55 and 56). The file of DTM data is searched to establish points which lie in the neighbourhood of the transformed point that can be used for the interpolation of the height of this particular point. As will be seen from line 60, the DTM point is used for the purpose

if it lies within a radius of 500 m from the point requiring rectification. If the number of such points reaches 4, then the search for further points may be stopped.

Next, the interpolation and calculation of the height of the point requiring rectification is carried out, followed by the computation of the corrections to the Eastings and the Northings arising from relief displacement. These are then applied to the transformed coordinates (X, Y) of the point and the results stored in array DIRECT (1,a). The program can then proceed to the next pair of digitizer coordinates. If one or both of the coordinates to be transformed happen to be negative (which indicates that the next set of (x,y) coordinates belong to another feature which had been digitized) then the program does not transform these coordinates but simply replaces them in arrays D and DIRECT by 999999.99 and 999999.99 in order to make them conform to the output data format (line 85). The program then proceeds to the next pair of digitizer coordinates. This continues until all the digitizer coordinates are exhausted.

Block 11. This block writes out, in the specified format, the rectified terrain coordinates and the feature identification codes stored in array DIRECT to a pre-created data file where they will be ready for plotting using program PLOTTER.

10.4.2.4 Detailed Explanation of the Program

<u>Line No.</u>	<u>Comments</u>
1	The title of the program.
2	Dimensions the arrays A, D, DIRECT, G2.
3-6	Comments on the function of the program.

- 7-8 Reads array A and gives details of its format.
- 9-10 Defines the number of digitized image points (639) and number of DTM points (898).
- 11-27 Gives the image-to-terrain transformation parameters already computed by PROGRAM POLY.
- 28-32 Gives the limits of the DTM in terms of its Easting and Northing values.
- 33-38 Gives the multiplying constant ($C9 = \frac{H}{Sg} = 2.737$); the average ground height ($h = 60$ m) and the angle (THETA) between the across-track direction of the flight and the Grid North.
- 39-41. Reads the string DTM data in a format as specified.
- 42-49 Transforms the image coordinates of a point to its terrain value.
- 50-51 Assigns X and Y to the transformed coordinates.
- 52-53 Checks whether the transformed point lies outside the DTM domain.
- 54-56 Sets the initial values to prepare for the height interpolation from the string DTM data.
- 57-64 Computes $Q_i h_i$ and Q_i .
- 65 If there is no point lying in the neighbourhood of the transformed point then it is accepted as it is (this did not actually happen in this experiment).
- 66 Computes the final interpolated height.
- 67-68 Calculates the elevation of the point with respect to the average terrain elevation.
- 69-72 If the point lies below average terrain height, then

- the relief error is calculated using the appropriate formulae and applied to the transformed coordinates.
- 73-75 If the point is above the average terrain height, then the relief displacement error is calculated using the appropriate formulae and applied to the transformed terrain coordinates.
- 76-80 Put $D(1,j) = DRECT(1,j) = 999999.99$ and $D(2,j) = DRECT(2,j) = 999999.99$ in order to conform to the output format of statement 190.
- 81-82 If the point cannot be rectified (i.e. there are no nearby DTM points) then store it in array DRECT. N.B. This did not actually happen in this experiment.
- 83 Continues the rectification.
- 84-85 Writes out array DRECT in the previously specified format.
- 86-87 Ends the execution of the program.

10.4.2.5 Listing of Program and Sample of Input and Output Data

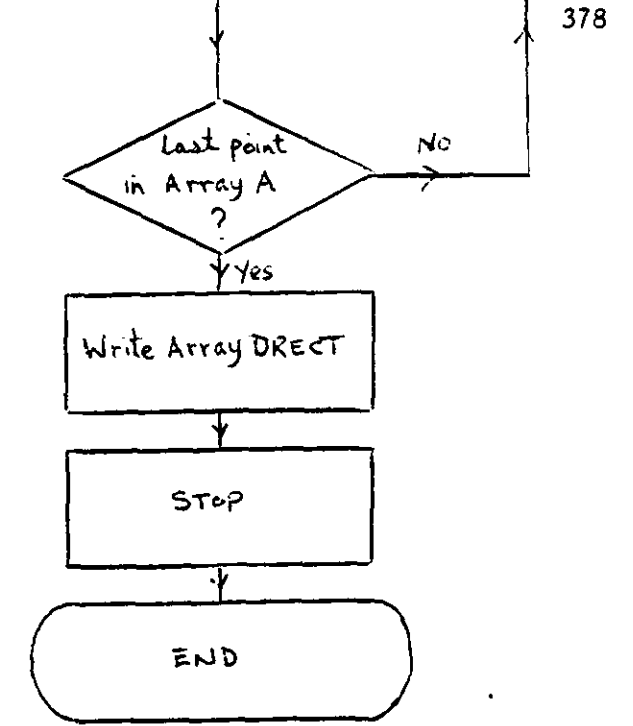
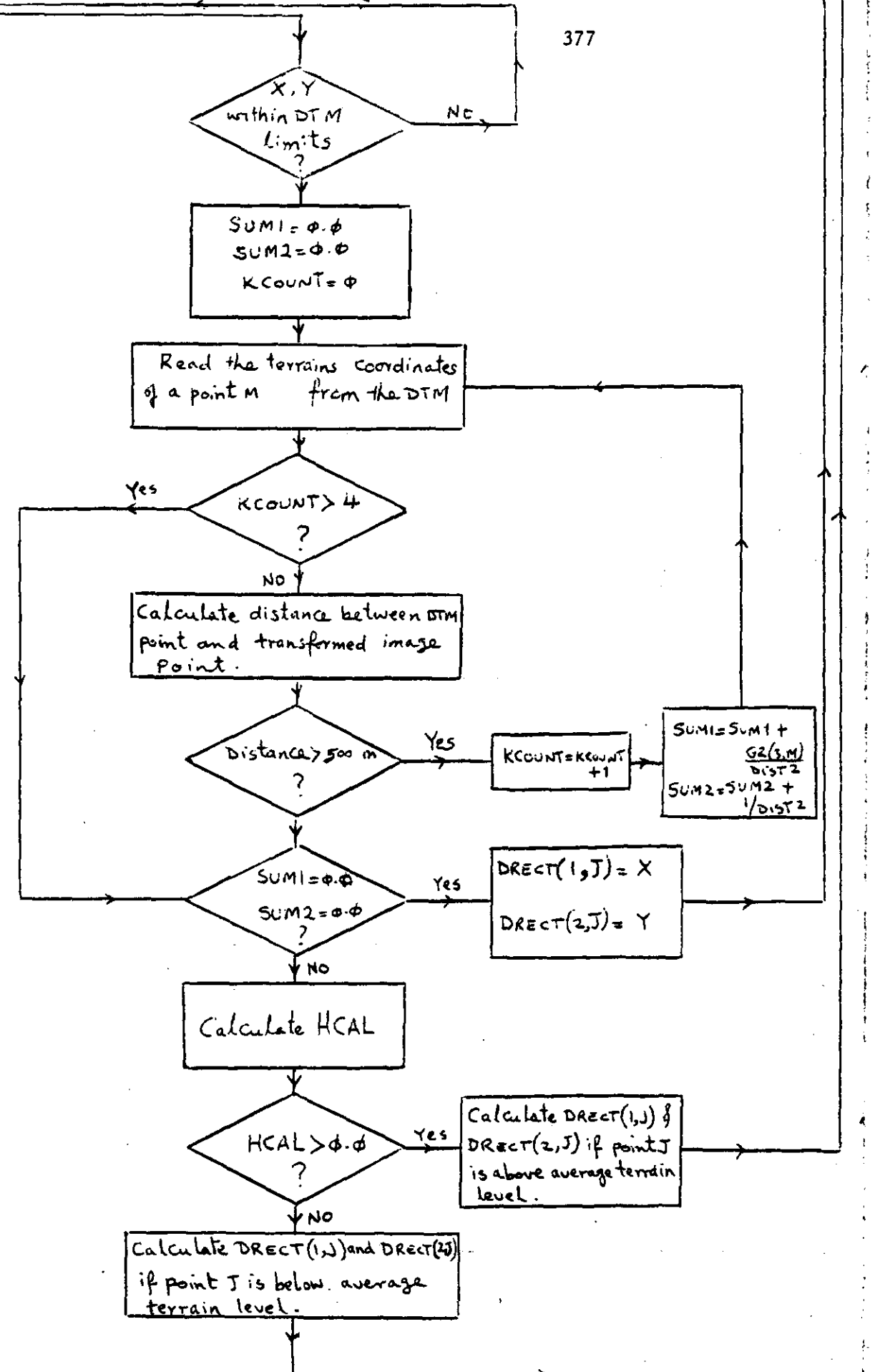
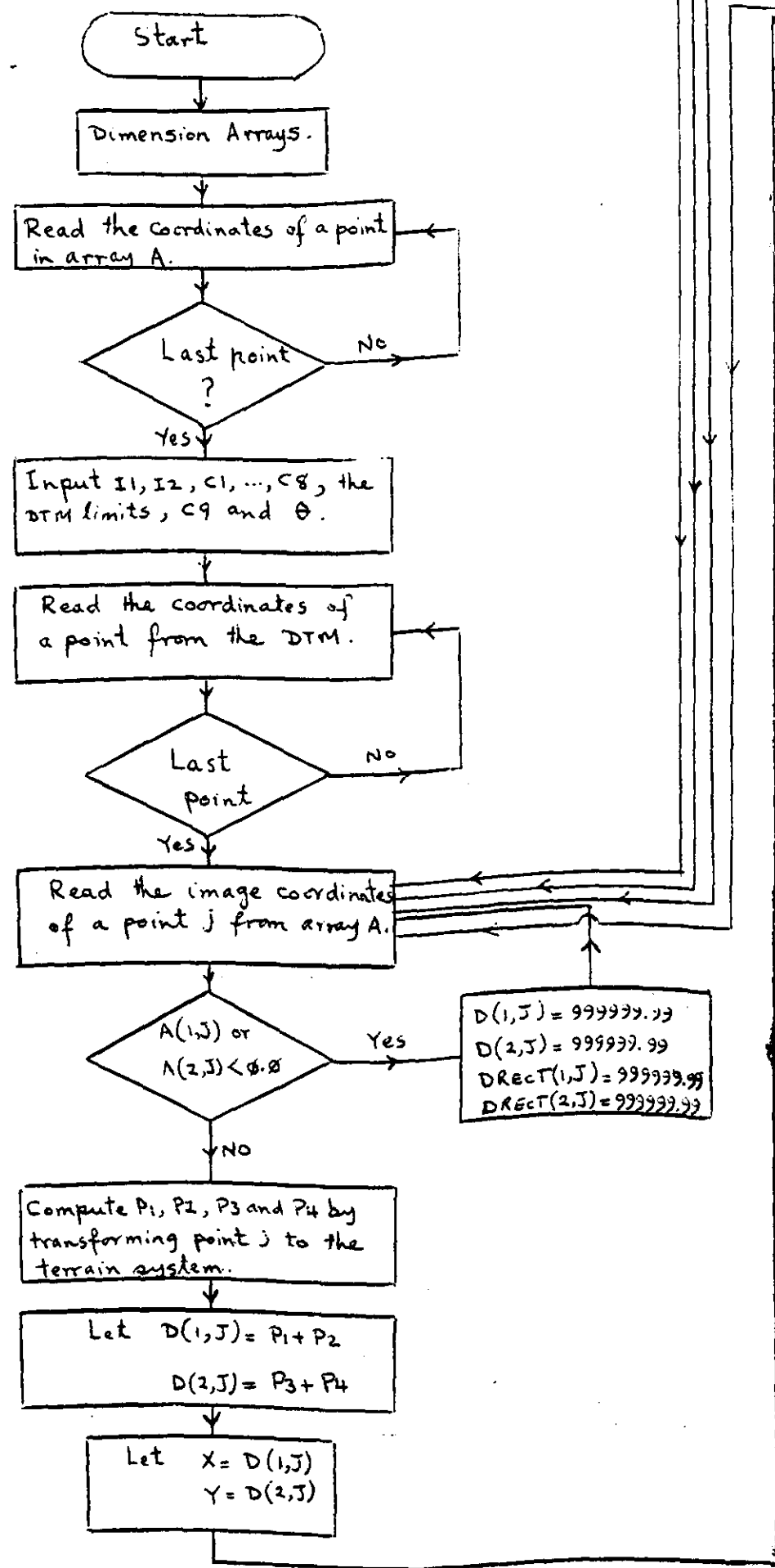
Fig 10.7 is the listing and Fig 10.7.1 the flow diagram of the Program FRECT. A sample of input data to the program is included as Fig 10.8 together with the corresponding output data (Fig 10.9).

10.4.3 Program PLOTTER

It was not possible to use the previous PLOTIR program which plotted out the individual vector errors resulting from the accuracy tests, since the digital monoplotting procedure involved the continuous plotting of line features. Thus, this program plots the

CONTAINS

PULLOUTS



(0001)2+01609+02157
 (0002)2+01606+02134
 (0003)2+01620+02132
 (0004)2+01624+02152
 (0005)2+01611+02153
 (0006)2-00018-00075 Header indicating the start of a new feature
 (0007)2+01531+02152
 (0008)2+01543+02146
 (0009)2+01548+02124
 (0010)2+01558+02128
 (0011)2+01564+02124
 (0012)2+01572+02119
 (0013)2+01576+02114
 (0014)2+01582+02104
 (0015)2+01576+02104
 (0016)2+01553+02117
 (0017)2+01551+02104
 (0018)2+01553+02096
 (0019)2+01548+02091
 (0020)2+01536+02094
 CONTINUE(Y OR N)?Y

(0021)2+01543+02112
 (0022)2+01534+02119
 (0023)2+01537+02132
 (0024)2+01522+02141
 (0025)2+01527+02153
 (0026)2+01537+02152
 (0027)2+01545+02145
 (0028)2+01550+02129
 (0029)2+01550+02128
 (0030)2+01553+02127
 (0031)2-00022-00070 Header indicating the start of a new feature

(0032)2+01572+02214
 (0033)2+01560+02208
 (0034)2+01565+02192
 (0035)2+01576+02197
 (0036)2+01572+02213
 (0037)2-00014-00073
 (0038)2+01502+02189
 (0039)2+01504+02185
 (0040)2+01492+02183
 CONTINUE(Y OR N)?Y

(0041)2+01488+02183
 (0042)2+01487+02180
 (0043)2+01483+02180
 (0044)2+01479+02176
 (0045)2+01471+02162
 (0046)2+01475+02160
 (0047)2+01469+02164
 (0048)2+01473+02169
 (0049)2+01466+02174
 (0050)2+01469+02181
 (0051)2+01449+02192
 (0052)2+01451+02198
 (0053)2+01484+02188
 (0054)2+01487+02188
 (0055)2+01487+02193
 (0056)2+01501+02193
 (0057)2-00020-00075
 (0058)2+01464+02105
 (0059)2+01477+02095
 (0060)2+01474+02089
 CONTINUE(Y OR N)?Y

(0061)2+01459+02098
 (0062)2+01464+02100
 (0063)2-00013-00074
 (0064)2+01480+02091
 (0065)2+01478+02087
 (0066)2+01489+02077
 (0067)2+01496+02082
 (0068)2+01482+02094
 (0069)2-00009-00069
 (0070)2+01245+02169
 (0071)2+01250+02166
 (0072)2+01238+02153
 (0073)2+01249+02142
 (0074)2+01268+02145
 (0075)2+01281+02147
 (0076)2+01276+02150
 (0077)2+01286+02160
 (0078)2+01283+02164
 (0079)2+01278+02161
 (0080)2+01276+02170
 CONTINUE(Y OR N)?Y

(0081)2+01272+02179
 (0082)2+01262+02173
 (0083)2+01245+02167
 (0084)2-00022-00075
 (0085)2+01215+02194
 (0086)2+01228+02183
 (0087)2+01217+02178
 (0088)2+01210+02186
 (0089)2+01212+02194
 (0090)2-00025-00073
 (0091)2+01308+02231
 (0092)2+01294+02206
 (0093)2+01278+02216
 (0094)2+01290+02237
 (0095)2+01304+02231
 (0096)2-00014-00065
 (0097)2+01093+02099
 (0098)2+01108+02080
 (0099)2+01083+02065
 (0100)2+01116+02002
 CONTINUE(Y OR N)?Y

(0101)2+01134+02000
 (0102)2+01134+01993
 (0103)2+01109+01995
 (0104)2+01063+02086
 (0105)2+01098+02100
 (0106)2-00014-00068
 (0107)2+01101+02096
 (0108)2+01146+02053
 (0109)2+01144+02051
 (0110)2+01149+02043
 (0111)2+01143+02034
 (0112)2+01141+02016
 (0113)2+01136+02015
 (0114)2+01129+02001
 (0115)2-00021-00068
 (0116)2+01126+02114
 (0117)2+01203+02048
 (0118)2+01233+02063
 (0119)2+01235+02071
 (0120)2+01266+02076
 CONTINUE(Y OR N)?Y

(0001) 582262.90 333688.30
(0002) 582405.30 333372.30
(0003) 582596.90 333457.70
(0004) 582490.50 333743.70
(0005) 582319.30 333653.40
(0006) 999999.99 999999.99
(0007) 581321.20 333006.50
(0008) 581519.10 333025.80
(0009) 581753.60 332787.40
(0010) 581848.30 332917.00
(0011) 581955.00 332913.80
(0012) 582094.60 332913.70
(0013) 582184.00 332881.90
(0014) 582337.80 332802.60
(0015) 582262.10 332755.30
(0016) 581871.10 332738.30
(0017) 581947.30 332558.40
(0018) 582034.80 332472.90
(0019) 582010.80 332370.60
(0020) 581836.20 332314.00
CONTINUE(Y OR N)?Y

(0021) 581784.10 332596.40
(0022) 581616.10 332613.70
(0023) 581552.60 332801.50
(0024) 581293.60 332796.40
(0025) 581262.90 332987.40
(0026) 581396.80 333053.90
(0027) 581552.20 333028.90
(0028) 581739.60 332866.30
(0029) 581747.50 332853.70
(0030) 581793.10 332864.80
(0031) 999999.99 999999.99
(0032) 581353.30 334115.90
(0033) 581249.40 333944.10
(0034) 581437.10 333781.80
(0035) 581536.20 333932.70
(0036) 581361.10 334103.30
(0037) 999999.99 999999.99
(0038) 580667.30 333243.40
(0039) 580723.60 333208.80
(0040) 580587.70 333088.70
CONTINUE(Y OR N)?Y

(0041) 580537.30 333057.10
(0042) 580547.90 333011.40
(0043) 580497.30 332979.80
(0044) 580478.10 332897.90
(0045) 580486.10 332658.70
(0046) 580552.30 332665.00
(0047) 580445.20 332668.10
(0048) 580456.80 332762.60
(0049) 580329.20 332770.40
(0050) 580312.40 332882.10
(0051) 579973.00 332863.30
(0052) 579951.50 332954.40
(0053) 580447.60 333088.60
(0054) 580485.60 333112.30
(0055) 580446.60 333175.10
(0056) 580623.40 333285.90
(0057) 999999.99 999999.99
(0058) 580842.70 331886.30
(0059) 581084.70 331862.60
(0060) 581093.70 331763.50
CONTINUE(Y OR N)?Y

(0061) 580834.30 331758.90
(0062) 580881.60 331823.30
(0063) 999999.99 999999.99
(0064) 581153.80 331835.80
(0065) 581159.70 331769.80
(0066) 581376.40 331730.30
(0067) 581425.60 331848.20
(0068) 581155.60 331889.30
(0069) 999999.99 999999.99
(0070) 577534.00 331009.90
(0071) 577624.10 331008.80
(0072) 577576.40 330752.10
(0073) 577810.40 330693.00
(0074) 578030.60 330874.80
(0075) 578181.70 330998.70
(0076) 578092.80 330999.00
(0077) 578139.90 331202.30
(0078) 578068.70 331230.60
(0079) 578028.40 331154.70
(0080) 577928.80 331254.50
CONTINUE(Y OR N)?Y

(0081) 577803.00 331339.50
(0082) 577722.30 331188.00
(0083) 577550.60 330984.30
(0084) 999999.99 999999.99
(0085) 576930.20 331111.90
(0086) 577194.40 331064.70
(0087) 577092.10 330919.40
(0088) 576932.00 330972.00
(0089) 576890.40 331090.20
(0090) 999999.99 999999.99
(0091) 577849.70 332271.30
(0092) 577869.30 331848.60
(0093) 577578.10 331856.90
(0094) 577564.50 332213.60
(0095) 577797.30 332241.40
(0096) 999999.99 999999.99
(0097) 576174.90 328971.40
(0098) 576541.90 328826.60
(0099) 576366.10 328436.90
(0100) 577354.70 327843.00
CONTINUE(Y OR N)?Y

(0101) 577589.80 327958.80
(0102) 577652.60 327865.80
(0103) 577334.60 327693.80
(0104) 575914.00 328574.60
(0105) 576229.90 329021.60
(0106) 999999.99 999999.99
(0107) 576305.40 328989.80
(0108) 577263.30 328754.80
(0109) 577256.10 328713.10
(0110) 577389.40 328645.80
(0111) 577395.30 328480.30
(0112) 577531.40 328226.30
(0113) 577479.40 328173.60
(0114) 577520.40 327932.50
(0115) 999999.99 999999.99
(0116) 576462.40 329414.60
(0117) 578017.30 329128.80
(0118) 578265.80 329554.80
(0119) 578223.90 329673.40
(0120) 578573.10 329976.70
CONTINUE(Y OR N)?Y

(0121) 578506.70 330025.30
(0122) 578245.30 329776.20
(0123) 578152.90 329809.90
(0124) 578064.90 329918.10
(0125) 578052.80 330018.30
(0126) 577914.20 330150.10
(0127) 577895.80 330424.10
(0128) 577883.60 330470.10
(0129) 577880.60 330557.10
(0130) 577880.60 330557.10
(0131) 577817.90 330626.60
(0132) 577675.90 330544.00
(0133) 577692.80 330518.20
(0134) 577777.10 330443.10
(0135) 577780.30 330356.10
(0136) 577735.30 330043.90
(0137) 577756.00 329768.60
(0138) 576705.40 329717.40
(0139) 576739.40 329480.80
(0140) 576455.00 329557.60
CONTINUE(Y OR N)?Y

(0141) 999999.99 999999.99
(0142) 577514.60 329624.50
(0143) 577777.40 329655.10
(0144) 577829.10 329468.80
(0145) 577813.90 329277.50
(0146) 577785.60 329186.90
(0147) 577562.10 329178.60
(0148) 577533.20 329435.60
(0149) 577520.00 329482.30
(0150) 577426.20 329517.30
(0151) 577510.50 329603.90
(0152) 577680.30 329614.80
(0153) 999999.99 999999.99
(0154) 578093.70 329629.80
(0155) 578131.60 329707.10
(0156) 578161.00 329580.80
(0157) 578072.80 329581.10
(0158) 578055.90 329606.80
(0159) 999999.99 999999.99
(0160) 576441.90 329365.80
CONTINUE(Y OR N)?Y

Header

image coordinates of all the digitized features after they have been transformed to the terrain system and rectified to eliminate the effect of relief displacement using the method described in Section 11.3.3. The type and characteristics of the plotter used for this task are the same as those mentioned previously in Section 8.7.

10.4.3.1 Definition of Variables

A(1,j), A(2,j) Eastings and Northings (respectively) of the point j which is to be plotted;

N Number of records in the file which contains the data to be plotted.

10.4.3.2 Definition of Arrays

A(2,m) Array containing the rectified terrain coordinates of the area.

10.4.3.3 Explanation of the Program

Block 1. This block gives the title of the program.

Block 2. This block explains the function of the program.

Block 3. In this block, the array A containing the data to be plotted is dimensioned.

Block 4. This fourth block gives the number of records in the data file containing the points to be plotted and the number of headers or feature identification codes (coordinates 999999.99, 999999.99 in this case).

Block 5. Reads array A in the special format specified in statement 100.

Block 6. This block calls the appropriate GHOST subroutines to prepare the plotter for plotting the data.

Block 7. This block calls GHOST subroutines to actually perform the plotting of the features; moving the pen to the start of a new feature whenever the values $X = 999999.99$ and $Y = 999999.99$ are encountered.

Block 8. Calls the GHOST subroutine GREND to end plotting after the list of coordinate data has been exhausted.

Block 9. This block ends the execution of the program.

10.4.3.4 Detailed Explanation of Program

<u>Line No.</u>	<u>Comments</u>
1	Title of the program.
2-4	Explains the function of the program.
5	Dimensions array A.
6	Gives the number of points to be used in the plotting operation.
7-8	Reads array A and defines its format.
9-18	Calls the appropriate GHOST routines to prepare the plotter for the plotting operation.
19	Calls GHOST routine POSITN to place the pen at the initial point.
20	Initializes the plotter by setting $I = 2$.
21-30	Calls the GHOST routines necessary to plot the features.
31	Calls GHOST subroutine GREND to end plotting.
32-33	Ends the execution of the program.

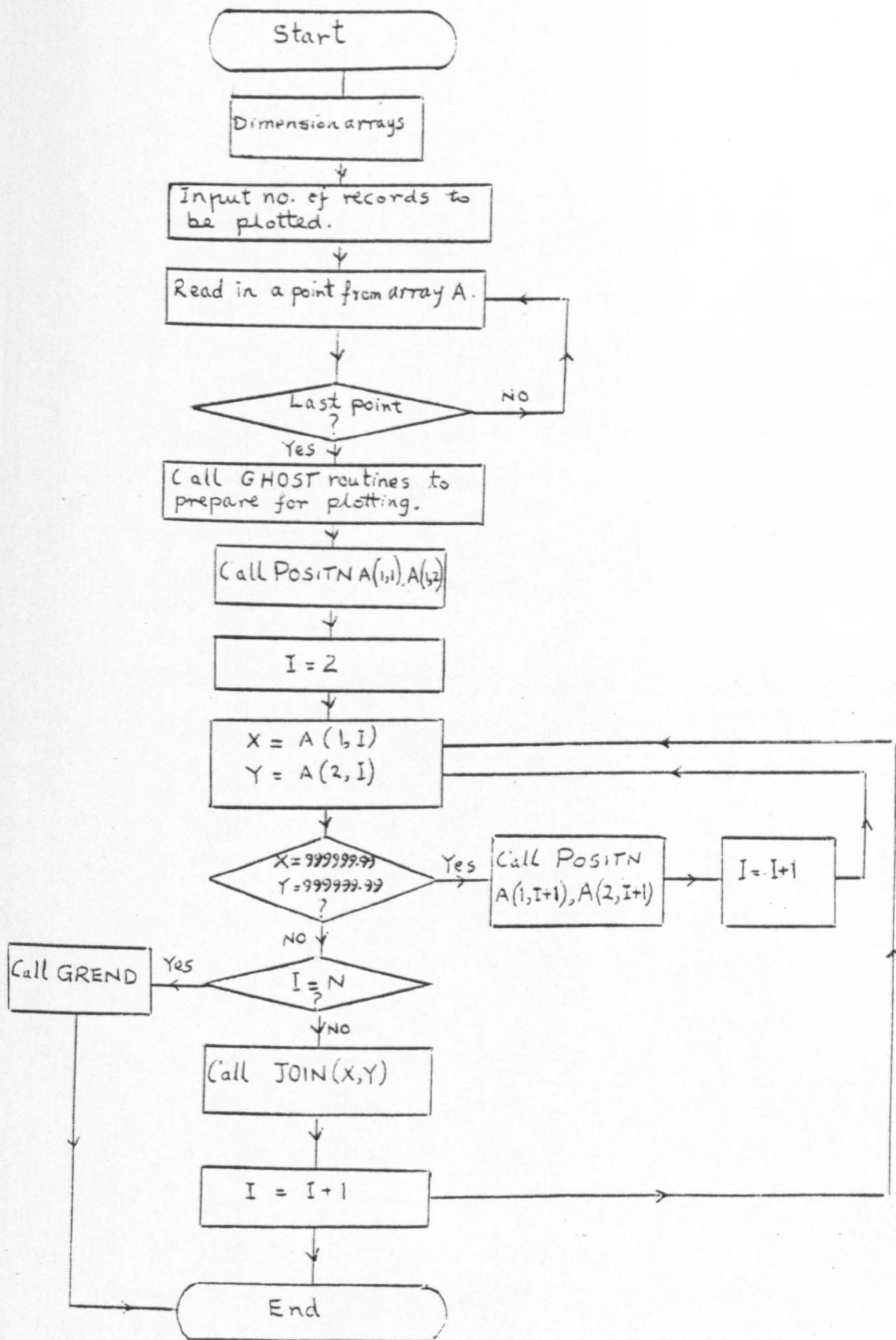
10.4.3.5 Listing of Program PLOTTER

Fig 10.10 is the listing of the Program PLOTTER supplemented by Fig 10.10.1 which is a flow diagram of the program. Fig 10.9 is

Fig 10.10 Listing of Program PLOTTER

(0001)	PROGRAM RADARMAP	(1)
(0002)C	TO PLOT TERRAIN COORDINATES OF PART OF EAST ANGLIA (RAGE AFTER	
(0003)C	CORRECTING THEM FROM THE EFFECT OF RELIEF DISPLACEMENT	(2)
(0004)C	GHOST ROUTINES ARE USED FOR PLOTTING	
(0005)	REAL A(2,639)	(3)
(0006)	N=639	
(0007)	READ(5,100) A	(4)
(0008) -100	FORMAT(1X,F9.2,1X,F9.2)	(5)
(0009)C	CALLING PLOTTING ROUTINES	
(0010)	CALL PAPER(1)	
(0011)	CALL PSPACE(0.1,0.95,0.1,0.95)	
(0012)	CALL MAP(572000.,592000.,322000.,342000.)	(6)
(0013)	CALL SCALES	
(0014)	CALL BORDER	
(0015)	CALL ITALIC(0)	
(0016)	CALL PLACE(10,3)	
(0017)	CALL TYPECS('DIGITALLY PLOTTED MAP',23)	
(0018)	CALL CTRMAG(5)	
(0019)	CALL POSITN(A(1,1),A(2,1))	
(0020)	I=2	
	CONTINUE(Y OR N)?Y	388
(0021) 105	X=A(1,I)	
(0022)	Y=A(2,I)	(7)
(0023)	IF(X.EQ.999999.99.AND.Y.EQ.999999.99) GOTO 110	
(0024)	IF(I.EQ.N) GOTO 120	
(0025)	CALL JOIN(X,Y)	
(0026)	I=I+1	
(0027)	GOTO 105	
(0028) 110	CALL POSITN(A(1,I+1),A(2,I+1))	
(0029)	I=I+1	
(0030)	GOTO 105	
(0031) 120	CALL BREND	(8)
(0032)	STOP	
(0033)	END	(9)
(0034)++END++		

Fig 10.10.1 Flow Chart of Program PLOTTER



a sample of the input data to the program while Fig 10.13a is a sample output map using the program PLOTTER.

10.5 Results of Digital Monoplotting Experiment

As an initial check on the effectiveness of the rectification process, the planimetric coordinates of the twelve control points used for the determination of the transformation parameters have been computed before and after rectification of the relief displacement errors. The resulting errors (as compared with the given values) are shown in the computer output listing as Fig 10.11. The vector plots of these errors at the twelve points before and after rectification are given in Figs 10.12a and 10.12b respectively. As can be seen, the r.m.s.e. in the X-direction improved very slightly from $\sigma_X = \pm 15$ to $\sigma_X = \pm 11$ m. However, in the Y-direction, the improvement is more noticeable, i.e. from $\sigma_Y = \pm 28$ m to $\sigma_Y = \pm 18$ m. It can also be seen from the vector plots that while the rectification did reduce the magnitude of the errors due to the topographic relief, substantial residual errors remained, still displaying the characteristic pointing in the cross-track direction visible in all the accuracy tests carried out with the Seasat SAR imagery. These findings may be viewed as being rather disappointing in view of the very large amount of effort and time that has been spent in attempting further rectification using digital monoplotting techniques. It is indeed difficult to account for the substantial residual systematic errors which these plots display.

The main object of the experiment was the production of a rectified planimetric map from the Seasat SAR imagery. This is included as Fig 10.13a, while Fig 10.13b is the map resulting from

plotting the unrectified data, i.e. without the application of the relief displacement corrections. The two maps have been plotted at the scale of 1:63,360 for comparison with the existing O.S. topographic map of the area (Fig 10.13c).

Comparison of the plot of the unrectified data (Fig 10.13b) with the O.S. topographic map (Fig 10.13c) shows that it does not fit the map too well. In particular, features such as the A148 main road and the lower part of the Roman Road (designated by "a") are in places well off target while most of the plotted woodlands do not register exactly with the map. The same remarks may be applied to the Sculthorpe Airport (though to a lesser extent), the Deer Park and most of the minor roads which have been interpreted, digitized and plotted, e.g. that at the top right of the plot designed by "b".

Comparison of the plot produced from the rectified data against the map reveals that overall there is only a slightly better fit of this plot to the map than that produced with the unrectified data. When comparing this plot with that produced from the unrectified data, it will be seen that the differences between the two plots are not substantial nor readily apparent due to the small scale at which the map has been plotted. However, that the rectification did actually take place can be seen from the comparison of the listings of the coordinates of part of Bunker's Hill forest and of Chantrey Hill forest before and after rectification (Fig 10.14). Substantial corrections - typically of the order of 15 to 25 metres - have been effected, corresponding to 0.25 to 0.4 mm at the map scale. However, these do not show up as marked differences between the two plots and they would need representation at much larger scales for the changes to be readily seen. In fact, as will be seen below,

RUN Fig 10.11 Discrepancies at control points before and after application of the relief displacement error.

* SEASAT.TRANSB 05 FEB 82 18:09:53

PT. NO	EASTINGS(M)	NORTHING2(M)	DE(M)	DN(M)	D1(M)
40	578101	329539	-20.1833	-26.8284	33
57	581339	334051	2.93158	-32.0229	32
59	585292	330396	13.6694	-40.5331	42
69	587893	334912	13.1895	-16.3581	21
72	587678	337596	-2.21845	2.45493	3
36	576646	328428	3.51712	6.3628	7
43	577855	331805	3.91659	1.34528	4
46	579209	330545	19.2566	26.7305	32
47	580127	330361	-27.0059	-5.21825	27
53	582206	331456	9.25193	44.338	45
60	586672	332925	-25.2391	39.3693	46
74	578269	328333	9.08006	-0.457047	9

RMSE IN X DIRECTION BEFORE RECTIFICATION= 14.6038

PRESS RETURN TO CONTINUE

RMSE IN Y DIRECTION BEFORE RECTIFICATION= 27.7522

RESIDUAL ERRORS AT CONTROL POINTS AFTER RECTIFICATION

POINT NO	EASTINGS(M)	NORTHINGS(M)	DE(M)	DN(M)	D2(M)
40	578101	329539	-21.4236	-29.2682	36
57	581339	334051	1.69129	-34.4627	34
59	585292	330396	12.4292	-22.973	26
69	587893	334912	5.5147	7.5592	9
72	587678	337596	6.46356	19.5339	20
36	576646	328428	2.27684	3.92295	8
43	577855	331805	-1.04455	-8.41411	8
46	579209	330545	18.0163	4.2906	18
47	580127	330361	-8.2462	-7.65809	11
53	582206	331456	-14.3135	-2.01907	14
66	586672	332925	-6.4794	16.9295	18
74	578269	328333	-2.08252	-12.4157	12

PRESS RETURN TO CONTINUE

RMSE AT CONTROL POINTS AFTER RECTIFICATION(X-DIRC.)= 11.2421

RMSE AT CONTROL POINTS AFTER RECTIFIC. IN Y DIRECTION= 17.5083

* .581 SECONDS USED 18:10:47

RUN

Fig 10.11 Discrepancies at control points before and after application of the relief displacement error.

* SEASAT.TRANSB 05 FEB 82 18:09:53

PT. NO	EASTINGS(M)	NORTHING2(M)	DE(M)	DN(M)	D1(M)
40	578101	329539	-20.1833	-26.8284	33
57	581339	334051	2.93158	-32.0229	32
59	585292	330396	13.6694	-40.5331	42
69	587893	334912	13.1895	-16.3581	21
72	587678	337596	-2.21845	2.45493	3
36	576646	328428	3.51712	6.3628	7
43	577855	331805	3.91659	1.34528	4
46	579209	330545	19.2566	26.7305	32
47	580127	330361	-27.0059	-5.21825	27
53	582206	331456	9.25193	44.338	45
66	586672	332925	-25.2391	39.3693	46
74	578269	328333	9.08006	-0.457047	9

RMSE IN X DIRECTION BEFORE RECTIFICATION= 14.6038

PRESS RETURN TO CONTINUE

RMSE IN Y DIRECTION BEFORE RECTIFICATION= 27.7522

RESIDUAL ERRORS AT CONTROL POINTS AFTER RECTIFICATION

POINT NO	EASTINGS(M)	NORTHINGS(M)	DE(M)	DN(M)	D2(M)
40	578101	329539	-21.4236	-29.2682	36
57	581339	334051	1.69129	-34.4627	34
59	585292	330396	12.4292	-22.973	26
69	587893	334912	5.5147	7.5592	9
72	587678	337596	6.46356	19.5339	20
36	576646	328428	2.27684	3.92295	8
43	577855	331805	-1.04455	-8.41411	8
46	579209	330545	18.0163	4.2906	18
47	580127	330361	-8.2462	-7.65809	11
53	582206	331456	-14.3135	-2.01907	14
66	586672	332925	-6.4794	16.9295	18
74	578269	328333	-2.08252	-12.4157	12

PRESS RETURN TO CONTINUE

RMSE AT CONTROL POINTS AFTER RECTIFICATION(X-DIRC.)= 11.2421

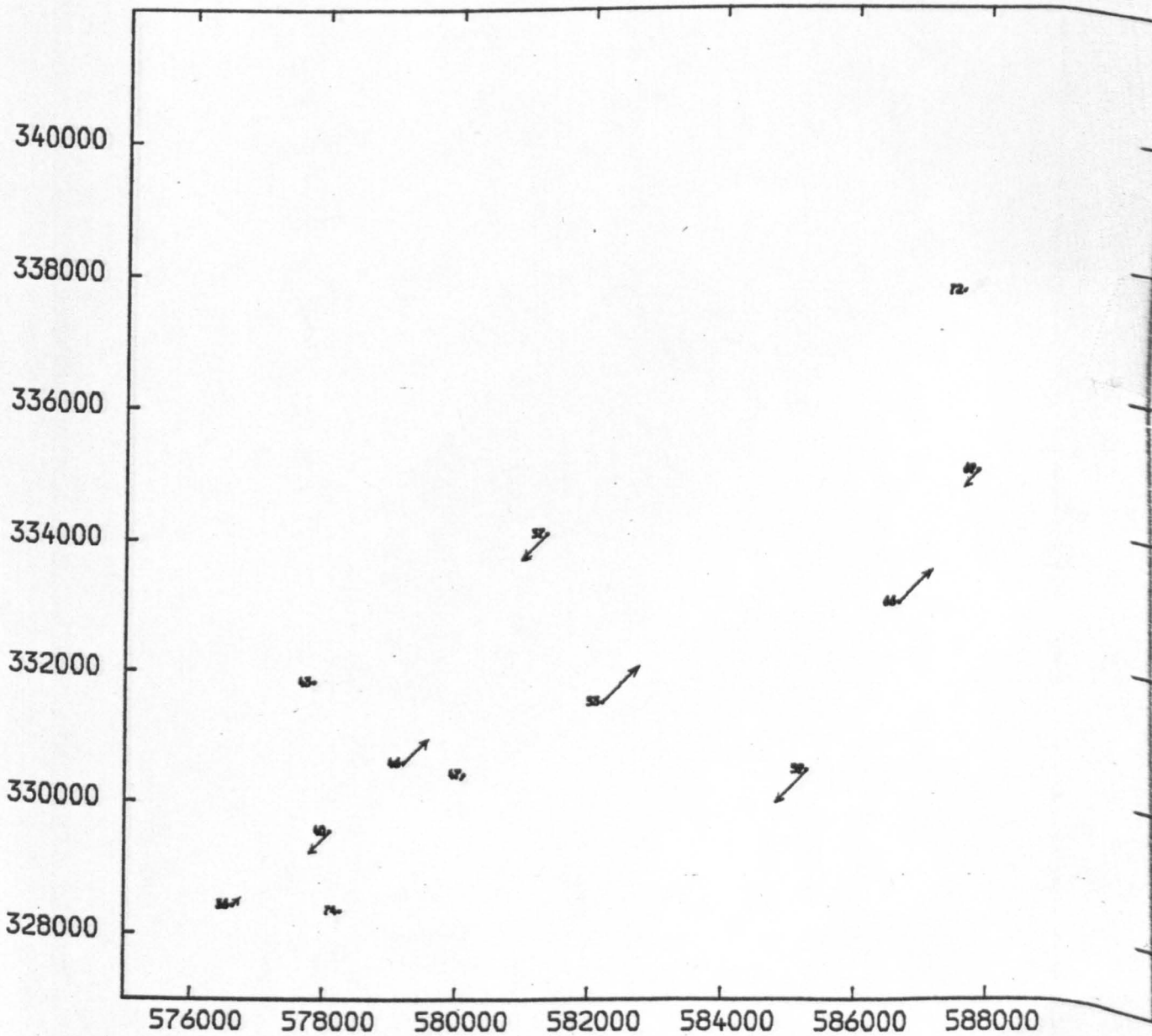
RMSE AT CONTROL POINTS AFTER RECTIFIC. IN Y DIRECTION= 17.5083

* .581 SECONDS USED 18:10:47

AFTER POLYMER TRANSFER
MAP SCALE 1/25000, VECTOR SCALE 1/20000

Fig 10.12a

VECTOR MAP OF POSITION ERRORS BEFORE RECTIFICATION



AFTER POSITION TRANSFORM
MAP SCALE 1/25000, VECTOR SCALE 1/20000

Fig 10.12b

VECTOR MAP OF POSITION ERRORS AFTER RECTIFICATION

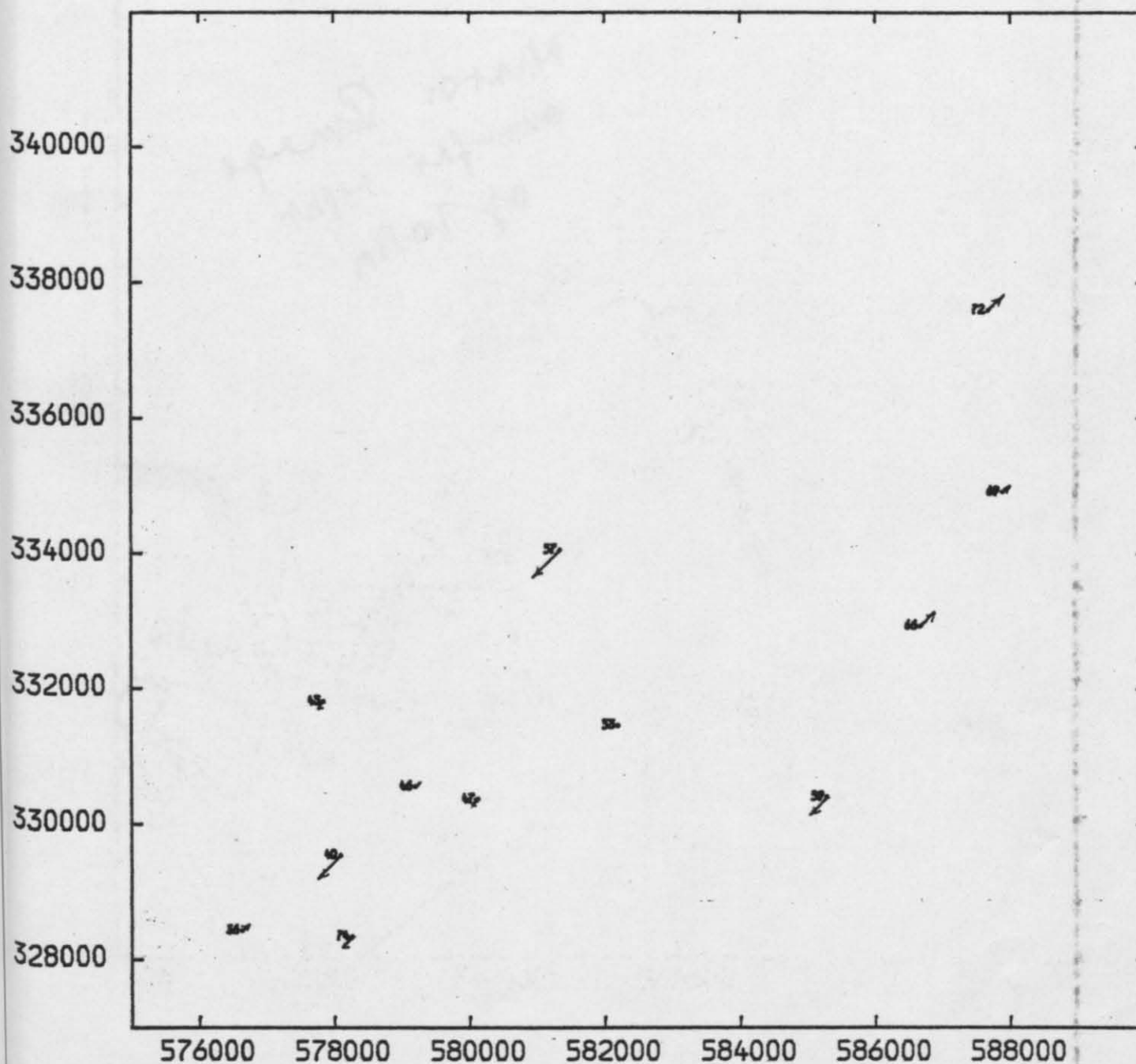


Fig 10.13a

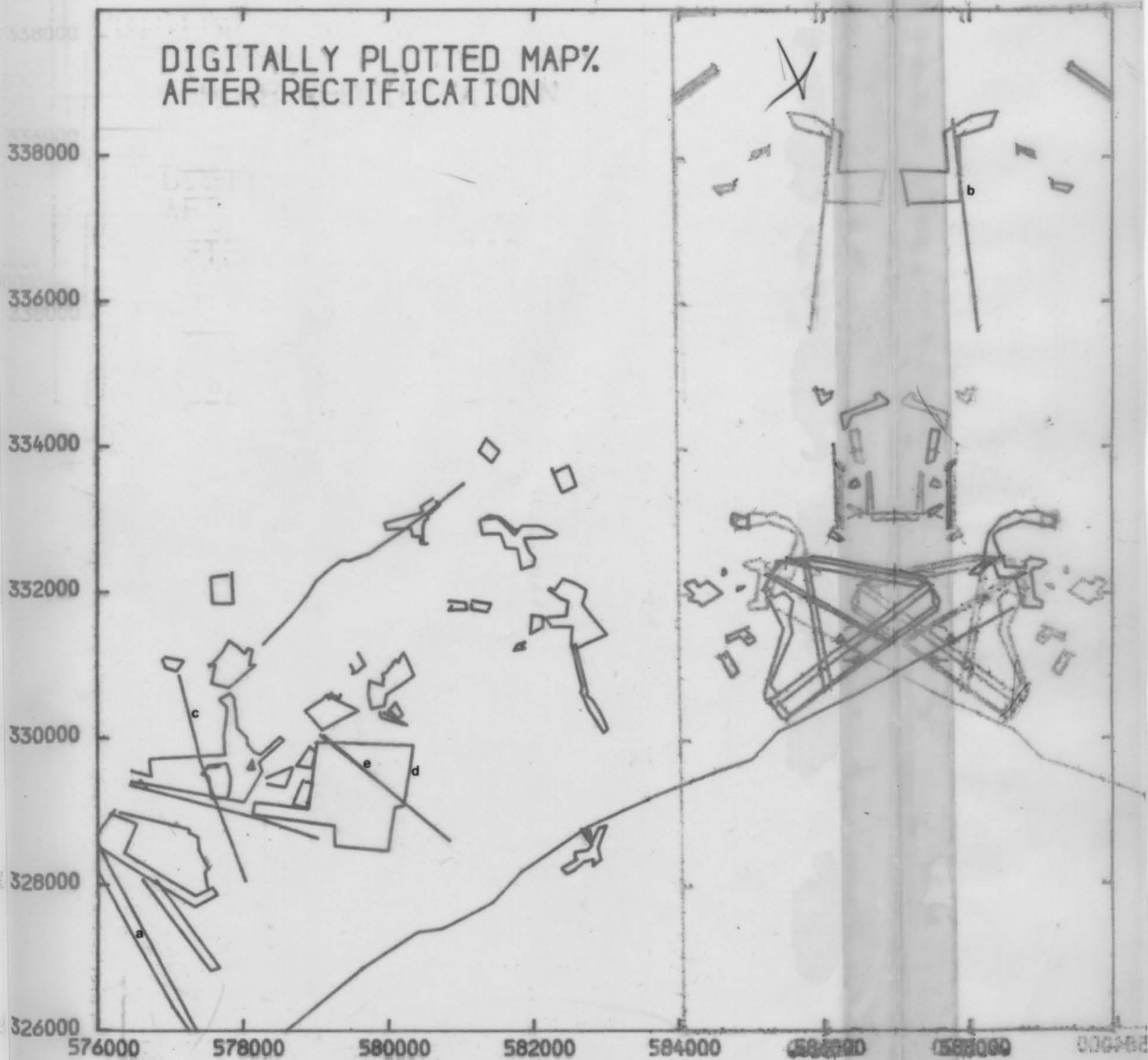


Fig 10.13b

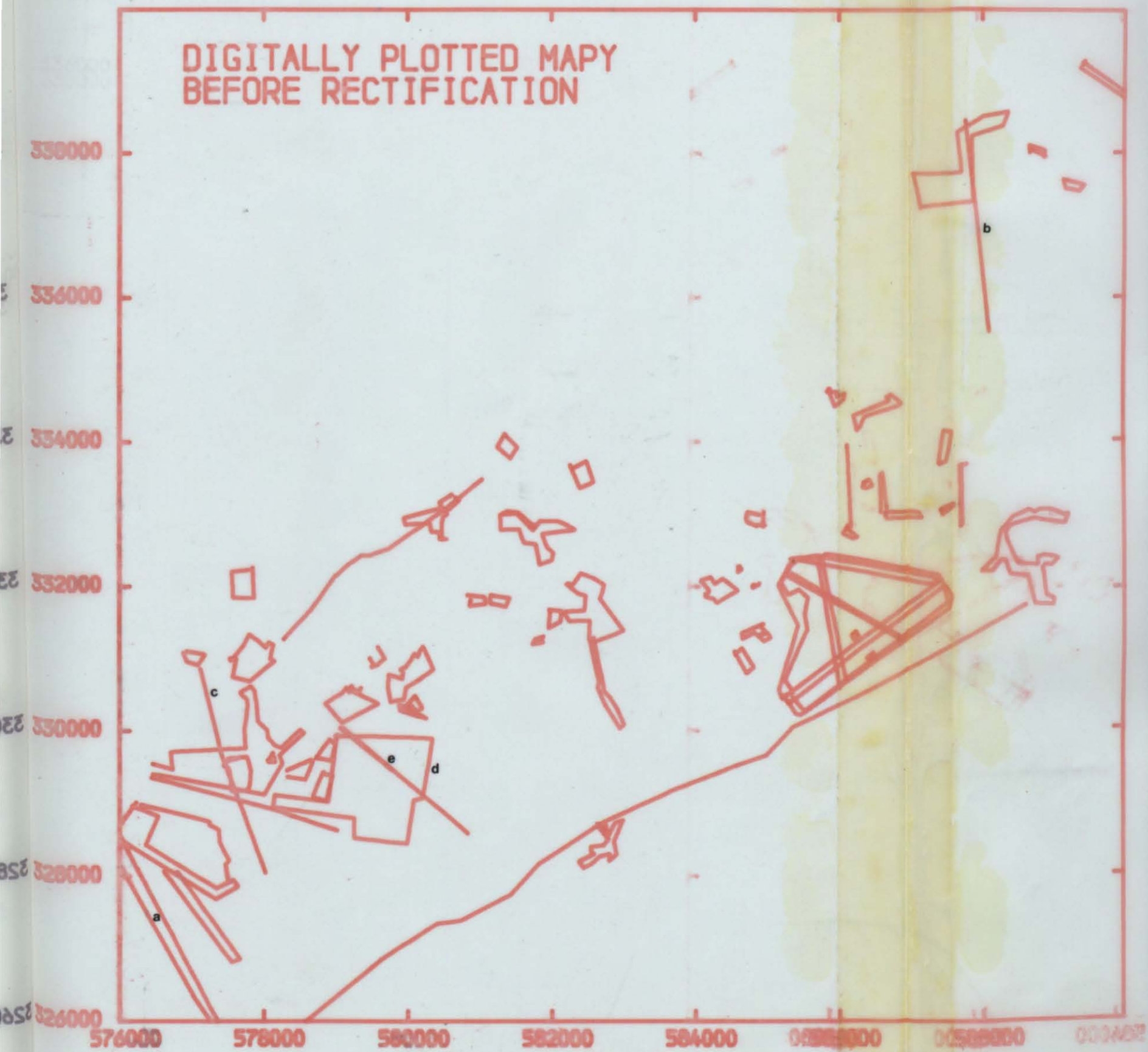
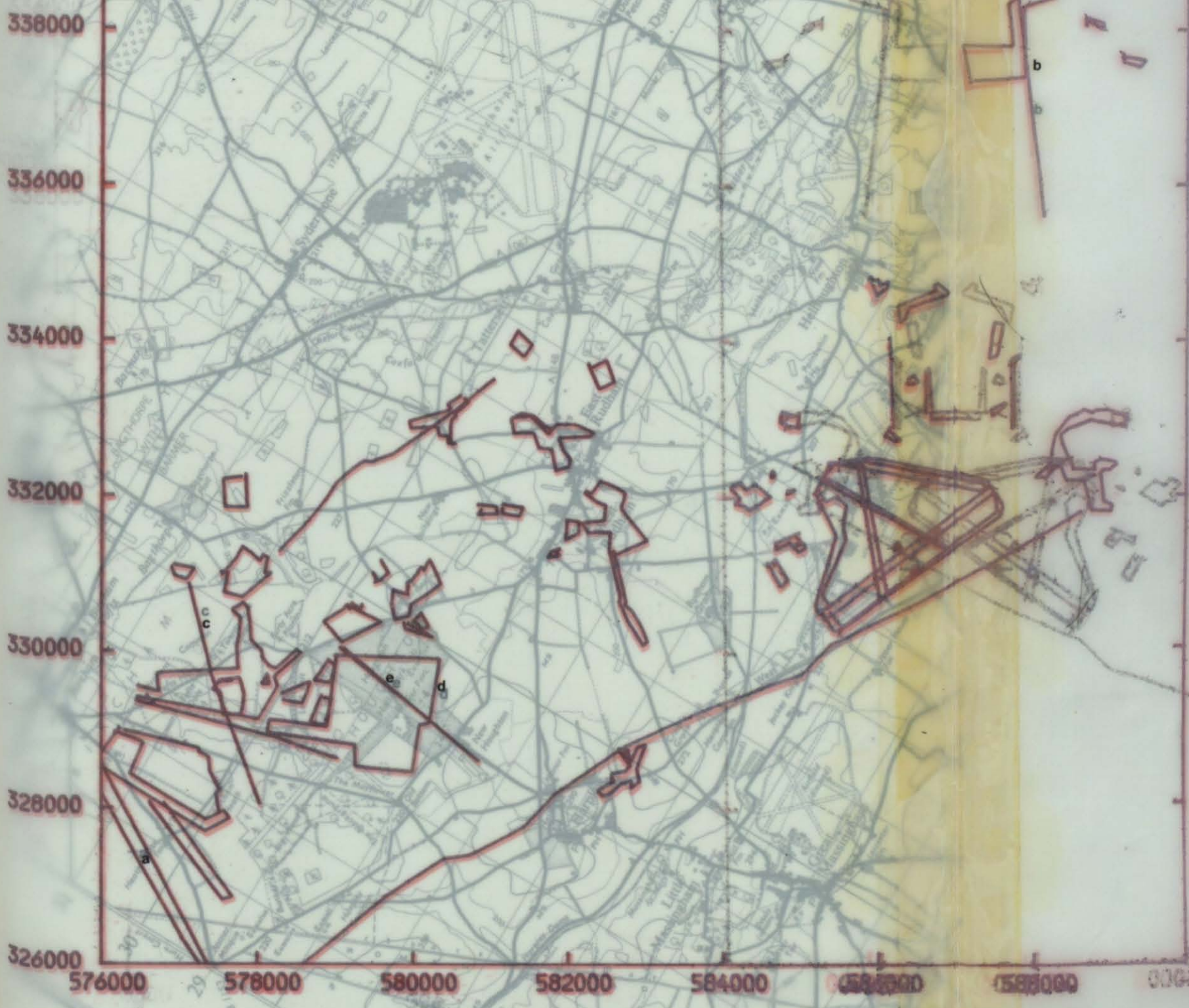


Fig 10.13c



Fig 10.13c
397 396
Fig 10.13b
Fig 10.13a

DIGITALLY PLOTTED MAP AFTER RECTIFICATION



: RUN

Fig 10.14 Two Features which have been Rectified

BUNKER HILL FOREST

BEFORE RECTIFICATION

AFTER RECTIFICATION

X(M)	Y(M)	X(M)	Y(M)
1. E+6	1. E+6	1. E+6	1. E+6
576445.	329400.	576461.	329412.
578000.	329107.	578016.	329126.
578251.	329540.	578265.	329552.
578216.	329657.	578223.	329671.
578556.	329967.	578572.	329974.
578505.	330005.	578506.	330023.
578230.	329761.	578244.	329774.
578146.	329810.	578152.	329807.
578050.	329896.	578064.	329916.
578035.	330000.	578052.	330016.

PRESS RETURN TO CONTINUE

577896.	330134.	577913.	330148.
577872.	330408.	577895.	330422.
577868.	330449.	577882.	330468.
577862.	330534.	577879.	330555.
577872.	330541.	577870.	330546.
577800.	330609.	577817.	330624.
577663.	330529.	577675.	330542.
577672.	330498.	577692.	330516.
577759.	330423.	577776.	330441.
577758.	330356.	577779.	330354.
577704.	330044.	577734.	330042.
577739.	329750.	577755.	329766.
576695.	329698.	576704.	329715.
576730.	329471.	576738.	329478.
576441.	329551.	576454.	329555.
1. E+6	1. E+6	1. E+6	1. E+6

* .401 SECONDS USED

23:42:55

399

RUN

CHANTREY HILL FOREST

BEFORE RECTIFICATION

AFTER RECTIFICATION

X(M)	Y(M)	X(M)	Y(M)
1. E+6	1. E+6	1. E+6	1. E+6
587134.	337256.	587120.	337237.
587028.	337730.	587022.	337781.
587711.	337742.	587708.	337746.
587651.	338291.	587649.	338285.
588026.	338511.	588015.	338501.
588372.	338571.	588361.	338555.
588294.	338374.	588281.	338365.
587852.	338242.	587834.	338239.
587877.	337339.	587859.	337330.
587173.	337278.	587160.	337261.

PRESS RETURN TO CONTINUE

1. E+6 1. E+6
* .230 SECONDS USED

1. E+6 1. E+6
23:45:17

400

the corrections resulting from the rectification were, in many cases, swamped by the errors resulting from wrong identification and measurement of the plotted boundaries.

Turning to specific classes of well defined features on this plot:-

- (i) The fit is relatively good for most of the plotted wooded areas. However, due to the difficulties encountered in the interpretation and delineation of the exact boundaries of the woodlands, the plotting of these features is not consistently good as can be seen from the many minor misfits of the wooded areas.
- (ii) Some minor roads such as that crossing the Big Wood forest, that passing to the east of it and that crossing the Deer Park (designated by c, d, and e respectively) do fit the O.S. map quite well. This is rather unexpected since all of these roads run roughly in the cross-track direction. On the other hand, as with the plot produced with the unrectified data, the A148 main road which runs approximately at right angle to the flight track is still displaced out-of-position along most of its plotted parts, compared with all the other features on the plot. Thus, there is little doubt that this main road has been wrongly identified and consequently wrongly measured and plotted, even though the image which was actually plotted appeared to be quite convincing as a road.
- (iii) The fit of the Sculthorpe Airport on this plot is reasonably good. Even the small blocks of buildings situated inside the air-field seem to conform to the details shown on the O.S. 1:63,360 scale map.
- (iv) The limits of the built-up areas such as the village of East

Rudham in the centre bottom of the map have not been plotted correctly or completely, the reason being that around this type of village there are a number of blocks of houses scattered in the country-side which also give bright returns. Thus during measurement, it was difficult to delineate the exact boundary of the village, and so only the centre of the village, where a coherent and consistent set of returns occur, has been delimited. However, it is also possible that the size of the village may have changed considerably over the time lag between the compilation of the map (1969) and the acquisition of the imagery (1978). This tends to be confirmed by a further comparison of the plotted map with the recently revised 1:50,000 scale O.S. map of the area.

Overall, it may be concluded that the technique adopted in this experiment to remove the effect of relief displacement errors from the Seasat SAR image data only improved the fit slightly, and it appears that the difficulties experienced with interpretation are those of paramount importance in the process of digital monoplotted of the Seasat SAR images. In particular, the roads of many different types which would provide the main framework of linear features on which the rest of the detailed plotting could be based proved to be singularly difficult to deal with. In many cases, the road image appeared to depart from the correct position in an unexpected manner and even prior knowledge of the orientation and location of a particular road would sometimes not help in correctly identifying and plotting it on the image as in the case of the A148 main road mentioned above.

Wooded areas pose their own special set of problems, though of a lesser magnitude than those associated with the roads. The

main difficulties associated with the digital monoplotted of wooded areas in the test image appear to stem from the fact that the types of trees dominant in some wooded areas produce relatively weak radar energy returns which makes them difficult to detect and interpret and hence to measure them with any confidence even though they are well depicted on the map.

Human settlements can be relatively easy to plot if sufficient image contrast exists. However, it is not always possible to plot individual blocks of houses; instead, a small settlement of possibly 100 m to 200 m in extent can be plotted as a single cluster which is not necessarily a defect on a relatively small-scale topographic map.

10.6 Conclusions and Recommendations of the Test

The present digital monoplotted experiment from Seasat SAR imagery was initiated in support of topographic mapping from side-looking orbital radar imagery. In particular, map revision was seen as an obvious application of the technique. The results are undoubtedly disappointing but since the scope and extent of the present test have been rather limited, the corresponding results must be viewed with this in mind. It must be said however that initial attempts to plot the digitally processed image of the Milford Haven test area using the same technique were even more disappointing than that of the East Anglian image due to the sheer lack of topographic detail which could be identified with any certainty.

Turning back to the East Anglian image, although individual well-defined image features did show some improvement in their overall positional accuracy after the application of the relief

displacement errors, the plotted detail certainly did not fit the ground as well as had been hoped for and many features required for inclusion in a topographic map have not been detected or plotted. Hence, one may conclude tentatively that the problems associated with digital monoplotting from SAR imagery are mainly associated with the detection and identification of image features rather than those of a geometric nature. These problems may lead to many gross errors being perpetrated in the measurement stage.

However, a more positive point towards digital monoplotting from radar imagery is that, even with its limitations, it may be of importance in the cloud-bound areas of the developing world, though, in these circumstances, a disadvantage is the need for advanced technology in the form of computers, digitizers, plotters etc, and of skilled personnel to implement the method. However, since this experiment is one of the first attempts to produce original line maps from satellite SAR images, further experiments of this type should be carried out over different types of terrain in various parts of the world to reach firm conclusions regarding the potential of digital monoplotting techniques from satellite SAR imagery for topographic mapping.

CHAPTER XI

INTERPRETATION OF SEASAT SAR IMAGERY FOR TOPOGRAPHIC MAPPING11.1 Introduction

It has already been seen in the previous two chapters that the efforts to establish the effectiveness and accuracy of the various procedures devised for rectification of the Seasat SAR imagery were severely constrained by the difficulties encountered in the detection and interpretation of the objects known to be present on the terrain and which should have been visible on the SAR image. No measurements, whether of individual point images as carried out in the tests of geometric accuracy or of continuous line plotting as attempted in the digital monoplotting experiment, can take place without some degree of interpretation, however secondary a function this might be. However, the sheer paucity of well-defined points experienced in the geometric accuracy tests, especially with the optically-processed images, and the obvious omissions, gaps and errors present in the plot produced as a result of the monoplotting experiment bring the matter of the interpretability of the Seasat SAR images to the fore. Therefore in this Chapter an attempt has been made to establish what can be discerned on the Seasat SAR imagery using the details required for standard small-scale topographic mapping as the yardstick for the study.

It will already have become apparent that, since a SAR image and a conventional aerial photograph are produced by entirely different sensors in terms of their wavelengths, methods of operation, geometry, etc, the appearance of the same piece of ground will be entirely different on the two images. What appears on the one image may not

appear on the other. Since the photographic interpretation process itself and the results likely to be produced from the interpretation of photographs at a given scale are very well known and established, while that of SAR imagery is unfamiliar, the main factors influencing SAR image interpretation will first be outlined. This is followed by an account of the actual experiments carried out on the four test images available to the author to establish what can (and cannot) be detected and interpreted on the Seasat SAR images in terms of topographic detail.

11.2 Factors Influencing Interpretability of SLR Images

Apart from the interpreter's own abilities and aptitudes, there are two main groups of factors which affect the interpretability of the image. These arise from:

- (i) the radar system geometry; and
- (ii) the back-scattering characteristics of the terrain and of the objects present on it.

11.2.1 Radar System Geometry

For the purpose of interpretation of SLR imagery, the most important geometrical parameters are: (i) the SLR system resolution; (ii) the direction in which the imaging is taking place; and (iii) the general characteristics of the terrain surface itself with respect to the incident energy of the SLR pulse.

(i) Radar Resolution: The detailed discussion regarding along-track and cross-track resolution of SLR images has already been given in Section 2.4 and needs no repetition here except to emphasize its fundamental importance in image interpretation. Wavelength is of

particular importance with the shorter wavelengths offering superior resolution. Obviously, objects with dimensions less than a resolution element will be very difficult to detect and identify on the SLR image.

(ii) Direction of Imaging: The distinction between along-track and cross-track resolution also raises the matter of the precise direction in which the imaging takes place and the resolution which results from this. Obviously, an object may be resolved when it is illuminated from one direction but not when illuminated from another depending on whether it is lying in the along-track or cross-track direction. Another aspect of the orientation of the object with respect to the imaging beam is that certain objects, e.g. an embankment or a line of trees, may well give a strong reflection when located roughly parallel to the flight direction but a weak or negligible return if oriented in any other direction. These are most important factors, in that the detection and interpretation of individual features on SLR images is to a certain extent arbitrary and a matter of sheer chance in a manner which is not experienced in the interpretation of conventional photographic images or those produced by other remote sensing devices.

(iii) Geometrical Characteristics of the Terrain Surface: As mentioned in Section 6.3.1.2, radar layover is a function of the height of the object being imaged and the radar elevation angle. Furthermore, it is also a function of the terrain slope γ (Fig 11.1). The incidence angle between the direction at which the SLR pulse strikes an object or surface and the normal to the surface imaged is also important in defining the conditions for the extent of the back-scatter and reflectivity of the incident pulse. Furthermore, the actual layover resulting from the presence of relief and slopes on the terrain can of course

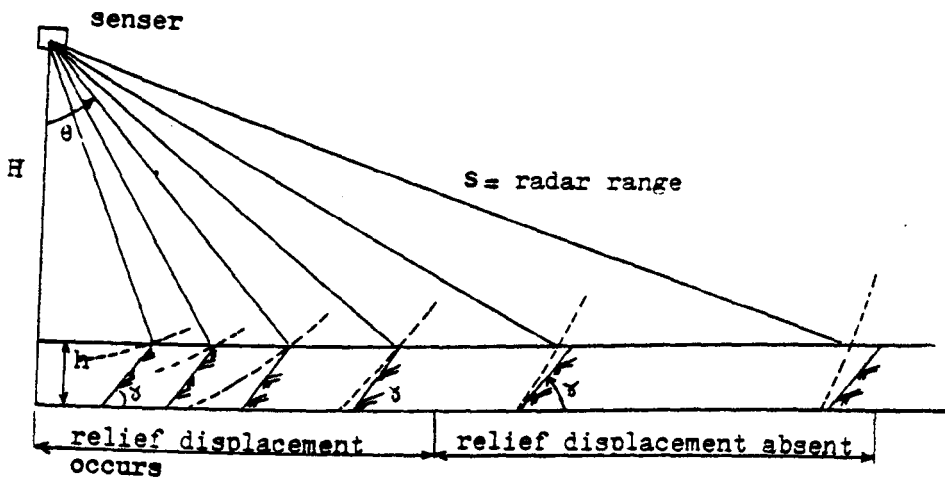


Fig 11.1 Effect of elevation angle and terrain slope on radar layover.

render features virtually uninterpretable especially in areas of mountainous terrain.

11.2.2 Back-Scattering Characteristics

The variations in the degree of reflection of the incident SLR pulse towards the antenna considerably influence the appearance of a certain target on a radar image and hence its detectability and interpretability. The actual backscatter which will be present is a function of both the system parameters and the terrain and object characteristics and of their interaction with one another.

(i) Surface Roughness: According to the Rayleigh Criterion, a surface imaged by an SLR is considered to be smooth in terms of the transmitted wavelength, if it is related to the wavelength by the following relationship:-

$$h_r = \frac{\lambda}{8 \sin \psi}$$

where h_r = surface roughness;
 λ = radar wavelength; and
 ψ = angle of incidence.

Thus the general rule is that the rougher the surface is as compared with the wavelength, the more energy will be reflected to the antenna. One may note that, for an X-band ($\lambda = 3$ cm) SLR, many features on the terrain will appear rough while for an L-band ($\lambda = 25$ cm) radar, relatively speaking, fewer features will appear rough on the radar image. It will be obvious too that the term surface roughness is concerned with very small features such as leaves, twigs, gravel, sand, etc, which are measured in centimetres and tens of centimetres rather than the topographic relief, e.g. hills, valleys, ridges, etc, whose dimensions are measured in hundreds of metres.

Normally several different categories of surface roughness may be distinguished. Specular reflection takes place when the surface is smooth, in which case, reflection follows Snell's Law by which the angle of reflectance is equal and opposite to the angle of incidence of the radar energy (Fig 11.2a). Virtually all the energy is reflected away from the antenna and the surface thus appears totally black on the image, i.e. it is a void. Surfaces which are predominantly specular are still water, paved roads, airfield runways, concrete surfaces, etc. Such surfaces give very low radar returns, except when they present a surface normal to the incident radar energy (Fig 11.2b) when a very strong return signal is produced which appears as a very bright image.

Also if a series of smooth surfaces combine to form a corner reflector, e.g. a combination of buildings or walls or a complex structure such as a bridge or pylon, then again a strong return signal will be produced. Towns and villages in particular exhibit many such reflectors at SLR wavelengths.

If, on the other hand, a surface has irregularities comparable with the wavelength, energy will be reflected in a quite different manner usually referred to as diffuse or scattered reflection (Fig 11.2c). Surfaces which produce scattered reflection are woodlands, forests, crops, parks, etc. The reflected energy will produce an image of intermediate brightness, its actual appearance being dependent on the proportion of the incident energy back-scattered to the antenna. This in turn will depend on the characteristics of the object itself and the degree of surface roughness which it exhibits.

The influence of the SLR wavelength already discussed above will also extend to include the degree of surface penetration. In general, the longer the wavelength, the greater will be the depth of

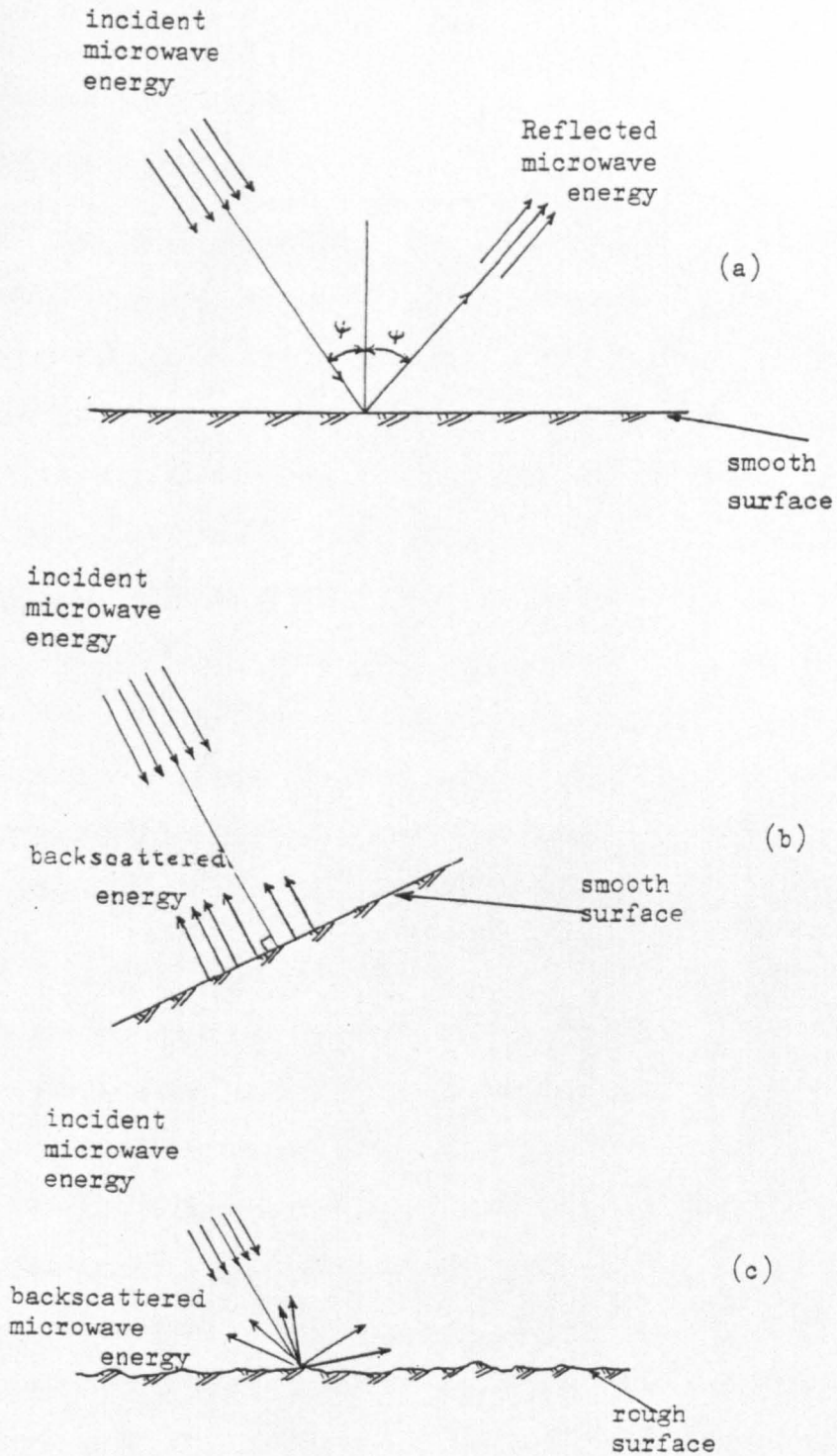


Fig 11.2 Specular and diffuse reflections

penetration and the stronger will be the effect of the sub-surface characteristics on the returning signal.

(ii) Dielectric Constant: The electrical properties of a surface as expressed in the dielectric constant (defined as the ratio between electric flux density in an object to that in a vacuum for the same electric field) critically affect radar return and SLR image interpretation. These properties are strongly dependent on water content so that the dielectric constant varies almost linearly with the moisture content. Thus in general terms, reflection is least with a surface with low moisture content while an increased moisture content leads to a marked reflectivity in the surface (Deane, 1973). Having said this, one must also remark that it appears very difficult to quantify or measure the dielectric properties of a surface and very little work of a definite nature has appeared in the literature so far.

(iii) Polarization: SLR imaging systems normally transmit horizontally plane-polarized electromagnetic radiation. When this radiation hits the terrain, part of it is depolarized and rotated to varying degrees depending on the nature of the reflecting object. The horizontal and vertical components of this reflected energy may be received separately using two different antennae. If the horizontal component of the radiation is picked up, i.e. the received energy has the same polarization as the transmitted pulse, then the resulting image is designated as HH. If, however, the vertically polarised component of the reflected radiation is received, the image so formed is designated by HV. Investigations of multi-polarized radar images, e.g. by Lewis et al (1969), Moore et al (1971), have indicated that the simultaneous use of horizontally and vertically polarized images is

very useful in carrying out successful image interpretation of vegetation, rock formations, etc. However, the Seasat SAR is a single polarization (HH) system, so it is not possible to investigate whether or not the interpretation of two cross-polarized images would be of advantage.

(iv) Radar Side-lobe Banding: This is a well-known phenomenon often encountered on SLR images. It is normally found in the near range part of an SLR image where it takes the form of a pattern of light and dark bands trending parallel to the flight line. These are the result of the returns from the subsidiary pulses emitted by the radar set called side-lobes. Since their strength is a function of the two-way travelling distance, thus weakening with range, this accounts for their occurrence at the near range parts of the image where ranges are shorter. With airborne SLR imagery, interpretation is often hindered by these side-lobe effects. For satellite-borne radars, side-lobe banding can be expected to be very small because of the much greater operating ranges involved.

11.3 Elements of SLR Image Interpretation

As will have been apparent from the preceding discussion, the SLR image of a specific area will inevitably be very different in appearance from the corresponding aerial photographic image of the same area taken by a conventional photogrammetric or reconnaissance camera. Thus the normal experiences and procedures derived from photographic interpretation will often have limited application to the interpretation of SLR images. It may be useful to review the usual set of factors - size, shape, shadow, tone, pattern, site (or location) and orientation - listed as important in aerial photographic interpretation and attempt

to assess their relevance to the particular case of SLR imagery.

(i) Size: As with aerial photographic images, the size of an object on an SLR image is an important clue as to an object's identity. By measuring the dimensions of an unknown object on a radar image, the interpreter can frequently eliminate from consideration certain possibilities as to the character of the objects imaged. In the context of SLR, the size of an object should normally be greater than the nominal image resolution for it to be detected and identified, although of course corner reflectors of a smaller dimension may give such a great reflectivity as to be visible. It should also be noted that measurements on the radar image may only be fruitful if large inherent geometric distortions are removed at a preliminary stage in processing.

(ii) Shape: Shape relates to the general form, configuration or outline of an individual object and, as such, these characteristics are just as important in recognizing objects on an SLR image as they are on photographic images. However, the direction from which the radar looks at an object can greatly affect the shape of that object recorded on the SLR image. Thus the shape may well be falsified or misleading in that certain features of the object may be visible or prominent on the image while others will not be present, solely due to the orientation of the object with respect to the imaging direction of the SLR set itself. As a result, it is not always easy to visualize how a particular ground object will be represented on the SLR image and to make allowances for the distortion in shape which will result from the inconsistencies in the signals back-scattered to the receiver arising from this effect.

(iii) Tone: As with photographic images, objects will often be distinguished by the differing tones or intensities appearing on the

SLR image. These are produced by the varying amounts of energy reflected to the antenna from the objects. As discussed in Section 11.2.2, the amount of back-scattered energy depends, among other factors, on the properties of a specific object, e.g. its composition (i.e. the material from which it is made), its surface roughness, its dielectric properties, its orientation with respect to the antenna at the time of imaging, etc. These are factors which are not always apparent to the interpreter who may find it difficult to take account of their effect in a particular set of circumstances even when their general influence or characteristics are known.

(iv) Pattern: is the spatial arrangement of the components of an image, e.g. man-made features may often exhibit a systematic pattern. SLR image patterns are very important for geologists and geomorphologists (Waite et al, 1971) but care has to be taken since the systematic pattern visible on a specific SLR image may result wholly or partly from the relationship of certain features to the imaging direction of the SLR system. Thus caution has to be exercised in basing interpretation on the patterns visible on a specific image. In view of these limitations, the detection or presence of patterns may not be as important in the context of radar image interpretation for topographic mapping as it is in aerial photography.

(v) Shadow: The presence of this characteristic may help interpretation, for it may show the shape of an object. For example, shadow shapes may allow the interpreter to infer information about the actual land forms present in the area and the relative terrain relief. However, in the context of an SLR image, it should be remembered that the shadows occurring on SLR images are in fact total voids in the

image whereas, on a photographic image, detail may still be discerned in the shadow areas. These image voids are of course a major difficulty in interpreting or mapping an SLR image for which there is no cure whatsoever.

(vi) Site (or location): The location of an object with respect to the surrounding terrain features is of course a most helpful item to employ in the detection and interpretation of a certain feature on an SLR image. Indeed, such were the difficulties experienced in interpreting the Seasat SAR images that, in many cases, it was only the knowledge gained from existing maps or other information that objects were located in a particular place which allowed them to be detected and interpreted. Without this locational information, the interpretation would have been still poorer and even more difficult than it was. This is a major defect in the use of SLR imagery especially if original topographic mapping is being contemplated and the collateral information in the shape of existing maps, photographs, etc, is not available.

11.4 Interpretation of Seasat SAR Imagery for Topographic Mapping Purposes

Having introduced the basic elements of SLR interpretation and the various factors which are likely to be involved in the process, it is now possible to see how the interaction of these factors affected the interpretation of the Seasat SAR images which were available to the author and had previously been used for the geometric tests described earlier in Chapters VIII and IX. These were the optically processed images which cover the area around the River Tay and the towns of Dundee and Perth in Scotland and the two digitally processed images, the one

covering parts of East Anglia in England and the other covering parts of Pembrokeshire in Southern Wales. The interpretation of the SLR images has been carried out on the basis of these two forms of processing. Each will be discussed separately and the results summarized by two tables given at the end of the chapter. However, it should be noted that the results of the interpretation set out in this chapter are not oriented towards the needs of specialized field scientists interested in mapping particular aspects of geology, forestry, vegetation, soil, land forms, hydrology, etc, since the present author does not have the reference level required for such studies. Instead, the studies have been concentrated on the basic question as to whether objects can be detected and identified on an SLR image in the context of the detail required for the construction of topographic maps at medium to small scales.

11.4.1 Interpretation of the Optically Processed Images

Interpretation of the two optically processed images of the River Tay area was carried out by viewing the image monoscopically through a mirror stereoscope equipped with large aperture 3X magnification oculars or using a 2X magnifying glass. In view of the difficulties experienced in viewing the SLR images which exhibited a great deal of background clutter or noise under quite moderate magnification, the 3X and 2X magnifications used seemed quite appropriate. Collateral information used to assist the interpretation was provided in the form of a 4X enlargement print of each image and the 1:63,360 scale O.S. map of the area.

The main features of interest from the point of viewing of compiling or revising a topographic map of the area were inspected in turn with the following results:-

11.4.1.1 Man-Made Features

(a) Roads and Highways: These are smooth man-made features which, generally speaking, should exhibit largely specular reflections. Thus they should show up as dark straight or curved line features on the SLR image. On the O.S. 1:63,360 topographical map series, the roads are classified into many categories - motorways (M-class), trunk and main roads (A-class), secondary roads (B-class), roads with 14 ft or over of metalling, roads with 14 ft or under of metalling, minor roads and gravel paths. Each of these categories is well depicted on the map by using different symbols and colours. Attempts to detect and interpret these various categories of roads on the optically processed images of the River Tay test area gave the following results:-

- (i) Motorways: Only very occasionally can even a very small portion of a motorway be detected on the SLR image, and even then, only when the motorway runs parallel to the flight line would it be possible to recognize it even with collateral information. In the situations when a motorway is oriented in a direction which is not parallel to the flight line, it is impossible to detect it on the SLR image as is the case with the M90 motorway lying between Perth and Loch Leven. This is compounded by the fact that this area is quite hilly which may have resulted in parts of the motorway being lost in the radar shadows.
- (ii) Trunk and Main Roads: As is the case with the motorways, very few of these are visible. Only when they happen to lie in the direction parallel or nearly parallel to the flight line do small sections appear and these are very difficult to discern against the background clutter which is such a strong feature of these optically processed images. When sections of them do appear, it is utterly impossible to classify them in terms of being a motorway, a trunk or a minor road.

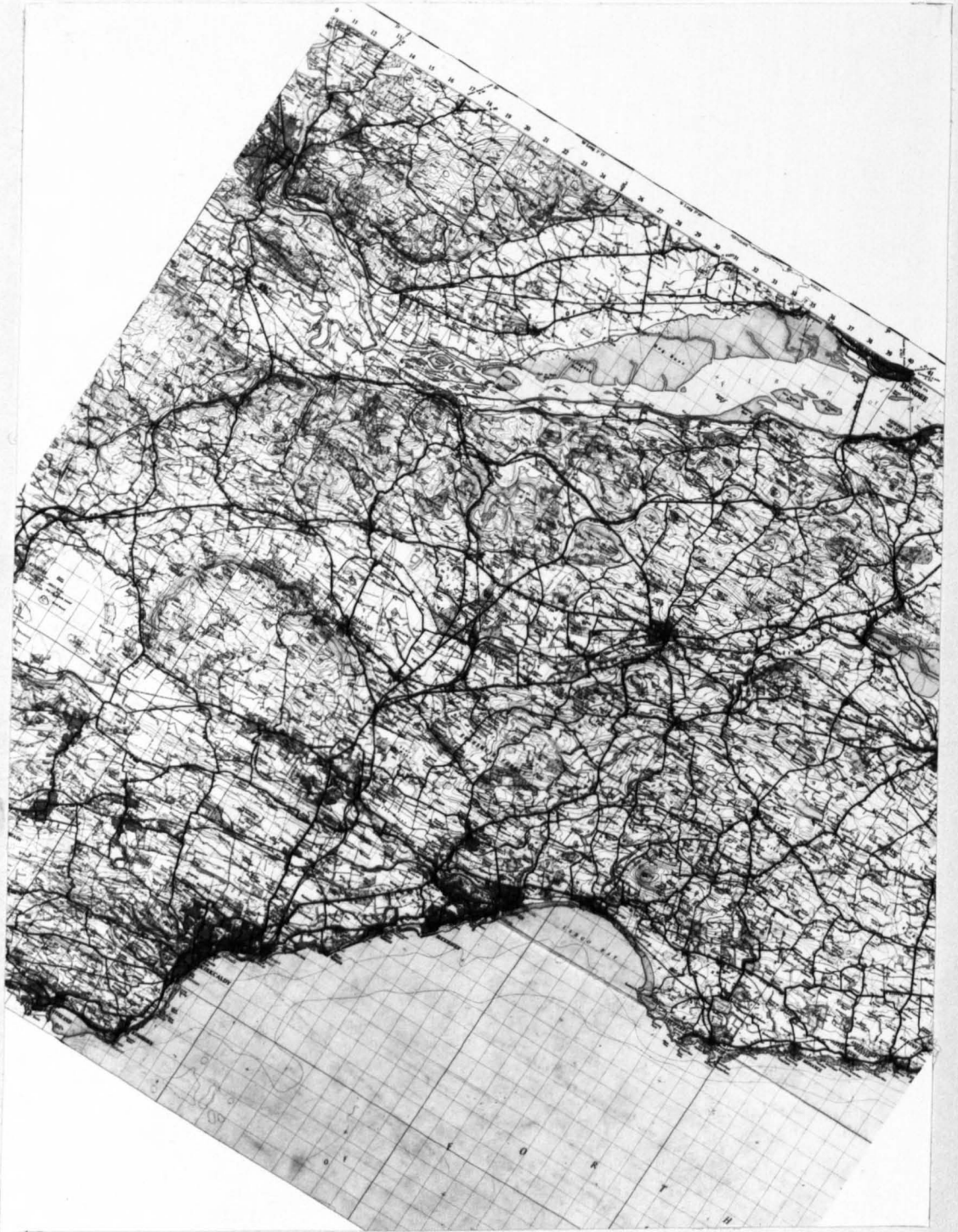
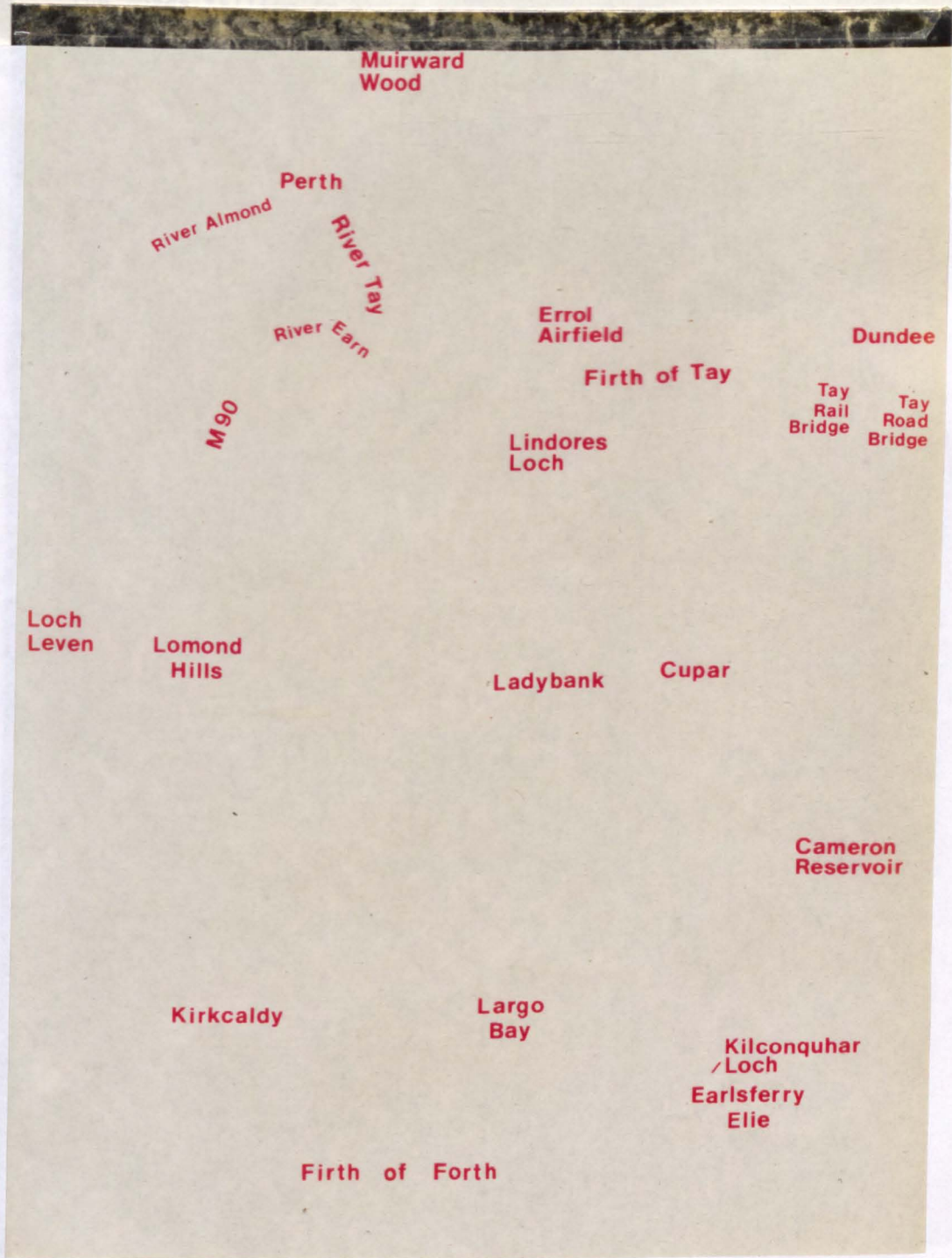


Fig 11.3

Topographic map of the River Tay test area

(iii) Roads with ...



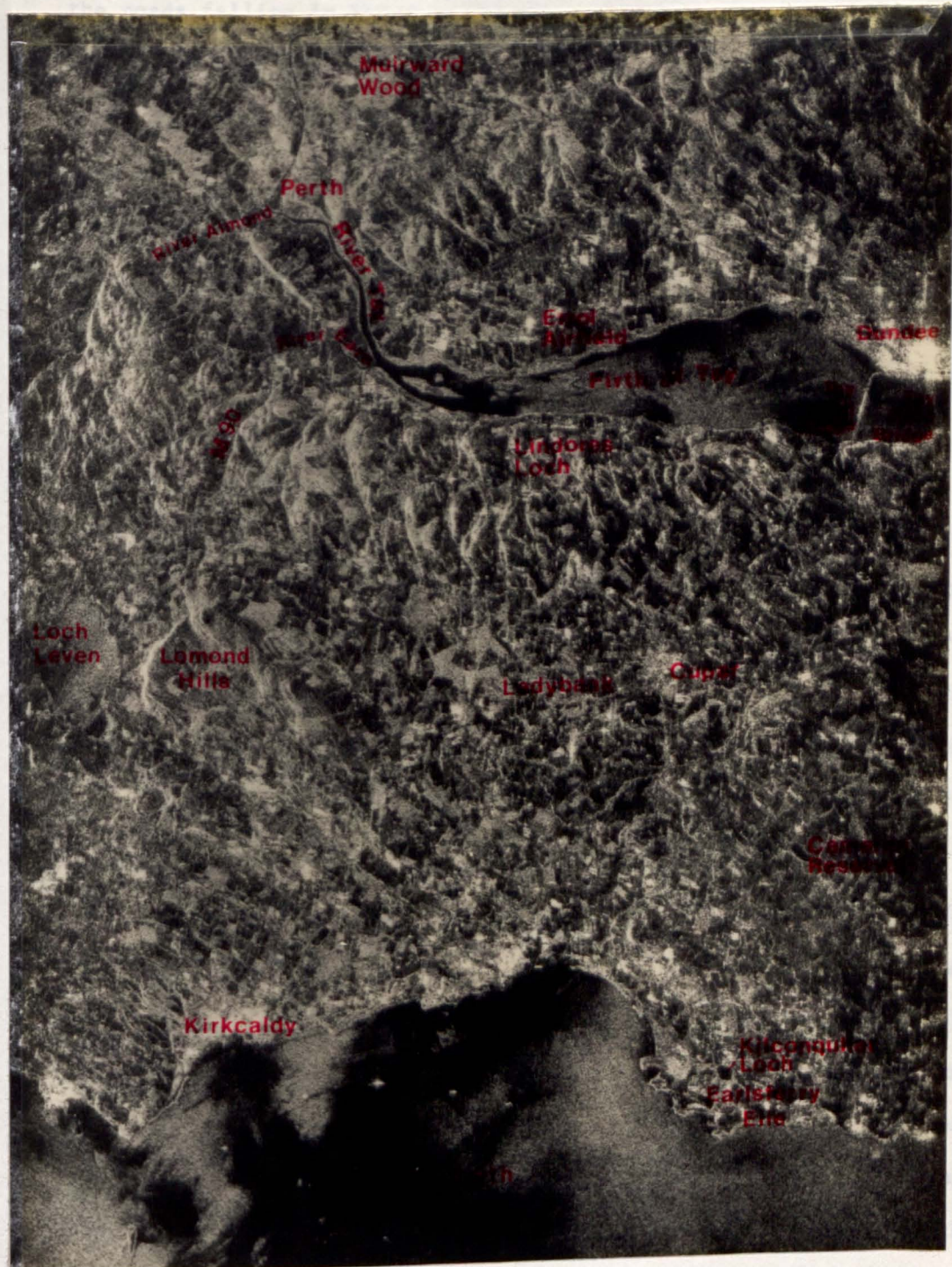


Fig 11.4 Features detected on the River Tay image

(iii) Roads with 14 ft Metalling: These are much smaller in size than the roads falling in the previous two categories and again very few of them can be detected and recognized. Their detection and recognition occurs occasionally more especially when they are running in a direction parallel to the satellite ground track but only with the help of an existing map. However, generally speaking, most of these roads are simply not visible on the SAR image.

(iv) Minor Roads: As would be expected, the detection of these features is extremely difficult on this type of imagery. Only a very small portion of a minor road running close to the coast between Kilconquhar and Earlsferry can be detected and identified.

(v) Gravel Paths: Quite a number of these features exist on this test area but they are of a very small dimension and none are visible on these two optically processed images.

In summary, one can say that a road of whatever category will sometimes show up on the image but only if it is located roughly parallel to the direction of flight. It is not, however, possible to decide into which category the detected road belongs.

(b) Railway Lines: These features are classified on the O.S. 1:63,360 scale map as multiple or single track lines. Quite a number of examples from each category are present on this test area. A few small isolated portions of both multiple and single-track railway lines can be detected and identified on the image wherever they run parallel or nearly parallel to the satellite track (Fig 11.4). However, whenever they substantially change their orientation from being near-parallel with respect to the satellite ground track, they almost invariably cease to be visible. As a single notable exception, the single-line railway running along

the east coast of Fife between Buckhaven and Anstruther can be detected for some kilometres of its length even though it runs in a direction roughly normal to the satellite track. The special circumstances permitting this to be visible are not apparent or known to the present author. It should also be noted that even if a railway line is detected and identified (in this respect, the long gradual curves aid in discriminating it from a road), it is not possible to classify it as single- or multiple-track.

(c) Bridges: There are five major bridges in this test area shown in the O.S. 1:63,360 scale map of the area. Three are located on the River Tay joining the two parts of the town of Perth, while the other two are the famous road and rail bridges crossing the Firth of Tay between Fife and Dundee. The three bridges in Perth are only just visible but only with prior knowledge of their position from the map. The very long Dundee bridges are very clearly visible (Fig 11.4). However, the numerous small bridges present in the area, located at the intersections of railway lines or motorways and at river crossings cannot be detected at all.

(d) Built-up Areas: These comprise the towns and villages of which many are present in this test area. Because the buildings may combine to act as good corner reflectors, most built-up areas, e.g. Dundee, Perth, Kirkcaldy, Cupar, etc, show up as very bright but ill-defined patches on the images. Even very small villages comprising a few houses can often be detected and identified with the help of a map though the image is rather amorphous and ill-defined and it is difficult to imagine that the information can be used for topographic mapping. In particular, though the presence of the built-up area can be identified it will be extremely difficult to define accurately the boundaries of a settlement.

(e) Airfields: There are three airfields in this area. One at Scone near Perth; the second at Riverside (Dundee Airport) and the third is a disused military airport at Errol. The Scone airfield near Perth has grass runways which cannot be seen. Errol is a disused military airfield whose runways can be seen with considerable difficulty and only after consultation of the map. Dundee's airfield is completely missing, although the overall grass area in which it is located shows up clearly.

(f) Power Lines: Many of these features exist in the test area and are shown on the 1:63,360 scale map. However, it is extremely difficult to detect a powerline without the help of the map and even then only when it runs parallel to the flight line. Again, virtually all of the power lines running in or near the direction normal to the satellite track are not visible, especially in the lower (southern) part of the images where, due to the many cultural features present, the lack of sufficient contrast did not allow power lines to be detected.

11.4.1.2 Hydrological Features

(a) Rivers: Because of their specular reflection, large rivers such as the Rivers Tay, Earn and Almond are very easily recognized with their very dark tones and gently twisting pattern and can be traced for the whole of their lengths on the image (Fig 11.4). However, the River Eden, although it is as wide as the River Almond, is hardly visible, even though it flows for a substantial part of its course through very flat flood plain areas. It may be noted again that its general orientation is at right angles to the flight line. The numerous other smaller rivers (e.g. the so-called burns) are very difficult to detect in these two optically processed images.

(b) Lakes: The largest lake in the test area is Loch Leven. It is indeed visible but contrary to what might be expected, it exhibits a medium grey tone especially at its boundary (Fig 11.4). The possible explanations are that, at the time of imaging, the wind might have been strong enough to cause waves on the surface of the Loch so that scattered reflection occurred instead of the specular reflection which would take place if the water surface had been calm. On the other hand, two much smaller lakes - Kilconquhar Loch and Lindores Loch - present in the eastern part of the image can easily be recognized by their very dark tones which contrast well with the bright surroundings of the woodlands located near them. It is however rather difficult to identify small lakes where they are surrounded by flattish terrain giving rather similar return signals.

(c) Reservoirs: These will of course be difficult to discriminate from the small lakes present in the area. Where a reservoir is surrounded by medium or high return features such as a forest or a woodland, it can be rather easily detected and identified on the image. It shows up as a very dark patch with a sharp boundary, e.g. Cameron Reservoir near St. Andrews (Fig 11.4). When the area surrounding a reservoir consists of fairly flat terrain often covered with grass as in the case of Carriston Reservoir near Markinch, it is then difficult to detect and identify. Also the series of reservoirs - Balla, Harperless, Holl, Arnott, etc. - located in the Lomond Hills are completely missing.

(d) Islands: The detection and identification of an island seems to depend on its size, surface cover and the condition of the surrounding water at the time of imaging. There are two islands in Loch Leven (Fig 11.4), one being approximately ten times the size of the other.

The small one is quite visible while the bigger one is completely missing. The reason for this appears to be that the small island has forest cover which gave medium intensity returns, thus rendering it visible against the relatively dark surroundings of the water. The bigger island seems to have been covered by grass or other low vegetation which has similar reflecting properties to those of the surrounding water.

(e) Shore-line: The general outline of the shoreline can be detected and identified but accurate tracing of the shoreline is extremely difficult. This is particularly true in the Firth of Tay where mud and sand banks make it very difficult to delineate the land/water boundary in the estuary area.

11.4.1.3 Vegetational Features

The various types of vegetation present on these two images are the woodlands, orchards, ornamental grounds and bracken and heath, all of which are well depicted on the map.

(a) Woodlands: Large woodlands or forests show up strikingly well on these images, e.g. the series of woods around Ladybank and Muirward Wood north of Perth (Fig 11.4). They almost always produce medium bright or grey tones and can be identified from this characteristic (Fig 11.4). However, on the two test images, many small woodlands could not be detected or identified at all, which suggests that they may contain deciduous trees with poorer reflecting properties than the larger forests which are frequently planted with coniferous trees. Another characteristic is that they do not contrast well with the surrounding features especially where located in or close to hilly and

built-up areas which may give rather similar tonal intensities and patterns. In such cases, the lack of contrast compared with these major features causes the wooded area to disappear completely.

- (b) Orchards: cannot be detected at all on these optically produced images.
- (c) Ornamental Grounds: Some of the parks present on this area can be detected but only with great difficulty and only with the help of the map, an example being the Scone Park near Perth.
- (d) Bracken and Heath: These features cannot be detected without the help of a map. Even then, their boundaries are very difficult to define and delineate and those so determined could not be used in the compilation of a topographic map.

11.4.1.4 Landforms

These elements include mountains, hills, valleys and other relief features which show up clearly on SLR images, e.g. mountainous areas can be recognized by their rather bright returns and their faces leaning forward towards the radar antenna, e.g. the Ochil or Lomond Hills in Fig 11.4. However, although the presence of such features is readily apparent, it is impossible to accurately define these features for the purpose of topographic mapping.

11.4.2 Interpretation of the Digitally Processed Images

The interpretation of the two digitally processed images has been carried out using the same simple devices and techniques used for the interpretation of the two optically processed images. A 4X enlarged print (at 1:40,000 scale) and the O.S. 1:63,360 scale maps were



Fig 11.5 Topographic Map of the East Anglian test area

East
Common

Fakenham

South
Creake

Sculthorpe
Airfield

River
Wensum

Colkirk

Helhoughton
Wood

B1454
Coxford
Wood

East
Rudham

West
Raynham
Airfield

Houghton
Park

West Rudham Common

A148

Disused
Airfield

Big Wood
Forest

Harpley

Great
Massingham

Roman Road



Fig 11.6 Features detected on the East Anglian image

again available for each area as collateral information sources. An important point regarding the interpretation of the digitally processed images is that they suffered less severely from the background clutter which is such a feature of the optically processed images. This allowed a greater enlargement of the image to be used for the interpretation and reduced somewhat the difficulties of detecting objects examined by the interpreter. However, clutter is still experienced to a considerable degree.

11.4.2.1 Man-Made Features

(a) Roads and Highways

- (i) Motorways: No motorways exist on either image.
- (ii) Trunk and Main Roads: A number of these exist on the East Anglian test area. The A148 which runs roughly at right angles to the satellite track seems to be visible for some short parts of its length on the image (Fig 11.6). The small part of the A1067 which runs nearly normal to the flight line and which passes through the Coxford Wood is also visible, but the rest of the road is completely absent. Also the whole of the A1065 running south-west from Fakenham and approximately at right angles to the flight line is missing.

On the Milford Haven image, nearly all the main roads run normal to the satellite path and none of them can be detected on the image.

- (iii) Minor Roads: There are only two classified roads of this type (the B1145 and the B1464) present on the East Anglian image, and these cannot be detected at all. Regarding other minor roads, it is only possible to detect them where they pass an area displaying medium reflecting properties so that suitable tonal variations are generated. This does in fact take place with the road crossing the Big Wood forest;

the road passing to the east of the Houghton Park and the one to the north of it (Figs 11.5 and 11.6), even when the road in question runs in a direction normal to that of the flight ground track. The Roman road, which is classified as a minor road on the map, stands out exceptionally clearly showing very bright returns. The reason for this unexpected appearance may be due to the fact that the road has a metal fence or banks parallel to the flight direction which act as excellent reflectors resulting in these bright returns.

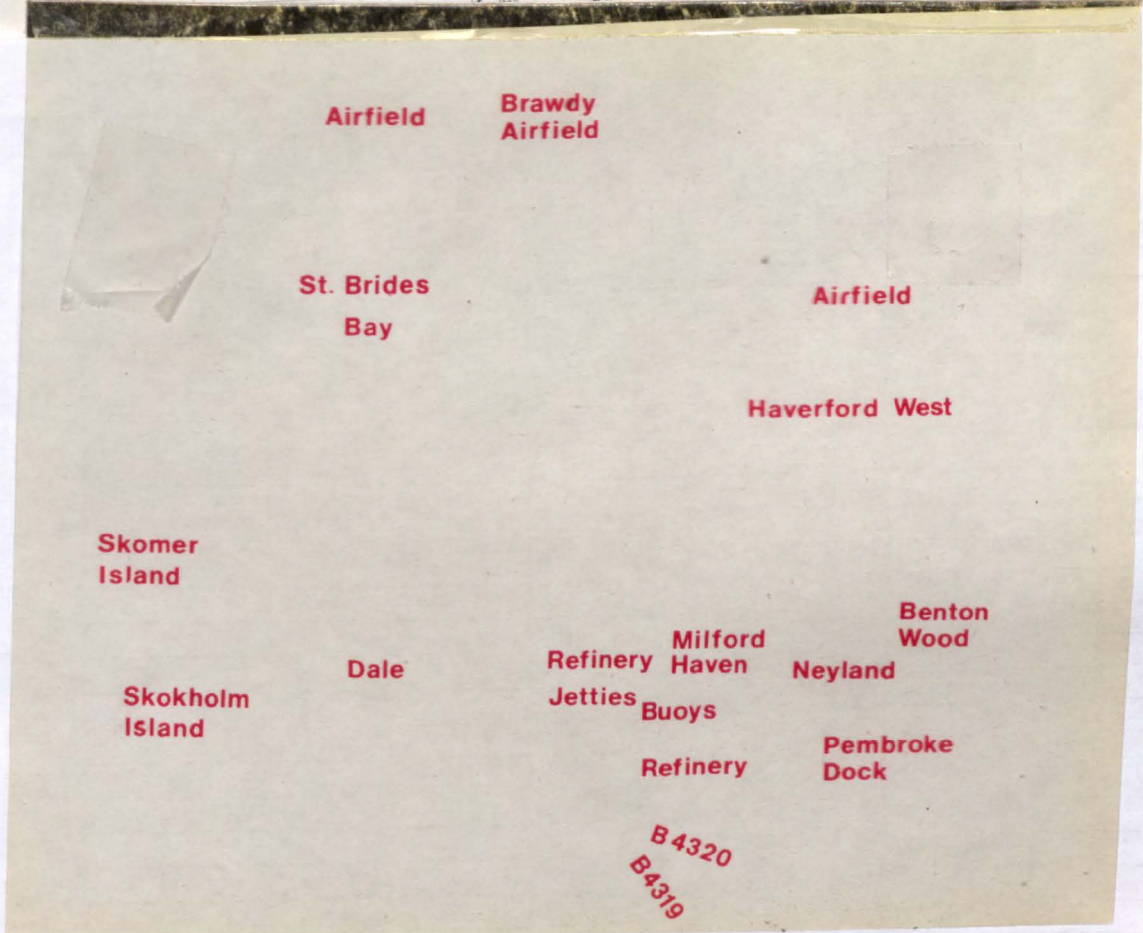
On the Milford Haven image, the B4320 is visible and can be identified and so are some parts of the B4319, possibly because they traverse an area containing medium return features which allows good tonal variations to be obtained. However, the B4341 and the B4327 are not visible at all. This comes as no surprise since they both traverse an area of considerable topographic relief with few definite features. Also it is probable that some parts are indeed lost in the substantial radar shadows present in the area. On the Milford Haven image, none of the unclassified minor roads could be detected.

(iv) Gravel Paths: Taking both digitally processed images, the only gravel path that can be detected is the one crossing the Big Wood in the East Anglian image which results in a break in the tree cover. The rest are completely missing.

(b) Railway Lines: Two single-track railway lines cross the East Anglian test area, the one running east-west and the other north-south. Some portions of each of these two lines are detectable and can be identified. However, wherever the railway line crosses a populated area or runs in a direction transverse to the satellite track it becomes difficult to detect even with prior knowledge of its position derived from the map.



(a)



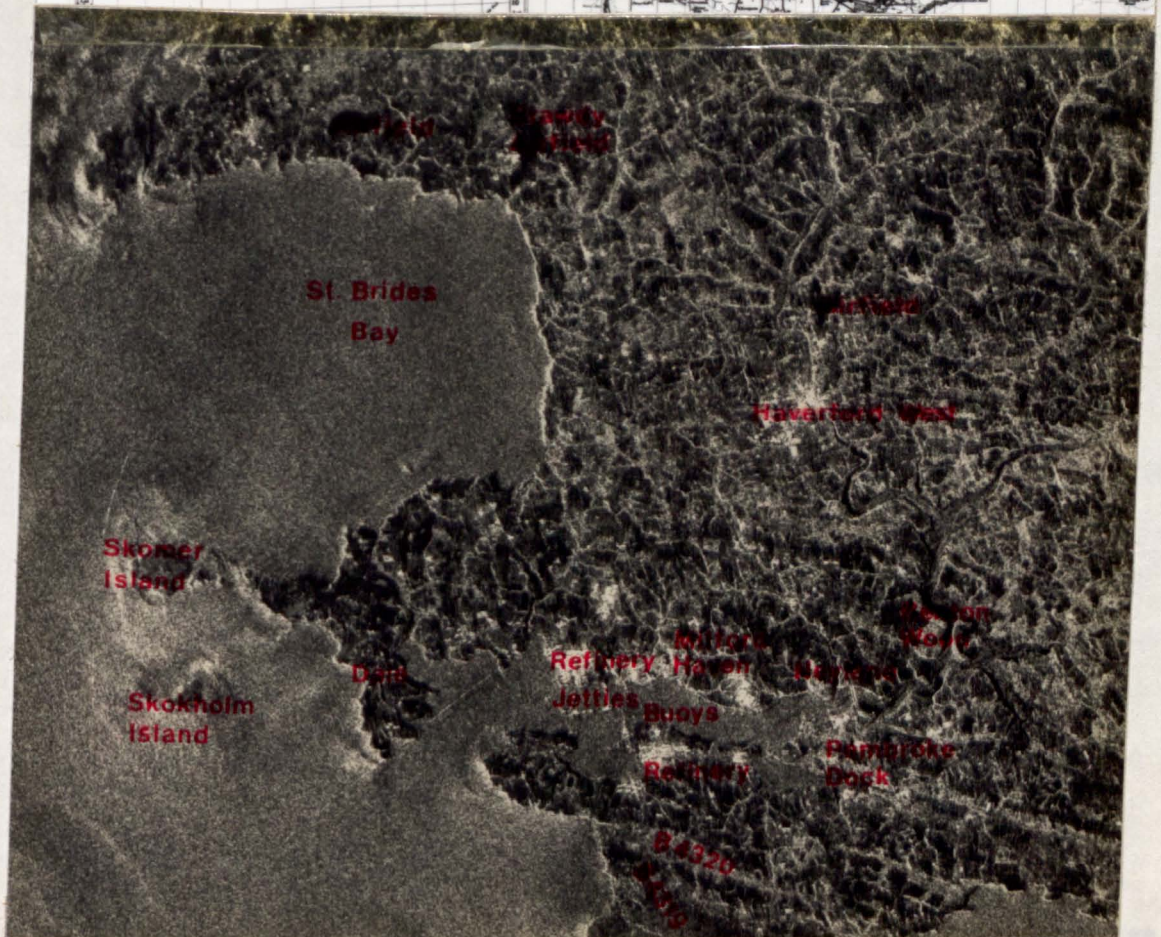
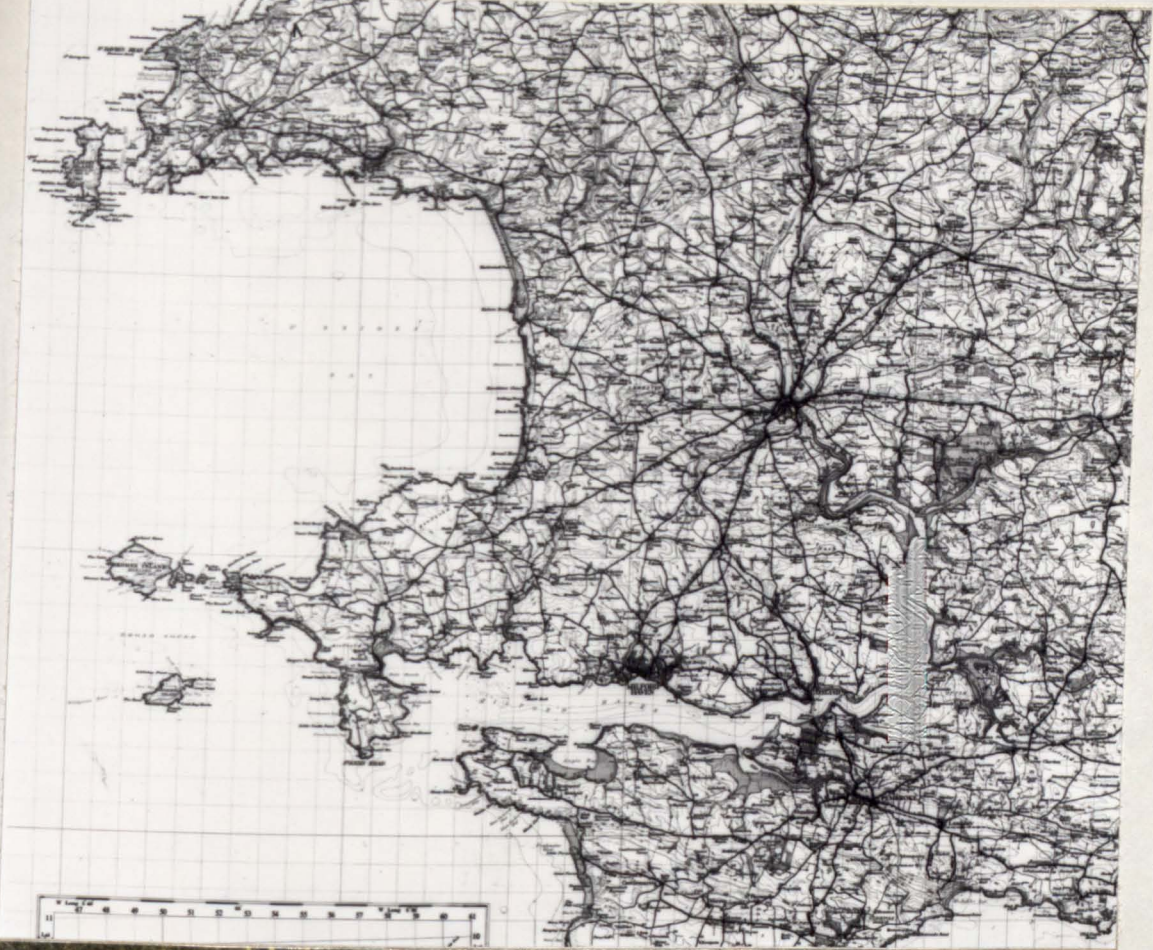


Fig 11.7 Features detected on the Milford Haven image

On the Milford Haven test area, only a single railway line exists - crossing the area from Milford Haven to Havenford West from South to North. Over parts of its length the line can be detected but with much difficulty. However, when the railway runs near to and parallel to a heavily vegetated river, it is very difficult to detect. In other areas, it is simply absent.

(c) Bridges: There is only one main bridge in the East Anglian test area, that carrying the railway across the River Wensum near the town of Fakenham. This bridge is not visible at all, possibly because it has been lost in the strong returns from the town and the woodlands surrounding it.

On the Milford Haven test area, a recently completed long bridge over Milford Haven connecting the towns of Pembroke Dock and Neyland can be clearly seen. However, the short railway bridge over River Pembroke near the town of Pembroke is completely absent on the image, apparently resulting from the fact that there are not enough tonal variations.

(d) Built-up Areas: As usual, these appear as large very bright patches on the imagery which, with the help of the existing map, can easily be recognized and interpreted. On the two digitally processed images, the boundaries of these features can be defined relatively better than on the optically processed images of the River Tay area but still with considerable uncertainty as to the exact limits of the built-up area. However, once again, if a built-up area is surrounded by or located adjacent to a woodland, it will be difficult to define its boundaries.

In the Milford Haven image, the two strongest reflecting areas are the two large oil refineries located on either side of Milford Haven,

no doubt due to the high reflectance produced by the refinery plant. Equally striking are the large buoys and lighthouses located in the channel of the Haven itself which are relatively small point objects but with a reflectance seen against the relatively poor reflectance of the surrounding water.

(e) Airfields: There are four military airfields on the East Anglian test area, two of which are currently disused. Two stand out most clearly in all circumstances, the runways being very visible, e.g. Sculthorpe and West Rudham airfields (Fig 11.6). The two disused airfields are much less distinct, e.g. that to the east of Great Massingham.

On the Milford Haven area, there are five airfields some of which have also been disused for some time. Three of these are clearly visible and can be identified and interpreted - particularly the large Brawdy military airfield (Fig 11.7a,b). The other two which are located in the south near Dale can also be detected but only with the help of the map.

(f) Power Lines: In the East Anglian image there is a complete absence of images of power lines.

On the Milford Haven area, only a short portion of the main power line can be detected and even then only after consultation of the map. It is difficult to account for this lack of response in these areas.

11.4.2.2 Hydrological Features

(a) Rivers: On the East Anglian area, there are three major rivers, none of which can be identified on the image. Not even the 60 m wide River Wensum can be traced. Along the area where it should appear, a broad grey band can be detected (Fig 11.6) which suggests that its banks

are heavily vegetated thus masking the actual river. On the Milford Haven image, again most rivers can only be located in the most general way via the presence of the grey band produced by the trees on their banks. Most other smaller rivers cannot be detected at all.

(b) Lakes: On both the two digitally processed images, lakes can only be identified if they are surrounded by woodlands or forests, otherwise they are extremely difficult to detect and identify.

(c) Reservoirs: These are difficult to detect on both images, e.g. the prominent reservoir between East and West Raynham is completely absent.

(d) Islands: There are no islands on the East Anglian test area, but on the Milford Haven image, where they are large in extent and are surrounded by sea rather than a lake, the presence of islands such as Skomer and Skokholm Islands can easily be identified (Fig 11.7a,b). However, as with the optically processed images, the actual boundaries or limits of these islands are difficult to define accurately, possibly due to the prevailing conditions of the sea at the time of imaging.

(e) Shore-lines: It is relatively easier to define the shoreline on the digitally processed image of Milford Haven than on the two optically processed images of the River Tay area. This may be due to the higher image resolution, but probably more important is the fact that the water is deep and close to the shoreline thus eliminating the difficulties experienced with the sand and mud banks in the estuary area of the Firth of Tay.

11.4.2.3 Vegetational Features

(a) Woodlands: As with the optically processed images, large woodlands such as the Big Wood, Coxwood, West Rudham Common and East Common on the East Anglian image (Fig 11.6) can easily be recognized, interpreted and mapped. However, successful interpretation of a woodland seems to depend also on the actual types of trees contained in a specific forest or woodland. This is apparent from the fact that some very large woodlands cannot easily be detected on the image without the help of the map, for example Helhouton Common appears a very mottled image of intermediate brightness. However, some very small forests can also be recognized on the image with their very bright tones.

On the Milford Haven image, there are virtually no forests present on the area. The only large wood - Benton Wood - is clearly visible as a mottled image.

(b) Orchards: Again, these features cannot be mapped on either of these digitally processed images.

(c) Ornamental Grounds: Some very large parks such as the Houghton Park on the East Anglia area appear as a mottled image and can be recognized without much difficulty, but one should note that this was only possible when the park is surrounded by extensive areas of low grass-covered terrain which give a good tonal contrast which allowed the park to be picked out. Other large parks such as Raynham Park and Crammer Park are completely missing and cannot be identified on the image probably because they are surrounded by mainly wooded areas.

(d) Bracken and Heath: Again, these are very difficult to delineate without the help of the map. They show up as dark grey lineations which are usually difficult to differentiate uniquely.

11.4.2.4 Land forms: Hilly areas and wide valleys can be recognized on the Milford Haven image, and can give some impression about relative terrain relief, but as with the River Tay area, no actual definitive mapping of the type needed for a topographic map can be undertaken.

11.5 Conclusion

Table 11.1 summarizes the interpretation results set out in this chapter. However these tables need to be supplemented by some additional comments. With linear man-made features such as roads, railways, power lines, etc, the orientation of an individual feature with respect to the flight direction is, in many cases, important if not decisive in detecting and identifying it. In particular, linear features running parallel or near-parallel to the satellite

TABLE 11.1 SUMMARY TABLE FOR THE DETECTABILITY OF FEATURES ON SEASAT SAR IMAGES

Elements shown on map (1:63,360 scale)	Optically processed images of the River Tay Test Area			Digitally processed images of East Anglia and Milford Haven		
	Detected on image	Recognized on image	Remarks	Detected on image	Recognized on image	Remarks
(1) <u>Communication Lines</u>						
Roads and Highways	*	* } }	Orientation very important	✓	* } }	Variable detection and recognition - very dependent on orientation
Railway Lines	*	* }		✓	*	
Bridges	✓	✓	large bridges only	*	*	
Gravel Paths	x	x		✓	*	
(2) <u>Man-Made Features</u>						
Built-up Areas	✓	✓		✓	✓	
Airfields	*	*		✓	✓	
Power Lines	*	*		*	x	
Reservoirs	✓	*		x	x	
(3) <u>Hydrological Features</u>						
Rivers	✓	*		x	x	
Lakes	✓	*		✓	*	
Shoreline	*	*		✓	✓	On Milford Haven
(4) <u>Vegetation</u>						
Woodland	✓	✓		✓	✓	
Orchards	x	x		x	x	
Ornamental Grounds	*	*		*	x	
Bracken and Heath	x	x		*	x	
(5) <u>Landforms</u>	*	*	cannot be mapped	*	*	cannot be mapped

✓ = Yes
x = No
* = Sometimes

track are often relatively easier to detect and identify. All of this makes for marked inconsistencies in terms of those features falling within a particular class and their actual detection and inclusion in the map. With regard to hydrographic features, their detection and identification on SAR imagery seems to be greatly affected by the amount of contrast available between a particular feature and those features on the terrain surrounding it. Thus if a lake falls in an area surrounded by woodlands which have medium reflectivity of the microwave energy, this lake will be visible on the radar image. In other situations, it may be quite absent.

The detection, identification and classification of vegetated areas is apparently governed by the size and type of trees or vegetation present in a particular forest or woodland. If the trees constituting such a forest or a woodland are of a type that has good reflecting properties of the incident microwave energy, then the forest will be visible.

Although the general outlines of the landforms, especially those of the mountains, hills, ridges and valleys, are sometimes clear and information about terrain relief can be inferred from this, it is really not possible to map these features in any meaningful way from a single radar image.

Finally some remarks must be made as to how frustrating and time-consuming the work of detecting, identifying and classifying objects on the present type of satellite SAR imagery can be. Yet in spite of the effort involved, the results are often unsatisfactory especially in terms of their completeness. A particular feature of

the Seasat SAR imagery which causes great difficulty in interpretation is the background clutter present in all the images, but especially in the optically processed examples. In this respect, the digitally processed images were much superior so aiding the interpretation considerably. However, even with these digitally processed images, the clutter is still quite troublesome and one must hope for much improvement in this respect in future if progress is to be made in mapping from satellite SAR images.

In conclusion, the particular point on which a heavy emphasis should be laid is that the direction of viewing of the SAR system is often decisive in deciding whether an object will appear on the image or not. Thus there is a certain arbitrariness as to the content of the SAR image which is not found in other types of imagery used for mapping. Since this is a fundamental matter for which a solution is at present not in sight it may be said that this is probably the limiting factor in conducting mapping operations from SAR imagery at the present time and for the foreseeable future.

CHAPTER XII

CONCLUSIONS AND RECOMMENDATIONS

12.1 General Conclusions

Since the results of the individual experiments have been discussed in detail in the previous chapters, it is not necessary to repeat these in this concluding chapter. However, it is quite appropriate to attempt to draw some general conclusions regarding the possibilities of topographic mapping from satellite SAR data based on the research work reported on in this dissertation.

(1) The first point is that the results obtained during the tests of geometrical accuracy confirm the fact that the planimetric accuracy attainable from the satellite SAR imagery available at the present time falls substantially below that of conventional photographic images and is not compatible with the accuracy specifications of any but the smallest scale topographic maps. However, the accuracy obtained depends significantly on the method of processing the SAR data (i.e. whether optical or digital processing) actually used in the production of the SAR imagery available to the user.

Nevertheless, it is indeed possible to extract metric information of an accuracy standard sufficient for the purposes of many developing countries which would allow the production of maps at scales of 1:250,000 and smaller. This is very important for certain regions of the world where continuous cloud cover is a major impediment to basic topographic mapping. However, the major problem would then be that the implementation of mapping from satellite SAR imagery would

require a difficult and expensive transfer of sophisticated technology from the advanced countries to the developing world, especially those concerned with SAR data reception and processing and with the subsequent stages of rectification using digital methods and the final hard-copy production. This could of course be carried out elsewhere as at present, but this would have considerable disadvantages from the point of view of the countries being mapped.

- (2) The analysis of the inherent geometric distortions occurring in SAR imagery has shown that these distortions can be modelled and corrected for mathematically using polynomials in such a manner as to eliminate or substantially reduce the errors present in an individual image. However, of special importance to the question of mapping from single radar images are the geometric distortions produced by the variations in the topography of the area imaged by the SAR system. The particular solution of this problem adopted in the present work - that of employing digital monoplotted techniques - shows a certain promise but the degree of success actually achieved was limited by the difficulties encountered in the detection, identification and interpretation of the features recorded by the SAR system.
- (3) This leads immediately to the root of the problem being experienced with the satellite SAR imagery which is currently available - that of deficiencies in image quality. The results obtained from the interpretation of the Seasat SAR imagery carried out in this project show that there are grave deficiencies in this particular aspect of the imagery. Partly these originate from the constraints in imaging direction which are inherent in all SLR imaging and give rise to the rather arbitrary series of responses which are a feature of all SLR

images. However, partly they appear to result from the special circumstances of operating an SAR system from a satellite. In particular, the background clutter which is a feature of both the optically and the digitally processed images is a deterrent to any type of mapping of other than major features. The source of this major defect is not obvious - whether it stems from the use of a discontinuous aperture with SAR can at present only be a speculation. But its removal during processing is quite essential if mapping from a satellite SAR system is to be fully effective.

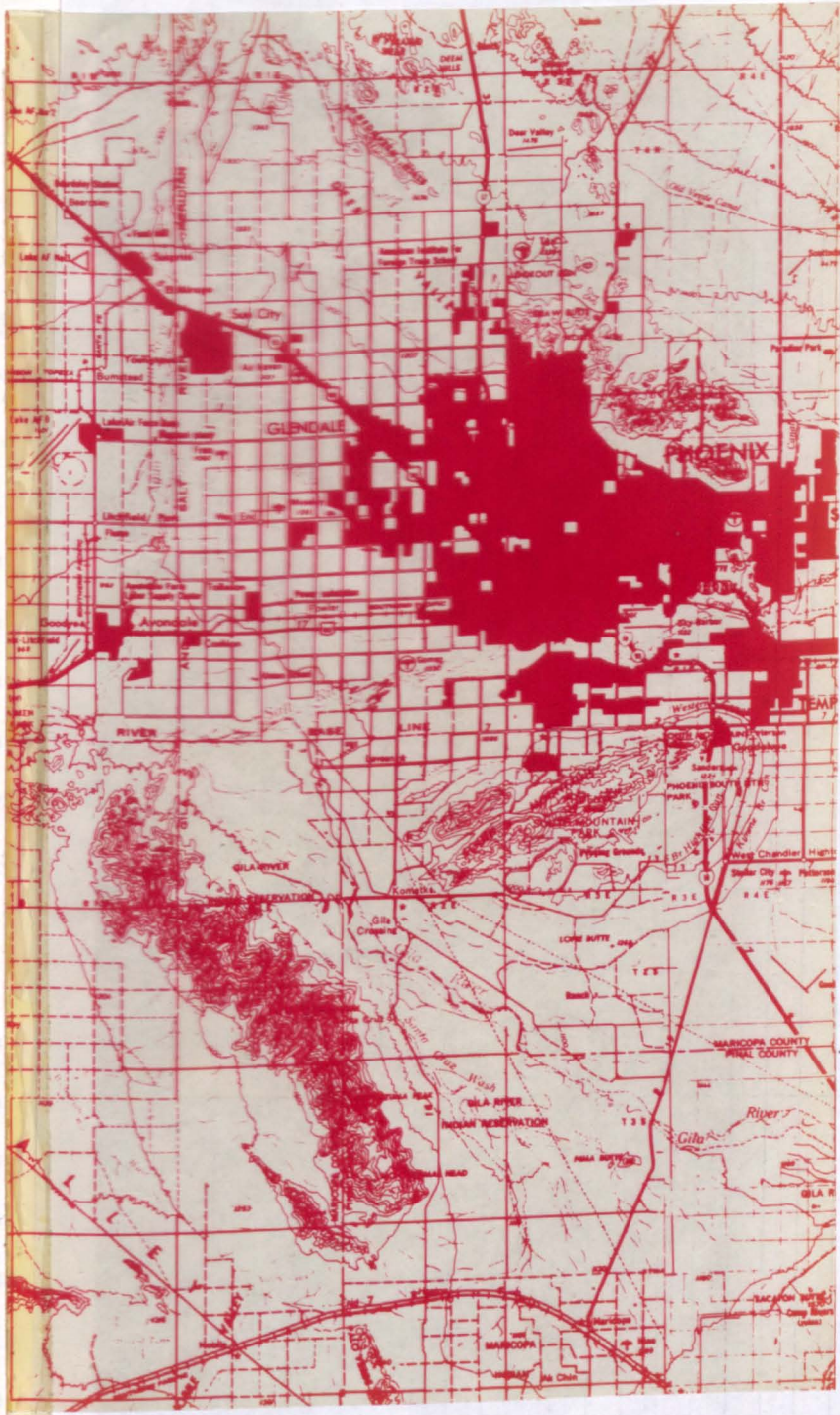
It is noticeable that this defect is far less apparent in aircraft SAR imagery as evidenced in the image (Fig 12.1) taken with Goodyear GEMS-1000 over the Phoenix area and used in the I.S.P. accuracy tests (Konecny, 1974) discussed in Section 7.5. It will be noticed that, while the nominal resolution of the Seasat SAR is 25 metres and that of the GEMS-1000 is 15 metres, there is a vast discrepancy in the quality of the image as delivered to the user.

Even with an improved quality of the image, the user/mapper must be aware of the special characteristics of the SAR images as exemplified by the variations in the occurrence of images of linear features resulting from their orientation relative to the flight direction of the SAR system. This will always cause inconsistencies both in the detail available for basic topographic mapping purposes and in that which needs to be detected for the purposes of map revision, which is of special interest to more highly developed countries with adequate existing map cover.

12.2 Recommendations for Further Future Work

There is no doubt that a number of unsolved problems of

Fig. 12.1 A Goodyear GEMS-1000 SAR image of Phoenix



varying degrees of importance and priority still exist in the development of methods of mapping from satellite SAR imagery.

- (1) In the first instance, there is an almost total lack of information about the geometric aspects of the SAR instrument itself. If mapping from satellite SAR imagery is to be contemplated on a regular basis, then it will be necessary to determine the necessary calibration parameters both initially during manufacture and regularly on an operational basis thereafter. The latter will become possible if the SAR device is launched and recovered from the Space Shuttle vehicle as indeed has been the case with the satellite SAR carried on the latest two proving flights of the Space Shuttle Columbia. Furthermore, the use of satellite SAR imagery for mapping would be assisted greatly if the information on the attitude and position of the sensor itself was made available to the users. This would allow the development of more rigorous analytical techniques with which to carry out the necessary rectification rather than the interpolative methods which are forced on the user, given the present lack of this information.
- (2) Some of the limitations and uncertainties encountered in the experimental work carried out in this present work arise from the lack of a large test field of suitably signalized points with accurately known positions. Any future researchers into this subject are recommended to invest in such a field of reflectors since it would eliminate many of the ambiguities and difficulties which arose from the use of poorly-defined natural points such as road intersections, river junctions, etc. The use of such a field of targetted control points would make it possible to judge the effectiveness of particular rectification procedures without the additional uncertainties arising

from the difficulties in accurately locating and measuring the control points. The construction and maintenance of the reflectors would undoubtedly cost a considerable sum of money, but only a minute fraction of that involved in the construction, maintenance and operation of a SAR mapping system, while the benefits could be great.

(3) The vector plots of the residual errors obtained throughout the series of tests carried out by the author displayed a highly systematic pattern in the cross-track direction. This was apparent even after application of polynomial corrections and those for known relief displacement. Since the reasons for these residual errors are not apparent, further work is recommended to find the source of these errors.

(4) The shortcomings in the Seasat SAR image quality have already been discussed above. It was evident that basic topographic mapping would be utterly impossible without the collateral information available to the present author in the form of existing maps. The use of this material is justified in a research project but obviously it will not be available in a real mapping operation. Hopefully, the image quality of satellite SAR images will be improved but, even if this takes place, there is a real need for an increased knowledge and appreciation of the different forms that the images of specific objects may take and further experiments and experience is required if mapping is to be attempted on a regular basis. In particular, a more complete knowledge and appreciation of the different terrain and system parameters and their interaction and effects on the radar back-scatter from the various objects to be mapped is necessary if the maximum information is to be acquired from the SAR image for mapping purposes.

The suggestions made above that further research is necessary may be viewed as an inevitable conclusion from any research work. The disappointment with the results of some of the research work undertaken in this present project must however be tempered by the knowledge that the Seasat SAR was an experimental system and that it was the first spaceborne SLR system whose data was available for civilian investigators. Improved SAR devices will certainly appear in future. Indeed, as this chapter is written, the first images from the Shuttle SAR systems have just been printed in the technical press and undoubtedly these will have made use of the experience gained with the Seasat system. Furthermore, it is expected that the European Spacelab will eventually carry a SAR on board the Shuttle as a preliminary to the incorporation of such a device in the E.R.S. (European Resources Satellite) expected to be launched in the second half of this decade. Thus the results obtained in this present research and the recommendations made for further future work will be a contribution towards a better understanding of the possibilities of satellite-borne SAR systems for the purpose of topographic mapping.

12.3 A Final Note

To conclude this study on a personal note, the author has benefitted greatly from the knowledge and skills acquired from carrying out this research work. For example, the author had not undertaken any serious computer programming before commencing this study. However, he has been able to make full use of the extensive facilities available in the Glasgow University Computing Service and has been able

to develop several relatively large and complex programs for his work in two different high-level computer languages. As a result, the techniques of devising suitable algorithms and of writing the appropriate computer programs to solve such algorithms have been thoroughly grasped.

However, the main benefit to the author has been the opening of the whole field of SLR mapping to him including data processing; image analysis, interpretation and measurements; the provision of control and test data; and the utilization of modern digitizers for image coordinate measurements. Furthermore, the digital monoplottting technique with its accompanying requirements for data processing, the preparation of a DTM and the plotting of the final digital map is still another area in which the author had no previous background prior to undertaking this project.

Thus besides the theoretical analyses carried out by the author, the experimental work carried out in the course of this research project has been invaluable in providing advanced training and experience in photogrammetry, remote sensing and computing. This will undoubtedly be of great benefit to the author's future career and hopefully this will in turn be of direct usefulness to his own country and to the University of Khartoum which have supported him in this research project.

BIBLIOGRAPHY

- Akovetskiy, W.I., 1968. Transformation of Radar Coordinates into the Geodetic System. Geod. Aerofotosjomka, (Translated from Russian).
- Allam, M., 1978. DTM Application in Topographic Mapping. Photogrammetric Eng. and Remote Sensing, Vol. 44, No. 12, P.1513-1520.
- American Society of Photogrammetry, 1975. Manual of Remote Sensing, First Edition (Two Volumes).
- Ausherman, D.A., 1977. Digital Versus Optical Techniques in Synthetic Aperture Radar Data Processing. Proceedings of the Society of Photo-optical Instrumentation Engineers (SPIE), Vol.119, P.238-257.
- Barnett, M.E., Smith, R.W. and Welford, W.T., 1978. Optical Decoding of Satellite-borne Synthetic Aperture Radars. Optica Acta, Vol. 25, No. 8, P.707-714.
- Bayma, R.W., Jordan, R.L. and Manning, B.N., 1977. A Survey of SAR Image-formation Processing for Earth Resources Applications. Proceedings of the 11th International Symposium on Remote Sensing of Environment, P.319-326.
- Bennett, J.R. and Cumming, I.G., 1979. A Digital Processor for the Production of Seasat Synthetic Aperture Radar Imagery. Presented Paper, SURGE Workshop, ESRIN, Frascati, Italy.
- Besenicar, J., 1976a. Digital Restitution from Single Photographs for Cadastral Purposes. M.Sc. Thesis, Dept. of Photogrammetry, ITC, Netherlands.
- Besenicar, J., 1976b. A Digital Monoplotting System for Cadastral Purposes. Presented Paper, Commission IV, I.S.P. Congress, Helsinki.

- Bosman, E.R. et al., 1971. Project KARAKA - The Transformation of Points from Side-looking Radar Images into the Map System. Final Report, Part 1, Netherlands Interdepartmental Working Community for the Application and Research of Remote Sensing Techniques, Delft.
- Bosman, E.R. et al., 1972. KARIN - A Program System for the Mapping of Remote Sensing Information. Presented Paper, Commission III, I.S.P. Congress, Ottawa.
- Bosman, E.R. and Clerici, E., 1975. A Report Submitted to the Working Group on the Geometry of Remote Sensing, Stuttgart, F.R.G.
- Brown, W.M., 1967. Synthetic Aperture Radar. IEEE Transactions on Aerospace and Electronic Systems, Vol. AES-3, P.217-229.
- Brown, W.M. and Porcello, L.J., 1969. An Introduction to Synthetic Aperture Radar. IEEE Spectrum, Vol.6, No. 9, P.52-62.
- Campbell, W.T., 1975. Geophysical Studies of Floating Ice by Remote Sensing. Journal of Glaciology, Vol.15, No. 7, P.305-328.
- Clynch, J., 1979. Ionospheric Residual Range Error Model. Proceedings of the Second International Geodetic Symposium on Satellite Doppler Positioning, Austin, Texas. P.113-134.
- Corr, G.D. and Haskell, A., 1978. A Digital SAR Processor for Seasat-A. Proceedings of the International Conference on Spacecraft On-board Data Management, Nice, France.
- Grandall, C.J., 1969. Radar Mapping in Panama. Photogrammetric Eng., Vol.35, No. 7, P.641-646.
- Cutrona, L.J. and Leith, E.N., 1960. Optical Data Processing and Filtering Systems. IRE Transactions on Information Theory, Vol. IT-6, P.97-111.
- Cutrona, L.J., Vivian, W.E., Leith, E.N. and Hall, G.O., 1961. A High Resolution Radar Combat Surveillance System. IRE Transactions on Military Electronics, Vol.MIL-5, P.127-131.

- Cutrona, L.J. and Hall, G.O., 1962. A Comparison of Techniques for Achieving Fine Azimuth Resolution. IRE Transactions on Military Electronics, Vol. MIL-6, P.119-121.
- Cutrona, L.J., Leith, E.N., Porcello, L.J. and Vivian, W.E., 1966. On the Application of Coherent Optical Image Processing Techniques to Synthetic Aperture Radar. Proceedings of IEEE, Vol.54, P.1026-1032.
- Deane, R.A., 1973. Side-looking Radar Systems and Their Potential Applications to Earth Resources Surveys. European Space Research Organization (ESRO) Report, No. ESRO-CR-136.
- Derenyi, E.E., 1974a. Planimetric Accuracy of Infra-red Line-scan Imagery. The Canadian Surveyor, Vol.28, No. 3, P.247-254.
- Derenyi, E.E., 1974b. SLAR Geometric Test. Photogrammetric Eng., Vol.40, No.5, P.597-604.
- Derenyi, E.E., 1975. Topographic Accuracy of Side-looking Radar Imagery. Proceedings of I.S.P. Commission III Symposium, Stuttgart, F.R.G., P.597-604.
- Derenyi, E.E. and Szabo, L., 1980. Planimetric Accuracy of Synthetic Aperture Radar Imagery. Proceedings of I.S.P. Congress, Commission III, Hamburg, F.R.G., Vol.B3, P.142-148.
- Dowideit, G., 1975. A Simulation System for Theoretical Analysis of Radar Restitution and Test by Adjustment. Proceedings of I.S.P. Commission III Symposium, Stuttgart, F.R.G., P.216-229.
- Drake, B. and Shuchman, R., 1974. Feasibility of Using Multiplexed SLAR Imagery for Water Resources Management and Mapping Vegetation Communities. Proceedings of the 9th Symposium on Remote Sensing of Environment, P.219-250.
- Dunbar, M., 1975. Interpretation of SLAR Imagery of Sea Ice in Nares Strait and the Arctic Ocean. Journal of Glaciology, Vol.15, No. 7, P.193-214.

- Ellis, A.B.E., 1978. Ground Processing of Seasat-A Data at an Earthnet Station. Proceedings of the International Conference on Spacecraft Onboard Data Management, Nice, France.
- Entres, S.L., 1970. Observation Limits of Low Power Space-borne Side-looking Radar for Earth Resources Applications. Royal Aircraft Establishment Technical Report, No. 70015.
- European Space Agency (ESA), 1979. Seasat-1. Earthnet Review, February.
- Forrest, R.B. and Hattaway, D.P., 1968. LR-1 Portable Line-Drawing Rectifier. Bendix Corporation Technical Journal, Vol.1, No. 2, P.81-82.
- Forrest, R.B., 1972. A Digital Portable Line-Drawing Rectifier. Bendix Corporation Technical Journal, Vol.5, No. 1.
- Goodyear, 1974. Preliminary Imagery Data Analysis - Goodyear Electronic Mapping System (GEMS). Goodyear/Aerospace Corporation Report GIB - 9342, Code 99696.
- Graham, L.C., 1970. Cartographic Applications of Synthetic Aperture Radar. Goodyear/Aerospace Corporation Report No. GERA-1831.
- Graham, L.C., 1974a. Synthetic Aperture Radar Applications to Earth Resources Development. Goodyear/Aerospace Corporation Report, No. GERA-2010.
- Graham, L.C., 1974b. Geometric Problems in Side-looking Radar Imagery. Proceedings of I.S.P. Commission III Symposium, Stuttgart, F.R.G., P.199-206.
- Greenberg, J.S., 1967. A System Look at Satellite-borne High Resolution Radar. RCA Review, No. 28.
- Greve, C. and Cooney, W., 1974. Digital Rectification of Side-Looking Radar. Proceedings of A.S.P. Annual Conference, Washington D.C. P.19-32.

- Guignard, J.P., 1980. The I.S.P. SAR Processing Workshop Group Activities. Proceedings of I.S.P. International Congress, Hamburg, F.R.G., Vol.B9, P.223-246.
- Hall, D., 1974. Digital Cartographic Compilation. Proceedings of A.C.S.M., 34th Annual Meeting, St. Louis, P.248-311.
- Hibler, W.D., Tucker, W.B. and Weeks, W.F., 1975. Techniques for Studying Sea Ice Drift and Deformation at Sites far from Land Using Landsat Imagery. Proceedings of the 10th International Symposium on Remote Sensing of Environment, P.595-610.
- Hockeborn, H.A., 1971. Extraction of Positional Information from Side-looking Radar. Bildmessung und Luftbildwesen, Vol.39, No.1, P.55-58.
- Jensen, H., Graham, L.C., Porcello, L.J. and Emmet, N.L., 1977. Side-Looking Radar. Scientific American, Vol.237, No.4, P.84-95.
- Konecny, G. and Derenyi, E.E., 1966. Geometric Considerations for Mapping from Scan Imagery. Proceedings of the 4th Symposium of Remote Sensing of Environment, P.327-337.
- Konecny, G., 1970. Metric Problems in Remote Sensing. ITC Publications Series A, No.50, P.152-177.
- Konecny, G., 1972. Geometric Aspects of Remote Sensing. Proceedings of the 12th I.S.P. Congress, Commission III, Ottawa.
- Konecny, G., 1974. Approach and Status of Geometric Restitution for Remote Sensing Imagery. Proceedings of I.S.P. Commission III Symposium, Stuttgart, F.R.G. p.188-198.
- Konecny, G., 1975. Analytical Relations for the Restitution of Dynamic Remote Sensing Imagery. Report Submitted to E.R.O.-E.T.L. Conference, University of Glasgow.
- Konecny, G., 1976. Mathematical Models and Procedures for the Geometric Restitution of Remote Sensing. International Archives of Photogrammetry, Vol.21, Part 3.

- Kovaly, J., 1976. Synthetic Aperture Radar. Artech House.
- Kozma, A., Leith, E.N. and Massey, N.G., 1972. Tilted Plane Optical Processor. Applied Optics, Vol.11, No.8, P.1766-1777.
- Kratky, V., 1980. Seasat Orbit Effects on Imaging Geometry of Synthetic Aperture Radar. Annales des Mines, April-May, P.81-89.
- Laprade, G.L., 1963. An Analytical and Experimental Study of Stereo for Radar. Photogrammetric Eng., Vol.29, No.3, P.294-306.
- Laprade, G.L. and Leonardo, E.S., 1969. Elevations from Radar Imagery. Photogrammetric Eng., Vol.35, No.4, P.366-371.
- Laprade, G.L., 1970. Subjective Considerations for Stereo Radar. Goodyear/Aerospace Corporation Report No. GIB-9169.
- Larsen, R.W. and Zelenka, J.S., 1971. A Microwave Hologram System. IEEE Transactions on Aerospace and Electronic Systems. Vol.AES-8, P.809-842.
- Leatherdale, J., 1981. Mapping Applications of Satellite and SLR Imagery. Evening Lecture, Dept. of Geography, University of Glasgow.
- Leberl, F., 1970. Metric Properties of Imagery Produced by Side-looking Airborne Radar and Infrared Linescan Systems. ITC Publications, Series A, No.50. P.125-151.
- Leberl, F., 1972. Evaluation of Single Strips of Side-looking Radar. Proceedings of the 12th I.S.P. Congress, Vol.19, Part 3.
- Leberl, F., 1974. Evaluation of SLAR Image Quality and Geometry for PRORADAM. ITC Journal, 1974/2. P.518-546.
- Leberl, F., 1975a. The Geometry of, and Plotting from Single Strips of Side-looking Airborne Radar Imagery. ITC Technical Report, No. 1, Enschede.
- Leberl, F., 1975b. Radargrammetry for Image Interpreters. ITC Technical Report, No. 2, Enschede.

- Leberl, F., 1975c. Radargrammetric Point Determination PRORADAM.
Proceedings of I.S.P. Comm. III Symposium, Stuttgart, P.207-215.
- Leberl, F., 1975d. Photogrammetric Interpolation. Photogrammetric Eng. and Remote Sensing, Vol.41, No.5, P.603-612.
- Leberl, F., 1975e. Sequential and Simultaneous SLAR Block Adjustment.
Photogrammetria, Vol.31, No.1, P.39-51.
- Leberl, F., 1975f. Lunar Radargrammetry with ALSE-VHF Imagery.
Proceedings of A.S.P., Fall Technical Meeting, Phoenix, Arizona,
P.266-285.
- Leberl, F., 1976a. Mapping Lunar Surface from Side-Looking Orbital
Radar Images. The Moon, Vol.15, P.329-342.
- Leberl, F., 1976b. Imaging Radar Applications to Mapping and Charting.
Photogrammetria, Vol.32, No. 1, P.75-100.
- Leberl, F., Farr, T., Bryan, L. and Elachi, C., 1976c. Study of Arctic
Sea Ice Drift from L-band Side-looking Radar. Proceedings of
A.S.P., 42nd Annual Convention, Washington D.C., P.597-611.
- Leberl, F., Jensen, H. and Kaplan, J., 1976d. Side-looking Radar
Mosaicing Experiment. Photogrammetric Eng. and Remote Sensing.
Vol.42, No.8, P.1035-1042.
- Leberl, F., 1980. Preliminary Radargrammetric Assessment of Seasat-A
SAR Images. Mitteilungen der Geodatischen Institut der Technischen
Universitat in Graz.
- Le Gal, Y. and Gilbert, J.C., 1978. Seasat-A SAR Ground Processing
With Standard Hardware Mitra 125 and PROPAL II. Proceedings of the
International Conference on Spacecraft Onboard Data Management,
Nice, France.
- Leith, E.N. and Ingalls, A.L., 1968. Synthetic Antenna Data Processing
by Wavefront Reconstruction. Applied Optics, Vol.7, No.3, P.539-544.

- Leith, E.N., 1971. Quasi-holographic Techniques in the Microwave Region. Proceedings of IEEE, Vol.59, No.9, P.1305-1318.
- Levine, D., 1960. Radargrammetry. McGraw Hill, New York.
- Lewis, A.J., MacDonald, H.C. and Simonett, D.S., 1969. Detection of Linear Cultural Features with Multipolarization Radar Image. Proceedings of the 6th International Symposium on Remote Sensing of Environment, P.879-894.
- Lodge, D.W.S., 1979. Seasat Data Reception and Dissemination at RAE. Paper Presented at the Remote Sensing Annual Conference, University of Dundee, Scotland.
- Lodge, D.W.S., 1980a. The Seasat-1 SAR: Introduction, Data Reception and Processing. EARSL Post Graduate Summer School on Remote Sensing Applications to Oceanography, Meteorology and Hydrology, University of Dundee, Scotland.
- Lodge, D.W.S., 1980b. Private Communication.
- Makarovic, B., 1973. Digital Monoplotters. ITC Journal, 1973-4, P.583-600.
- Masry, S.E. and McLaren, R. 1977. Digital Techniques for Map Revision and Checking Digitized Data. Technical Report No.40, Dept. of Surveying Engineering, University of New Brunswick, Canada.
- McCandless, S.W. and Thompson, T.W., 1975. The U.S. Seasat Program. Proceedings of the 12th Space Congress, Cocoa Beach, Florida, U.S.A.
- McCandless, S.W., 1977. Data Processing for NASA's First Space-based Synthetic Aperture Radar. Proceedings of the 11th International Symposium on Remote Sensing of Environment, P.1079-1081.
- Mikhail, E.M., 1976. Observations and Least Squares. IEP-Dun-Donnelley, New York.
- Moffit, F.H. and Mikhail, E.M., 1980. Photogrammetry. International Textbook Company, Scranton.

- Moore, R.K. and Thomann, G.C., 1971. Imaging Radars for Geoscience Use. IEEE Transactions on Geoscience Electronics, Vol.GE-9, P.155-164.
- Norvelle, F.R., 1972. AS-11A Radar Program. Photogrammetric Eng., Vol.38, No.1, P.77-82.
- Parashar, S.K., Biggs, A.W., Fung, A.K. and Moore, R.K., 1974. Investigation of Radar Discrimination of Sea Ice. Proceedings of the 9th Symposium on Remote Sensing of Environment, P.323-332.
- Parry, D.E. and Trevett, J.W., 1979. Mapping Nigeria's Vegetation from Radar. The Geographical Journal, Vol.145, Part 2, P.265-281.
- Petrie, G., 1974. Mapping from Earth Satellites. Road Design, Paper XI, Planning and Transport Research and Computation Co. Ltd., London.
- Petrie, G., 1978. Geometric Aspects and Cartographic Applications of Side-looking Radar. Paper Presented to the 5th Annual Conference of the Remote Sensing Society held at Van Mildert College, University of Durham, England.
- Porcello, L.J., Jordan, R.L., Zelenka, J.S., Adams, G.F., Phillips, R.J., Brown, W.E., Ward, S.H. and Jackson, P.L., 1974. Apollo Lunar Sounder Radar System. Proceedings of IEEE, Vol.62, P.769-782.
- Raney, R.K., 1977. A Solution to the Problem of SAR Range Curvature. Proceedings of the 11th International Symposium on Remote Sensing of Environment, P.1255-1258.
- Sabins, F.F., 1978. Remote Sensing, Principles and Interpretation. Freeman Press, San Francisco.
- Sherwin, S.W., Ruina, J.P. and Rawcliffe, R.D., 1962. Some Early Developments in Synthetic Aperture Radar Systems. IRE Transactions on Military Electronics, Vol.MIL-5, P.111-115.

- Shuchman, R. and Lowry, R.T., 1977. Vegetation Classification with Digital X-band and L-band Dual Polarized SAR Imagery. Proceedings of the 4th Canadian Symposium on Remote Sensing, Loews Le Concorde, Quebec, Canada, P.444-458.
- Skolnik, I.M., 1970. Radar Handbook. McGraw Hill, New York.
- Teleki, P.G. and Ramseier, 1978. The Seasat-A Synthetic Aperture Radar. Proceedings of the International Symposium on Remote Sensing for Observation and Inventory of Earth Resources and the Endangered Environment, Freiburg, F.R.G.
- Thompson, T.W. and Bradie, R.A., 1971. Progress Report on 25 cm Radar Observations of the 1971 AIDJEX Studies. NASA Contract Report No. NA57-100.
- Tiernan, M., Roth, L., Thompson, T.W., Elachi, C. and Brown, W.E., 1976. Lunar Cartography with Apollo-17 ALSE Radar Imagery. The Moon, Vol.15, No. 1/2, P.155-163.
- Van Roessel, J. and Godoy, R., 1974. SLAR Mosaics for Project RADAM. Photogrammetric Eng., Vol.40, No.6, P.583-595.
- Waite, W.P. and MacDonald, H.C., 1970. Snowfield Mapping with K-Band Radar. Remote Sensing of Environment, Vol.1, No.1, P.143-150.
- Wells, D.E., 1974. Doppler Satellite Control. Ph.D. Thesis, Dept. of Surveying Engineering, University of New Brunswick, Canada.
- Wong, K.W., 1968. Geometric Calibration of Television Systems for Photogrammetric Applications. Presented Paper, I.S.P. Congress, Lausanne.

APPENDIX AA.1 Least Squares Adjustment Using Observation EquationsA.1.1 Definitions

(i) Mathematical Model: This is defined as a theoretical system or an abstract concept by which one describes a physical situation or a set of events. Such a description is not necessarily meant to be complete or exhaustive, but to relate only to those aspects or properties that are under consideration (Mikhail, 1976).

(ii) Observation: The term "observation" (or measurement) is often used in practice to refer to both the operation or process itself, as well as the actual outcome of such operation.

A.1.2 Procedure and Derivation

Relating the n observations as functions of the minimum number of the unknown variables (m), then

$$m = (n - r)$$

where r = the number of redundant observations.

Let the linearized form of these equations be of the form:

$$\bar{x} = AX + A_0 \dots\dots\dots \quad (\text{A.1})$$

where \bar{x} = the vector of unknown adjusted observations ($nx1$);

A = the coefficient matrix of the unknown variable (nxm);

X = the vector of unknown variables ($mx1$); and

A_0 = the vector of constants.

Equation A.1 can be expressed in another form, as

$$(x_0 + v) = A(X_0 + \Delta X) + A_0 \dots\dots\dots \quad (\text{A.2})$$

where x_0 = the observed values;

v = the unknown corrections to the observed values (or residual errors after adjustment);

X_0 = approximate values for the unknown variables X ; and

ΔX = the unknown corrections to the approximate values X_0 .

Re-arranging the terms, the observation equations become:

$$v = A \cdot \Delta X - (x_0 - AX_0 - A_0)$$

$$\text{or } v = A \Delta X - L \dots\dots\dots (A.3)$$

where L = the new vector of constants.

Now, imposing the least squares condition,

$$E = v^T G^{-1} v = \text{minimum,}$$

where G is the cofactor matrix of observed quantities.

One may write this as:

$$\begin{aligned} E &= (A\Delta X - L)^T G^{-1} (A\Delta X - L) \\ &= (\Delta X^T A^T - L^T) G^{-1} (A \cdot \Delta X - L) \\ &= (\Delta X^T A^T G^{-1} - L^T G^{-1}) (A \cdot \Delta X - L) \\ &= \Delta X^T A^T G^{-1} A \cdot \Delta X - L^T G^{-1} A \cdot \Delta X - \Delta X^T A^T G^{-1} L + L^T G^{-1} L \dots (A.4) \end{aligned}$$

For E to be minimum, equate the quantities $\frac{\partial E}{\partial \Delta X_1}$, $\frac{\partial E}{\partial \Delta X_2}$,

$\frac{\partial E}{\partial \Delta X_3}$,, $\frac{\partial E}{\partial \Delta X_n}$ to zero.

$$\begin{aligned} \therefore \frac{\partial E}{\partial (\Delta X)} &= A^T G^{-1} A \cdot \Delta X + (A^T G^{-1} A)^T \Delta X - (L^T G^{-1} A)^T - A^T G^{-1} L \\ &= A^T G^{-1} A \cdot \Delta X + A^T G^{-1} A \cdot \Delta X - A^T G^{-1} L - A^T G^{-1} L = 0 \end{aligned}$$

$$\therefore \frac{\partial E}{\partial (\Delta X)} = 2(A^T G^{-1} A \cdot \Delta X) - 2(A^T G^{-1} L) = 0$$

$$\therefore A^T G^{-1} A \cdot \Delta X = A^T G^{-1} L \dots\dots\dots (A.5)$$

Equation A.5 may be written in the following form:

$$N \cdot \Delta X = F \dots\dots\dots (A.6)$$

$$\begin{aligned} \text{where } N &= A^T G^{-1} A; \text{ and } \} \\ F &= A^T G^{-1} L \} \dots\dots\dots (A.7) \end{aligned}$$

Equation A.6 is the set of normal equations (of which there are of course as many equations as unknowns). The unknowns themselves may be found from:

$$\Delta X = N^{-1}F \dots\dots\dots (A.8)$$

Equations A.7 and A.8 are those programmed and used in the present study.

A.2 Application of the Least Squares Adjustment Method to the Polynomial Transformation used in the Present Study

When implementing these equations, one starts from equation A.3 where the observation equations are first formed. For the polynomial transformation, these equations take the form:

$$\begin{aligned} v_x &= n_0 + n_1x + n_2y + n_3xy + n_4x^2 + n_5x^2y + n_6x^3 + n_7x^3y - X \\ v_y &= m_0 + m_1x + m_2y + m_3xy + m_4x^2 + m_5x^2y + m_6x^3 + m_7x^3y - Y \end{aligned} \quad (A.9)$$

where v_x and v_y are the residual errors in Northings and Eastings respectively. These equations can be written as follows:

$$\begin{aligned} v_x &= \begin{bmatrix} 1 & x_i & y_i & x_i y_i & x_i^2 & x_i^2 y & x_i^3 & x_i^3 y \end{bmatrix} \begin{bmatrix} n_0 \\ n_1 \\ n_2 \\ n_3 \\ n_4 \\ n_5 \\ n_6 \\ n_7 \end{bmatrix} - \begin{bmatrix} X \end{bmatrix} \\ \text{and } v_y &= \begin{bmatrix} 1 & x_i & y_i & x_i y_i & x_i^2 & x_i^2 y & x_i^3 & x_i^3 y \end{bmatrix} \begin{bmatrix} m_0 \\ m_1 \\ m_2 \\ m_3 \\ m_4 \\ m_5 \\ m_6 \\ m_7 \end{bmatrix} - \begin{bmatrix} Y \end{bmatrix} \end{aligned}$$

In matrix notation, this can be written in the form of equation A.3:

$$v = A.\Delta X - L \dots\dots\dots (A.10)$$

where A = coefficient of knowns;
 v = the vector of residual errors; and
 ΔX = the vector of unknowns; and
 L = the vector of known coordinates.

Equation A.10 includes a pair of observation equations that arise for each point of known coordinates in both the X and the Y directions. Obviously for each direction, eight such points are necessary and sufficient to compute the eight unknown parameters. Whenever more than eight points are given, a least squares adjustment becomes necessary. The general situation in this case is to consider both x and y as observations.

Using the least squares adjustment technique, as mentioned above, the matrix of the unknowns ΔX can be computed from equation A.10, i.e.

$$\Delta X = N^{-1}F$$

where $N = A^T G^{-1} A;$

A^T = transpose matrix of A;

G = cofactor matrix of observed quantities; and

$F = A^T G^{-1} L.$

If x and y are considered as uncorrelated and of equal measurement precision, then $G^{-1} = I$ (unity) (e.g. see Mikhail, 1976; Moffit and Mikhail, 1980). This condition is assumed throughout the program and no attempt has been made to assign any weights or weighting functions to the observed quantities.

This assumption has been adopted since there is no evidence that a certain observation is more reliable than the others.

Having established the transformation parameters, the computer program can then calculate the transformed terrain coordinates at the control points. Comparison of these computed values with the given coordinate values for these points allows the computation of the individual residual errors at each point. From these, the root mean square error (r.m.s.e.) may be derived by using the formula:

$$\sigma_r = \sqrt{\frac{\sum vv}{(n-u)}}$$

where σ_r = r.m.s.e. at the control points;
 v = residual error (or discrepancy) at a control point;
 n = number of control points used; and
 u = minimum number of control points required, to solve the system of equations.

The program can then proceed to compute the transformed coordinates of the check points, from which the individual residual errors and the r.m.s.e. values may be deduced in a similar manner to that above using the formula:

$$\sigma_c = \sqrt{\frac{\sum vv}{n}}$$

where σ_c = r.m.s.e. at the check points;
 v = residual error (or discrepancy) at a check point; and
 n = the number of the check points used.